Retinal Ensemble Coding under Dynamic Conditions

León Mauricio Juárez Paz

geboren am 7. Februar 1977 in Mexiko-Stadt, Mexiko

Zusammenfassung

In einer natürlichen Umgebung ist die Verarbeitung von visuellen Bewegungsinformationen oftmals überlebenswichtig. In der Regel beinhalten visuelle Eindrücke mehr als eine Eigenschaft wie z.B. Lichtintensität, Textur und Farbe. Daher muss Bewegung auch bei unterschiedlichen Lichtbedingungen zuverlässig erkannt und geschätzt werden, um korrekte Verhaltensentscheidungen treffen zu können. Es wird allgemein angenommen, dass die Bewegungserkennung von Primaten und Menschen in den visuellen Zentren des Gehirns stattfindet. Allerdings konnte für einige Tierarten, wie z.B. bei Kaninchen, Fisch und Schildkröten gezeigt werden, dass die Bewegungserkennung bereits in der Retina beginnt. Da alle dem Gehirn zur Verfügung stehenden visuellen Informationen von den Ganglienzellen der Retina stammen, ist anzunehmen, dass Ganglienzellenantworten viele visuelle Merkmale simultan kodieren. Dennoch ist der zugrunde liegende Kodierungsmechanismus in der Retina nicht vollständig bekannt.

Der erste Teil dieser Studie widmet sich der Untersuchung wie Antworten retinaler Ganglienzellen Bewegungsinformationen unter konstanten Lichtbedingungen kodieren. Hierfür wurden an Retinen von Schildkröten (*trachemys scripta elegans*) sowie von Karpfen (*cyprinus carpio*) extrazelluläre Ableitungen von Ganglienzellen durchgeführt, die mit bewegten Stimuli gereizt wurden. Im zweiten Teil dieser Studie wird näher auf den möglichen Mechanismus eingegangen, welcher den Ganglienzellen die Kodierung von Bewegungsinformationen bei variablen Lichtbedingungen erlaubt. Hierfür wurden die Antworten der Ganglienzellen einer Karpfenretina auf bewegte Stimuli unter wechselnden Lichtbedingungen verwendet.

Zur Analyse der Ganglienzellantworten wurden in dieser Studie zwei unterschiedliche publizierte Metriken verwendet, die speziell zur Analyse von Aktionspotentialfolgen entwickelt wurden: "Spike Cost-Based Metrics" und "ISI Metrics". Die "Spike Cost-Based Metrics" ermöglicht den Vergleich der Spikerate mit der zeitlichen Struktur der Ganglienzellenantworten auf verschiedenen Zeitskalen als potenzielle Kodierungsstrategien für Bewegungsinformation. Die "ISI Metrics" wurde verwendet, um die Bedeutung der zeitlichen Struktur für die Kodierung der Bewegungsinformation weiter zu analysieren. Zudem wurde untersucht, ob die Kombination der Aktivität mehrerer Ganglienzellen die Kodierung der Bewegungsinformation verbessern kann. Hierfür wurden drei Hypothesen der Kombination von Aktivitäten getestet: "Pooled Population", "Labelled Line" und "Functional Group".

Die Ergebnisse des ersten Teils dieser Studie zeigten, dass die Ganglienzellantworten von Schildkröten und Karpfen die Bewegungsgeschwindigkeit und deren Veränderung kodieren. Weiter konnte gezeigt werden, dass sowohl die Spikerate, als auch die zeitliche Struktur der Spikes eine Bedeutung bei der Kodierung von konstanter Bewegung spielen. Im Gegensatz dazu spielte die zeitliche Spikestruktur bei der Kodierung von Änderungen der Bewegung eine größere Rolle als die Spikerate. Die kombinierte Aktivität von Ganglienzellen verbesserte die Kodierung der Bewegungsinformation, besonders wenn sich die Geschwindigkeit der Bewegung veränderte. Insbesondere die Hypothesen "Labelled Line" und "Functional Group", die zwischen Spikes verschiedener Neurone unterscheiden, ermöglichten eine effiziente Kodierung.

Im zweiten Teil dieser Studie konnte gezeigt werden, dass die Ganglienzellantworten der Karpfenretina gleichzeitig Informationen über Bewegung und Lichtintensität kodieren. Jedoch reichen die Antworten einer einzelnen Ganglienzelle nicht aus, um Änderungen dieser beiden Eigenschaften zuverlässig schätzen zu können. Die kombinierte Aktivität mehrerer Ganglienzellen ermöglichte eine Verbesserung insbesondere der simultanen Kodierung der Stimuluseigenschaften und deren Änderungen. Auch wenn die Spikerate sich grundsätzlich als Kodierungsstrategien eignete, gewann die zeitliche Feinstruktur der Antworten für die Schätzung von Bewegungsinformationen an Bedeutung, wenn die Lichtbedingungen sich änderten.

Basierend auf diesen Ergebnissen kann vermutet werden, dass eine Kombination der Spikerate und der zeitlichen Struktur neuronaler Aktivität eine plausible Kodierungsstrategie für retinale Ganglienzellen darstellt. In der Literatur finden sich Hinweise auf die Verwendung aller drei der hier untersuchten Hypothesen zur Kombination mehrerer Zellantworten im visuellen und anderen sensorischen Systemen. Somit ist es möglich, dass Karpfen- und Schildkrötenretinen diese Kodierungsstrategien für die simultane Verarbeitung von Bewegungsinformationen und anderer visueller Stimuluseigenschaften verwenden.

Abstract

In a natural environment, the processing of visual motion information is crucial for survival tasks. Moreover, natural scenes are generally composed by more than one visual feature. Therefore, in order to ensure correct behavioural responses, the detection and estimation of motion has to be performed robustly regardless of other information cues, such as light intensity, texture or colour. It has been proposed that in primates and humans, the processing of motion information starts in the primary visual cortex of the brain. However, it also has been found that in other animals, such as rabbit, turtle and fish, the processing of motion information starts already in the retina. Since the brain relies on the responses of retinal ganglion cells as its only source of visual information, these responses should encode several features of visual scenes simultaneously. Nevertheless, the coding mechanisms that the retina could utilise remain elusive.

The first part of this study was dedicated to investigate how the activity of retinal ganglion cells could encode information about motion features under constant light intensity conditions. This investigation involved the extracellular recording of retinal ganglion cell responses to a moving stimulus. For the recordings, turtle (*trachemys scripta elegans*) and carp (*cyprinus carpio*) were used as animal models. The second part of this study further explored the possible mechanisms that could allow the simultaneous encoding of information about motion features and changing light intensities. For this task, retinal ganglion cell responses were extracellularly recorded from one carp retina.

Two spike train metrics were used to analyse the recorded responses of retinal ganglion cells; spike cost-based metrics and ISI metrics. The spike cost-based metrics allows testing the spike firing rate of the responses of retinal ganglion cells, as well as different time scales of their temporal structure, as plausible coding strategies for visual motion. In turn, the ISI metrics was used as complementary method to test the relevance of the temporal structure for encoding tasks. Moreover, it was also explored if the combined activity of cells could enhance the encoded information about visual stimulus features. Here, three joint activity coding hypotheses were tested; Pooled Population, Labelled Line and Functional Group.

The results obtained for the first part of this study show that the activity of retinal ganglion cells in turtle and carp retinae encodes information about motion velocity as well as velocity changes. Moreover, the spike firing rate and the temporal structure show to be suitable coding strategies for constant motion features. In contrast, the temporal structure gains relevance

for the encoding of changing motion features, while the opposite happens for the spike firing rate. Furthermore, the combined activity of retinal ganglion cells allows enhancing the encoded information about motion features, especially about the ones that involve changes in motion velocity. Additionally, the hypotheses distinguishing spikes coming from different neurons, i.e., Labelled Line and Functional Group, show to encode more efficiently information about motion features.

The results for the second part of this study show that the activity of single retinal ganglion cells of the carp encodes information about motion features and light intensities simultaneously. However, this activity performs poorly for the encoding of individual changes in these two stimulus features. In turn, the joint activity of retinal ganglion cells allows enhancing the performance, especially for the simultaneous encoding of the two stimulus features, as well as the encoding of their changes. Furthermore, while the spike firing rate and the temporal structure show to be suitable coding strategies for all cases, finer time scales of the temporal structure gain relevance for encoding tasks when changes in light intensity are present.

Based on the results obtained in this study it can be suggested that the spike firing rate and the temporal structure of neuronal activity are plausible coding strategies for retinal ganglion cells. Moreover, since the three joint activity coding hypotheses tested in this study have been reported in different sensory systems, including the visual system. It is possible that turtle and fish retinal ganglion cells utilise them for the processing of visual motion and the simultaneous encoding of stimulus features.

Contents

Chapter 1

Introduction

Everyday situations like walking through crowds, driving a car or playing soccer, involve the visual detection and estimation of motion. Moreover, for animals in a natural environment, the detection and estimation of motion play an important role in many behavioural important functions, such as camouflage breaking, detecting threatening objects and the perception of depth. Therefore, in order to enhance the chances of survival, all these functions should be robustly performed regardless of the luminance, shape, color, and texture of the visual objects. Within this context, it is very likely that all animals with vision have mechanisms for motion processing. Nevertheless, it is still not entirely understood how the processing of motion information is performed by the visual system.

The present study is focused on the first stage of motion detection and estimation in the visual system; the retina. Here, utilising the turtle (*trachemys scripta elegans*) and carp (*cyprinus carpio*) as animal models, it was investigated how the activity of retinal ganglion cells encode information about the motion features of a moving stimulus. For both animal species, the analyses were performed considering the extracellular activity of single and populations of retinal ganglion cells. Here, it was assessed how relevant the spike firing rate and the temporal structure of the responses of retinal ganglion cells are, for the encoding of motion information. Additionally, this study includes the test of three different hypotheses that deal with the mechanisms by which the activity of retinal ganglion cells could jointly encode information about motion features.

Because the detection and estimation of motion have to be accomplished under dynamical light conditions, a further aspect of this study tested the capacity of carp retinal ganglion cells to encode simultaneously, information about motion features and light intensities.

The sense of vision in many animal species is the primary source of information about the outside world. For survival in a natural environment, many animal species rely on this sense to perform the correct behavioural task to either escape from a predator, or catch a prey. In humans, vision has a strong direct influence in mental processes like vection (self-motion perception) (Prothero et al., 1995) and memory (Leibovic, 1990), and it has been also indirectly related to mental time travel (Miles et al., 2010). Furthermore, reflex responses, like the optokinetic nystagmus can be induced by continuous movement of the whole or a part of the visual field (Cohen et al., 1977). Besides the fundamental role that vision plays in many animal species, the research interest in this sense, specially in the retina, is also based on the fact that the gained knowledge can contribute in a great manner to understand the function of the nervous system (Dowling, 1987).

Although all parts of the eye play an important role in vision, the retina is the one responsible for the transduction of the time dependent visual image into electrical signals and the transmission of these signals to the brain. The retina is a filmy piece of tissue with a thickness of roughly half a millimetre that lines the back of the eyeball (Kolb, 2003). This tissue develops from the embryonic forebrain and thus, it is considered to be part of the brain (Dowling, 1987). All of the visual information from the outside world undergoes an early stage of processing and compression at the retina and then, it is further transmitted to the brain by ensembles of retinal ganglion cells in the form of action potentials, which are also known as spikes. Moreover, it has been proposed that by the processing of the spatio-temporal intensity changes of the image that has been sensed by the two dimensional array of photoreceptors, the first stages of visual detection and estimation of motion are already carried out in this tissue (Dellen and Wessel, 2009).

The only source of information available to the brain about the visual experience is contained in the spikes arriving from the retinal ganglion cells. Here, much research has been done in the attempt of understanding how the retina processes and finally encodes the visual information. This research covers, among others, the molecules that the different types of retinal cells use as neurotransmitters, the gap junctions that these cells use to communicate among each other, and the electrical activity that these cells utilise to process and further transmit the visual information. Within the framework of the latter research field, the retina offers great experimental advantages to explore the way in which the activity of retinal ganglion cells could encode the visual information that they send to the brain. One of these advantages is that the retina is a flat tissue with a layered structure, in which cells of a certain type are located at defined depths. Additionally, the retina can be readily stimulated using its natural sensory input, i.e., photorecep-

tors, and the responses to these stimuli can be registered with relative ease by extracellular recordings. In this sense, the advances in microelectrode recording techniques (Meister et al., 1994; Nordhausen et al., 1996; Stoppini et al., 1997; Borkholder et al., 1997; Nicolelis et al., 1998; Segev et al., 2004), as well as the processing power of actual computers, have enabled a better understanding of the functional aspects of the retina.

Since the first experiments to record the neural activity in different animal species and in different sensory systems succeeded (Adrian and Zotterman, 1926a,b; Adrian and Matthews, 1927, 1928), it has been proposed that sensory information is conveyed in the time varying firing rate of the neuronal responses. In the case of the retina, there is evidence suggesting that the temporal structure of the neuronal activity contributes to enhance the information that the spike trains carry (Berry et al., 1997; Victor, 1999; Greschner et al., 2006; Gollisch and Meister, 2008; Cerquera and Freund, 2011). Therefore, many studies have focused on the characterisation of the responses of retinal ganglion cells. Nevertheless, this is not a trivial task due to the variability in the spike firing rate and the spike timing of neuronal responses to the same stimulus, mostly provoked by extrinsic influences and intrinsic noise, such as synaptic noise. Several methods have been developed in order to measure the reproducibility of the properties of neuronal responses to a repeatedly stimulus and thereby, find which properties of neuronal responses encode sensory information (Victor and Purpura, 1996; van Rossum, 2001; Schreiber et al., 2003; Kreuz et al., 2007).

Due to the limited number of axons that form the optic nerve, and the assumption of parallel information processing in the nervous system, different hypotheses have been proposed to explain how the activity of retinal ganglion cells encodes visual stimuli. Here, most of the hypotheses suggest that the encoding of visual information is carried out by the joint activity of retinal ganglion cells, rather than by the independent activity of single neurons. However, the joint activity coding hypotheses are sometimes contradictory proposing on the one hand, that the ganglion cells are mainly non-redundant or independent encoders of information (Fernandez et al., 2000; Nirenberg et al., 2001) and on the other hand, that the activity of these cells is repetitive and redundant (Puchalla et al., 2005).

The first chapter of this study comprises four sections. Section 1.1 includes a brief introduction into the architecture of the vertebrate retina. Here, the stages of visual information flow within the retina are explained by making a short and general description of the function and interconnections of the major retinal cell types. Section 1.2 introduces the current hypotheses about how the features of neuronal activity could serve in the encoding of visual information. These features include the spike firing rate and the tem-

poral structure of the activity of single, as well as populations of neurons. Moreover, this section presents three hypotheses about how the activity of single neurons could be combined in order to jointly encode sensory information. Section 1.3 makes a brief description of the properties of the natural images that the visual system of animals has to deal with, and their relation to the function of neurons in the visual system. Finally, Section 1.4 includes a short review about some stimulus reconstruction methods, and the approaches followed in this study to test how the activity of retinal ganglion cells encode different features of visual stimuli.

The second chapter of this study includes three sections, which are devoted to the performed experiments and the applied methods to analyse the acquired data. Section 2.1 describes the extracellular recordings performed in the isolated retinae of turtles and fish, as well as the stimuli used for the electrophysiological experiments. Section 2.2 describes the acquired data and the pre-analysis stages that comprise spike sorting and cell classification. Furthermore, this section introduces the rationale behind the construction of small cell populations to test ensemble coding hypotheses. Finally, Section 2.3 introduces the analysis methods applied in this study to investigate how the activity of retinal ganglion cells encodes information about visual stimuli. Moreover, this section describes the methods used to quantify the performance of the tested hypotheses for the encoding of visual stimuli features.

The third chapter contains the results obtained from the analyses of the activity of single and small populations of retinal ganglion cells. Here, Section 3.1 and Section 3.2 are dedicated to the experiment protocols followed in this study. In turn, both sections include the description of the performance allowed by the different properties of the responses of retinal ganglion cells for the encoding of visual information.

While the fourth chapter of this study is dedicated to the discussion of the obtained results, the last chapter of this study addresses the conclusions that can be drawn from them.

1.1   Architecture of the Retina

The retina is a thin piece of tissue with a thickness, depending on species, between 100 μm and 500 μm that lines the inside of the eyeball and is located at the posterior part of it. The retina owns both, sensory neurons that perform the transduction of light into electrical signals, and neurons that form intricate circuits to carry out the first stages in the processing of visual information. Remarkably, the architecture of the retina is similar for many

animal species, having the same layer arrangement and the same five principal cell types. Furthermore, many of the neurotransmitters used in the retina are the same across many animal species (Meister and Berry II, 1999). However, depending on the species, the anatomical microcircuitry of the retina shows some differences. For instance, the diversity of neurons like the horizontal and amacrine cells decreases in higher mammals, in which more complex visual processing is thought to be relegated to the neocortex (Schiller, 2010). In contrast, animal species whose retinae perform more visual information processing, have specialised retinal regions with cells that fulfil a defined function, e.g., the detection of fast movements by cells in the visual streak of turtles (Ammermüller and Kolb, 1996) and rabbits (Barlow and Hill, 1963; Oyster et al., 1981).

A simplified diagram of the architecture of the retina can be observed in Figure 1.1. Here, it can be observed that the structure of retina consists of different distinguishable layers. These layers are called nuclear or plexiform layers, in function of whether they contain cell bodies (somata) or neuron processes (i.e., dendrites or axons), respectively. Additionally, the layers are named outer or inner layers in relation to their distance from the eyeball centre. In this sense, the outer nuclear layer is where the bodies of the photoreceptors can be found. Immediately anterior to this layer is the outer plexiform layer, which contains the neuron processes that make the synaptic connections between photoreceptors, horizontal and bipolar cells. Moving in the same direction, the next layer is called the inner nuclear layer. This layer contains the somata of horizontal, bipolar and amacrine cells in its outer, center and inner segments, respectively. The inner plexiform layer contains the neuron processes of bipolar, amacrine and retinal ganglion cells. The next layer is the ganglion cell layer, which contains the somata of the retinal ganglion cells. Finally, the most anterior layer of the retina is the nerve fibre layer, which contains the axons of the retinal ganglion cells.

The first step in the processing of visual information is performed by the photoreceptors, which are the neurons that transduce the light into changes in their membrane potential. As mentioned before, the photoreceptors are located in the outer part of the retina and therefore, light has to pass through all the layers of the retina before it reaches these cells. After the transduction process carried out by the photoreceptors, the further processing and transmission of visual information is accomplished by changes in the membrane potential of the different types of neurons in the retina. Here, the most direct pathway for the flow of visual information through the retina is constituted by the photoreceptors, bipolar cells and retinal ganglion cells. Nonetheless, the processing of visual information that takes place in the retina also includes longer pathways that involve the interaction of photoreceptors and
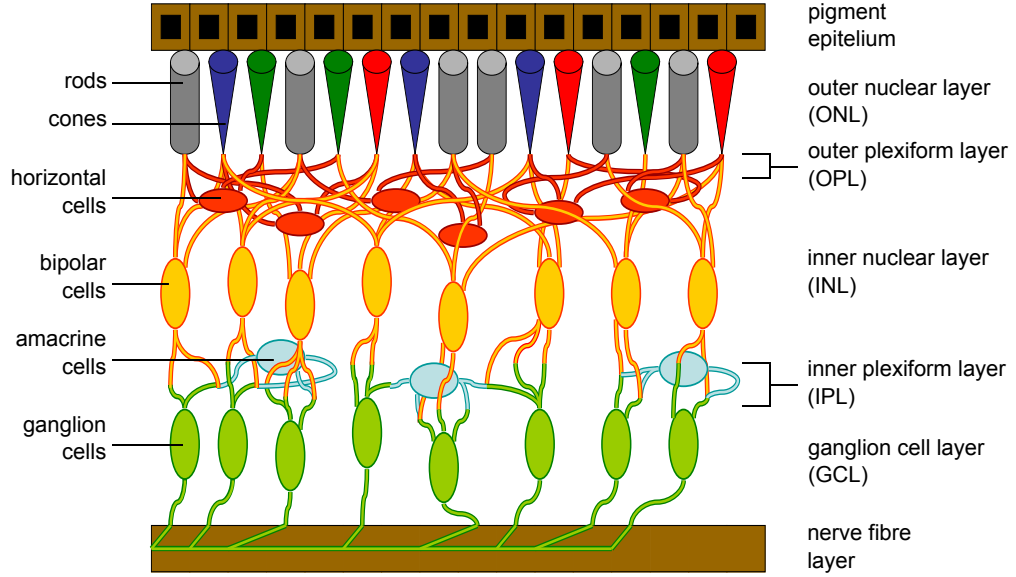
Figure 1.1: Simplified diagram of the architecture of the retina showing the different type of neurons and their organization in different layers.

bipolar cells with horizontal cells, and the interaction of bipolar and retinal ganglion cells with amacrine cells. The final stage in the processing of visual information by the retina is reached at the retinal ganglion cells. Moreover, these cells are different to the rest of the neuron types in the retina in the sense that they, and some types of amacrine cells, are the only capable of producing action potentials (Dowling, 1987; Zhou and Fain, 1996; Habermann et al., 2003; Segev et al., 2004). The axons of retinal ganglion cells build the optical nerve, which in turn conveys all the visual information to the brain in the form of temporal sequences of action potentials.

The turtle has been one of the animal models used by electrophysiologists due in part to the ease and stability of its retina in electrophysiological recordings. Moreover, besides the fact that turtles have good colour vision, the structure of their retina is characterized by a region of specialized cells running above the optic nerve called visual streak. The cells in this region allow the turtle to detect fleeting movements and orient them relative to the horizon. Therefore, it has been proposed that retinae with this streak structure can process information about features of image motion and therefore, perform more vision processing in comparison with retinae with fovea (Kolb, 2003). Other animal models like fish have also been long used to study the function of the retina. Here, within the framework of this study, turtle and

fish retinae were used as models in order to gain some insights about the similarities in the encoding of visual information by the retina across animal species.

In the following sections, the general location and function of the different types of retinal cells are briefly described. Additionally, for each of the cell types, the description addresses shortly the identified cells in turtle an fish retina.

1.1.1 Photoreceptors

The retina in most vertebrates has at most two types of photoreceptors; rods and cones. In this sense, the skate retina seems to be an exception due to the fact that only rods appear to be present in its receptor layer (Dowling and Ripps, 1970; Ripps and Dowling, 1990; Reuter, 2011). The rods are responsible for monochromatic vision and are generally used for dim-light vision. Moreover, these cells usually respond to slow changes in light fluctuations. In contrast, cones are responsible for chromatic vision and are used for daylight and bright-coloured vision. Furthermore, these cells have the ability to respond to rapid light changes.

The outer segments of the photoreceptors are in contact with the pigment epithelium, which is located at the most posterior side of the retina. One of the functions of the pigment epithelium is to absorb the incoming photons and prevent their back reflection into the photoreceptors, avoiding in this way the blurring of images. Furthermore, the pigment epithelium protects the photoreceptors from excessive exposure to light radiation.

The outer segments of the photoreceptors contain disks filled with photopigments. Here, depending on the photoreceptor, the photopigments are comprised by the chromophore 11-*cis*-retinal and one class of the protein opsin (Lamb and Pugh Jr., 2004; Lamb et al., 2007). Thereby, in the rods, this complex is called rhodopsin, whereas in the cones, it is called iodopsin. Here, the difference in the spectral sensitivity of the cones is determined by the light wavelengths that their photoreceptor protein opsin is likely to absorb (Brown and George, 1963, 1964; Marks et al., 1964; Dowling, 1987; Purves et al., 2001). When light hits one photoreceptor, it provokes a conformational change of the molecule 11-*cis*-retinal to *all-trans*-retinal. In turn, this change gives rise to a biochemical cascade that is the basis of the transduction of light into changes in the membrane potential of the photoreceptors. In order to ensure the further phototransduction, the re-isomerisation of the *all-trans*-retinal to 11-*cis*-retinal has to be undertaken. This process takes place in the pigment epithelium (Lamb and Pugh Jr., 2004).

Counterintuitively, rods and cones are hyperpolarised when exposed to

light and depolarised in the dark. When the photoreceptors are depolarised, their synapses release glutamate and depending on the neurotransmitter receptors of the postsynaptic cells, they will induce an inhibitory or an excitatory response. All photoreceptors make synaptic contacts with horizontal and bipolar cells at the outer plexiform layer (OPL). Nonetheless, rods and cones have different pathways for the transmission of visual information. Here, the rod pathways involve the indirect transmission of visual information through the connection between rod bipolar and AII amacrine cells (Kolb, 1979, 1997, 2003). This pathway is going to be described in more detail in Section 1.1.4. Furthermore, the synaptic connections through the rod pathway are more convergent than for the cone pathway. This higher convergence degree allows the rod pathway to be a better detector of light at the expense of acuity. In contrast, the the rod pathway provides better acuity at the expense of light detection.

As mentioned before, turtles have a very good colour vision, which can be inferred by the fact that they have at least six types of cones that are sensitive to light in a wide range of wavelengths. The spectral sensitivity of cones can be inferred from the colour of the oil droplets that they contain (Table 1.1). In contrast, rods in the turtle retina lack these droplets (Ammermüller and Kolb, 1996; Ammermüller et al., 1998). The cones of the turtle retina influence the responses of neighbouring cones of opposite spectral type through electrical junctions among each other, i.e., gap junctions. Here, it has been proposed that the interaction between antagonist and same spectral cone types might provide a sharpening of the spatial image to a better resolution than the one provided by the tiling of the photoreceptors (Ammermüller and Kolb, 1996). Regarding the connections that photoreceptors in the turtle retina make with other cells, rods contact only one type of horizontal cell (H1), whereas cones contact the four types of identified horizontal cells (H1, H2, H3 and H4)(Table 1.1). In addition, cones in the turtle retina contact all types of bipolar cells (11 morphologically identified cells, see Ammermüller and Kolb (1996)), sharing one bipolar cell type (small bipolar cell) with the rods (Dacheux, 1982).

In the case of fish, it has been found that goldfish and carp own well developed colour vision. For both species, three types of cones with similar spectral sensitivities have been found (Marks, 1965; Tomita et al., 1967). The spectral sensitivities for the different cones in the goldfish and the carp retina have shown to be between 611 nm and 625 nm for the red-sensitive cones, between 529 nm and 530 nm for the green-sensitive cones, and between 455 nm and 462 nm for the blue-sensitive cones. Concerning the further connections that photoreceptors make in the fish retina, cones contact three types of horizontal cells (H1, H2 and H3), whereas rods contact only one kind of these

Oil droplet colour	Colour sensitivity	Wavelength	Postsynaptic horizontal cell
Red	Red	620 nm	H1
Red and orange	Red	630 nm	H1 and H4
Red and yellow	Red	623 nm	H1 and H4
Yellow	Green	540 nm	H1 and H2
Green/Colourless	Blue	460 nm	H2 and H3
Colourless	Ultraviolet	360 nm	H2 and H3

Table 1.1: Cones in the turtle retina. The spectral sensitivity of cones can be inferred by the oil droplets they contain. The cone types in the turtle retina make specific postsynaptic contacts with different types of horizontal cells.

cells (rod horizontal cells, see Stell and Lightfoot (1975)). Additionally, cones contact the two types of bipolar cells identified morphologically in fish (large M and small C cells). Nonetheless, one of the types of bipolar cells (large M cells) receives also input from rods (Famiglietti Jr et al., 1977).

1.1.2 Horizontal Cells

The dendrites of horizontal cells invaginate photoreceptors terminals and this way, receive direct input from these cells. Horizontal cells respond to light with graded sustained hyperpolarising potentials that have a high degree of spatial summation. This almost linear spatial summation is due to the direct electrical coupling of adjacent horizontal cells of the same type via gap junctions. Depending on the animal, retinae could have between one and three types of horizontal cells; Luminosity cells (L-type), which hyperpolarise for light in the whole light spectrum and have been found in all of the studied retinas so far, biphasic Chromatic cells (C-type), which hyperpolarise for short wavelengths and depolarise for long wavelengths, and triphasic C-type, which hyperpolarise for monochromatic light from both extremes of the spectrum and depolarise for wavelengths in the intermediate spectral region (Svaetichin and MacNichol Jr., 1959; Twig et al., 2003). In addition, horizontal cells can be morphologically classified in external and intermediate horizontal cells, where external cells are located in layers close to the photoreceptors and intermediate cells are located in more anterior layers (Kaneko, 1979).

Horizontal cells receive input from several photoreceptors and are electrically coupled with adjacent homologous horizontal cells. These facts together explain their wide receptive fields. Furthermore, it is known that horizontal

cells give negative feedback to cone photoreceptors through the release of the neurotransmitter GABA (γ-aminobutyric acid). In turn, cones feedforward the signal further to the bipolar cells they contact. The function of the horizontal cells is nowadays still not fully understood, but they have shown to mediate light adaptation. This process regulates the response of the photoreceptors by decreasing their response sensitivity for bright light conditions and increasing it for dim-light conditions. Less is known about the effects that the action of horizontal cells have on bipolar cells. Nonetheless, they appear to be involved in the first stages of image sharpening by adding an On- or Off-surround signal to Off- or On-bipolar cells, respectively (Kolb, 2003).

Four different morphological types of horizontal cells have been found in the turtle retina; H1, H2, H3 and H4. From these cells, the H1 cell is the only one that consist of two morphologically different structures; L1 and L2. Moreover, rod photoreceptors only make postsynaptic connections with the L1 structure of this cell. Conversely, cone photoreceptors contact all types of horizontal cells. The presynaptic connections that the horizontal cells in the turtle retina make with the cone photoreceptors are listed in Table 1.1. Regarding the spectral responses of horizontal cells, H1 cells respond to light in the whole spectrum but nevertheless, exhibit their maximum response for long wavelengths. In contrast, H2 and H3 cells exhibit biphasic responses depending on the wavelength of light. Here, depolarisation of both cell types is produced by red light, whereas hyperpolarisation is provoked by green and blue light, respectively for the H2 and H3 cells. The responses of H4 cells still remain not well understood and are often confused with those of H1 cells (Ammermüller and Kolb, 1996).

In the carp retina, four types of horizontal cells have been identified. The H1, H2 and H3 horizontal cells are located close to the photoreceptor layer (external horizontal cells) and contact only cone photoreceptors. The rod horizontal cells, located more anterior that the external horizontal cells, contact only rod photoreceptors. H1 and rod horizontal cells have hyperpolarising monophasic responses to green, yellow and red light. Nonetheless, H1 cells have their maximum response for red light, whereas rod horizontal cells have it for green light. H2 cells have a biphasic response, hyperpolarising for green and yellow light and depolarizing for red light. Finally, H3 cells own a triphasic response with hyperpolarisation for red light and depolarisation for green and yellow light (Kaneko and Stuart, 1984).

1.1.3 Bipolar Cells

The bipolar cells serve as bridge for the flow of visual information from the photorecetors to the amacrine and retinal ganglion cells. Here, the dendrites of bipolar cells make synaptic contact at the OPL with the photoreceptors, from which they receive their input signal with glutamate as neurotransmitter. The transmission of the visual information through parallel channels begins already at these synapses. In mammals for instance, only one type of bipolar cell contact rod photoreceptors, whereas as much as eight different types of bipolar cell could contact one single cone photoreceptor (Wässle, 2004). At the other extreme of the bipolar cells, their axons contact amacrine and retinal ganglion cells, using also glutamate as neurotrasmitter for the further transmission of visual information.

The responses of bipolar cells are graded potentials, whose polarity and dynamics are defined by the type of glutamate receptors on their dendrites. In this sense, bipolar cells with excitatory glutamate receptors depolarise in dark and therefore, activate the Off-pathway, which allows the detection of dark images against a bright background. In contrast, bipolar cells that have inhibitory glutamate receptors depolarise with light and this way, activate the On-pathway, which in turn allows the detection of bright images on a dark background. As mentioned before, the type of glutamate receptors in the dendrites of bipolar cells also effects the dynamics of their responses, allowing that bipolar cells respond either to fast or slow changes of the visual scene. This decomposition of the temporal aspects of visual information in different pathways accounts for the claim that the processing of temporal information of visual scenes starts already at the first synapse in the retina (DeVries, 2000).

Bipolar cells have receptive fields that are organised in a concentric antagonistic manner. Here, the receptive field centre of the bipolar cells seems to be produced by the input of the photoreceptors, whereas the surround appears to be mediated by the indirect action of horizontal cells (Kaneko, 1979). This organisation of the bipolar cells' receptive fields contributes in the transmission of information about the contrast of a visual scene.

At least twelve types of bipolar cells have been identified in the turtle retina. Here, the classification of these cells has been made according to the stratification patterns of their axons within the five strata of the inner plexiform layer (IPL). Furthermore, the responses evoked by the bipolar cells, either On- or Off-centre, can be sometimes inferred from the type of connections that they make with photoreptors and their axonal terminations within the IPL. In this sense, it has been observed that Off-centre bipolar cells have axons in the two most distal strata of the IPL (B4 and B5), as well as in the

three most proximal strata (B3, B9 and B10). In contrast, On-centre bipolar cells have axons exclusively in the three most proximal strata of the IPL (B1, B2, B6 and B7). Finally, it has been found that all bipolar cells in the turtle have an antagonistic receptive field organization. Here, the centre and surround of these receptive fields receive input primarily from red-sensitive cones and in a less number, from green-sensitive cones (Ammermüller and Kolb, 1996).

As mentioned before, two morphological types of bipolar cells have been identified in the fish retina (large M and small C cells). The responses of these cells can, as in the case the turtle retina, be inferred by the location of their axonal terminations within the five strata of the IPL. In this sense, Off-centre M and C cells have axons in the two most distal strata of the IPL, whereas On-centre M cells have axons in the two most proximal strata of the IPL, and C cells have axons only in the most proximal stratum (Famiglietti Jr et al., 1977).

1.1.4   Amacrine Cells

Back to the studies carried out in the retina by Ramón y Cajal (1892), he found some cells in the IPL that seemed to lack an axon. Due to this property, these cells were named amacrine cells. However, nowadays it is known that some types of amacrine cells own an axon like process and moreover, that some of these cells are able to produce action potentials. Based on morphological studies, many types of amacrine cells have been identified. Nonetheless, the function that these cells have in the processing of visual information is still a main research focus.

Amacrine cells act like intermediary cells in the pathway from bipolar to ganglion cells by making synaptic contacts with both types of retinal cells within the IPL. In fish (Tachibana and Kaneko, 1988) and rat retina (Hartveit, 1999), it has been found that between amacrine and bipolar cells, there are reciprocal contacts that allow the amacrine cells to receive input from bipolar cells and at the same time, feedback onto them, broadening in this way the operating range of bipolar cells. In these reciprocal synapses, it has been proposed that bipolar cells signal amacrine cells using glutamate as neurotransmitter, whereas the signalling from amacrine to bipolar cells is done using GABA as neurotransmitter (Dong and Werblin, 1998). Among the functions of the amarine cells, it has been proposed that for the rod pathway, the interaction in the IPL of bipolar, amacrine and retinal ganglion cells works as a mechanism to collect and amplify scattered light for twilight and night vision (Kolb, 2003). Moreover, it has been found that the underlying mechanism for the direction selectivity in the responses of some retinal

ganglion cells relies in the inhibition action of certain types of amacrine cells (Taylor and Vaney, 2003). Finally, it has been also proposed that amacrine cells introduce a temporal domain to the visual information transmitted to the retinal ganglion cells for the encoding of contrast (Dong and Werblin, 1998).

Based on the diameter of the dendritic extension of amacrine cells, they have been classified into narrow-field (30-150 μm), small-field (150-300 μm), medium-field (300-500 μm) and wide-field (<500 μm) amacrine cells (Kolb et al., 1981). Additionally, amacrine cells have also been classified based on the location of their dendrites within the strata of the IPL. Here, at least four different categories have arisen; broadly stratified, bistratified, monostratified and diffuse amacrine cells. The functional relevance of the stratified patterns of the amacrine cells lies on the fact that it has been observed that Off-amacrine cells confine their dendrites to the sublamina a of the IPL (strata 1 and 2), whereas ON-amacrine cells do it for the sublamina b (strata 3, 4 and 5). In contrast, On-Off amacrine cells have shown to have dendrites in both sublaminae (Kaneko, 1979).

The physiological properties of amacrine cells have allowed the identification and classification of these cells into different groups. Within the framework of this study, only some of the representative amacrine cells are going to be briefly described. The AII amacrine cell is probably the most studied amacrine cell in the vertebrate retina. Moreover, this amacrine cell is the most common type in the mammalian retina. In contrast to most of the amacrine cells, which are GABAergic, AII amacrine cells are glycinergic. Due to the fact that rod bipolar cells do not have direct synaptic contact with retinal ganglion cells, these narrow-field (30-70 μm) cells play an important role in the function of the rod-pathway. Here, AII cells receive input from rod bipolar cells at the lower sublamina b of the IPL, and they subsequently signal retinal ganglion cells by different postsynaptic contacts. In this way, most of the postsynaptic contacts of AII cells are located at the sublamina a of the IPL, where they make connections with Off-centre cone bipolar and Off-centre retinal ganglion cells. Additionally, AII cells signal On-centre cone bipolar cells via gap juntions in the sublamina b of the IPL and these cells in turn, feedforward On-centre retinal ganglion cells. By the use of both circuits mentioned before, the AII amacrine cells allow that the rod signal reaches the On- and OFF-centre retinal ganglion cells (Kolb, 1979, 1997). Another amacrine cell involved in the rod pathway is the A17 cell. Due to the wide-field nature of this amacrine cell, it receives inputs from several thousands of rod bipolar cells. Moreover, A17 cells make reciprocal synapses with rod bipolar cells and by this mechanism, it is though that they are able to amplify the rod signal for low light intensities (Kolb, 1997).

An example of an amacrine cell that contributes to the cone pathway is the A8 cell. Although these cells receive some input from On-centre bipolar cells, most of their input comes from Off-centre cone bipolar cells in the sublaminae a and b of the IPL. A8 cells are glycinergic, have transient Off-responses and contact Off-centre retinal ganglion cells in the sublamina a of the IPL (Kolb, 1997).

A special type of amacrine cells are the starburst cells, which name is derived from their fireworks exploding appearance. Starburst are medium-field (200-800 μm) amacrine cells that use acetylcholine (ACh) and GABA as excitatory and inhibitory neurotransmitters, respectively (Vaney and Young, 1988). These cells receive input from Off-centre cone bipolar cells and AII cells, and are organised in the IPL in a vertically two-cell-mirror-symmetric arrangement. Here, it has been observed that besides retinal ganglion cells, this type of amacrine cell is also able to produce action potentials (Bloomfield, 1992). Furthermore, it has been found that starburst amacrine cells respond more strongly to images moving away from their soma than to images moving towards it (Taylor and Vaney, 2003). Because starburst cells are though to make selective connections with On-Off and On-retinal ganglion cells in the IPL (Famiglietti, 1987, 1991; Briggman et al., 2011), it has been proposed that the distinguished responses of starburst cells to a moving image are responsible for the direction selectivity of some retinal ganglion cells in rabbits and turtles (Kolb, 1997).

In the turtle retina, 45 types of amacrine cells have been found based on morphological and physiological studies. Based on the responses of amacrine cells, they have been classified in four groups; On-sustained, Off-sustained, On-transient and Off-transient. In this sense, some relations between the morphology and physiology of the amacrine cells have been found. For example, both types of sustained amacrine cells seem to be monostratified cells that follow the general bisublamination rule in the IPL, i.e., Off-cells are found in the sublamina a, whereas On-cells are found in the sublamina b. Furthermore, monostratified amacrine cells with transient responses and those with direction selectivity are found in the middle of the IPL. Finally, the amacrine cells that have been proposed to mediate the direction selectivity of retinal ganglion cells are the A15, A5, A9 and A6 cells, from which A15, A5 and A9 are thought to use acetylcholine as neurotransmitter (Ammermüller and Kolb, 1996).

Based on the responses of amacrine cells in the carp retina, they have been classified in sustained and On-Off transient amacrine cells. Here, as in the case of the turtle retina, there are some relationships between their morphology and physiology. In this sense, it has been found that sustained amacrine cells are monostritified, whereas the transient amacrine cells are ei-

ther bistratified or multistratified. Furthermore, sustained On-amacrine cells are found in the strata 4 of the IPL, they have a high degree of spatial summation and red light elicits their maximum response. In contrast, although Off-amacrine cells are rarely found in the carp retina, their dendrites seem to be confined to the sublamina a of the IPL. Finally, On-Off amacrine cells have dendrites in both sublaminae (Famiglietti Jr et al., 1977).

1.1.5 Retinal Ganglion Cells

The retinal ganglion cells are the last stage in the processing of visual information at the retina. These cells collect all the visual information that has been pre-processed by the vertical (i.e., photoreceptor and bipolar cells) and horizontal (i.e., horizontal and amacrine cells) pathways in the retina. Furthermore, the axons of the retinal ganglion cells are organised in bundles that build the optical nerve, which in turn contacts the brain. In turn, retinal ganglion cells receive their input from bipolar and/or amacrine cells and subsequently, they transmit the visual information to the brain in the form of action potentials. In vertebrates, retinal ganglion cells have long been classified based on their morphology (Ramón y Cajal, 1894). Nonetheless, further studies on the primate (e.g., Polyak (1941)) and cat retina (e.g., Boycott and Wässle (1974)) have made it possible to find associations between the morphology and physiology of these cells.

In the cat retina, as well as in some other vertebrates like monkeys, frogs and rabbits, it has been found that almost all retinal ganglion cells have receptive fields that are organised in a concentric manner, having a centre with light responses of certain polarity, and an antagonistic surround (Kuffler, 1953; Hubel and Wiesel, 1960; Barlow, 1953; Barlow et al., 1964). Moreover, from the first studies in cat retina, it was found that some cells showed responses with direction selectivity (Stone and Fabian, 1966). In Enroth-Cugell and Robson (1966), the authors of the study were able to classify the retinal ganglion cells of the cat in two different classes based on their responses. In this sense, X-cells were found to have sustained responses to light stimuli, whereas Y-cells showed transient responses. Moreover, the same study proposed a Gaussian model for the centre and surround of the retinal ganglion cells' receptive fields. Here, it was found that the Gaussians describing the centre and surround responses of the X-cells summed almost linearly allowing therefore, the cancellation of them when each half of the receptive field was stimulated with complementary light intensities. In contrast, Y-cells showed always responses to the light stimulus independently of its spatial phase. Therefore, it was proposed that these cells do not sum linearly the signals coming from the different areas of their receptive fields. Due to this non-

linear summation, Y-cells are sensitive to small stimulus movements within and far away from their receptive field centre. Additionally, the signals from the Y-cells are the first to arrive to the brain and therefore, it is thought that these cells are involved in turning on visual attention (Wässle, 2004). Moreover, it has proposed that in vertebrates, Y-cells could be involved in the processing of motion direction in higher brain areas (Demb et al., 2001). Further studies (Stone and Hoffman, 1972; Stone and Fukuda, 1974) introduced a new type of retinal ganglion cell; the W-cells. These cells showed differences with the X- and Y-cells in their conduction velocity and receptive field properties.

In a study by Boycott and Wässle (1974), the authors classified the retinal ganglion cells based on the relationship between the size of their dendritic field and the size of their soma. In this sense, the cells were grouped in four categories; alpha- (α), beta- (β), gamma- (γ) and delta- (δ) cells, being the latter class a subtype of the γ-cells. Now it is know that α-cells constitute approximately 3% of all retinal ganglion cells in the cat and it is thought that parasol cells in the primate retina are their counterpart. In contrast, β-cells constitute almost 50% of all retinal ganglion cells in cat and are thought to be the counterpart of the midget ganglion cells in the primate retina, where they account for 70% to 80% of all retinal ganglion cells. Because of the high density and small dendritic field of β-cells, they have been proposed to account for the acuity system of mammals (Wässle, 2004). In addition to the morphological classification of the retinal ganglion cells, Boycott and Wässle (1974) proposed a relationship between the morphological cell classes and the physiological cell classes described in Enroth-Cugell and Robson (1966). Thereby, the β-cells were suggested as the counterpart of X-cells, the α-cells the counterpart of Y-cells and finally, the γ-cells as the counterpart of the W-cells.

Regarding the distribution of the retinal ganglion cells in the retina, it has been found in that each type of cell tiles the retina with an overlap depending on the cell type Wässle (2004). In the mammalian retina, the dendrites of α-cells have a low overlap, whereas the dendrites of β-cells have a high overlap. Furthermore, the size of the dendritic field of α- and β-cells seems to be proportional to their eccentricity (Boycott and Wässle, 1974). Retinal ganglion cells, as in the case of bipolar cells, have different stratification patterns depending on the polarity of their light responses. Here, Off-α retinal ganglion cells have dendrite arborations in the sublamina a of the IPL, whereas On-α cells have them in the sublamina b. Moreover, direction selective cells have dendrites in both sublaminae (Nelson et al., 1978; Wässle, 2004). The tiling of the retina by the different types of retinal ganglion cells, together with their differentiated stratification patterns within

the IPL, have been proposed to allow the retinal ganglion cells to transmit different features of the visual environment through parallel pathways (Peichl and Wässle, 1983; Wässle, 2004).

In the turtle retina, Granda and Fulbrook (1989) classified the retinal ganglion cells based on their responsiveness to certain features of the visual stimulus and this way, suggested eight groups of retinal ganglion cells; simple, On-sustained, annular, wavelength-sensitive, direction selective, bar-shaped, large field, and velocity. Here, direction selective cells comprised approximately 40% of the sample of recorded retinal ganglion cells and they were found to have On-, Off- and On-Off responses. Later studies (Ammermüller and Kolb, 1995; Ammermüller et al., 1995; Ammermüller and Kolb, 1996) have found 27 types of ganglion cells based on morphological analyses. Furthermore, as in the case of the amacrine cells, the retinal ganglion cells could be classified in four physiological groups; On-sustained, Off-sustained, On-transient and Off-transient retinal ganglion cells. In this sense, monostratified sustained retinal ganglion cells follow the bisublaminate stratification rule, whereas monostratified transient cells have their dendrites at stratum 3. In the turtle, G18, G19, G24, G15, G14a and G20 retinal ganglion cells have been found to be direction selective. Here, all of these cells have at least one branch of their dendrites in stratum 1 of the IPL, and they can be mono- (G18 and G20), bi- or multistratified.

In fish, Off- and On-centre retinal ganglion cells seem to obey the bisublamite stratification rule (Kaneko, 1979). Here, Off-centre retinal ganglion cells seem to have large cell bodies and have their maximum response to red light. In contrast, On-centre retinal ganglion cells have small cell bodies and are rarely found (Famiglietti Jr et al., 1977). Moreover, as in other animal species, it has been found that retinal ganglion cells in fish have centre-surround antagonistic receptive fields (Kaneko, 1971).

As mentioned before, in contrast to all the neurons in the retina, retinal ganglion cells and some types of amacrine cells are the only cells capable of generating action potentials. Here, the spike trains generated by the former cells are the only source of information about the visual environment for the brain. Due to the fact that retinal ganglion cells have shown to have selective responses for certain features of visual scenes, it has been proposed that these cells decompose the visual image in different parallel neuronal images that are encoded by different features of the generated spike trains. The following sections will be dedicated to the introduction of the coding hypotheses based on the activity of retinal ganglion cells.

1.2   Neural Coding Strategies

Since the first recordings of neural activity in amphibians and mammals by Adrian and Zotterman (1926a,b), it was observed that the responses of stretch receptors in muscles varied their characteristics depending on the intensity of the applied stimulus. In further studies, Adrian and Matthews (1927, 1928) were able to record light responses of optical nerve fibres of the eel. The findings in the optical nerve fibres confirmed the results found previously in the muscle nerve fibres. Here, the intensity and frequency of the optical nerve fibres' activity depend on the magnitude of the applied stimulus. Moreover, Adrian and Matthews (1927, 1928) also suggested that the interaction between neurons could account for the transmission of sensory information.

In a later study by Hartline (1938), the author was able to record the action potentials of single fibres of the frog's optical nerve. Here, although some of the recorded retinal ganglion cells showed similar responses to the same stimulus, it was observed that not all of them elicited the same number of action potentials in response to the same stimulus. Moreover, the author observed that in addition to the variability of the response features among neurons, the number of action potentials and the temporal structure of the elicited spike trains changed in the course of the application of the light stimulus. In this way, based on the properties of the responses of retinal ganglion cells, Hartline found a relationship between these and the changes in the light intensity of the stimulus, suggesting in this way, On-, Off- and On-Off response classes.

Nowadays, much has been learned about how visual sensory information is processed and transmitted within and out of the retina. In the case of the latter process, different approaches have been tested to find which features of the spike trains are important for the transmission of visual information to the brain. The most common and first approach was to take the number of spikes within a time-window of a certain width, and relate this spike rate to the presented stimulus. This approach however, has been suggested to be unable to account for the encoding of all the features of visual stimuli. Therefore, in recent years the relevance of the temporal structure of the spike trains for the encoding of visual information has been assessed. One argument supporting this approach is that for the fast processing of sensory information, the time of occurrence of the first spikes after stimulus changes would convey information in a faster way than the count of spikes in long time windows. Furthermore, certain types of neurons could act as coincidence detectors, whose output will depend more on the absolute time of arrival of input spikes, rather than in the number of incoming spikes within a certain

period of time. Finally, another argument supporting the relevance of the temporal structure of spike trains for the encoding of information considers the interspike time intervals. Here, the effect of a spike in a post-synaptic neuron can depend significantly on the period of time since the occurrence of earlier spikes (Victor and Purpura, 1997).

1.2.1 Rate Code

As mentioned before, since the first experiments to record the activity of neurons succeeded, the rate code hypothesis was proposed as the first approach to understand how the activity of neurons encodes information about sensory stimuli. The basic idea behind this hypothesis is that the number of spikes elicited by a neuron, or a population of neurons in a defined period of time, would carry information about features of a given stimulus. So far, three different approaches to average the number of elicited spikes have been proposed for this coding hypothesis; average of spikes in time, average of spikes in response to different repetitions of the same stimulus and average of the spikes elicited by a population of neurons. These approaches are not mutually exclusive and therefore, depending on the matter subject to study, they can be combined to calculate the mean firing rate.

Spike average over time

The spike average over time *(F)* is usually expressed in spikes per second or Hertz, and it is obtained basically by counting the number of spikes *(S)* in a period of time *(T)* and then, dividing the result by this period of time (Equation 1.1).

$$F(T) = \frac{S(T)}{T} \tag{1.1}$$

In the case of the applied force in Adrian and Zotterman (1926a,b), the spike average over time proves to account for the transmission of information about features of constant or low frequency varying stimulus. Nonetheless, the major drawback of this approach is that for the detection of fast stimulus changes, usually short presentation times are available to living organisms. Therefore, there should be a more efficient mechanism to allow the fast detection and classification of stimulus changes, than averaging spikes over time. For instance, it has been found that the house fly can perform corrective flying manoeuvres in response to a visual stimulus within 40 ms (Land and Collet, 1974). In this direction, humans have shown to be capable of detecting visual stimuli that have been presented for 20 ms (Thorpe et al., 1996).

Furthermore, neurons in the temporal lobe have showed responses 100 ms after visual stimulus presentation. Here, the minimum number of synapses between the photoreceptors and the face selective neurons in the temporal lobe has been suggested to be ten. Therefore, a maximum of ~10 ms per synapse are available to integrate the spike firing rate, making very unlikely that the neurons use the spike average over time for encoding tasks (Thorpe and Imbert, 1989).

Spike average over trials

The spike average over several repetitions (K) of the same stimulus (also known as Peri-Stimulus-Time histogram or PSTH) is obtained by calculating a histogram of the spike frequency elicited by a neuron, where the total period (T) of stimulus presentation is divided in time bins (Δt). The results for each bin are then divided by the length of the time bins and the number of repetitions, see Equation 1.2.

$$F(t) = \frac{1}{\Delta t} \frac{S(t; t + \Delta t)}{K} \tag{1.2}$$

The PSTH allows the investigator to get some insight about the time variations of neural responses to a stimulus. Nevertheless, this form of coding sensory information is rather unlikely to occur in nature due to the fact that living organisms usually do not have a second chance for the detection of, e.g., a threatening condition.

Population spike average

The last approach for the rate code is to average the spikes across a population of neurons. The rationale behind this approach is that many neurons elicit similar responses to the same stimulus and additionally, make further synapses with defined populations of neurons, e.g., the M and P ganglion cells in primate, which project into the magnocellular and parvocellular layers of the geniculate, respectively. In this sense, it has been proposed that to overcome the rather irregular spiking pattern of single neurons for the transmission of neural information, the activity of an homologous neuron population would be able to vary fast enough to follow fast changes of stimulus conditions (Knight, 1972; van Vreeswijk and Sompolinsky, 1996; Gerstner, 2000). The mean firing rate of a population of N cells can be calculated by counting the spikes (S_{Pop}) that this population of neurons fire in the time $t + \Delta t$, and dividing the result by the number of neurons N and the time

interval Δt, see Equation 1.3.

$$F(t) = \frac{1}{\Delta t} \frac{S_{Pop}(t; t + \Delta t)}{N} \tag{1.3}$$

One drawback of this approach is that real neurons have always a certain degree of heterogeneity. For instance, it has been observed that each type of retinal ganglion cells tiles the retina. Here, although some overlap is observed in the receptive fields of retinal ganglion cells from same type, no sharing of the same receptive field for two cells of the same time will occur (Wässle, 2004). Therefore, for certain tasks such as the detection of small moving objects, the spatial summation over a population of cells could be counterproductive for spatial resolution.

1.2.2 Temporal Code

Additional to the spike firing rate of neurons, it has also been proposed that the encoding of additional sensory information could be achieved by the temporal structure of neuronal responses. Here, it has been suggested that temporal patterns in neuronal activity are highly specific symbols. In turn, these symbols would encode information by selectively eliciting the response of neurons that are able to decode them (Strehler and Lestienne, 1986). The proposal of a temporal code mechanism can be traced back to the time when Hartline (1938) recorded the responses of retinal ganglion cells of frogs to a light stimulus. Here, the author observed that the responses of distinct retinal ganglion cells exhibited different temporal patterns to the same stimulus. Moreover, Hartline (1938) observed that even the responses of the same retinal ganglion cell exhibited temporal differences in the course of the stimulus presentation. Thereby, the temporal structure of neuronal responses has shown to play a role in the encoding of different sensory information. In cats for instance, cortical neurons seem to use the temporal spike patterns of single cells to perform sound localisation (Middlebrooks et al., 1994), whereas in humans, it has been found that the relative timing of the first spikes of an ensemble of primary sensory neurons carries information about features of tactile stimuli (Johansson and Birznieks, 2004).

Different studies have reported that responses of retinal ganglion cells in turtles, salamanders, rabbits, cats and primates exhibit precise temporal patterns with small time variations across repetitions of the same stimulus (Greschner et al., 2006; Berry et al., 1997; Kara et al., 2000; Uzzell and Chichilnisky, 2004; Gollisch and Meister, 2008). These observations suggest on one hand, that the temporal structure of neuronal responses could be a consequence of the stimulus dynamics. However, on the other hand, the

temporal structure could also arise as a consequence of the intrinsic properties of the neurons (e.g., stimulus selectivity, refractory period). In this direction, the finding of precise temporal patterns in retinal ganglion cell responses do not necessarily imply that these neurons utilise a temporal code to encode visual information. Nevertheless, based on the observations made in other sensory systems, it is plausible that the visual system also makes use of a temporal code mechanism. With this in mind, the role of the temporal structure of neuronal responses for the encoding of sensory stimuli has been mainly analysed considering the following three aspects; latency, interspike time interval and spike timing.

Latency

Latency can be generally defined as the time difference between two events. However, when considered as a neural coding mechanism, this difference in time can be regarded as an absolute or a relative latency. Absolute latency is defined as the time delay between stimulus onset and the first spike of the elicited neuronal responses. In contrast, relative latency can be described as the time difference between e.g., the responses of a population of neurons and the first spike of the elicited neuronal responses (Kretschmer et al., 2012). Moreover, the relative latency can also be the time difference between the first elicited spikes from two neurons (Thomson and Kristan, 2006; Gollisch and Meister, 2008). First spike latency has been proposed by Thorpe (1990), amongst others, as a mechanism to encode sensory stimulus information. This proposal is based on the fact that living organisms often need to detect stimuli or perform corrective motor actions in time periods comprising only a few milliseconds. Because in these short time periods neurons would not be able to fire many spikes, it has been proposed that the time of arrival of the first elicited spike should carry sensory information.

It has been found that the absolute spike latency conveys information about the location of sound sources in the auditory system of e.g., guinea pigs (Zohar et al., 2011). Moreover, it has been found that in bats, the absolute spike latency is a more plausible strategy than spike firing rate for echolocation (Fontaine and Peremans, 2009). In this direction, (Sestokas et al., 1991) found that the responses of X- and Y-cells in the retina, as well as in the lateral geniculate nucleus of cats show variable absolute latencies depending on the stimulus spatial frequency and contrast. Furthermore, years later (Gawne et al., 1996) found similar results in the responses of cortical neurons of monkeys to changes in stimulus contrast. Therefore, it has been suggested that the visual system could also use the absolute latency as coding mechanism.

The proposal of absolute latency as coding mechanism appears to be plausible if the time of stimulus onset is available to the nervous system. However, the nervous system has no direct access to this information. To cope with this problem, some studies have suggested different mechanism that could be used by the nervous system as reference points for response latency. For instance, this is the case of the theta rhythm of the electroencephalograms of freely moving rats. Here, the place cells in the hippocampus have shown to fire spikes at phases of the theta rhythm that were correlated with the spatial location of the animal (O'Keefe and Recce, 1993). In the primary cortex of cats, Eggermont (1998) found that local field potentials could be used as reference point for the relative latency in order to encode information about sound azimuth. Furthermore, in rabbits it has been found that the activity of several ganglion cell types are suppressed during a saccade (Roska and Werblin, 2003). These findings support the concept of a snapshot mechanisms in the visual system, in which the suppression of activity of certain cells could work as a reset to mark the beginning of the transmission of new visual information (Gollisch, 2009).

Additionally, it has been proposed that the relative latency could be determined based on the response onset of populations of neurons (Levick, 1973). However, the definition of the response onset is not straightforward and thus, several approaches have been developed to cope with this problem. For instance, one of the developed methods consist of a cumulative sum technique based on PSTH (Ellaway, 1978). Here, a complement to this technique by second order differences to identify the onset and offset of stimuli has been proposed by Falzett et al. (1985). Furthermore, Berényi et al. (2007) has proposed a double sliding-window technique, which involves the statistical comparisons between the probes contained in the sliding windows to detect stimulus onsets. Thereby, using modelled responses of neurons of the auditory system of cats, Chase and Young (2007) assessed the efficiency of the absolute and relative latency as coding mechanism. The authors found that the relative latency encoded slightly more information about sound location than the absolute latency. Here, the Chase and Young (2007) defined the relative latency with respect to stimuli onsets based on the activity of pseudopopulations of neurons. Additional studies in the turtle and archer fish retina have found found that information about velocity changes Cerquera et al. (2008) and the velocity Cerquera and Freund (2011); Kretschmer et al. (2012) of a moving pattern of dots is encoded by the relative latency of the responses of retinal ganglion cells.

The time delay between the first spikes of different neurons has also been tested as relative latency coding strategy. Here, Thomson and Kristan (2006) have found that based on the relative latency between the responses of pairs

of P cells in the leech, these cells can encode and decode information about touch location. Additional evidence for the same information encoding mechanism has been found in the auditory cortex of ferrets (Bizley et al., 2010). Here, the authors found that the relative latency across neurons in a population encoded information about the periodicity of auditory stimuli. Moreover, in the salamander retina, Gollisch and Meister (2008) have found that the relative latency in the responses of certain retinal ganglion cells encodes the spatial structure of briefly presented stimulus. Here, the authors found that this coding mechanism was robust to fluctuations in the absolute latency and was not affected by stimulus contrast.

Thorpe (1990) proposed an additional encoding mechanism that makes use of the firing sequence of the first spikes of neurons from a population. Here, the author suggested that this encoding mechanism could be used to allow the recognition of visual stimuli in shorts periods of time. In a subsequent study, Thorpe et al. (2001) named this mechanism the rank order code and provided, based on simulations, some evidence about the far greater efficiency of this mechanism for the encoding of information in comparison to the rate code. Some experimental evidence supporting this hypothesis has already been provided by (Johansson and Birznieks, 2004). Here, the authors found that in humans, the sequence of firing of the first spikes of an ensemble of primary sensory neurons carries information about features of tactile stimuli. Moreover, analysing the activity of M/T cells in frogs, (Junek et al., 2010) found that the first spike sequence of a population of M/T cells encode information about odour identity and concentration in a more reliable way than the spike firing rate.

Interspike time interval

The interspike time interval is defined as the time between two spikes. This temporal structure of spike trains has also been proposed to be involved in the encoding and transmission of sensory information. The proposal of interspike time intervals as an efficient encoding mechanism for sensory information dates back to the work of Lorente de Nó (1939), where based on his studies of the anatomical connectivity of the brain, he suggested that messages with different informational content could be transmitted by the time differences of spikes. Years later, Perkel et al. (1967) revisited the statistical techniques available at that time for the analysis of interspike time intervals of single spike trains. Furthermore, Strehler (1969) suggested that some synapses in neurons have a spatial configuration which would enable them to recognise certain presynaptic spike patterns allowing in this way, spatial summation in the postsynaptic neuron for the further generation of spikes. In this sense,

Strehler (1969) proposed at least two coordinated time intervals, which he called triplets, as the simplest spike patterns. For the definition of triplets, it was not necessary that the interspike time intervals were consecutive. With this in mind, Strehler (1969) proposed that triplets served as a multiplexing mechanism. In turn, this mechanism would allow the transmission of several '*pulse-train-coded*' symbols by a single axon in several time scales, where different triplets would be specific for different stimuli (refer to Lestienne and Strehler (1988) for a summary of this hypothesis).

Some evidence to support the interspike time interval coding hypothesis arrived years later, when Larson et al. (1986) found that some neurotransmitter receptors are sensitive to interspike time interval patterns. Furthermore, in Strehler and Lestienne (1986) and Lestienne and Strehler (1987), the authors found triplets that were stimulus specific in the recorded activity of visual cortex cells of the rhesus monkey. Here, the authors also found that these triplets could be decoded in later stages by spatial summation. Additional evidence was obtained years later by Abeles and Prut (1996). In this study the authors analysed the responses of frontal cortex neurons of monkeys when the animals were performing localisation and problem solving tasks. Here, Abeles and Prut (1996) found that there were some temporal patterns in the responses that consisted of three spikes. Furthermore, these patterns conveyed more specific information than all the spikes of a single unit.

The interspike time intervals have been suggested to provide an estimate of the spike firing rate (Kreuz et al., 2007). In this context, based on extracellular recorings of turtle retinal ganglion cells, Cerquera et al. (2008) and Cerquera and Freund (2011) tested if additional to the latency, the following interspike time intervals carried information about the motion velocity and velocity changes of a dot pattern. Although in these studies the authors found that the first spike latency, relative to response onset, encodes information about motion features of the pattern, a slight but significant enhancement of information is allowed by the following two interspike time intervals.

Spike timing

The precision with which spikes from a presynaptic neuron arrive to a postsynaptic neuron has also been proposed as a neural coding strategy (MacKay and McCulloch, 1952). Here, overlaps between the definitions of latency, interspike time interval and spike timing could arise. Nonetheless, spike timing is different to latency in the sense that it can consider more than one spike from the spike train. In contrast, the interspike time intervals distinguish them selves from the spike timing in the sense that spike trains could have

similar interspike time intervals that nonetheless, occur at different times. In this sense, one objection to the proposal of spike timing as a coding mechanism is the need for the precise measurement of spike arrival times (Bialek et al., 1991).

Based on the study of moderate complex synaptic circuits, MacKay and McCulloch (1952) have long proposed the hypothesis that the time precision with which a neuron fires spikes in response to stimuli is a more efficient mechanism to encode sensory information than the firing rate alone. Furthermore, MacKay and McCulloch (1952) proposed that neurons act as coincidence detectors, where only spikes with time intervals shorter than 0.15 ms would allow spatial summation in a postsynaptic neuron. In following years, some evidence supporting this hypothesis arose from models of brain cells. Thereby, Abeles (1982) tested the influence of synchronous and asynchronous presynaptic spikes for the generation of spikes in postsynaptic cells using a model of a cortical neuron. The author confirmed the hypothesis proposed by MacKay and McCulloch (1952) tha cortical neurons would act mainly as coincidence detectors rather than integrators. Therefore, Abeles (1982) proposed the temporal structure of the neural activity, and not the firing rate, as the appropriate encoding mechanism for higher cortical functions. Moreover, in a later study based on a model of a pyramidal neuron, Softky (1995) stated that some neurons could utilise fine temporal scales of presynaptic spike patterns to modulate their activity and in turn, transfer information in a more efficient way than a rate code could allow.

Some experimental evidence for the relevance of spike timing in the encoding and transmission of neuronal information arrived with the studies by Richmond et al. (1987, 1990). In these studies, the authors applied the principal component analysis to examine the responses of primary visual, as well as inferior temporal cortex neurons of monkeys to visual stimuli. Richmond et al. (1987, 1990) found that besides the firing rate of the responses, the temporal structure of the responses of neurons carried information about visual stimulus. Moreover, in a later study by Middlebrooks et al. (1994), they found that single auditory neurons in the cat encode information about the approximate location of sounds by the temporal timing of spikes. More recently, Reyes (2003) tested the transmission of neural information in a multilayer feedforward network of neurons in an *in vitro* slice preparation. In his study, he found that the firing rate was represented by a classical rate code in the initial layers, but switched to a synchrony-based code in the deeper layers suggesting thus, that spike synchrony was involved in propagating in a stable manner the rate signals to subsequent layers.

The synchronised and coordinated activity of neurons has also been proposed as information processing mechanism for different sensory systems

(Bair, 1999; Meister and Berry II, 1999; Shlens et al., 2009). For instance, it has been suggested that the synchronised activity of visual cortical neurons would serve to bind the distributed neuronal activity into unique representations (Engel et al., 1992). Furthermore, Middlebrooks et al. (1994) suggested that in the auditory cortex of cats, the coordinated activity of a population of neurons would allow the precise location of sound sources. Some experimental evidence supporting the role of the temporal structure of the activity of neurons for the encoding of information was found by Aronov et al. (2003) in the primate cortex of monkeys. In this study, the authors found that the temporal structure of pairs of neurons carried information about the spatial phase of a stationary visual stimulus.

1.2.3 Relevant Time Scale

From Sections 1.2.1 and 1.2.2, it can be observed that several hypotheses regarding either a rate code or a temporal code have been proposed to explain how sensory information is encoded, transmitted and processed by the activity of neurons. Furthermore, based on experimental data, all of the mentioned hypotheses have been found suitable to perform these tasks. Nevertheless, it is still not clear which properties of sensory information are encoded by which features of the neuronal activity.

The approach followed by Theunissen and Miller (1995) to explore suggested coding strategies, consisted on first proposing a definition for the rate and temporal codes, based on the properties of the information to be encoded by these mechanisms. The authors stated that the stimulus features to be encoded defined the parameters that are involved in the rate and temporal codes, like for instance, the length of the encoding window. Theunissen and Miller (1995) suggested that the length of the encoding window should be long enough to allow good acuity, and short enough to decrease the reaction time. Additionally, in order to fulfil the Nyquist theorem, the length of the encoding window should correspond to at least the double of the frequency of the stimulus properties that are going to be encoded. With this in mind, Theunissen and Miller (1995) stated that if information about a constant stimulus parameter is conveyed by the number of fired spikes, or if the frequency components of a stimulus signal are correlated with the same or lower frequency patterns of spike firing, then a rate code is involved in the information encoding process. In contrast, if higher-order moments of the neuronal responses are involved in the encoding of constant stimulus or dynamic stimulus features, then a temporal code is the encoding mechanism. Based on these definitions and on several studies in the mammalian visual system, Theunissen and Miller (1995) suggested that a significant amount

of information is encoded in the temporal spike patterns of populations of neurons, and that the nature of the encoded information by these patterns is different from that encoded by the spike firing rate.

Around the same time, Shadlen and Newsome (1994) on the rate code side, and Softky and Koch (1993) on the temporal code side, held one noteworthy discussion about which coding strategy is the most suitable for encoding neuronal information. Based on recordings on the V1 and MT area of awake monkeys, and on compartmental models that tried to explain the variability of the recorded neuronal responses (Softky and Koch, 1993; Softky, 1994, 1995), the authors alleged that the variability in the responses of the recorded cortical neurons could only be reproduced by the models, if a strong synchronization of the synaptic inputs was given. Conversely, the variability of the responses was absent for modelled neurons that temporally integrated their synaptic inputs. In turn, Shadlen and Newsome (1994) proposed a balanced inhibition-excitation integrate-and-fire model. In their study, the authors found that integrate-and-fire models that lacked the inhibition consideration were unable to reproduce the variability observed in the responses of cortical neurons. However, once inhibition was added to the model, the variability in the responses of the modelled neurons was similar to that of the recorded cortical neurons. Finally, although Shadlen and Newsome (1995) offered evidence to support their proposal about a noisy and redundant rate code in the cortex, they also admitted that albeit missing evidence, the efficient temporal code proposed by Softky and Koch (1993) could also be suitable. This idea was reinforced by a review from Ferster and Spruston (1995), which pointed out the possibility that in hippocampal place cells, a temporal code could be simultaneously superimposed on a rate code. On this line of investigation, newer studies have provided some evidence to the claim that both encoding mechanism are present in the cortex. For instance, Nicolelis et al. (1998) found that populations of broadly tuned neurons located in different areas of the somatosensory cortex of monkeys could encode the location of tactile stimulus by using simultaneously a firing rate and a temporal code. Moreover, Reyes (2003) found that for *in vivo* slide preparations of rat's cortex, the synchrony did not encode temporally precise inputs, but instead, it ensured that rate signals propagated in a stable manner across cortex layers.

The possibility that different coding strategies serve to encode different sensory information was addressed by Gautrais and Thorpe (1998). In this study the authors pointed out the relevance and convenience for the nervous system to use the spike firing rate as encoding mechanism for specific situations, specially for stimuli with constant or slow changing features. For example, information about the force that has to be developed by a muscle

can be encoded by a rate code, which would allow, through the number of fired spikes, the regulation of neurotransmitter release. However, Gautrais and Thorpe (1998) also proposed that for fast changing stimuli or when the processing of information has to be performed rapidly, other coding strategies, like the temporal code, could be better suited. Furthermore, in the review by Oram et al. (2002), the authors suggest that neuronal activity could encode different features of a given stimulus using different temporal resolutions. As first, they suggested that information of the overall stimulus class could be encoded by the spike firing rate over time windows of several milliseconds. Moreover, they proposed that details of the stimulus could be encoded by intermediate time scales of the neuronal responses and finally, that information about, e.g., the degree of attention to a presented stimulus could be encoded by fine time scales. In the case of the retina, although the spike firing rate of the activity of retinal ganglion cells convey information about visual stimuli, it has been suggested that the temporal structure of the responses would allow to enhance the encoding of visual information (Berry et al., 1997; Meister and Berry II, 1999; Van Rullen and Thorpe, 2001; Jacobs et al., 2009).

1.2.4   Joint Activity Coding Hypotheses

The question of how the visual information about the environment is encoded by the joint activity of retinal ganglion cells is still an ongoing debate. For instance, it has been proposed that the correct interpretation of spike firing synchrony of neighbouring retinal ganglion cells by the brain would allow a higher spatial resolution of the visual scene (Meister and Berry II, 1999). Here, the joint activity of neurons would allow the encoding of information of one stimulus feature. Nonetheless, different time scales of the individual responses of the neurons in the population could encode different features of a stimulus (Theunissen and Miller, 1995; Gautrais and Thorpe, 1998; Oram et al., 2002). Thereby, it has been proposed on one hand, that retinal ganglion cells are non-redundant or mostly independent encoders of information (Fernandez et al., 2000; Nirenberg et al., 2001) and on the other hand, that the activity of retinal ganglion cells is repetitive and redundant (Puchalla et al., 2005).

In this direction, it has been found that the joint activity of neurons allows to encode more sensory information, than the activity of single neurons. For instance, Warland et al. (1997) tested if the activity of small populations of retinal ganglion cells in the salamander retina could encode the light intensity of a stimulus. In their study, it was found that only when cells with different response properties were considered, i.e., On- and Off-cells, the estimation

of light intensity allowed by the population of neurons was better than the one yielded by the activity of single cells. Furthermore, they observed that the information encoded by the joint activity of one On- and one Off-cell was equivalent to the sum of the information encoded by the activity of each individual cell. Hence, this finding suggested that the retinal ganglion cells encoded independently information about different stimulus properties. Similar results were found by Aronov et al. (2003) when the authors analysed the responses of pairs of neurons in the V1 area of monkeys. Here, they found that the combined activity of similar cells slightly enhanced the encoded information about the spatial phase of a stationary visual stimulus. However, the combined activity of cells with different response properties yielded a lower redundancy index.

Based on the responses of turtle retinal ganglion cells, Fernandez et al. (2000) tested if the spike firing rate, latency and first interspike time interval carried information about the wavelength and light intensity of a stimulus. They found that the estimation of wavelength and light intensity based on the activity of a population of cells outperformed the estimation allowed by the activity of single retinal ganglion cells. Moreover, a later study by Greschner et al. (2006) tested if the activity of small populations of turtle retinal ganglion cells encoded information about light intensity changes. For the analysis, the authors considered different features of the transients period of the retinal ganglion cell responses, e.g., spike count, latency and second interspike time interval. Greschner et al. (2006) found that although all of the considered cells were of the On-Off type, the estimation performance increased for larger population sizes.

In this direction, besides testing the relevance of the spike firing rate and the temporal structure of neuronal responses for the encoding of information about features of visual stimuli, one of the aims of this study is also to test if the joint activity of retinal ganglion cells would enhance information encoding. Therefore, three different joint activity coding hypotheses were tested; Pooled Population, Labelled Line and Functional Group (see Figure 2.6).

Pooled Population

From the first integrate-and-fire model proposed by Lapicque (1907), it was suggested that the membrane of a neuron integrates its synaptic inputs towards a threshold and once this threshold is reached, the neuron will generate an action potential and reset the membrane potential. For this mechanism and considering the number of interconnections among neurons, it is possible that the dendrites of single neurons pool the responses of many individual neurons to further transmit sensory information by the generation of action

potentials. This is the rationale behind the Pooled Population hypothesis. Here, it is assumed that all the activity of neurons in a population have equal weight and thus, the knowledge of the neuron of origin of each spike is irrelevant for the encoding of sensory information. This hypothesis was first proposed by Adrian and Zotterman (1926a). In this study, the authors stated that due to the irregular interspike time intervals of single neuron activity, an instantaneous estimate of spike rate can only emerge from the pooled responses of many individual neurons. Although the assumption of equally weighted activity may appear unrealistic, it has shown to be helpful to explore the fast propagation of fire rates in layered networks of noisy neurons (van Rossum and Turrigiano, 2002).

Labelled Line

Since the times of the proposal of a '*law of specific nerve energies*' made by Müller (1826), it was investigated how the information about different sensory inputs allow the perception of different sensations. This idea evolved into the proposal of a Labelled Line coding, with which it was tried to explain the perception of different stimulus properties within each sense, e.g., in vision, the perception of different colours of light. The Labelled Line coding states that different parts of a sensory area are sensitive to defined stimulus properties and that in turn, the nature of perception is defined by the pathway over which the sensory information is carried. This coding mechanism was explored by von Helmholtz (1863) in his '*place theory of pitchperception*' hypothesis. Here, the author suggested that the location of the maximum vibration of the basilar membrane in the cochlea, defined the group of auditory nerve fibres that were maximally excited and this in turn, determined the subjective pitch. Evidence to support the Labelled Line coding strategy was found in the late XIX century in the skin surface, where different spots showed to be selectively sensitive to either pain, touch, cool and warm (for a Review see Norrsell et al. (1999)). Nevertheless, it was not until years later that the hypothesis of Helmholtz was confirmed by von Békésy and Wever (1960).

In contrast to the Pooled Population hypothesis, the Labelled Line hypothesis proposes that the knowledge of the neuron of origin of each spike is relevant for stimulus encoding. Here, based on the selective responses of neurons, their differentiated activity would allow to encode in parallel different stimulus properties. In this direction, (Buck, 2004) have found that different odourants are detected by the combined activity of odour receptors. However, the activity of each odour receptor serves as individual component for the encoding of these odourants. Based on the same principles as in the

olfactory system, the Labelled Line hypothesis has been also proposed for the encoding of information about taste (Lemon and Katz, 2007). Moreover, the Labelled Line coding can be found in the retina of humans and monkeys. Here, in the fovea region, the midget cell pathway involve one-to-one connections between cone photoreceptors and midget bipolar cells, as well as between midget bipolar cells and midget retinal ganglion cells (Wässle, 2004).

Functional Group

The last hypothesis explored in this study, Functional Group, is a combination of both previous hypotheses. This hypothesis states that for the encoding of stimulus features, the knowledge about the type of cell that fires each spike, rather than the exact neuron, has a high relevance. The rationale behind this hypothesis is that some neurons elicit similar responses to the same stimulus properties and additionally, they make further selective synapses with the same populations of neurons. Thus, (Gerstner and Kistler, 2002) have proposed that under this hypothesis, the proportion of active neurons in the presynaptic population would be the relevant feature for the processing of neural information. Furthermore, it has been suggested that the combined activity of a population of homologous neurons could be able to follow fast changes of stimulus conditions (Knight, 1972; van Vreeswijk and Sompolinsky, 1996; Gerstner, 2000).

It seems plausible that the Functional Group coding can be used by the visual system. This suggestion is supported by the fact that the visual information that the retina sends to the brain is decomposed in parallel pathways (Warland et al., 1997; Schiller, 2010). One example of these pathways are the M and P ganglion cells in primate, which project into the magnocellular and parvocellular layers of the geniculate. Additionally, it has been found that cells with similar physiological functions are organised in vertical columns in the primary visual cortex of cats and monkeys (Hubel and Wiesel, 1962, 1977). Furthermore, along the processing stages in cortical areas of mammals, ith has been found that there is extensive interaction across different functional areas (Engel et al., 1992; Singer and Gray, 1995).

Population Coding and Ensemble Coding

Sections 1.2.1 and 1.2.2 revisited some of the hypotheses on how sensory information can be encoded by the spike firing rate and the temporal structure of neuronal activity. These two response properties are not only confined to

the activity of single neurons, but can also be extended to the activity of populations of neurons. Therefore, Theunissen and Miller (1995) and Lestienne (2001) proposed two rigorous definitions to describe how the joint activity of neurons could encode sensory information; population coding and ensemble coding.

Lestienne (2001) defined the *population coding* as a mechanism where the encoding of information is based on the spike firing rate of a population of neurons. Here, each neuron contributes to the population in the proportion of its spike firing rate. In contrast, Theunissen and Miller (1995) and Lestienne (2001) defined the *ensemble coding* as a mechanism that involves the temporal coordination of the activity of a population of neurons for the encoding of information.

An example of population coding is the population spike average (Section 1.2.1). Here, it has been suggested that the activity of several neurons with similar functions can be integrated by a postsynaptic neuron. In turn, the relevant feature for the processing of neural information would be the proportion of active neurons in the presynaptic population (Gerstner and Kistler, 2002). An additional possible mechanism for the encoding of information based in a population spike average considers neurons with distinct response properties for the same stimulus features. Here, instead of simply pooling the activity of the neurons, a weighted sum of their spike firing rate is performed (population vector coding). This mechanism has been found to encode information about arm position in the motor cortex neurons of monkeys (Georgopoulos et al., 1986).

Ensemble coding has been suggested as a mechanism with which neurons in a population could encode information in a synergistic way. This suggestion is supported on the proposal that the temporal patterns of the activity of single neurons are highly specific symbols (Strehler and Lestienne, 1986). Therefore, Theunissen and Miller (1995) have suggested that the activity of a population of neurons would allow to encode more information due to the increase of possible coding symbols. Nonetheless, the amount and efficiency of the encoded information by these symbols could be limited by the following factors: 1) The possibility that different symbols could encode the same stimulus, 2) Symbols could occur too seldom to be characterised and 3) The postsynaptic neural decoder may not be able to extract the encoded information from these symbols.

1.3   Natural Visual Scenes

As can be noticed from the preceding section, much research has been focused on understanding how the activity of single and population of neurons encodes visual stimuli. However, so far it has not been mentioned which kind of information the visual system of animals has to deal with. Natural visual scenes vary depending on the environment and thus, have different statistics. Nevertheless, natural visual images from different environments also show common characteristics. For instance, natural visual images are not Gaussian (Dong and Atick, 1995b) and although they appear to be random, they often show structures with high redundancy (Simoncelli and Olshausen, 2001). Considering that it has been long suggested that the environment influences the function of sensory neurons through evolutionary and developmental processes (Simoncelli and Olshausen, 2001), it would not be pointless to have a good comprehension of the kind of information that natural visual scenes contain, in order to obtain a better understanding of the function of the visual system.

Natural visual scenes are composed by several spatio-temporal features like, e.g., colour, contrast, luminance, motion, etc. Moreover, many of the features that compose natural visual scenes have to be encoded and processed simultaneously by the visual system of animals, since this information could be crucial for survival tasks. Therefore, the activity of neurons in the visual system should contain all the information about the relevant features of visual scenes. Nevertheless, not all animals have the same needs for survival, and what for one animal species could seem threatening, for another animal species could be regarded as appetizing. Based on these facts, Barlow (1961) proposed that the function of sensory systems of animals was tuned by their environment, and that the sensory systems should have something like a password mechanism to allow relevant features for survival to be encoded in a faster way.

As mentioned earlier, natural visual scenes have been found to be statistically redundant, showing strong spatial and temporal correlations. In this context, Attneave (1954) suggested that in visual scenes, much information is concentrated along the edges, where abrupt colour changes are frequently found. Moreover, he suggested that further non-redundant information could be found in edges that abruptly change their direction. In a latter study by Kersten (1987), the author measured the content of information in individual pixels of natural images and found that redundancy ranged from 46% to 74%, for images of foliage and human faces, respectively. Furthermore, Field (1987) analysed the spatial correlations in natural images by calculating the amplitude spectrum of them. He found that in the spectrum of

natural scenes, lower spatial frequencies have the highest amplitudes, and that the spectrum could be characterised by $1/f^2$, where f corresponds to the spatial frequency. In a later study, Ruderman (1994) quantified the spatial correlations in natural images of foliage. Here, the author found that pixels contained information about the features of the neighbouring pixels and moreover, that the information decayed exponentially with the distance. Additional to the spatial correlations, features of natural visual images like, e.g., intensity, do not change randomly over time and thus, natural scenes are though to be also highly correlated in time. Dong and Atick (1995b) studied the spatial and temporal correlations of natural scenes. They found that in general, the spatial and temporal spectra depended on each other and were only independent in the regime of high temporal and low spatial frequencies. In the context of the spatio-temporal correlations of natural images and due to the fact that the responses of neurons have certain constrains for the transmission of sensory information, Attneave (1954) and Barlow (1961) proposed that one of the functions of sensory neurons would be to recode the information of the input signals to decrease their redundancy and this way, extract the relevant information from them.

Some experimental evidence supporting the hypothesis that the environment shapes the function of visual systems of animals has already been found. For instance Laughlin (1981) found that the probability distribution of contrasts in the natural environment of flies match the one of the response-contrast function of the large monopolar cell of the animal and suggested thus, that matching the input-output function of neurons with the expected distribution of the incoming signals could be a strategy to maximize the capacity of neurons to transmit information. Moreover, in a later study by Srinivasan et al. (1982), the authors found that first-order interneurons of the fly show similar inhibition surrounds to the ones required to suppress spatial correlations in natural visual scenes. In this direction, Atick and Redlich (1992) found that kernels that relate the responses to light of X- and P-pathway retinal ganglion cells in cats and monkeys, respectively, perform a spatial decorrelation, i.e., whitening of natural images and suggested additionally, that this whitening could be useful to compress the photoreceptor input signal. Regarding colour vision, Ruderman et al. (1998) found that in foliage scenes, information about illumination changes, and opponencies of blue-yellow and red-green are uncorrelated. Therefore, information about these features can be represented by a three dimensional space. Interestingly, these three dimensions are also found in the responses of cones in humans. Based on these observations, it has been suggested that in order to reduce the redundancy in natural visual scenes, the retina spatially decorrelates the incoming signals. Nonetheless, temporal correlations of natural images are

still present in the activity of retinal ganglion cells. Thus, Dong and Atick (1995a) suggested that the temporal decorrelation of the incoming signals could be performed in the lateral geniculate nucleus. Here, based on the statistics of natural visual scenes, the authors calculated the spatio-temporal receptive fields that could achieve the temporal decorrelation of the signals. The results of this study pointed out that these receptive fields remarkably matched the *lagged* and *nonlagged* responses of lateral geniculate neurons.

So far, the study of the visual system has been carried out making use of rather simple stimuli like, e.g., bars, grating or spots. This research approach is explained by the fact that simple stimuli, as well as the responses of neurons to them, are easy to control and characterise. Nonetheless, because these stimuli do not resemble the natural environment that the visual system has to deal with, it is sometimes difficult to draw conclusions from the characterisation of the responses of neurons to these stimuli. Therefore, it would be desirable to use of natural stimuli to characterise the responses of neurons. However, these stimuli are more difficult to control and characterise. Therefore, the knowledge about the statistics of natural scenes could be useful to design stimuli that remain simple but nevertheless, still resemble the characteristics of natural images to further characterise the function of the visual system.

1.4   Stimulus Reconstruction

In the pursuit of understanding how the neural information is encoded and transmitted by the activity of neurons, several approaches have been suggested (Rieke et al., 1999). For instance, one approach is to create models that reproduce the neuronal responses observed in *in vitro* or *in vivo* experiments (Lapicque, 1907; Hodgkin and Huxley, 1952; Berry II et al., 1999; Thiel et al., 2006; Baccus et al., 2008). Here, hypothetical mechanisms necessary for the encoding of neural information can be tested.

Additional approaches test certain properties of neuronal responses individually, e.g., spike firing rate, temporal patterns, latency, autocorrelations, etc. Here, one approach involves the characterisation of the neuronal responses based on these properties (Gawne et al., 1996; Berry II et al., 1999; Greschner et al., 2002; Arkadir et al., 2004). Moreover, based on the information theory, the amount of information conveyed by these response properties can be assessed (Borst and Theunissen, 1999). Nonetheless, this approach does not provide further details about the kind of information that is conveyed by the neural activity (Lewen et al., 2001). Here, the mutual information measure becomes helpful to cope with this problem. This approach has

been utilised to measure the amount of conveyed information about visual stimulus by the activity of retinal ganglion cells of turtle (Ferrandez et al., 2002) and guinea pigs (Koch et al., 2004), as well as to asses the performance for texture discrimination allowed by the rat whisker pathway (Arabzadeh et al., 2006). However, in order to take advantage of the mutual information approach, the reconstruction or estimation of sensory stimuli has to be previously undertaken.

Several methods to reconstruct sensory stimuli based on neuronal responses have been developed. Here, depending on the research interest, these methods can additionally offer information about the features of neuronal activity that carry sensory information. For instance, artificial neuronal networks have been used to control a robotic arm based on the activity of motor cortex neurons of rats (Chapin et al., 1999). Moreover, applying this method it has been possible to reconstruct visual stimuli based on the activity of complex cells in the primary visual cortex of monkeys (Kjaer et al., 1994), or retinal ganglion cells (Warland et al., 1997; Ferrández et al., 1999; Greschner et al., 2002). Nevertheless, although this method allows to measure the amount of information conveyed by the activity of neuron populations, it is hard to draw conclusions about which features of the population activity are the ones responsible of encoding sensory information (Abbott, 1994).

An additional method for stimulus reconstruction makes use of non-linear filters with linear decoding algorithms. This approach has shown to be able reconstruct visual stimulus in a fast way based on the activity of H1 cells of the fly (Bialek et al., 1991), as well as responses of retinal ganglion cells of salamander (Warland et al., 1997) and turtle (Wilke et al., 2001). The attractiveness of this method lies in its simplicity. However, its drawback lies on the difficulty to find a filter that ensures a good performance in the estimation of several stimulus properties. Moreover, the chosen filters need to be robust when the interaction among neurons is considered (Warland et al., 1997). Other linear approaches make use of weighted vector summation (Georgopoulos et al., 1986) or adjust parameters for a defined estimation task. However, the drawback of these models is that they only serve to perform the estimation of certain stimulus features, e.g., the motion speed of a visual stimulus (Chichilnisky and Kalmar, 2003; Frechette et al., 2005), or the position of a robotic arm (Carmena et al., 2003), but fail to generalise to other stimulus features.

Another approach is the Linear Discriminant Analysis. Here, different properties of neuronal responses can be fed to the analysis to test their relevance in the encoding of sensory information. This analysis has been applied successfully to test the relevance of the spike firing rate, latency, spike time intervals, and temporal patterns of the responses of turtle retinal ganglion

cells, for the encoding of information about light intensities and wavelengths (Fernandez et al., 2000), instantaneous changes in light intensity (Greschner et al., 2006), or motion features (Cerquera et al., 2008; Cerquera and Freund, 2011).

A further approach for stimulus reconstruction relies on the Bayes' rule. Here, based on the prior probability distribution of the stimuli $P(\mathbf{s})$, the conditional probability, i.e., likelihood, $P(\mathbf{r}|\mathbf{s})$, that a neuronal response was elicited by a stimulus, and the probability distribution of the neuronal responses $P(\mathbf{r})$, it is possible to find $P(\mathbf{s}|\mathbf{r})$, which is the probability of each stimulus given a neuronal response. As with the Linear Discriminant Analysis, this approach allows to test individual properties of neuronal responses for the reconstruction of stimuli. Here, the approach has been tested in different sensory systems. For instance, it has been applied to estimate the position of rats based on the activity of their hippocampal place cells (Zhang et al., 1998), as well as in the motor system of monkeys, where the prediction of movement was done based on the activity of neurons in the supplementary motor area (Averbeck and Lee, 2003). In the visual system, this method has been applied to estimate different features of visual stimuli based on responses of retinal ganglion cells of archer fish (Segev et al., 2007), turtle (Thiel et al., 2007), mouse (Jacobs et al., 2009) and monkey (Pillow et al., 2005). The Bayesian framework for stimulus reconstruction has proven to be robust and has a low computational cost, making it suitable for on-line reconstruction tasks, like in brain computer interfaces (Shenoy and Rao, 2004).

The drawback of methods like the Linear Discriminant Analysis and the one based on the Bayes' rule, lies on the fact that sometimes it is difficult to identify the properties of neuronal activity that should serve as input for the analysis. Therefore, other approaches analyse the raw neuronal activity to find which properties are relevant for stimulus encoding. Here, some of these approaches are based on the assumption that neuronal responses evoked by a repeatedly presented stimulus should show less dissimilarities among them, than responses elicited by different stimuli. Thereby, the stimulus reconstruction is done based on the pairwise similarities or dissimilarities of spike trains. Section 2.3.3 presents a detailed explanation of how the stimulus reconstruction is carried on by using this assumption. In this context, several methods or metrics have been developed to assess the similarity between spike trains in terms of distance (Victor and Purpura, 1996; van Rossum, 2001; Hunter and Milton, 2003; Aronov, 2003; Schreiber et al., 2003; Kreuz et al., 2007). Within the scope of this study, two approaches were applied to the responses of retinal ganglion cells to estimate different features of visual stimuli; Spike cost-based metrics (Victor and Purpura, 1996; Aronov, 2003), and the ISI metrics (Kreuz et al., 2007).

The spike cost-based metrics approach allows to test the relevance of the spike firing rate and different time scales of the temporal structure of neuronal responses for the encoding of neural information. Furthermore, due to its binless nature, it respects the hybrid topology of the spike trains allowing in turn, a robust estimation of the relevance of neuronal response features for stimulus encoding (Victor, 2002). This method is described in detail in Section 2.3.1. The spike cost-based metrics has been applied to study different sensory systems in various animal species. Examples of the applications include the gustatory sensory system of rats (Di Lorenzo and Victor, 2003; Di Lorenzo et al., 2009), the auditory system of grasshoppers (Machens et al., 2003) and cats (Chase and Young, 2006, 2007, 2008) and the somatosensory system of humans (Saal et al., 2009). In the visual system, the spike cost-based metrics has allowed to distinguish which properties of the activity of single neurons in the primary visual cortex (Victor and Purpura, 1998; Reich et al., 2001a; Mechler et al., 1998, 2002), and the MT area (Sachsa et al., 2011) of monkeys are relevant for the encoding of visual stimuli features. Furthermore, this method has also been applied to study the visual system of flies (Grewe et al., 2003) and to validate models that reproduce the responses of retinal ganglion cells of salamander to light stimuli (Pillow et al., 2005). The spike cost-based metrics has the ability to test the relevance of the spike firing rate, as well as different time scales of the temporal structure of neuronal activity, for the encoding of information. In turn, this ability represent the main advantage of this method because the individual test of time scales allows to discard or keep them according to their relevance for encoding tasks (Samonds and Bonds, 2005). However, the interpretation of the relevant time scales is not straightforward. Here, it has been suggested that for spike trains that include different time scales (i.e., regular and transient or bursting spiking), the role of the relevant time scales for the encoding of visual information could be misinterpreted (Kreuz et al., 2007; Paiva et al., 2010; Chicharro et al., 2011).

An extension of the spike cost-based metrics, the multi-unit metrics, was developed by Aronov (2003). This extension allows to test different joint activity coding hypotheses (see pages 29-32). This method is explained in detail in page 57. The multi-unit metrics has been applied in monkeys to study how the joint activity of pairs of neurons in the V1 area encodes features of visual stimuli (Aronov et al., 2003). Here, the method allowed to test how important it is to distinguish the spikes coming from each neuron for information encoding tasks. The results in (Aronov et al., 2003) show that when no distinction between the spikes was made (i.e., Pooled Population), the joint activity of neurons encode more information than the activity of single cells. Moreover, the distinction of spikes coming from different neurons

(i.e., Labelled Line) can enhance the conveyed information, especially if the cells show different activity tuning for the same stimulus. Within the scope of this study, the multi-unit metrics have been used as an extension of the spike cost-based metrics and the ISI metrics to test the three joint activity coding hypotheses proposed in Section 1.2.4.

The ISI metrics is a method that has been developed to assess the synchrony between pairs of spike trains. Here, the ISI metrics assesses the synchrony (i.e., similarity) between a pair of spike trains based on the temporal integration of the ratio between their spike time intervals. Section 2.3.2 describes the method in detail. This method has been mainly applied to validate or characterise the behaviour of neuronal models (Dodla and Wilson, 2009; Ying and Qi-Shao, 2010; Ying et al., 2010) but also, to measure the variability of ampullary receptor responses of weakly electric fish (Engelmann et al., 2010), and neurons of the entorhinal cortex of rats (Haas et al., 2010). In contrast to the spike cost-based metrics, the ISI metrics is a self adaptive analysis method that identifies automatically the time scales that are relevant for stimulus encoding. Moreover, the ISI metrics finds the relevant time scales even if changes in the temporal structure within the same spike train occur (Kreuz et al., 2007). These abilities of the ISI metrics are important because it has been proposed that responses elicited by the same neuron could encode different features of sensory information by using different time scales (Oram et al., 2002). Therefore, the ISI metrics allows to test the relevance of the temporal structure of neuronal responses for encoding tasks. However, this method provides no additional information about which are the relevant time scales for encoding tasks. Furthermore, the ISI metrics shows some drawbacks for spike trains with phase lags and additionally, this metrics is not able to recognize when a pure spike rate code is relevant for stimulus encoding. In this study, the spike cost-based metrics and the ISI metrics were applied as complementary methods. By doing so, it was thought that the advantages of one of the metrics could help to cope with the limitations of the complementary metrics for the study of the retinal code.

Chapter 2

Materials and Methods

As exposed in the previous chapter, the retina is comprised by different types of neurons that play a specific role in the early stages of visual information processing. At the final stage in the retina, the processed information is sent to the brain in the form of action potentials that are generated by the retinal ganglion cells. The aim of this study is to gain some insight into the strategies that the retinal ganglion cells use to encode the visual information that they send to the brain. In this context, the retina offers two major advantages to achieve this goal. First, it can be relatively easy stimulated and the output of this system can be known by performing electrophysiological experiments. Second, the flatness of the retina, as well as its layered structure, and the fact that the retinal ganglion cells are located at the innermost layer of this tissue, facilitate the extracellular recording of the responses of these cells to a visual stimulus. Additionally, although much has been learned about how visual information is encoded in the activity of single retinal ganglion cells, the development in the past two decades of new techniques, that allow the simultaneous recording of several neurons using planar (e.g., Nordhausen et al. (1996); Nicolelis et al. (1998)) and three dimensional (e.g., Meister et al. (1994); Stoppini et al. (1997); Borkholder et al. (1997); Segev et al. (2004)) multi-electrode arrays, have open the possibility to explore how the encoding and processing of neuronal information can be done by the activity of populations of neurons.

In order to investigate how the activity of retinal ganglion cells encodes information about visual stimuli, extracellular recordings of the responses of these cells to visual stimuli were performed in isolated retinae of turtle and fish using a multi-electrode array. The acquired data consisted of sequences of action potentials which were fired in response to the visual stimuli. In this sense, the approach in this study was to test the performance in the estimation of the applied stimulus based on the responses of retinal ganglion

cells. In turn, the stimulus estimation was performed by applying two analysis methods that consider different features of neuronal activity, and the obtained results were evaluated.

The following sections describe the utilised experimental set-up and stimuli, as well as the data acquired from the experiments. Additionally, the pre-processing stages of the data, as well as the analysis methods are going to be exposed.

2.1 Experiment

The data analysed in this study was originated from electrophysiological experiments in isolated turtle and fish retinae. The protocol for all of the experiments in the turtle ($n = 3$) and for most of the ones performed in the fish ($n = 5$) was previously described in Thiel et al. (2007). This protocol involved the stimulation of the retinae by a moving pattern of dots. Additionally, a different protocol that involved the same moving stimulus and changes in the light intensity with which the pattern was projected onto the retina was used only in the fish ($n = 1$) retina. Figure 2.1 shows a simplified diagram of the experimental set-up used for this study.

2.1.1 Preparation and Recordings

The recordings of extracellular activity of retinal ganglion cells were performed in isolated retinae of turtle (*trachemys scripta elegans*) and carp (*cyprinus carpio*). First, animals were killed according to the University of Oldenburg Ethical Committee and ECC rules (86/609/ECC). Posteriorly, eyes were enucleated and then, in the case of the turtle, the retina was dissected with the pigment epithelium attached to it. In contrast, for recordings using carp as animal model, the pigment epithelium was removed from the retina. The dissected retina was in turn placed over a thin layer of agarose and fixed to it using micro filter paper. The agarose layer with the fixed retina was then placed on a transparent surface. This arrangement allowed to project a visual stimulus onto the retina through the transparent surface and at the same time, place a multi-electrode array on top of the retina to register the extracellular activity of retinal ganglion cells (see Figure 2.1).

The register of the responses of retinal ganglion cells was performed using a three dimensional 10 x 10 multi-electrode array (Utah Array, BlackRock Microsystems, Salt Lake City, Utah, USA) that was placed from the photoreceptor side into the ganglion cell layer of the isolated retina. The electrodes in this array were arranged in a matrix form with a minimal separation of
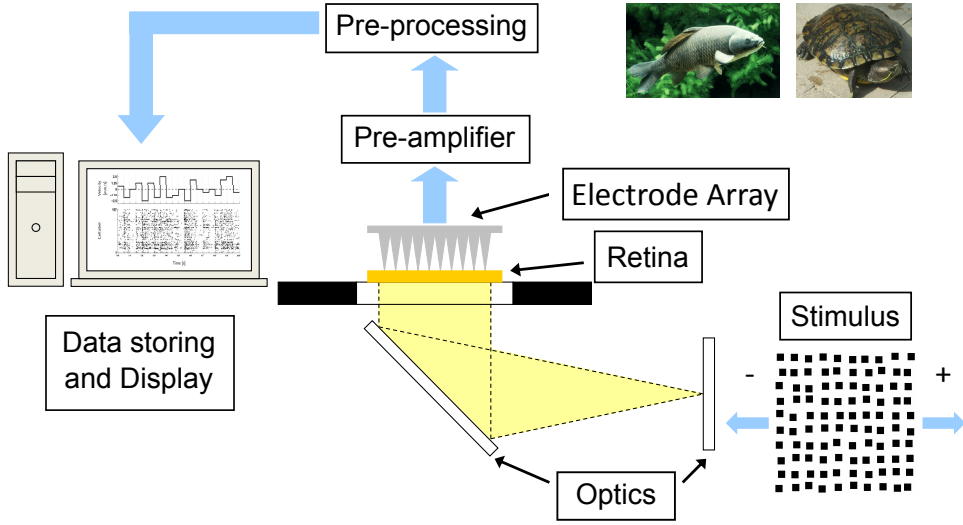
Figure 2.1: Simplified diagram of the experimental set-up used to record the extracellular activity of retinal ganglion cells of turtle and fish retinae. The pattern of dots (bottom right) was projected on to the retina trough optic devices and its motion was created by a miniature mirror system. A multi-electrode array was placed onto the retina to register the extracellular activity of retinal ganglion cells. The acquired data was stored in a personal computer.

400 μm. Here, due to the electrode separation, the probability that two neighbouring electrodes register the activity of the same cell is very low. The output of the array was connected to a pre-amplifier and this in turn, to the Bionic 100 channel neural signal acquisition system (Cyberkinetics, Foxborough, Massachusetts, USA) in the case of the turtle experiments, and to the Cerebus system (BlackRock Microsystems) in the case of the fish experiments. Both systems were utilised to amplify, threshold and store the extracellular activity of the retinal ganglion cells for posterior offline analysis.

In order to be able to register the activity of retinal ganglion cells, the retinae were superfused continuously with a Ringer solution during the entire duration of the experiment. The solution used for the turtle retina comprised 120 mM NaCl, 5 mM KCl, 2 mM $CaCl_2$, 2 mM $MgCl_2$, 10 mM glucose and 22 mM $NaHCO_3$. In turn, the solution for the carp retina consisted of 102 mM NaCl, 2.6 mM KCl, 1 mM $CaCl_2$, 1 mM $MgCl_2$, 5 mM glucose and 28 mM $NaHCO_3$. In both cases, the solution was bubbled with 95% O_2-5% CO_2 to keep the solution at a pH of 7.4.

2.1.2   Stimuli

The stimulus used in all of the experiments consisted of a pattern of squares that when projected onto the retina, moved along one of its axes. The squares of the projected pattern were 200 μm x 200 μm. Furthermore, their position was set by randomly shifting it relative to the position they would have if they were arranged on a regular lattice with a vertical and horizontal separation of 200 μm. Here, for the shifted squares, a minimal separation of 80 μm was kept between squares. The shift in the squares' position was to avoid the artificial firing synchronisation of retinal ganglion cells (Thiel et al., 2007). A section of the pattern of squares used on the experiments is shown in Figure 2.1.

Motion experiment

For the experiments in the turtle retina, the moving pattern consisted of dark squares on a bright background, whereas for the experiments with fish retina, the squares were bright on a dark background. As mentioned earlier, this protocol was utilised in $n = 3$ experiments carried out with turtle retina, and in $n = 5$ experiments performed with fish retina. Here, the experimental protocol only involved the motion of the pattern of squares.

The motion of the pattern of squares was achieved by a X-Y miniature mirror system (Datrouik, Rastede, Germany), which in turn was controlled by a personal computer. For this protocol, the pattern of squares was projected onto the retina with a constant light intensity and moved along one axis for 500 ms with a constant velocity. After this period, the velocity changed instantaneously to remain constant for another 500 ms and so on. Nine different velocities were used for this protocol. The velocities were obtained by combining two motion directions with four different speeds between 0.625 mm/s and 2.5 mm/s, with increments of 0.625 mm/s. Here, negative and positive velocities were defined by two opposite directions. Additionally, the absence of movement, i.e., 0 mm/s, was also considered as a velocity for this protocol. The sequence of velocities was created by combining all of the possible values in a pseudo-random way, ensuring that all velocities and transitions between velocities had the same occurrence frequency. In this sense, in a full sequence each velocity value was presented 80 times to the retina allowing in this way, that each of the 72 possible transitions between velocities appeared 10 times per sequence. Finally, depending on the conditions of the experiment, the sequence was presented to the retinae between eight and ten times. A fragment of the temporal sequence of the stimulus for this protocol can be observed on the top of Figure 2.3.

Light-motion experiment

An additional protocol was used for an experiment on the fish retina ($n = 1$). This protocol added changes in the light intensity with which the pattern of squares was projected onto the retina. Here, the velocity and light intensity of the projected stimulus were abruptly changed every second in an alternate way. This procedure yielded periods of 500 ms of constant velocity and light intensity. Five different velocities and four different light intensities were used for stimulation. Velocities were obtained by combining two different motion directions with speeds of 1.25 mm/s and 2.5 mm/s. Additionally, the absence of movement was also considered. Negative and positive velocities corresponded to motion in opposite directions. In turn, the projected light intensities onto the retina were 0.63 μW/cm^2, 2.08 μW/cm^2, 7.21 μW/cm^2 and 26.18 μW/cm^2. The sequence of combinations of the four constant light intensities and five velocities was created by concatenating all the 20 possible combinations in a pseudo-random way, ensuring that all combinations had the same occurrence frequency. In a full stimulus sequence, each of the 20 light intensity and velocity combinations was presented 96 times to the retina. Finally, the sequence was presented to the retina eight times. A segment of the temporal sequence of the stimulus that was presented to the retina for this protocol is shown in Figure 2.4.

2.2 Pre-analysis of the data

The aim of this study is to analyse how the activity of single and small populations of retinal ganglion cells encodes features of visual stimuli. To achieve this goal, the extracellular activity of the neurons was registered by a recording system that continuously sampled each of the electrodes in the array with a rate of 30 kHz. In turn, the detection of action potentials from the extracellular activity was done by manually setting a threshold for each of the electrodes. Nonetheless, depending on the experiment conditions, fluctuations in the extracellular activity that lack the classic form of an action potential can cross the threshold and could be wrongly regarded as spikes. Moreover, in extracellular recordings it is common that an electrode registers the activity of more than one neuron at a time. For these reasons, a pre-processing stage for the recorded activity by each electrode comprised the separation of spurious spikes from the real ones, as well as the grouping of the spikes corresponding to each of the registered cells. Additionally, the pre-processing of the data in this study involved the classification of retinal ganglion cells based in their responses to the applied motion stimulus.

2.2.1   Spike Sorting

Spike sorting refers to the process of differentiating action potentials from background '*noise*' in recorded extracellular activity. Additionally, for the electrodes in the array that were able to register the activity of retinal ganglion cells, this process also includes the discrimination of spikes originated by one neuron, from others evoked by neighbouring neurons.

The rationale behind spike sorting is that if an electrode registers the activity of more than one neuron, it would be possible to distinguish the activity of each neuron based on the waveforms of the evoked spikes. Here, within the framework of this study, spike sorting was performed on the recorded extracellular data using a commercial software (Offline Sorter V 2.8.8, Plexon Inc., Dallas, Texas, USA) that combines the Principal Component Analysis of the waveforms of the recorded action potentials, with an Expectation-Maximisation T-Distribution clustering method. Using these techniques, the software can perform spike sorting in an automatic manner for the different electrodes. The results after the automatic spike sorting consist in the creation of different so called units, which correspond to putative different neurons from which the electrodes have registered activity (see Figure 2.2).

For this study, the first step for spike sorting consisted of an automatic procedure for each of the electrodes in the array. After the automatic spike sorting, the results were controlled for each of the electrodes. The control consisted of a visual inspection of the created units in order to assure that no over classification was made, and that the waveforms of the obtained units possessed the shape of an action potential. Here, it is worth mentioning that due to the minimal distance between electrodes of 400 μm, the probability that two electrodes registered the activity of the same cell was rather low. The responses of retinal ganglion cells obtained after spike sorting for both experimental protocols can be observed in the lower sections of Figures 2.3 and 2.4. For the motion experiment, Table 2.1 displays the number of identified units after spike sorting, for each of the experiments performed utilising turtle ($n = 3$) and fish ($n = 5$) retina.

2.2.2   Cell Classification

For both experimental protocols used in this study, it was analysed how the activity of retinal ganglion cells encode information about motion features of a moving stimulus. Here, the recorded responses of some retinal ganglion cells showed to tune their firing rate depending on the speed and direction of movement of the pattern of squares. Therefore, for the motion experiment protocol, additional to the pre-processing stage of spike sorting, retinal gan-
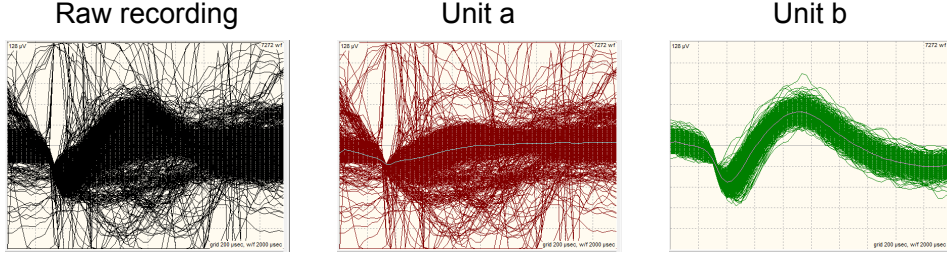
Figure 2.2: Registered extracellular activity by an electrode (raw recording). After spike sorting, two units were created. Unit a contains waveforms that were classified as noise and artefacts and hence, was not considered for further analysis. Unit b contains waveforms with a classical action potential shape.

glion cells were classified according to the tuning of their responses. This classification grouped the retinal ganglion cells in three categories; Left- and Right-direction selective cells (Left-DSC and Right-DSC, respectively), and symmetrically tuned Non-direction selective cells (Non-DSC).

The classification of retinal ganglion cells was performed based on the spike firing rate probability distributions of their responses to the different velocities of the moving stimulus. In turn, these probability distributions were obtained considering the 500 ms periods for which a constant velocity was presented to the retinae (Figure 2.5b). Here, in the case of the motion experiment protocol, four pairs of distributions originated from velocities with the same speed and opposite direction were obtained. Thereby, as first step for the cell classification, a two-sample Kolmogorov-Smirnov test was applied to each of the distribution pairs. If a cell showed significant differences for more than two distribution pairs ($p \leq 0.005$), it was considered as direction selective cell. In turn, the cell was grouped in the direction class for which the mean firing rate of the distributions showed to be maximum. Here, cells that showed to have preferred directions corresponding to negative velocities were classified as Left-DSC. Conversely, the opposite criterion applied for Right-DSC. A further analysis was performed for cells whose firing rate distributions did not allow to classify them as direction selective cells. This analysis comprised the comparison of the firing rate distributions over the different speeds. Here, if the analysed cells showed significant differences across more than two speeds ($p \leq 0.005$), they were classified as Non-DSC. In contrast, if the cells did not show significant differences, they were not considered for further analysis.

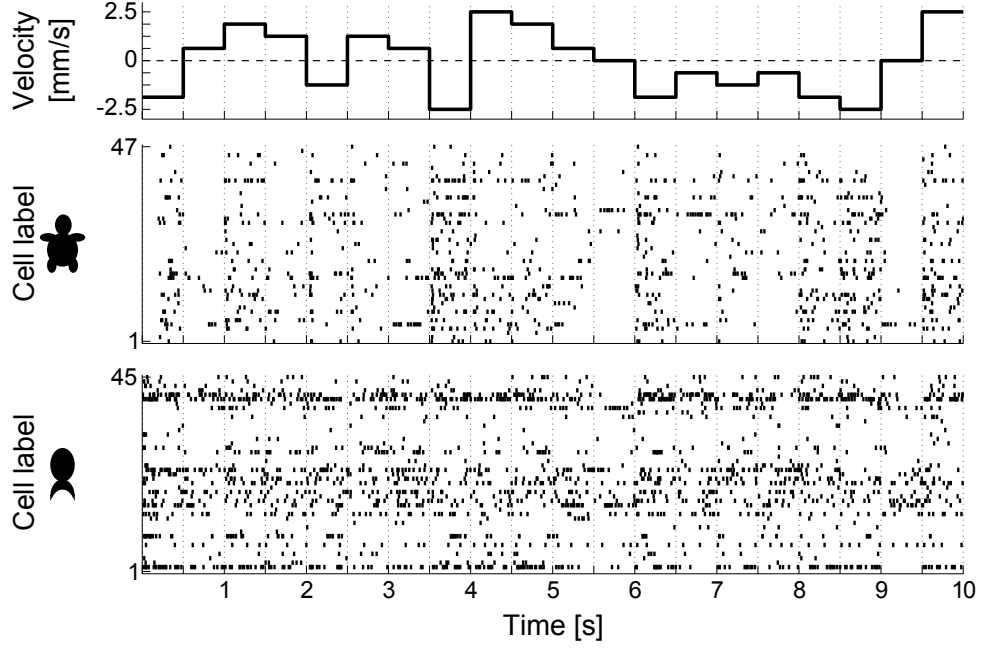For the motion experiment protocol, the percentage of cells that were

Figure 2.3: Segment of 10 s from the motion experiment. Time course of the different velocities with which the pattern of squares was moving (top). Responses, after spike sorting, of 47 and 45 cells recorded from experiments in the turtle and carp retina, respectively (middle and bottom).

grouped in a defined class varied among experiments and animal species. In the case of the experiments with turtle retinae ($n = 3$), the percentage of cells that tuned their activity to different speeds was between 70 % and 79.2 %. These cells include direction and non-direction selective cells. In turn, the percentage of cells that were direction selective was between 40.4 % and 50 % (upper section in Figure 2.5a).

For experiments conducted with carp retinae ($n = 5$), the percentage of cells that tuned their activity to the different speeds, including direction and non-direction selective cells, was between 16.9 % and 43.3 %. Here, the percentage of direction selective cells was between 4.3 % and 23.3 % (lower section in Figure 2.5a). For each of the experiments carried out in turtle and fish retina, the number of cells that were classified in each of the three categories, and hence considered for further analyses, is shown in Table 2.1.

Animal	Registered electrodes	Recorded units	Left-DSC	Non-DSC	Right-DSC
Turtle ($n = 3$)	99	40	8	8	12
	99	53	13	17	12
	99	47	11	14	8
Fish ($n = 5$)	95	77	9	2	2
	96	45	3	9	2
	96	30	6	6	1
	96	23	1	5	0
	96	61	2	4	4

Table 2.1: For the experiments carried out in this study, most of the electrodes in the 10 x 10 array registered extracellular activity. After spike sorting, the activity of retinal ganglion cells was identified for a reduced number of electrodes. In turn, only some of the identified cells showed tuned activity to the different speeds of the experiment protocol.

2.2.3   Selection of Cells

Additional to the classification of the retinal ganglion cells in the three classes described in Section 2.2.2, for the Motion Experiment protocol, a preliminary analysis was performed to select the cells that were used to test the three joint activity coding hypotheses introduced in pages 30-32. Thereby, the selection of cells was based on their performance for the estimation of motion velocity. The assessment of the estimation performance is going to be addressed in detail in Section 2.3.4.

More in detail, in the case of the turtle experiments, a preliminary analysis by applying spike-cost based metrics to estimate the motion velocity was performed. In turn, this preliminary analysis was carried out for all of the retinal ganglion cells that could be classified either into Left-, Right-, or Non-DSC. Furthermore, the analysis considered the responses of these cells within the 500 ms interval. In this sense, cells that allowed estimation performances similar to chance level were not further considered. Here, depending on the number of remaining available retinal ganglion cells for each of the experiments, a number between six and nine cells from each of the three cell classes were selected (see Table 2.2).

In the case of the fish experiments, due to the limited number of cells that could be classified either into Left-, Right- or Non-DSC, the maximum

Animal	Recorded units	Selected cells	Left-DSC	Non-DSC	Right-DSC
Turtle (n = 3)	40	25	8	6	9
	53	21	8	6	7
	47	20	8	6	6
Fish (n = 5)	77	6	2	2	2
	45	6	2	2	2
	30	6	2	3	1
	23	6	1	5	0
	61	6	2	2	2

Table 2.2: Number of selected cells for each of the experiments carried out in this study.

number of selected cells from each class was two. Nevertheless, as mentioned before, there were some experiments for which the number of cells of a defined class was either zero or one (see Table 2.2).

2.2.4   Combination of Neuronal Activity

As mentioned in Section 1.2.4 (pages pages 30-32), three joint activity coding hypotheses were tested in this study; Pooled Population, Labelled Line and Functional Group. Here, for each of the tested hypotheses, the activity of the retinal ganglion cells was combined in a specific way to build small populations. In order to build the populations, cells belonging to each of the three groups, i.e., Left-, Right- or Non-DSC (see Section 2.2.2) were considered. Moreover, the populations were built with an equal number of cells from each of the three cell classes. For instance, in the case of the turtle experiments, populations of size $n = 6$ comprised two Left-, two Right- and two Non-DSC cells. However, these considerations were not always fulfilled for the fish experiments. This situation was due to the fact that for these experiments, certain functional classes of RGC were either absent or rarely found (see lower section of Figure 2.5a). Additionally, the reduced number of recorded RGC in fish did not allow the test of the Functional Group hypothesis.

The idea behind the Pooled Population hypothesis is that for the encoding of sensory information, the knowledge about the neuron of origin of each spike is irrelevant (page 30). Therefore, to test this hypothesis, the spike trains of the considered retinal ganglion cells were pooled into a single spike train,

and no further distinctions were made (Aronov et al., 2003).

In contrast, the Labelled Line hypothesis considers that the knowledge about the exact neuron of origin of each spike is relevant for the encoding of stimulus information. Here, it is proposed that information is first encoded by the activity of single retinal ganglion cells on independent channels and then, the information coming from each channel is integrated (page 31). Thus, in terms of the metric methods applied in this study (Section 2.3), the distance matrices for the responses of each of the cells comprising the populations have to be first calculated, and then these matrices have to be summed (Aronov et al., 2003).

The Functional Group hypothesis is a combination of both previous hypotheses. In this sense, this hypothesis proposes that for the encoding of stimulus features, the knowledge about the type of cell that fires each spike, rather than the exact neuron, has a high relevance. Thereby, for this hypothesis it is suggested that the information about the features of visual stimulus is first encoded by the integrated activity of retinal ganglion cells of the same class on independent pathways and then, the information coming from the different pathways is integrated (page 32). Therefore, in terms of the analyses carried out in this study, the responses of retinal ganglion cells belonging to the same class were first pooled together. Then, the distance matrices for the responses of each of the cell classes were calculated and finally, the matrices were summed together. Figure 2.6 shows a simplified diagram that points out the three principles with which the activity of RGC was combined.

Regarding the test of the different joint activity coding hypotheses, ten populations of sizes $n = \{6, 9, 12, 15 \text{ and } 18\}$ were built for each of the experiments in turtle retina. Here, the populations were built considering the same number of cells from each of the three classes. For each of the built populations, the procedure involved the random draw of the necessary number of cells from the group of selected cells.

In the case of the experiments in fish retina, due to the fact that only few cells were selected, five populations of six cells were analysed. Here, each of the populations corresponded to each of the analysed experiments. As mentioned before, for two of the experiments in fish retina, it was not possible to build the populations with the same number of RGC of each class.
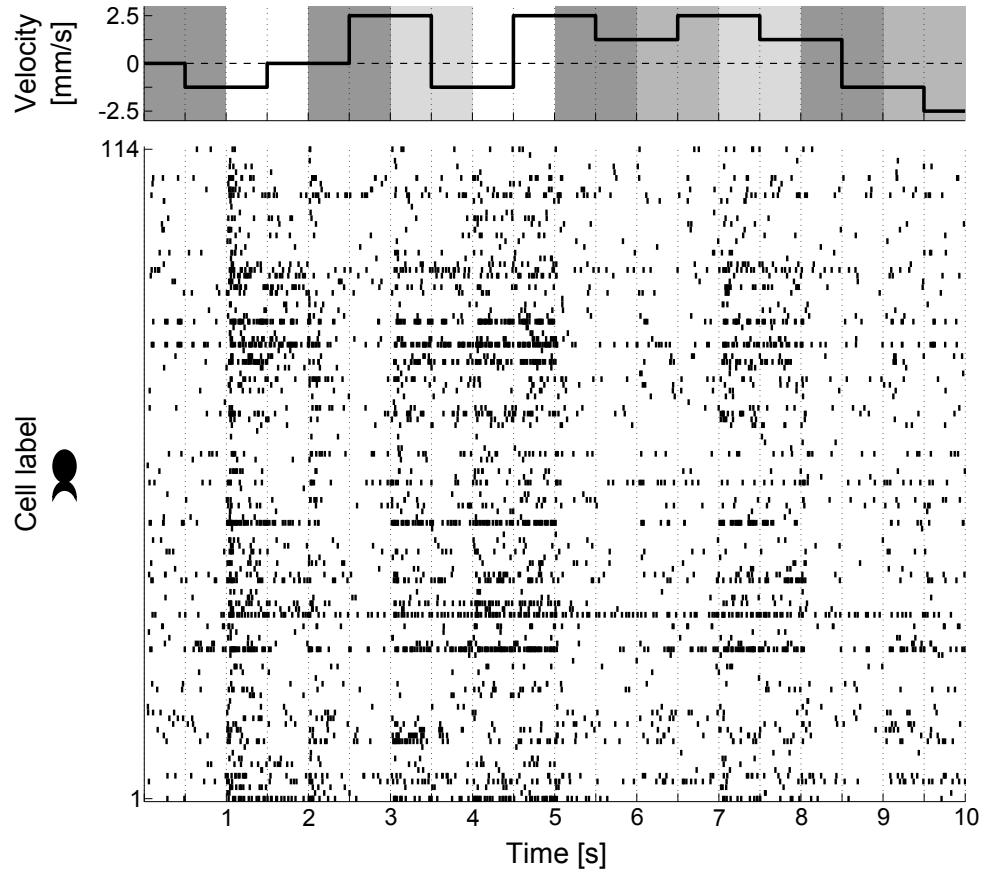
Figure 2.4: Segment of 10 s from the light-motion experiment. Time course of the different projection light intensities and velocities with which the pattern of squares was moving (top). Responses, after spike sorting, of 114 cells recorded from an experiment in the carp retina (bottom).
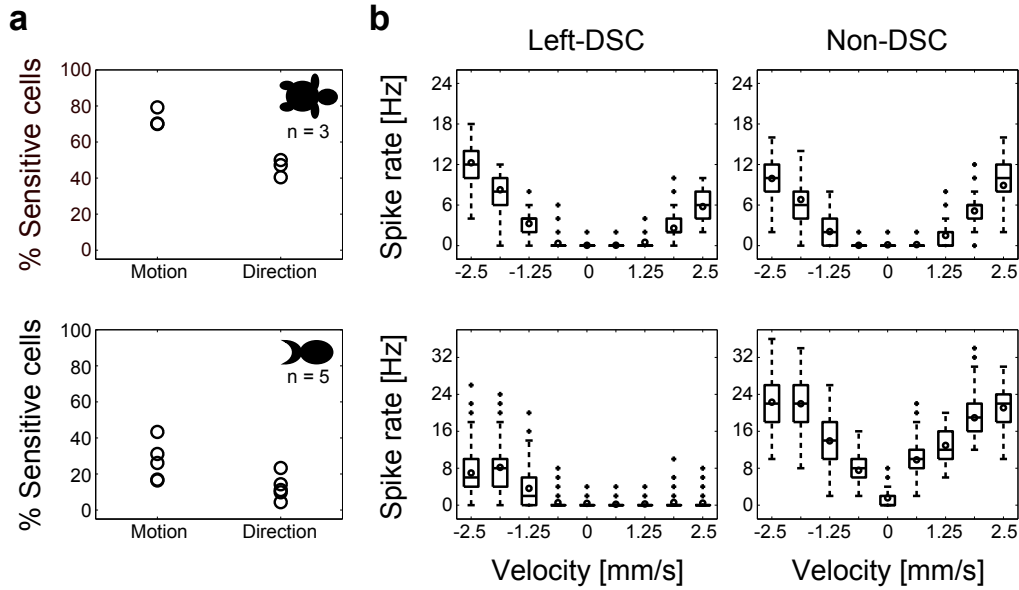
Figure 2.5: Classification of retinal ganglion cells of turtle (top) and carp (bottom) based on the tuning of their responses to different velocities. a) Percentage of identified motion and direction selective cells for each of the performed experiments. b) Firing rate probability distributions of individual cells, which were classified as Left-DSC or Non-DSC. Each box plot corresponds to each of the velocities utilised in the experiment protocol. For the cells shown, the central mark within the box plots depicts the median, whereas the edges of the box plots refer to the 25th and 75th percentiles of the spike firing rate. In turn, whiskers extend to the most extreme spike firing rates which are not considered outliers. Finally, the circles depict the mean firing rate.
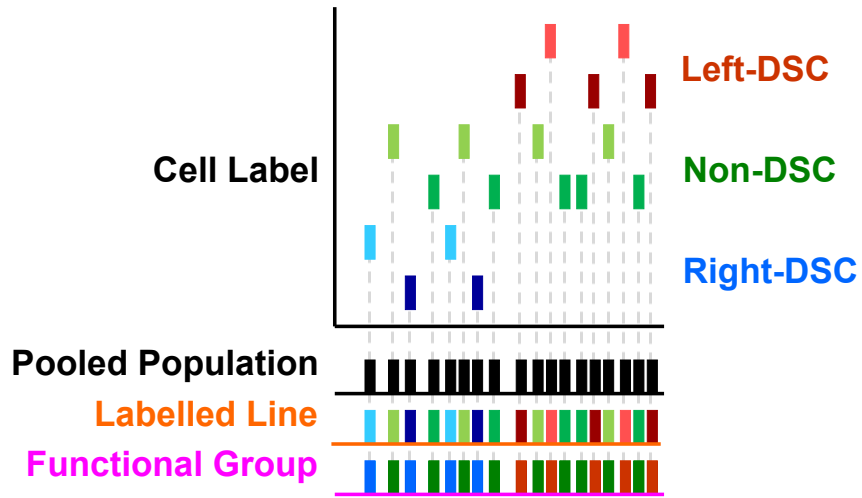
Figure 2.6: Diagram to illustrate how the activity of different neurons was combined to test different joint activity coding hypotheses. For each hypothesis, the knowledge about the cell that originated the neuronal activity has a different relevance for stimulus encoding. For the Pooled Population hypothesis, this knowledge has no relevance. For the Labelled Line hypothesis, the knowledge of the exact neuron of origin is relevant. For the Functional Group hypothesis, the knowledge of the cell type of origin is relevant.

2.3 Analysis methods

To analyse how the activity of retinal ganglion cells encodes information about visual stimuli, the approach followed in this study was to test if the features of the presented stimulus could be estimated based on the responses of these cells. Here, the basic assumption for the estimation of stimulus features, is that neuronal responses elicited by a repeatedly presented stimulus would show more similarity among them, than responses elicited by different stimuli. Therefore, this assumption allows to infer that it would be possible to estimate the stimulus features that were presented to the sensory system, based on the similarities and dissimilarities between the elicited responses. Nevertheless, due to the variability in the spike count and spike time precision of the neuronal responses, the measure of similarity or dissimilarity between spike trains is not a trivial task. Consequently, several spike train dissimilarity measures have been developed (for a review see Paiva et al. (2010)). Within the framework of this study, two different methods were applied to the recorded data in order to assess the similarity of pairs of spike trains; spike cost-based metrics (Victor and Purpura, 1996; Aronov, 2003) and ISI metrics (Kreuz et al., 2007).

Once the pairwise similarity of spike trains was calculated, the spike trains were assigned to the stimulus class that elicited responses to which they showed the highest similarity. In turn, the assignment was done applying a clustering method suggested by Victor and Purpura (1996). After the clustering procedure, the performance on the estimation of the different stimulus features was assessed by either calculating the percentage of correct estimations or the estimation normalised error.

2.3.1 Spike Cost-Based Metrics

Spike train cost-based metrics (Victor and Purpura, 1996) is a binless analysis method that allows to test the relevance of spike train features, i.e., spike firing rate and temporal structure, for the encoding of neural information. Here, the binless nature of this method respects the hybrid topology of spike trains. This topology refers to the discrete character of spike trains, which should have an integer number of spikes, and at the same time, to their continuous character, which points out the fact that spikes are elicited on a continuous time line.

To achieve its goal, spike train cost-based metrics assesses the difference between pairs of spike trains in terms of distance. This distance is calculated in a rigorous way by comparing the spike firing rate or the temporal structure of pairs of spike trains. In this sense, the method states that the features that

are relevant for stimulus encoding are the ones that minimize the distance between neuronal responses evoked by the same stimulus and at the same time, maximize the distance between responses elicited by different stimuli.

The analysis by this method was carried out using the Spike Train Analysis Toolkit, which is available at http://neuroanalysis.org/, and was developed by the laboratory of neuroinformatics of the Weil Medical College of the Cornell University. In turn, this toolbox was run in MATLAB V R2008a (The Mathworks Inc., Natick, Massachusetts, USA).

Single-unit metrics

Single-unit metrics considers only spike trains of single neurons for the analysis and is thus, the simplest application of spike train cost-based metrics. Here, the method quantifies the dissimilarity between a pair of spike trains by finding the minimal cost to transform a given spike train into another one. In turn, this transformation cost is considered as the distance between both spike trains. The transformation of spike trains is done based on three basic operations (Figure 2.7a):

- Inserting a spike, which has a cost $= 1$.

- Deleting a spike, which has a cost $= 1$.

- Shifting a spike in time, which has a cost $= q\Delta t$

The first two basic operations assure that any given spike train can be transformed into another, whereas the third basic operation confers spike timing sensitivity to the method by means of the parameter q. Hence, by setting different values for the parameter q, which units are s^{-1}, the temporal structure of neuronal responses can be tested for distinct time scales.

The robustness of this method relies on the fact that the distance between two spike trains is defined as the sum of the individual costs for the minimal number of necessary transformation operations. To express this formally, the minimal transformation pathway for a pair of spike trains S_a and S_b, with spikes times denoted by $\{a_1, a_2, ..., a_m\}$ and $\{b_1, b_2, ..., b_n\}$, can be obtained by applying the recursive algorithm shown in Equation 2.1. Here, $D_{i,j}^{spike}$ refers to the distance between spike trains S_a and S_b for their first i and j spikes, respectively.

$$D_{i,j}^{spike} = min\{D_{i-1,j}^{spike} + 1, D_{i,j-1}^{spike} + 1, D_{i-1,j-1}^{spike} + q|a_i - b_j|\} \qquad (2.1)$$

This algorithm should be regarded as a two dimensional m x n spreadsheet (for the particular case of spike trains S_a and S_b), where the first row

corresponds to $D_{0,j}^{spike} = j$, and the first column to $D_{i,0}^{spike} = i$. These first row and column represent the minimal path between a spike train with no spikes, and another one with i or j spikes, respectively. For these cases, the minimal path is the difference in the number of spikes. In turn, the three terms under the minimum argument of Equation 2.1 start to be meaningful for spike trains with at least one spike. Here, the first two terms correspond to the cost of adding one spike to either of the spike trains, whereas the third term refers to the time shift of the spike. Because the history of the transformation operations has to be followed in order to find the minimal path, the calculation of the entries for the remaining cells of the spreadsheet involve the values contained in the cells immediately on the left and above the one of interest, which in turn correspond to the first and second term of Equation 2.1, respectively. Finally, to find the minimal pathway for $q > 0$, the cost of shifting a spike in time should be less than deleting the spike and inserting it in the proper time location. Expressed more formally, $| a_i - b_j | < 2/q$. This last consideration is allowed by the insertion of the third term in Equation 2.1. Following this algorithm, the cell of the spreadsheet in the m row and the n column corresponds to the distance between spike trains S_a and S_b, for all of their spikes. This distance is denoted by $D^{spike}[q](S_a, S_b)$.

Due to the fact that the cost of shifting a spike in time is proportional to the value of the parameter q and thus, $1/q$ defines how far a spike can be shifted in time without increasing the distance between a pair of spike trains substantially, single-unit metrics offers the possibility to test the relevance of different time scales of the temporal structure of neuronal responses for the encoding of stimulus information. In general terms, this method states that precise time scales are relevant for the encoding of stimulus, provided that distances between spike trains elicited by the same stimulus are minimised for great q values and at the same time, distances for spike trains evoked by different stimuli are maximised. Conversely, if these results are obtained for small q values, then coarser time scales are relevant for stimulus encoding. A special case for this method occurs for $q = 0$ s^{-1}. Here, because there is no cost in shifting a spike in time, the minimal transformation cost is obtained by the difference in the number of elicited spikes between the considered pair of spike trains and thus, the firing rate is regarded as encoding mechanism (Figure 2.7b). For this study, single-unit metrics were applied considering $q = \{ 0, 1, 2, 4,..., 128 \text{ s}^{-1} \}$.

Multi-unit metrics

As already commented in Section 1.2.4, there are some hypotheses that suggest that sensory information could be encoded and processed by the activity
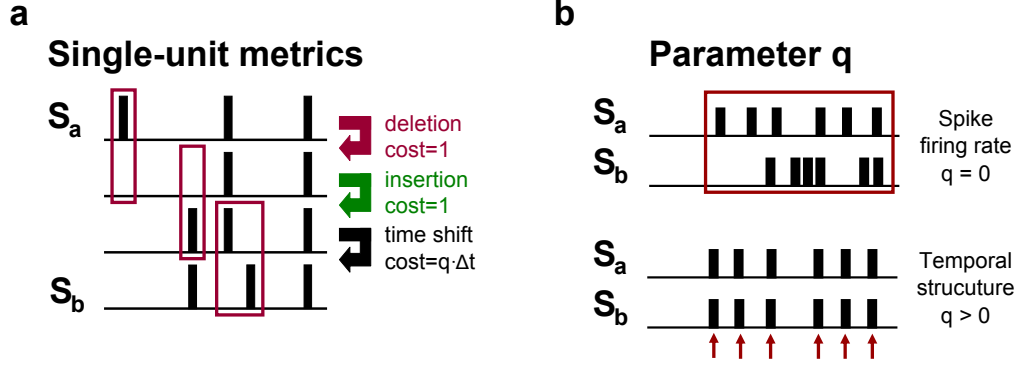
Figure 2.7: Single-unit metrics. a) Minimal transformation pathway illustrating the three possible basic operations of deletion, insertion and time shift of a spike. b) An insight into how the parameter q is used to test the relevance of spike trains properties for the encoding of stimulus features.

of populations of neurons, rather than by the activity of individual cells. In this context, it has been found that additional to the classical On-, Off- or On-Off responses, some retinal ganglion cells tune their activity in response to certain features of a moving stimulus, e.g., motion direction and/or speed. Therefore, one of the aims of this study was to test if the combined activity of such retinal ganglion cells encodes information about features of moving visual stimuli in a complementary way. To test this hypothesis, an extension of the single-unit metrics method, proposed by Aronov (2003), was applied on the responses of small populations of retinal ganglion cells. Multi-unit metrics, besides testing the relevance of the spike firing rate and the temporal structure of neuronal responses, tests if the knowledge about the cell of origin of each spike is relevant for the encoding of stimulus information.

As first step for the analysis, multi-unit metrics assigns labels to spikes according to their cell of origin and then, pools all spikes into a single spike train. Like the single-unit metrics, this method assesses the distance between a pair of spike trains based on the basic operations of inserting, deleting, or shifting spikes in time. Nevertheless, this method introduces an additional new parameter to find the shortest transformation path between two spike trains. This parameter, which is denoted as k and has no units, refers to the cost of changing the label of a spike, i.e., cell of origin (Figure 2.8a). The parameter k can have values $0 \leq k \leq 2$. Here, based on the different possible values of k, the method evaluates the importance of knowing the cell of origin of each spike for stimulus encoding. In this sense, for the case in which

$k = 0$, there is no cost in changing the spike label and therefore, all spikes are considered as been originated by the same cell. In contrast, for $k = 2$ the cost of re-labelling a spike is the same as deleting and inserting a new spike and thus, each spike will keep always its original label. With this in mind, multi-unit metrics states that the knowledge about the cell of origin of each spike for stimulus encoding will not be relevant, if distances between spike trains provoked by the same stimulus are minimised for $k = 0$ at the same time that distances between spike trains from different stimulus are maximised. In contrast, if such results are obtained for $k = 2$, the knowledge of the cell of origin of each spike will be relevant for stimulus encoding (Figure 2.8b).

In this study, multi-unit metrics was applied to analyse data sets of up to 18 cells with all possible combinations of the q parameter values used in the single-unit metrics, and values of $k = \{ 0, 2 \}$. Here, the cell populations were built considering retinal ganglion cells of each of the three classes found by the analysis of the cells' spike firing probability distributions, i.e., Left- and Right- DSC and Non-DSC (see Section 2.2.2). The procedure to calculate the distances between spike trains for the two values of k used in this study was as follows. For the case in which $k = 0$, the responses of the retinal ganglion cells that were considered to build the population were pooled into a single spike train and then, the minimal transformation pathway was found applying the recursive algorithm used for the single-unit metrics (Equation 2.1). In contrast, in the case of $k = 2$, the pairwise distance between spike trains of a population was equivalent to the sum of the individual pairwise distances of cells comprising the population (Aronov et al., 2003).

The decision to perform the analysis with values of $k = \{ 0, 2 \}$ was based on three major considerations. The first was the ease to interpret the results obtained with these values, in contrast to values within this range. The second consideration was that with these values, the multi-unit metrics can be easily extended to spike train metrics other than the spike cost-based metrics, i.e., ISI metrics. Finally, the third consideration was concerned with the time needed to calculate the pairwise distances. Here, in the case of the spike cost-based metrics, the time needed for $k = 0$ is proportional to N^2, where N is the number of spikes in the spike trains. For $k = 2$, the total time needed is proportional to $\sum_{l=1}^{L} N(l)^2$, where L is the number of neurons (Labelled Line) or neuron classes (Functional Group). In contrast, for values of k between these extremes, the time needed is N^{L+1} (Aronov et al., 2003).

2.3.2 ISI Metrics

In this study, an additional approach to estimate the dissimilarity between pairs of spike trains, in terms of the distance between them, was used to test
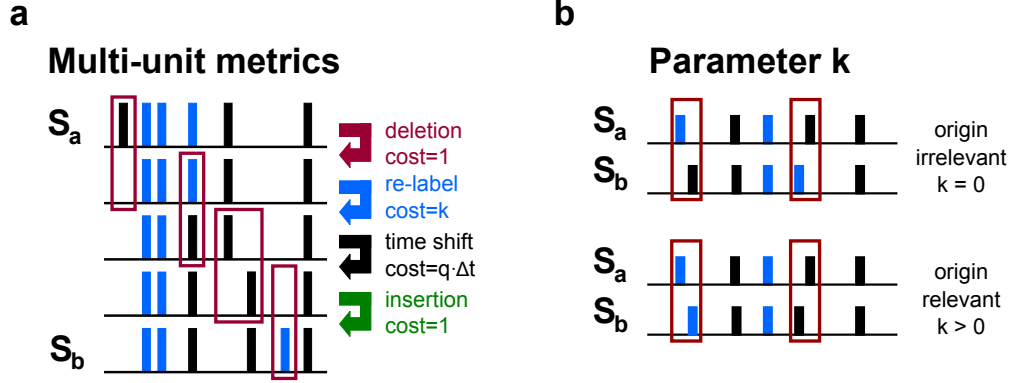
Figure 2.8: Multi-unit metrics. a) Minimal transformation pathway for a pair of spike trains elicited by two neurons to illustrate, additional to the three possible basic operations used in the single-unit metrics, the additional operation of label change. b) The additional parameter k tests the relevance of the knowledge of the neuron of origin of each spike for the encoding of information about stimulus properties.

how the activity of retinal ganglion cells encode visual information. The ISI metrics approach is based on the ratio between the interspike time intervals (ISI) of the analysed spike trains (see Figure 2.9). Here, the ISI are regarded as an instantaneous estimation of the spike firing rate and by this means, the method tests if the temporal structure of the spike firing rate of neuronal responses encodes sensory information. Furthermore, the ISI metrics uses no binning of the spike trains and therefore, it has a high time resolution that preserves the exact time stamps of single spikes. Thereby, allowing the visualisation of the relative timing of a pair of spike trains. Finally, the ISI metrics is parameter free and self adaptive, so no optimisation is necessary (Kreuz et al., 2007).

For the ISI metrics, the first step to obtain the distance between two spike trains is to calculate the instantaneous ISI of both spike trains (middle section of Figure 2.9). Here, for the spike train $S_a = \{ a_1, a_2, ..., a_m \}$, the ISI is assigned to each time instant t based on Equation 2.2.

$$S_a^{ISI}(t) = arg\ min\{a_i | a_i > t\} - arg\ max\{a_i | a_i < t\},\ a_1\ <\ t\ <\ a_m \quad (2.2)$$

Once the time resolved ISI sequences $S_a^{ISI}(t)$ and $S_b^{ISI}(t)$ are obtained, the ratio between these two series, $I(t)$, has to be calculated based on Equa-
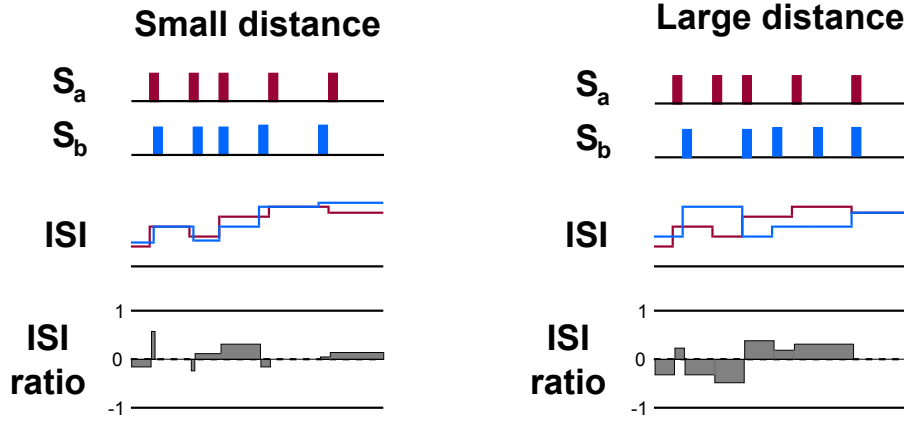
Figure 2.9: ISI metrics. Pairwise distance between similar (left) and dissimilar (right) spike trains. Instantaneous interspike intervals for the spike trains (middle). The integral in time of the interspike interval ratio defines the distance between spike trains.

tion 2.3.

$$
I(t) = \begin{cases} \frac{S_a^{ISI}(t)}{S_b^{ISI}(t)} - 1 & if \ S_a^{ISI}(t) \le S_b^{ISI}(t) \\ -(\frac{S_b^{ISI}(t)}{S_a^{ISI}(t)} - 1) & else \end{cases} \tag{2.3}
$$

The ratio obtained by Equation 2.3 is normalised. In this sense, it becomes zero in case of iso-frequent behaviour, and approaches -1 if $S_b^{ISI}(t)$ is infinitely greater as $S_a^{ISI}(t)$. Conversely, it approaches 1 if the opposite happens (lower section of Figure 2.9).

Finally, the pairwise distance, $D^{ISI}(S_a, S_b)$, between spike trains S_a and S_b is obtained by integrating in time the absolute value of the ISI ratio, as illustrated in Equation 2.4 (area inside the curves in the lower section of Figure 2.9).

$$
D^{ISI}(S_a, S_b) = \int_{t=0}^{T} |I(t)| dt \tag{2.4}
$$

The ISI metrics was applied to analyse the responses of individual and small populations of retinal ganglion cells that were recorded by performing the motion experiment protocol in turtle retinae. Here, as in the case of the spike cost-based metrics, the analyses involving the activity of small populations of retinal ganglion cells tested the relevance of the knowledge of the neuron of origin of each spike for the encoding of information about visual

stimulus, i.e., $k = \{ 0, 2 \}$. These analyses were carried out as described in the previous section.

2.3.3   Stimulus-Dependent Clustering

So far, the different methods to quantify the dissimilarity between pairs of spike trains from single and small populations of retinal ganglion cells have been described. Nevertheless, in order to quantify the extent to which distances between individual responses of retinal ganglion cells depend on the stimuli, the clustering approach proposed in Victor and Purpura (1996) to assign responses to stimulus classes was utilised in this study. The proposed clustering method works in an unsupervised way, makes no further assumptions and uses only the spike train pairwise distances for the classification of the responses. Here, the latter two properties of the clustering method are the strongest arguments why this method was utilised in this study. For the case of spike cost-based metrics, this is because two parameters (i.e., q and k) were used to test different features of the responses of retinal ganglion cells and therefore, it was desired to trace the effect of these parameters on the encoding of information about features of visual stimuli. On the other hand, if the classification results obtained with the spike cost-based metrics and the ISI metrics are to be compared, the results should be obtained using the same clustering methods.

For spike cost-based metrics and ISI metrics, the pairwise distance for all spike trains $S_{\beta,\alpha}$, was obtained. Here, β refers to the spike train label ($1 \geq \beta \geq n$, for n spike trains), and α to the stimulus class ($1 \geq \alpha \geq c$, for c stimulus classes) that provoked the response. In turn, all pairwise distances between spike trains were organised in a n x n distance matrix (see left section of Figure 2.10).

In order to perform the stimulus-dependent clustering, the mean distance of each spike train to the spike trains elicited by each stimulus class has to be calculated. This mean distance is denoted as $\hat{d}(S_\alpha)$, and can be obtained as illustrated in Equation 2.5. Here, for the calculation of $\hat{d}(S_\alpha)$, the spike train under study (S) is excluded from the responses (S') considered for each stimulus class.

$$\hat{d}(S_\alpha) = [\langle (D(S, S'))^z_{S' \ elicited \ by \ \alpha} \rangle]^{1/z} \qquad (2.5)$$

After all distance averages between the spike train S, and all other spike trains S' elicited by the different c stimulus classes are obtained, the spike train S will be assigned to the stimulus class γ for which the average distance $\hat{d}(S_\gamma)$ is the minimum of all average distances $\hat{d}(S_c)$. In this concern, $\langle \ \rangle$ in

Equation 2.5, refers to the distance average across spike trains generated by the stimulus class α. Moreover, the distances in Equation 2.5 are averaged following a power transformation by means of the exponent z. Here, negative values of z will bias the average to the shortest distance between S and the responses provoked by α and therefore, will assign the spike train S, to the stimulus class with the closest match. Conversely, for large positive values of z, the spike train S will be assigned to the stimulus class for which the distance to the furthest outlier is minimized. For this study, $z = 1$ was used.

In the case that more than one stimulus class show the minimum average distance, the spike train would be assigned to all of these stimulus classes. Therefore, the occurrence frequency f in which a spike train is assigned to a certain stimulus class will be inversely proportional to the number of classes p to which this spike train is assigned, i.e., $f = 1/p$. This consideration is important because in order to keep track of how spike trains were assigned to stimulus classes, the occurrence frequency f serves as the input for a c x c confusion matrix. This matrix will begin with all of its cells having a value of zero and then, each time a spike train elicited by a stimulus class α is assigned to a stimulus class γ, the occurrence frequency f will be added to the value contained in the cell (γ, α) of the c x c matrix (confusion matrix in Figure 2.10).

2.3.4 Performance Assessment

In order to quantify the degree in which the responses of retinal ganglion cells allow the estimation of the visual stimulus that evoked them, the estimation performance yielded by the analysis methods used in this study had to be assessed. This assessment was achieved by two different measures; the correct estimation percentage and the estimation mean absolute error.

Correct estimation percentage

The correct estimation percentage (Equation 2.6) was chosen as performance measure because it allows to compare easily the estimation performance of different analysis methods, coding strategies and joint activity coding hypotheses. Furthermore, its calculation is fast and the results can also be easily interpreted.

For Equation 2.6, γ is the stimulus class to which a response S_β, evoked by stimulus class α, was assigned. Additionally, δ represents the delta function, where $\delta(0) = 1$, and 0 otherwise. In this sense, the calculation of the correct estimation percentage was done considering the n responses for all visual
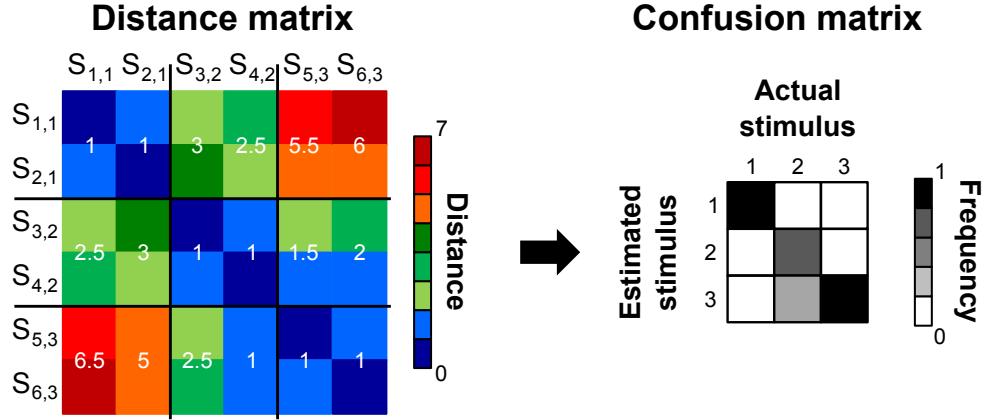
Figure 2.10: Stimulus-dependent clustering. Distance matrix whose entries correspond to the calculated pairwise distance between $n = 6$ spike trains elicited by $c = 3$ stimulus classes (left). Confusion matrix whose entries correspond to the normalised occurrence frequency in which a spike train elicited by the α stimulus class (actual stimulus) is assigned to a γ stimulus class (estimated stimulus). Each spike train is assigned to the stimulus class γ for which the mean distance across spike trains $\hat{d}(S_\gamma)$ (white numbers inside the distance matrix) has its minimum.

stimulus features recorded in the experiments.

$$E^c(n) = \frac{100}{n} \sum_{\beta=1}^{n} \delta(\gamma(S_\beta) - \alpha(S_\beta)) \tag{2.6}$$

In this study, different features, i.e., stimulus classes, of the visual stimulus presented to the retinae were estimated based on the responses of retinal ganglion cells. Here, the estimated features depended on the experiment protocol that was used. For instance, the motion experiment protocol involved the estimation of the motion velocity and the motion direction of the moving stimulus, as well as the instantaneous velocity changes. On the other hand, for the light-motion experiment protocol, the intensity of the projection light and the instantaneous changes in light intensity were estimated, additional to the motion stimulus features.

One of the drawbacks of the correct estimation percentage measure is that small deviations in the estimation of the stimulus features have the same influence in the percentage of correct estimations as large deviations. Additionally, because velocity is described as a speed in a given direction, the sole estimation of the stimulus motion velocity would not be sufficient to

gain knowledge about the type of information that is encoded in the activity of retinal ganglion cells. Therefore, the assessment of the performance in the estimation of motion direction, in the case of the estimation of motion features, is necessary to understand better which kind of information is encoded in the activity of retinal ganglion cells. In this sense, for the assessment of the estimation performance for motion direction (Equation 2.7), slight modifications to Equation 2.6 were necessary due to the fact that for the different velocities values used in both protocols, only three motion directions were possible; -1 and 1 for negative and positive velocities, respectively, and 0 for absence of movement (see Equation 2.8).

$$E^d(n) = \frac{100}{n} \sum_{\beta=1}^{n} \delta(sign(\gamma(S_\beta)) - sign(\alpha(S_\beta))) \tag{2.7}$$

with

$$sign(a) = \begin{cases} 1 & a > 0 \\ 0 & a = 0 \\ -1 & a < 0 \end{cases} \tag{2.8}$$

Estimation mean absolute error

Because of the drawback of the correct estimation percentage measure commented in the last paragraph, an additional measure that is more sensitive to error magnitudes was also utilised in this study. In this sense, the mean absolute error in the estimation of the visual stimulus features allows to obtain a better insight into the nature of the information encoded by the activity of retinal ganglion cells. In the case of the estimation of motion velocity, this measure is useful to understand the degree of the deviations in the estimation of motion speed, which in contrast to velocity, is a unsigned scalar quantity. Nonetheless, the calculation of the estimation mean absolute error can be also applied to the estimation of light intensities.

The calculation of the mean absolute error in the estimation of stimulus features was normalised to chance level (i.e., the expected error when the actual stimulus feature is compared with values drawn in a random manner) and was obtained using Equation 2.9.

$$E^e(n) = \frac{1}{chance} \frac{1}{n} \sum_{\beta=1}^{n} \|\gamma(S_\beta)| - |\alpha(S_\beta)\| \tag{2.9}$$

with

$$chance = \frac{1}{c^2} \sum_{v,v'=1}^{c} \| |\alpha(v)| - |\alpha(v')| \| \qquad (2.10)$$

In Equation 2.9, the mean absolute error is calculated for all the n responses recorded in the performed experiments. Furthermore, the chance level was obtained considering all the c stimulus classes, e.g, velocity values in the case of motion features, of the experimental protocols.

Maximum performance index

For the motion experiment protocol, an additional analysis was carried out based on the results yielded by the activity of single RGC. Thereby, because the spike cost-based metrics allows to assess individually the relevance of different time scales by means of the parameter q (see Section 2.3.1), it was tested if the time scales involved in the encoding of a certain motion feature vary depending on the value of this feature.

The analysis consisted in calculating first, how often a stimulus value c was correctly estimated for a given time scale q (Correct Estimation Index). In turn, this index was normalised by dividing it by the number of repetitions n_c for which each of the stimulus values was presented to the retinae (Equation 2.11).

$$E^C(c) = \frac{1}{n_c} \sum_{\beta=1}^{n_c} \delta(\gamma(S_\beta) - c)) \qquad (2.11)$$

For Equation 2.11, $E^C(c)$ is the Normalised Correct Estimation Index for the stimulus class c. Here, γ is the stimulus class to which a response S_β, evoked by stimulus class c, was assigned and additionally, δ represents the delta function, where $\delta(0) = 1$, and 0 otherwise.

The next step in the analysis calculated how often a stimulus value c' was incorrectly estimated as corresponding to the stimulus class c (Incorrect Estimation Index). This index was normalised by dividing it between the number of repetitions $n_{c'}$ for which the stimulus values, not belonging to stimulus class c, were presented to the retinae (Equation 2.12).

$$E^I(c) = \frac{1}{n_{c'}} \sum_{\beta=1}^{n_{c'}} \delta(\gamma(S_\beta) - c)) \qquad (2.12)$$

The Normalised Incorrect Estimation Index $E^I(c)$ was used as a penalty factor for the analysis. Hence, it was subtracted from one. In turn, the

value obtained after the subtraction was multiplied by the Correct Estimation Index to obtain $E^p(c)$, which is a compensated version of the Correct Estimation Index (Equation 2.13).

$$E^p(c) = [1 - E^I(c)] \cdot E^C(c) \tag{2.13}$$

In this sense, in the case that for a certain time scale q a stimulus value is often correctly estimated but nevertheless, an overestimation of the same stimulus value is present, the Correct Estimation Index will decay proportional to the occurrence frequency of this overestimation.

Based on the obtained values of $E^p(c)$ for each of the stimulus classes, it was calculated how often a certain value of q allowed the maximum estimation performance across the set Q of tested time scales ($O(c, q)$ in Equation 2.14).

$$O(c, q)_{q \in Q} = \sum^q \delta(E^p(c, q) - arg\ max(E^p(c, Q))) \tag{2.14}$$

Finally, the Maximum Performance Index was obtained by calculating the $O(c, q)$ for all the analysed RGC and in turn, normalising the results by dividing them by the number of analysed cells n_{RGC} (Equation 2.15).

$$F(c, q) = \frac{1}{n_{RGC}} \sum_{x=1}^{x=n_{RGC}} O(c, q, x) \tag{2.15}$$

Significance of the results

For the characterisation of data or the performance of significance tests, the mean is often the statistic utilised. However, in order for the mean to give useful information about the data, the normality condition should be fulfilled. Here, it is often the case that some uncertainties arise when trying to fulfil this condition. In order to cope with this problem, the median has been proposed as a statistic capable of providing as much information about the data as the mean. Thereby, the median of a population, as in the case of the mean, has a unique value. Furthermore, it can be calculated far more quickly. However, the primary advantage of the median over the mean is that the information that can be obtained from its value is robust, regardless of the probability distribution of the data (Crowe, 1933; Savur, 1937). In this study, no assumptions were made regarding the probability distributions of the obtained results. Therefore, it appeared meaningful to use the median for the graphical representation of the data.

In this direction, the Wilcoxon sum-rank-test was utilised to assess the significance of the results (Wilcoxon, 1945). This significance test has proved

to have a similar power as the *t*-test for situations where the condition of normally distributed data is fulfilled. However, when this condition is violated, the Wilcoxon sum-rank test has proved to offer larger power advantages, especially for high skewed distributions (Bridge and Sawilowsky, 1999). The Wilcoxon sum-rank test is a non-parametric statistical paired difference test. In turn, it compares pairwise samples from independent observations in order to assess if one of the samples tend to have larger values (Hollander and Wolfe, 1999).

The assumptions of the Wilcoxon sum-rank test are:

- that the two samples are randomly and independently drawn.

- that the dependent variable is intrinsically continuous and capable of producing measures carried out to the nth decimal place.

- that the measures within the two samples have the properties of an ordinal scale of measurement.

The Wilcoxon sum-rank-test was tested to assess the significance in the difference across coding strategies and joint activity coding hypotheses, as well as to test if the results were significantly better than those expected by chance. For the test, the distributions of both samples are equal under the null hypothesis. This means that it is equally likely that an observation from sample A exceeds an observation from sample B, or that the opposite occurs. The test was run using the function *wilcox.test* in R version 2.15.0 (The R Foundation for Statistical Computing, Vienna, Austria).

Chapter 3

Results

3.1   Motion Experiment

This study aims to assess the relevance of different properties of retinal ganglion cell (RGC) activity for the encoding of information about features of moving visual stimuli. Therefore, the activity of RGC from turtle (*traquemys scripta elegans*) and carp (*cyprinus carpio*) retinae was recorded extracellularly. The approach involved the estimation of the motion velocity and the instantaneous velocity changes of a moving pattern of squares based on the responses of single and populations of RGC.

In Section 2.2.2, it has been shown that some of the recorded RGC tune their activity to different motion speeds. Moreover, some direction selective cells (DSC) were also found (Figure 2.5). Figure 3.1 shows the responses of a turtle RGC that showed a symmetrical tuning of its activity to the stimulus velocities (Non-DSC). Here, the depicted responses were elicited by five different instantaneous velocity changes. In turn, each velocity change involves a previous and a post velocity. In the case of Figure 3.1, the velocity changes are the result of five different previous velocities and a common post velocity. From the raster plots and the peristimulus time histograms (PSTH) (Figure 3.1b and c, respectively) it can be observed that although the velocity after the instantaneous stimulus changes is the same, the responses of the Non-DSC show differences. More precisely, with the exception of the '*Speed down'* condition (first column to the left in Figure 3.1), the raster plots and the PSTH show larger activity fluctuations within the first milliseconds after the instantaneous velocity changes, than the fluctuations observed for the responses' late period. This observation points out that the information carried by the activity of RGC is dynamically changing over time, and that different time intervals within the responses carry

different information about the stimulus. Moreover, based on the probability distributions of the spike count and the interspike time intervals (ISI), it could be possible to discriminate some of the velocity transitions (Figure 3.1d and e). Here, the probability distributions are measured over the 100 repetitions and considering the entire 500 ms interval of stimulus presentation (see page 44). Furthermore, although the '*Speed up*' and '*Direction change*' conditions show similar spike count probability distributions, the ISI distributions show differences that could allow to discriminate both transitions. Conversely, the '*Speed up*' and '*Speed up direction change*' conditions show similar ISI probability distributions, but nevertheless their spike count distributions show great differences. This characterisation suggests that the encoding of information about motion features is not only carried out by one feature of the responses of RGC. Here, the spike count probability distribution points out the relevance of the number of fired spikes for the encoding of stimulus information, whereas the ISI probability distribution indicates the importance of one feature of the temporal structure of the responses of RGC.

As mentioned in Section 2.1.2, the stimulus used in the Motion Experiment protocol was a pattern of squares that moved with a constant velocity for 500 ms. After this period, the velocity was abruptly changed and held constant for another 500 ms and so on. Nine different motion velocities were involved in this experiment protocol. Thereby, in order to explore which kind of information is carried in distinct time intervals within the 500 ms periods, the results in this section were obtained by analysing the responses of RGC within three time intervals. These time intervals were the whole 500 ms, the first 200 ms after the instantaneous velocity change, and the last 200 ms before the next velocity change. In turn, these time intervals correspond to the transient activity (first 200 ms interval), the sustained activity (last 200 ms interval), and a mixture of both activities (500 ms interval). Moreover, the results shown in this section were obtained considering the activity of single, as well as populations of RGC of different sizes ($6 \leq n \leq 18$). To build the RGC populations, members corresponding to at least two of the groups obtained by classifying the cells based on their spike firing probability distributions, i.e., Left-, Right- or Non-DSC, were considered (see Section 2.2.2). Furthermore, three hypotheses regarding the way the activity of RGC is combined, i.e., Pooled Population, Labelled Line and Functional Group, were tested in order to assess the influence of these three combination procedures in the encoding of motion stimulus features (see Section 2.2.4).

The rationale behind the analyses performed in this study considered the assumption that responses of RGC to a certain stimulus should show some similarity as long as the stimulus remains the same and in turn, show differences as soon as the stimulus is changed. Therefore, the spike cost-
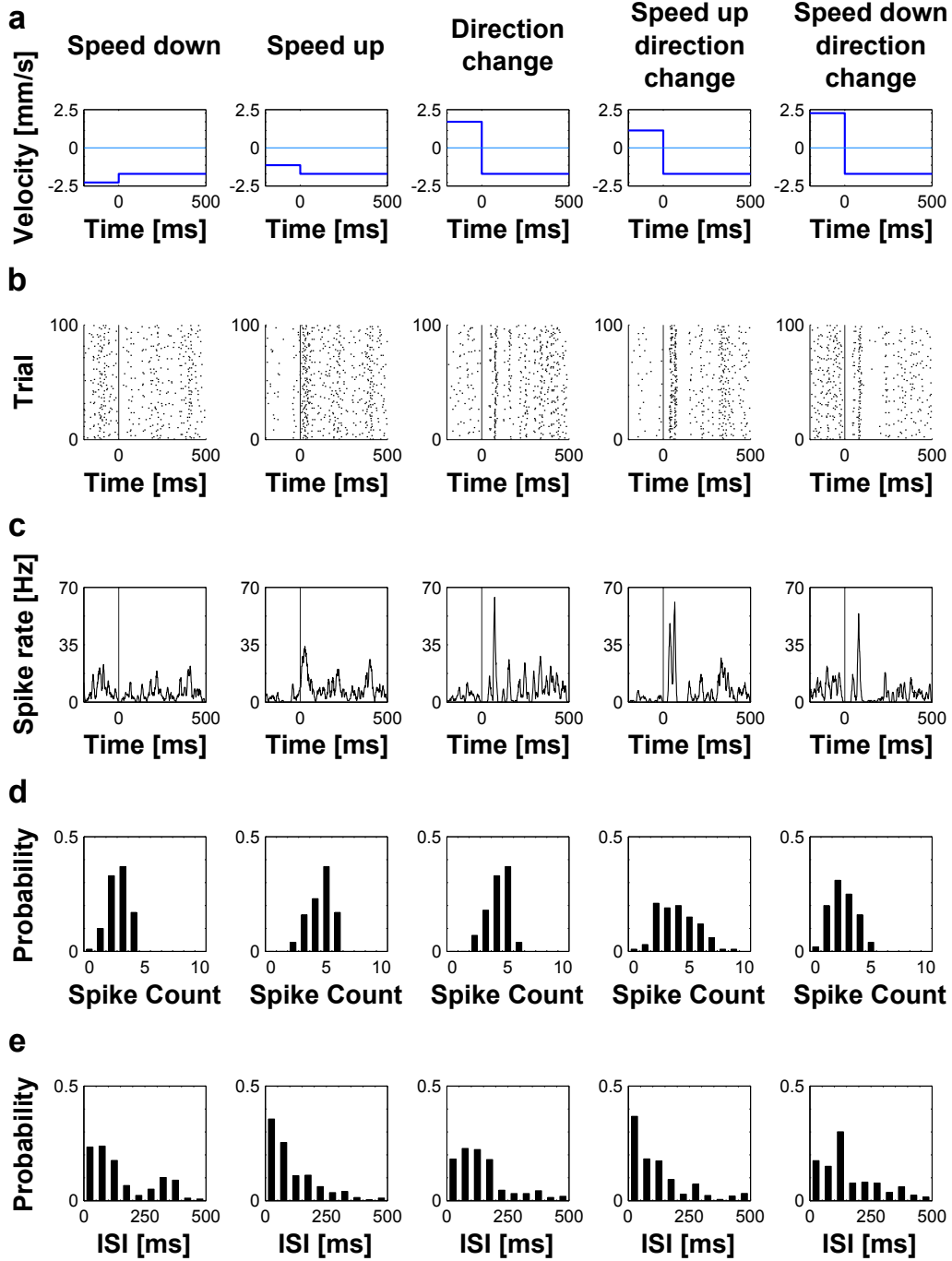
Figure 3.1: Characterisation of the responses of a turtle Non-DSC to a moving pattern of squares. a) The stimulus consisted of instantaneous velocity changes with a common post velocity. b) Raster plot of the responses of the Non-DSC for each of the trials. c) PSTH with a time resolution of 1 ms. The spike rate has been averaged across trials and smoothed with a rectangular sliding window of 10 ms. d) Spike count probability measured over all the 100 presentations, and considering periods of 500 ms and bins of 1 spike. e) Interspike time interval probability measured over all the 100 presentations, and considering periods of 500 ms and bins of 50 ms.

based metrics and the ISI metrics were applied to the responses of single, and populations of RGC to assess the similarity or difference between RGC responses evoked by the same and different stimulus features.

In the particular case of the spike cost-based metrics, the assessment of the similarity between RGC responses is performed by means of the parameter q (see Section 2.3.1). Thereby, the different values assigned to this parameter allow to explore the relevance of the spike firing rate and different time scales of the temporal structure of RGC responses, for the encoding of visual information. In the following paragraphs, some of the times the description of the results is going to be made based in a rough classification of the tested time scales. Hence, time scales in the range between 8 ms $\leq 1/q \leq 31$ ms are referred to as fine time scales, whereas the ones in the range between 62 ms $\leq 1/q \leq 250$ ms, are called medium time scales. Finally, coarse time scales are the ones falling in the range between 500 ms $\leq 1/q \leq 1000$ ms.

3.1.1   Single Cell Coding

This section describes the estimation results for the motion features of the moving pattern of squares obtained based on the activity of single RGC. Here, the representation of the estimation results obtained by the spike cost-based metrics and the ISI metrics, was done making the following considerations:

- In addition to the RGC responses obtained for the entire 500 ms interval of stimulus presentation, the activity during the transient period (first 200 ms) and the sustained period (last 200 ms) were analysed separately.

- For each of the three time intervals, the figures display the results obtained by different time scales for the spike cost-based metrics (right), and the results obtained for the ISI metrics (left).

- The depicted results correspond to the cells that were selected by the procedure described in Section 2.2.3.

- The results are individually represented for each of the three cell classes in which the cells were grouped, i.e., Left-, Right- and Non-DSC.

- For each of the cell classes, the estimation results allowed by the considered RGC of all experiments were pooled together. The procedure to assess the estimation performance is described in Section 2.3.4.

- With the exception of the post velocity, post direction and post speed (pages 90-95), the markers in the graphs correspond to the median,

whereas the error bars depict the minimal and maximal estimation performances across all considered RGC from all experiments.

- For the post velocity, post direction and post speed, the markers in the graphs correspond to the median of the estimation performance, while the error bars depict the median of the estimation performance differences between the post motion features and the motion features alone.

- The Wilcoxon sum-rank-test, considering different values of α ($\alpha > p$), was applied to assess the significance of the results (see page 67).

Velocity

For both animal species, the maximum median in the estimation performance for the motion velocity was obtained for the 500 ms interval. Here, the time scale $1/q = \infty$ led to estimation performances that reached 28.5% and 23.5% for single turtle and fish RGC, respectively.

For the *spike cost-based metrics*, the estimation performance for the motion velocity, obtained based on the activity of single RGC from both animal species, was qualitatively similar for the three analysed time intervals and the three tested RGC classes. Thereby, fine time scales led generally to estimation results that were close to the ones expected by chance, i.e., 11.11%. Nonetheless, estimation performance improved for coarser time scales, i.e., larger $1/q$ values. Thus, coarse time scales yielded generally the maximum estimation performances. Quantitatively, better estimation results were obtained when the 500 ms interval was considered for the analysis. Furthermore, the velocity estimation performances were quantitatively similar for the first and last 200 ms intervals (Figure 3.2).

In the case of single *turtle RGC*, the estimation performance for motion velocity appeared to reach a plateau at medium time scales. Moreover, the estimation performance allowed by medium and coarser time scales was significantly above chance level ($p < 0.005$). In contrast, the plateaus in the estimation performance for single *fish RGC* were less evident. Furthermore, only coarse time scales of the activity within the 500 ms and the first 200 ms intervals led to estimation results significantly above chance level for all cell classes ($p < 0.01$ and $p < 0.05$, respectively).

When applying the *ISI metrics* on the activity of turtle and fish RGC, the median of the estimation performances across time intervals was similar for each of the tested cell classes. In turn, for both 200 ms intervals, the estimation results obtained for the ISI metrics were quantitatively similar to

those obtained by the optimal time scales for the spike cost-based metrics. These results were not obtained for the 500 ms interval, which showed a tendency to yield lower estimation performances for the ISI metrics (Figure 3.2). Nonetheless, for the three tested cell classes and the three analysed time intervals, the activity of *turtle* and *fish RGC* yielded estimation results that were significantly above chance level ($p < 0.005$ and $p < 0.01$, respectively). The maximum estimation results for the motion velocity, obtained for both of the applied metrics, are summarised in the table in page 257, which can be found in the appendix of this study.

In order to gain more knowledge about the kind of information that is encoded in the activity of RGC, the estimation of velocity was further decomposed into the estimation of motion direction and speed.

Direction

The activity of single turtle RGC within the 500 ms interval led to the maximum median in the estimation performance for the motion direction. Here, the time scale $1/q = 1000$ ms led to estimation performances that reached 50.7%. In contrast, the ISI metrics led to the maximum estimation results for single fish RGC. In turn, these results reached 46.8% for the last 200 ms interval.

In the case *spike cost-based metrics*, the estimation performance for the motion direction was qualitatively similar for the three tested RGC classes and the three analysed time intervals. Thereby, fine time scales of the activity of RGC from both animal species led generally to estimation results clearly below chance level, i.e., 40.74%. As in the case of the motion velocity, coarser time scales allowed the improvement of the estimation performance, which showed to reach a plateau at medium time scales. Nevertheless, the estimation performance for medium and coarser time scales remained close to that expected by chance (Figure 3.3). The much lower than chance estimation performance yielded by fine time scales can be explained by the overestimation of the absence of movement for all velocities. This phenomenon is going to be analysed more in detail in the following paragraphs and in Section 4.2.

In the particular case of single *turtle RGC*, the median of the estimation performance was below chance level for all the tested time scales of the three cell classes in both 200 ms intervals. However, coarse time scales of the activity of DSC within the 500 ms interval, led to estimation results for the motion direction that were significantly above chance level ($p < 0.005$). In contrast, for the three tested classes of *fish RGC*, the estimation performance for motion direction was not significantly above chance level for any
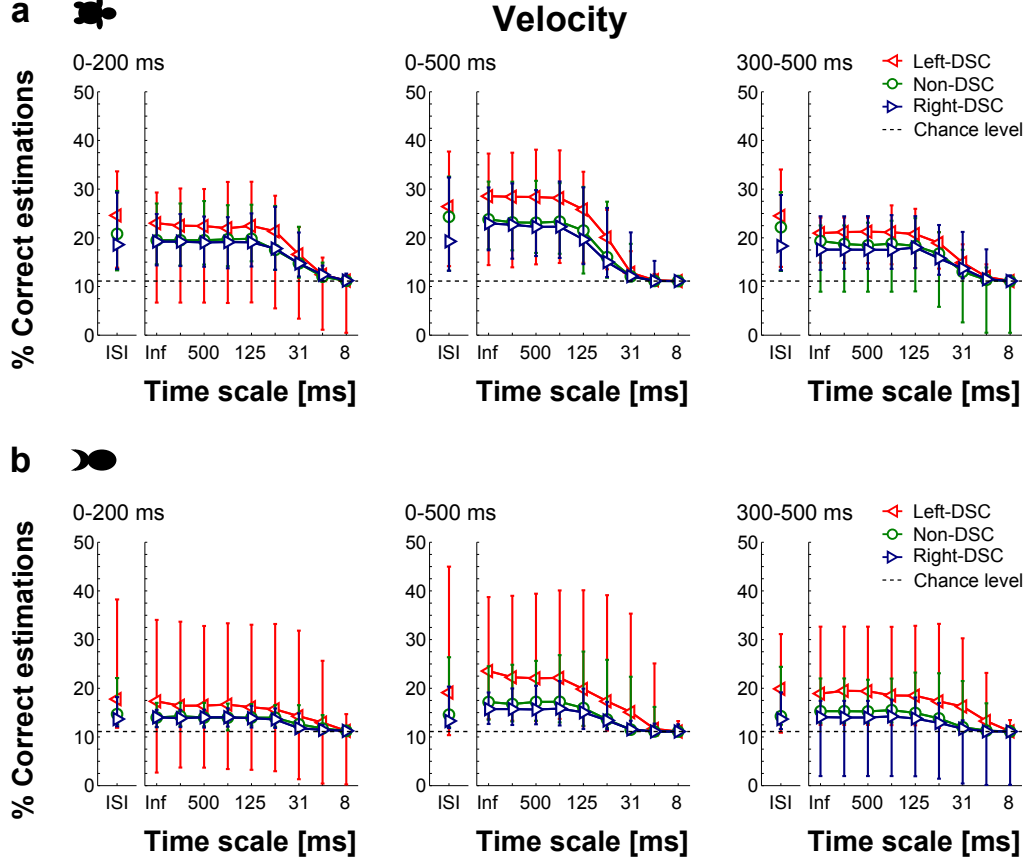
Figure 3.2: Estimation performance for the motion velocity of the moving stimulus. The estimation was carried out by applying spike cost-based metrics and ISI metrics on the activity of the selected RGC from all experiments within the three tested time intervals. Markers indicate the median, whereas error bars represent the range between maximum and minimum estimation performance. a) Turtle retinae: Three experiments; $n = 22$ Left-DSC, $n = 18$ Non-DSC and $n = 22$ Right-DSC. b) Fish retinae: Five experiments; $n = 9$ Left-DSC, $n = 14$ Non-DSC and $n = 7$ Right-DSC.

of the three analysed time intervals.

For the *ISI metrics*, the estimation performance for the motion direction was similar across the three analysed time intervals for each of the tested cell classes. Thereby, the estimation results allowed by the three tested cell classes of both animal species were close to chance level (Figure 3.3). However, in the case of *turtle RGC*, the results obtained based on the activity of Left-DSC were significantly better than those expected by chance for the three analysed intervals ($p < 0.05$). The maximum estimation results for the motion direction, obtained for both of the applied metrics, are summarised in the table in page 258.

Speed

For both animal species, the lowest median in the estimation error for the motion speed was obtained for the 500 ms interval. Here, the time scale $1/q = \infty$ led to normalised absolute errors that reached 0.6 and 0.7 for single turtle and fish RGC, respectively.

Although for the *spike cost-based metrics*, the absolute normalised estimation error for the motion speed showed quantitative and qualitative differences for both animal species, some common aspects were observed. In this sense, for the three analysed time intervals, fine time scales of the activity of all the tested RGC classes generally led to estimation errors much worse than those expected by chance. However, as in the case of the motion velocity and direction, coarser time scales led to estimation error reductions (Figure 3.4). The overestimation of the absence of movement yielded by fine time scales can explain, as in the case of motion direction, their much higher than chance estimation errors for the motion speed.

For most of the analysed *turtle RGC*, a plateau in the motion speed estimation performance was reached at $1/q \geq 500$ ms for the 500 ms interval. Moreover, coarse time scales of the activity of the three tested RGC classes within this time interval yielded estimation errors significantly below chance level ($p < 0.005$). In contrast, for both 200 ms intervals, the plateau in the estimation performance was already observed for time scales $1/q \geq 125$ ms. However, for these time scales, only the activity of Left- and Non-DSC within the first 200 ms interval led to estimation errors significantly below chance level ($p < 0.005$). In the case of *fish RGC*, coarse time scales generally led to lower estimation errors for the motion speed than fine time scales. However, estimation errors significantly below chance level were only observed for coarse time scales of the activity of Left-DSC within the 500 ms interval ($p < 0.05$).

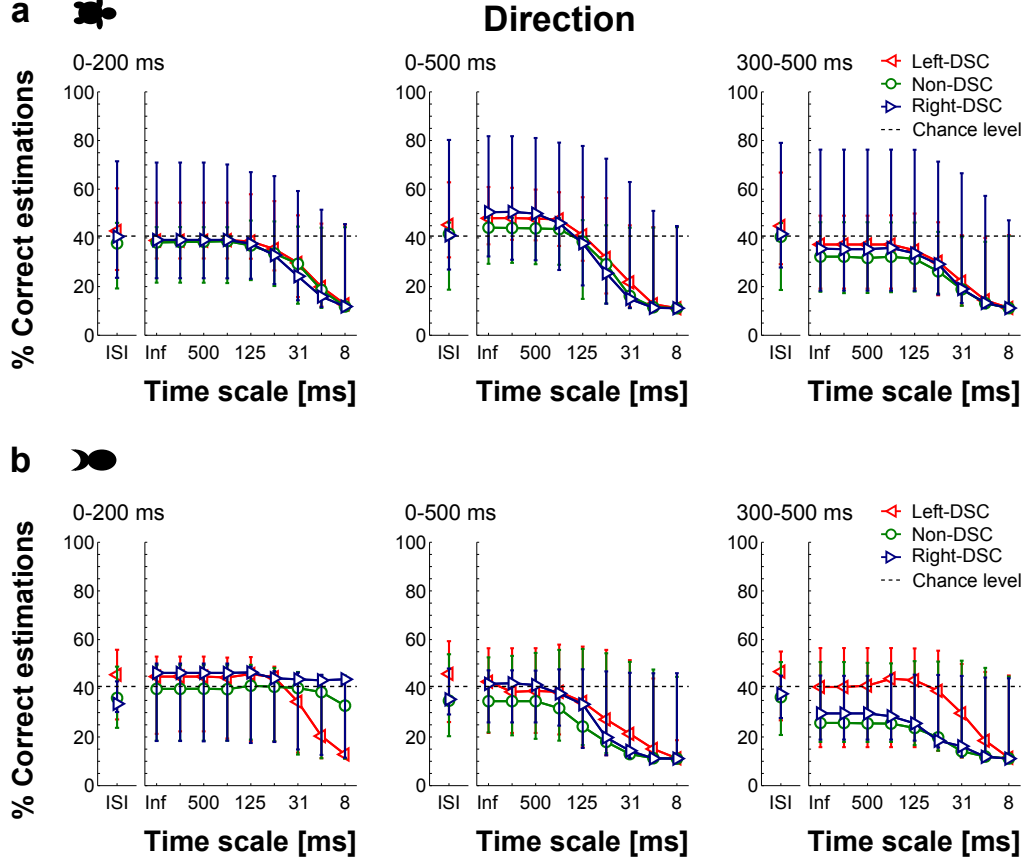Regarding the estimation errors for the motion speed obtained for the

Figure 3.3: Estimation performance for the motion direction of the moving stimulus. The estimation was carried out by applying spike cost-based metrics and ISI metrics on the activity of the selected RGC from all experiments within the three tested time intervals. Markers indicate the median, whereas error bars represent the range between maximum and minimum estimation performance. a) Turtle retinae: Three experiments; $n = 22$ Left-DSC, $n = 18$ Non-DSC and $n = 22$ Right-DSC. b) Fish retinae: Five experiments; $n = 9$ Left-DSC, $n = 14$ Non-DSC and $n = 7$ Right-DSC.

ISI metrics, some differences were observed across both animal species. Here, for the three tested *turtle RGC* classes, the median of the absolute error in the estimation of the motion speed was lower than that expected by chance for three analysed time intervals. However, only the activity of Left-DSC and Non-DSC showed a significant difference ($p < 0.05$). In contrast, for the *fish RGC*, only the activity of Left-DSC within the three analysed time intervals led to estimation errors whose median was below the chance level. However, these results were only significant for the last 200 ms interval ($p < 0.05$). The lowest estimation errors for the motion speed, obtained for both of the applied metrics, are summarised in the table in page 259.

Analysis of estimation errors

A more detailed representation of the estimation of all motion velocities, obtained by applying the spike cost-based metrics and the ISI metrics on the activity of a turtle Left- and a Non-DSC, can be observed in Figure 3.5. Here, the analysis was carried out considering the activity within the 500 ms interval. Thereby, in the case of the spike cost-based metrics, the time scale $1/q = 250$ ms was the one that allowed the best velocity estimation results for both cells. For the shown matrices, a perfect estimation of the motion velocities would draw a black diagonal on the matrix cells where the estimated and actual velocities coincide, and leave all other matrix entries blanc. In this sense, for both of the applied metrics, it can be observed that for the Left- and Non-DSC, the estimation performance was almost perfect for the absence of movement. Moreover, faster velocities were better estimated than slower ones. In contrast, the matrices of both cell classes show that slow velocities were often misclassified as absence of movement. This effect explains the worse than chance estimation performance for motion direction and speed described in pages 74- 76. Comparing both cell classes, two mirrored diagonals can be observed in the case of the Non-DSC. This finding indicates that additional to the assignment of speed values adjacent to the actual speed, errors in the estimation of velocities are due to the confusion in the motion direction. On the other hand, for the Left-DSC, the dark diagonal is clear only for velocities in the preferred direction, whereas velocities in the anti-preferred direction are mostly estimated as absence of movement. Furthermore, as in the case of the Non-DSC, errors in the estimation of velocities in the preferred direction for DSC are also due to the assignment of adjacent speed values.

In the case of the results obtained for the *spike cost-based metrics*, the time scales that allowed the maximum estimation performance for the dif-
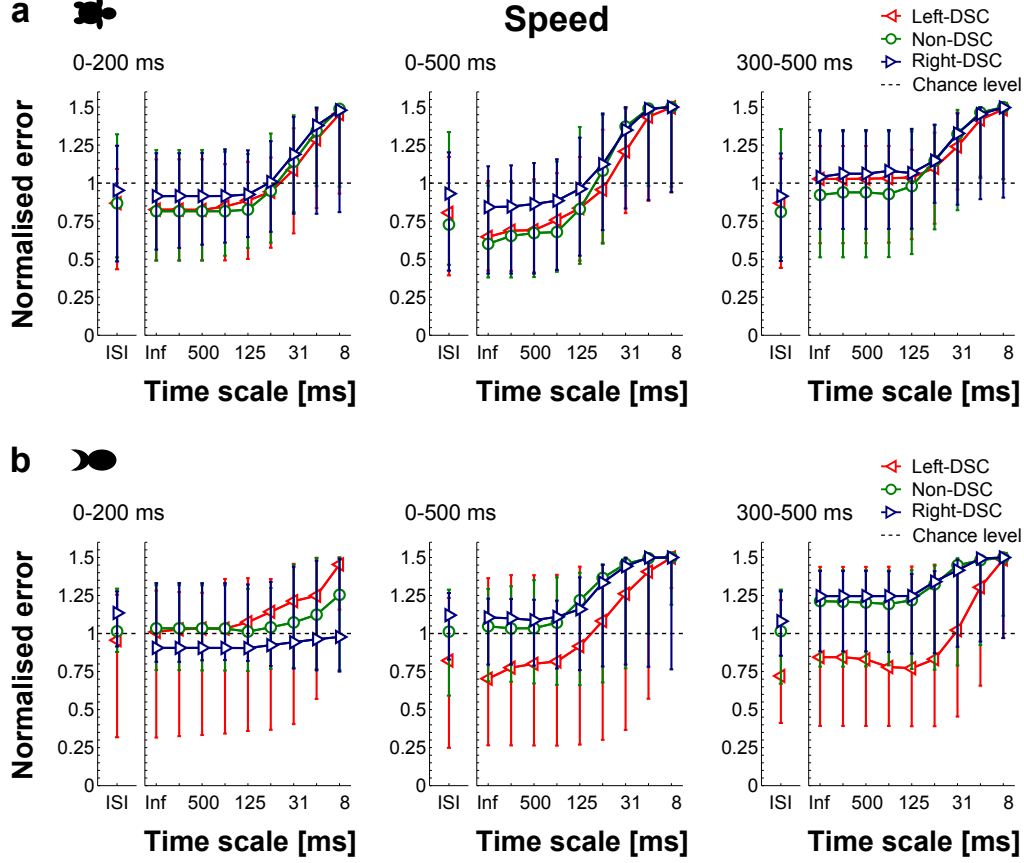
Figure 3.4: Absolute normalised estimation error for the motion speed of the moving stimulus. The estimation was carried out by applying spike cost-based metrics and ISI metrics on the activity of the selected RGC from all experiments within the three tested time intervals. Markers indicate the median, whereas error bars represent the range between maximum and minimum estimation performance. a) Turtle retinae: Three experiments; $n = 22$ Left-DSC, $n = 18$ Non-DSC and $n = 22$ Right-DSC. b) Fish retinae: Five experiments; $n = 9$ Left-DSC, $n = 14$ Non-DSC and $n = 7$ Right-DSC.
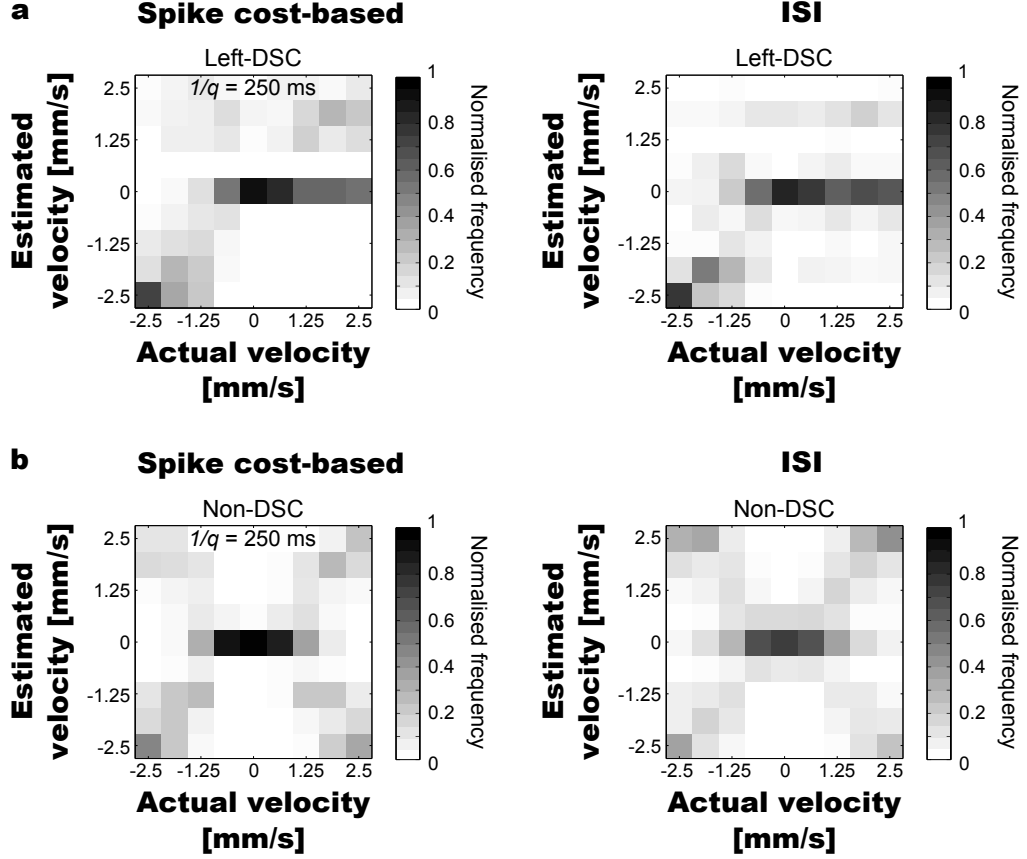
Figure 3.5: Distribution of the estimation performance for the nine motion velocities, obtained by applying the spike cost-based metrics and the ISI metrics on the activity of single turtle RGC within the 500 ms interval. In the case of the spike cost-based metrics, the time scale $1/q = 250$ ms allowed best estimation results for both of the displayed cells. In all cases, errors due to the assignment of adjacent velocities are observable. a) The activity of a Left-DSC allows better performance for velocities in the preferred direction but fails in the estimation of velocities in the anti-preferred direction. b) The activity of Non-DSC allows a good estimation of speed but fails in the estimation of the motion direction.

ferent motion velocities, directions and speeds, were variable across cells. Figure 3.6 shows the histograms of the normalised occurrence frequency with which a time scale allowed the maximum estimation performance for a certain value of the motion velocity, direction and speed for the turtle experiments (i.e., maximum performance index). In turn, these histograms were calculated based on the estimation result obtained for all the tested RGC of the three analysed turtle experiments (n =62). The procedure to compute the histograms is described in page 66.

For the 500 ms interval, time scales $1/q \geq 62$ ms allowed frequently the maximum estimation performance for all the velocities and speeds (Figure 3.6a and c). Nevertheless, besides the absence of movement, which was clearly best encoded by coarse time scales, there was not a clear tendency for either time scale to be relevant for the encoding of certain velocity or speed values. In contrast, for both of the 200 ms intervals, time scales $1/q \geq 125$ ms allowed frequently the estimation of the fastest velocities and speeds, as well as the absence of movement, whereas for the rest of the velocities and speed values, time scales 31 ms $\leq 1/q \leq 125$ ms showed a tendency to allow frequently the maximum estimation performances.

In the case of the motion direction, for the 500 ms interval, time scales $1/q \geq 250$ ms allowed frequently the maximum estimation performances for the different directions, whereas for both 200 ms intervals, these results were obtained for time scales $1/q \geq 62$ ms (Figure 3.6b).

Velocity changes

For the motion experiment protocol, additional to the estimation of the nine different velocities, it was also tested if the activity of single RGC carries information about the instantaneous velocity changes. Here, the correct estimation of each of the possible velocity changes requires the right estimation of the velocities present before and after the instantaneous transitions. Because the motion experiment protocol included nine different velocities, there was a total of 72 possible instantaneous velocity changes. In turn, this number of possible transitions leads to a low chance level, i.e., 1/72.

For both animal species, the maximum median in the estimation performance for the instantaneous velocity changes was obtained for the 500 ms interval. Here, the ISI metrics led to estimation performances that reached 10.1% and 6.7% for single turtle and fish RGC, respectively.

For the *spike cost-based metrics*, the estimation results for the instantaneous velocity changes showed some common aspects for both animal species. For instance, for each of the three analysed time intervals, similar estimation results were obtained for the three tested RGC classes. Moreover, medium
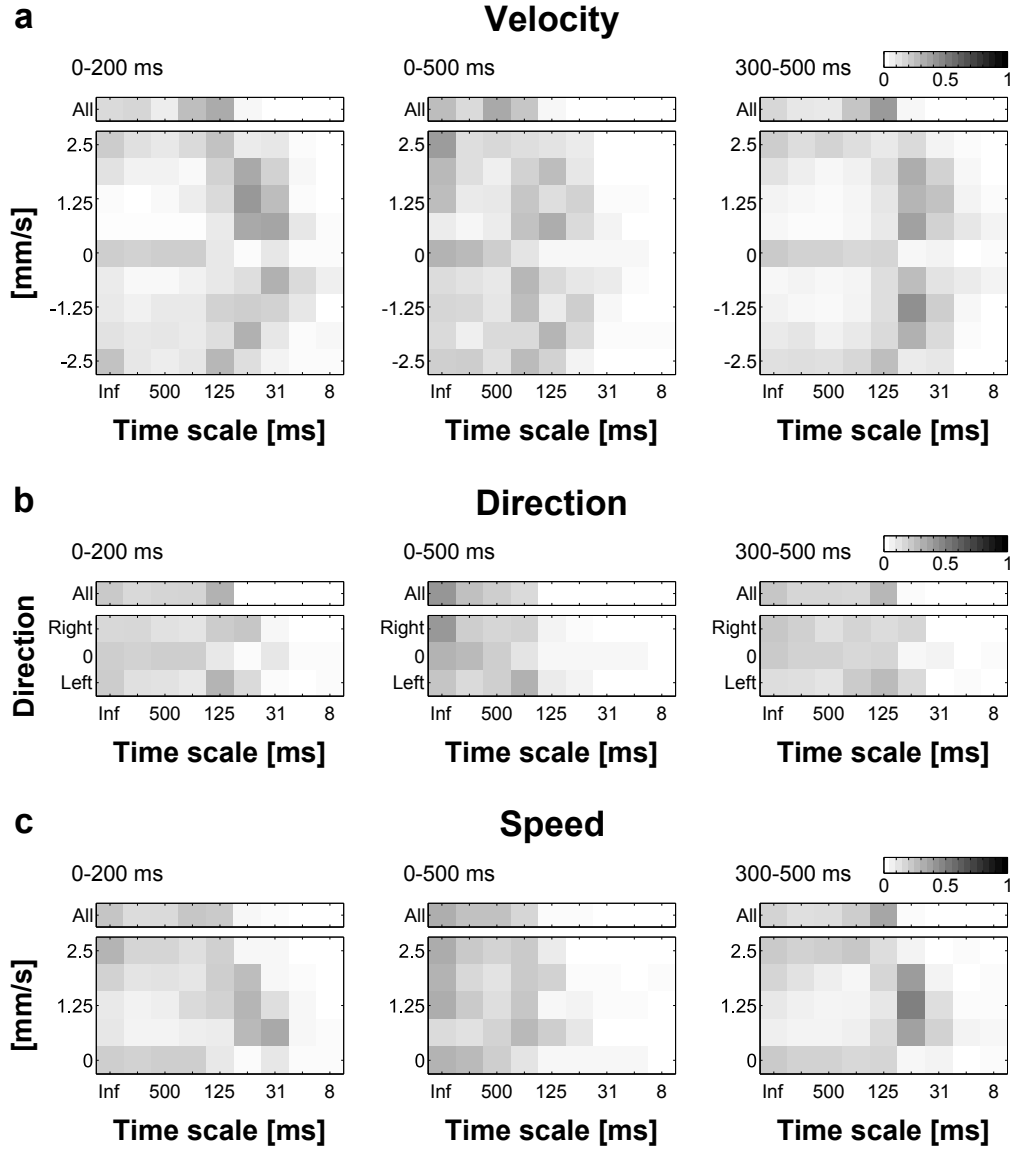
Figure 3.6: Histograms of the normalised occurrence frequency with which the tested time scales $(1/q)$ allowed the maximum estimation performance for a defined value of a stimulus motion feature. The histograms correspond to the activity of all the tested turtle RGC ($n =62$) within the three analysed time intervals. a) For each of the nine possible velocity values (bottom) and across all velocities (top). b) For each of the three possible direction values (bottom) and across all directions (top). c) For each of the five possible speeds values (bottom) and across all speeds (top).

time scales of the activity within the 500 ms interval led to the highest estimation performances. In contrast, the last 200 ms interval yielded the lowest estimation results for all time scales (Figure 3.7).

In the case of single *turtle RGC*, their activity within the three analysed time intervals led to estimation results significantly above chance level, i.e., 1.39% ($p < 0.005$). However, the 500 ms and the first 200 ms intervals led to better estimation results, for which time scales 31 ms $\leq 1/q \leq 125$ ms showed a tendency to be optimal for the encoding of information about the instantaneous velocity changes. In the case of the three tested *fish RGC* classes, although the activity within the first 200 ms led to rather poor estimation results, these were significantly above chance level for the time scale $1/q = 125$ ms ($p < 0.05$). Moreover, for the 500 ms interval, this time scale also led to the optimal estimation performance, which was in turn significantly better than chance ($p < 0.01$).

For the three analysed time intervals, the results obtained by applying the *ISI metrics* on the activity of the three tested classes of *turtle* and *fish RGC* led to estimation results significantly above chance level ($p < 0.005$ and $p < 0.01$, respectively). Nonetheless, the estimation results for the 500 ms and the first 200 ms intervals were better than those obtained for the last 200 ms interval. Moreover, for these two time intervals, these results were quantitatively similar to those yielded by the optimal scales for the spike cost-based metrics, particularly for the turtle RGC. The maximum estimation results for the instantaneous velocity changes, obtained for both of the applied metrics, are summarised in the table in page 260.

Due to the fact that the estimation of the previous and post velocities is inherent to the estimation of the instantaneous velocity changes, the estimation of these velocities was analysed separately in order to explore more in detail the information that is encoded in the activity of single RGC. Moreover, the estimation of the previous and post velocities was further decomposed in order to test if the activity of single RGC carries information about their motion direction and speed.

Previous velocity

For both animal species, the maximum median in the estimation performance for the previous velocity was obtained for the 500 ms interval. Here, the ISI metrics led to estimation performances that reached 20.4% and 19.1% for single turtle and fish RGC, respectively.

Generally, for the *spike cost-based metrics*, the activity of single RGC within the last 200 ms interval led to estimation results close to those ex-
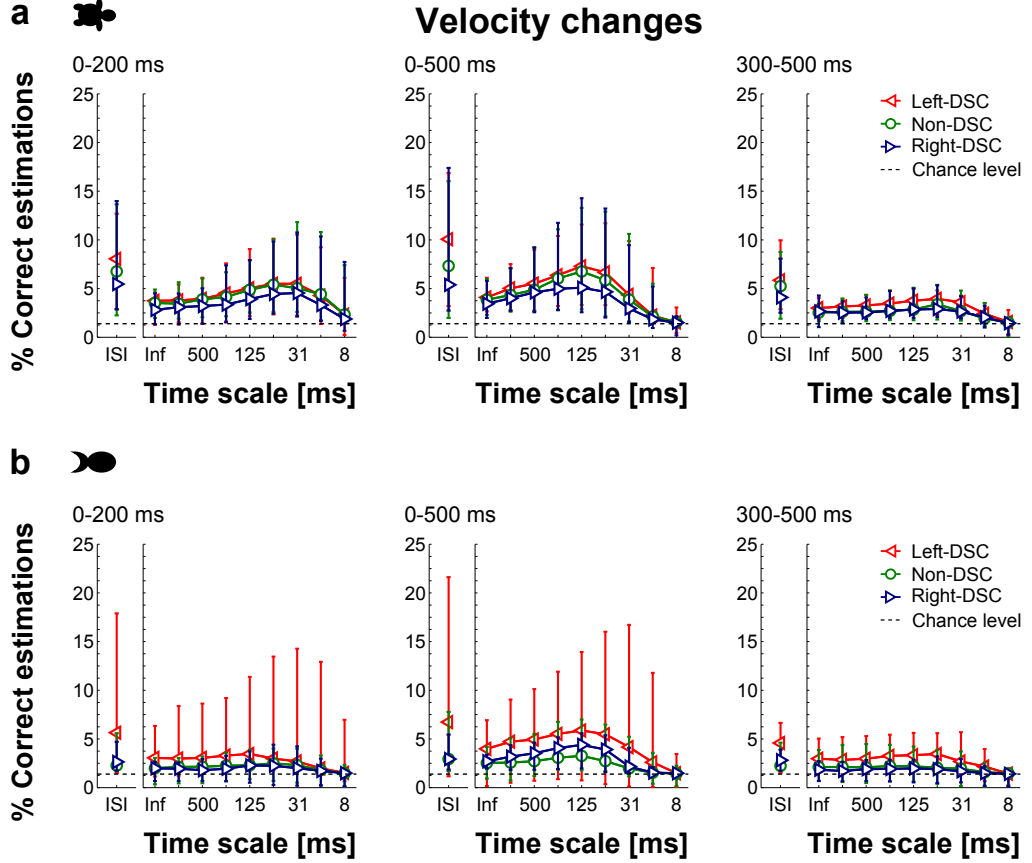
a

Velocity changes

Figure 3.7: Estimation performance for the instantaneous velocity changes of the moving stimulus. The estimation was carried out by applying spike cost-based metrics and ISI metrics on the activity of the selected RGC from all experiments within the three tested time intervals. Markers indicate the median, whereas error bars represent the range between maximum and minimum estimation performance. a) Turtle retinae: Three experiments; $n = 22$ Left-DSC, $n = 18$ Non-DSC and $n = 22$ Right-DSC. b) Fish retinae: Five experiments; $n = 9$ Left-DSC, $n = 14$ Non-DSC and $n = 7$ Right-DSC.

pected by chance. Here, the previous stimulus was already absent for 300 ms. In contrast, and particularly for time scales $1/q$ *geq* 31 ms, the activity of RGC within the 500 ms and the first 200 ms intervals allowed estimation results whose median was above chance level (Figure 3.8). Furthermore, for these time intervals, the estimation performance allowed by the optimal time scales was significantly above chance level for the three tested classes of *turtle* and *fish RGC* ($p < 0.005$ and $p < 0.01$, respectively).

In contrast, the *ISI metrics* led to estimation performances significantly above chance level for the three analysed time intervals and the three tested classes of *turtle* and *fish RGC* ($p < 0.005$ and $p < 0.01$, respectively). Here, the activity within the 500 ms and the first 200 ms intervals showed a tendency to allow better estimation results, which were in turn, quantitatively similar to those yielded by the optimal time scales for the spike cost-based metrics. The maximum estimation results for the previous motion velocity, obtained for both of the applied metrics, are summarised in the table in page 263.

Previous direction

For both animal species, the maximum median in the estimation performance for the previous direction was obtained for the 500 ms interval. Here, the ISI metrics led to estimation performances that reached 49.9% and 47.9% for single turtle and fish RGC, respectively.

The analysis of the responses of single RGC from both animal species with the *spike cost-based metrics* led to estimation results close to those expected by chance. Moreover, these was observed for all of the tested time scales of the activity within the three analysed time intervals (Figure 3.9). However, for the 500 ms and the first 200 ms intervals, and particularly for fine time scales, the estimation results obtained for the three classes of *turtle* and *fish RGC* were slightly, but significantly above chance level ($p < 0.005$ and $p < 0.01$, respectively).

In the case of the *ISI metrics*, the estimation performance for the three analysed time intervals and the three tested RGC classes from both animal species was quantitatively similar to that obtained by the spike cost-based metrics. Thereby, the 500 ms and the 200 ms intervals allowed estimation performances slightly, but significantly above chance level for the three tested classes of *turtle* and *fish RGC* ($p < 0.005$ and $p < 0.05$, respectively). The maximum estimation results for the previous motion direction, obtained for both of the applied metrics, are summarised in the table in page 263.
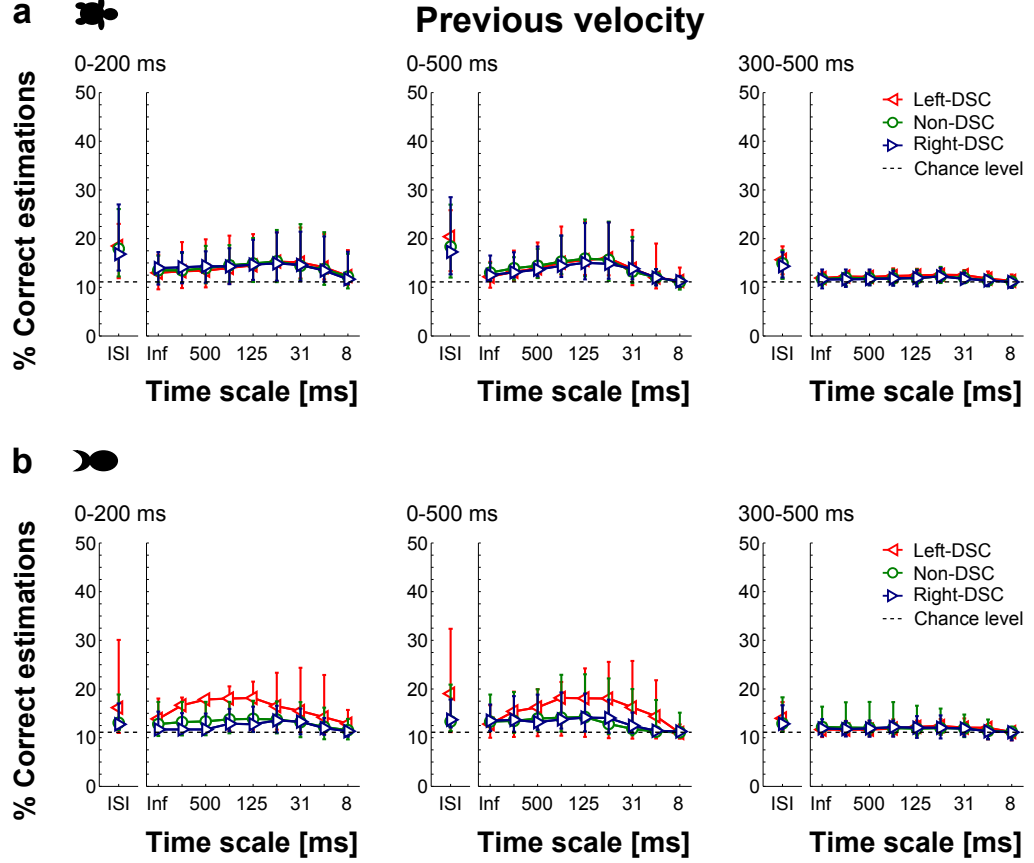
Figure 3.8: Estimation performance for the motion velocity of the moving stimulus before the instantaneous velocity changes. The estimation was carried out by applying spike cost-based metrics and ISI metrics on the activity of the selected RGC from all experiments within the three tested time intervals. Markers indicate the median, whereas error bars represent the range between maximum and minimum estimation performance. a) Turtle retinae: Three experiments; $n = 22$ Left-DSC, $n = 18$ Non-DSC and $n = 22$ Right-DSC. b) Fish retinae: Five experiments; $n = 9$ Left-DSC, $n = 14$ Non-DSC and $n = 7$ Right-DSC.
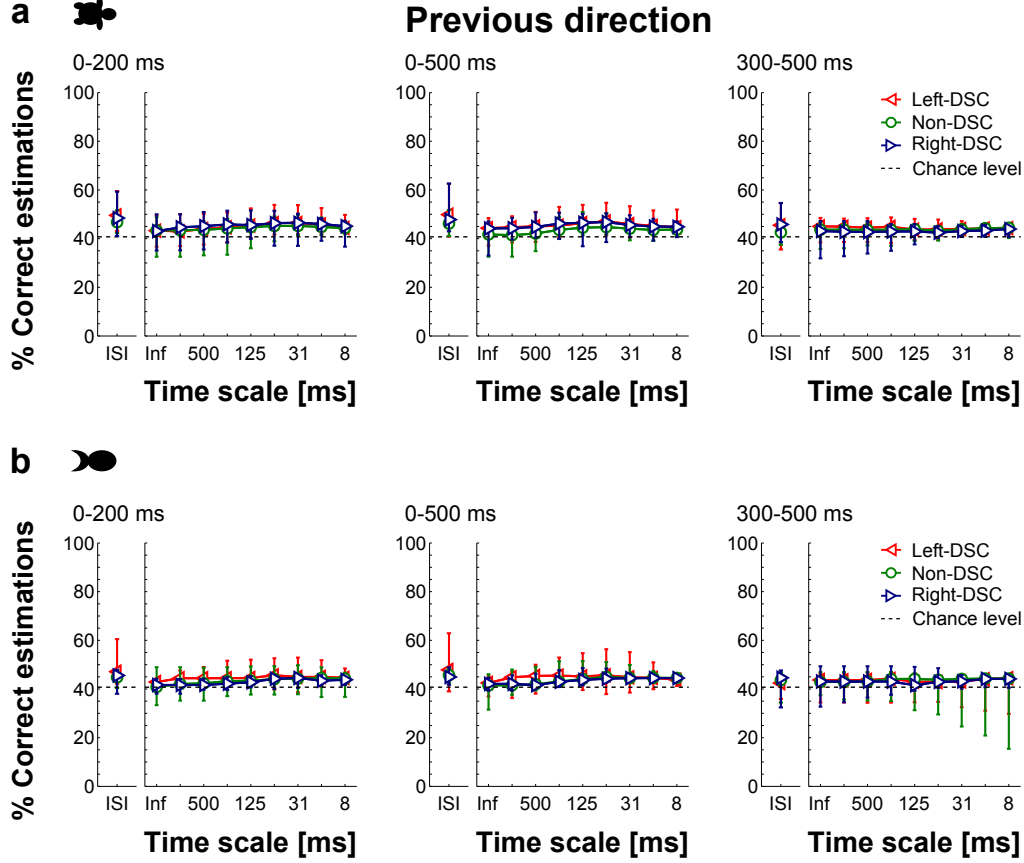
Figure 3.9: Estimation performance for the motion direction of the moving stimulus before the instantaneous velocity changes. The estimation was carried out by applying spike cost-based metrics and ISI metrics on the activity of the selected RGC from all experiments within the three tested time intervals. Markers indicate the median, whereas error bars represent the range between maximum and minimum estimation performance. a) Turtle retinae: Three experiments; $n = 22$ Left-DSC, $n = 18$ Non-DSC and $n = 22$ Right-DSC. b) Fish retinae: Five experiments; $n = 9$ Left-DSC, $n = 14$ Non-DSC and $n = 7$ Right-DSC.

Previous speed

The activity of single turtle RGC within the first 200 ms interval led to the lowest median in the estimation errors for the previous speed. Here, the ISI metrics led to normalised absolute errors that reached 0.79. In contrast, the time scale $1/q = 62$ ms led to the lowest estimation errors for single fish RGC. In turn, these errors reached 0.81 for the 500 ms interval.

The estimation errors for the previous motion speed, obtained by analysing the activity of single RGC from both animal species with the *spike cost-based metrics*, were similar to those expected by chance for the three analysed time intervals. However, the estimation results showed a tendency to be better for the 500 ms and the first 200 ms intervals (Figure 3.10). Here, in the case of the three tested classes of *turtle RGC*, the activity within these two time intervals yielded estimation errors significantly below chance level for medium time scales ($p < 0.005$). In contrast, for the three tested classes of *fish RGC*, these time scales led to significantly lower than chance estimation errors only for the 500 ms interval ($p < 0.05$).

For the *ISI metrics*, the activity of RGC within the 500 ms and the first 200 ms intervals generally led to lower estimation errors than the ones yielded by the last 200 ms interval. Moreover, for the 500 ms and the first 200 ms intervals, the estimation errors were significantly below chance level for the three tested *turtle RGC* classes ($p < 0.005$). These results were not found for *fish RGC*, for which only the activity of Left- and Non-DSC led to significantly lower than chance estimation errors ($p < 0.05$). The lowest estimation errors for the previous motion speed, obtained for both of the applied metrics, are summarised in the table in page 263.

Analysis of estimation errors

Figure 3.11 shows the distribution of the estimation performances for the nine previous motion velocities yielded by both of the applied metrics. Here, the analyses were performed considering the 500 ms interval and the same cells presented in Figure 3.11. In the case of the *spike cost-based metrics*, the time scale $1/q = 62$ ms allowed the best estimation results for both cells. In this sense, Figure 3.11 shows clear differences in the kind of information that is gained by the analyses carried on by both of the applied metrics. For the spike cost-based metrics, the estimation results yielded by the activity of the Left-DSC show an overestimation of the the fast motion velocities in the anti-preferred direction, whereas in the case of the activity of the Non-DSC, the overestimation is mostly for the absence of movement. In turn, the results obtained by applying the *ISI metrics* on the activity of both cell classes show
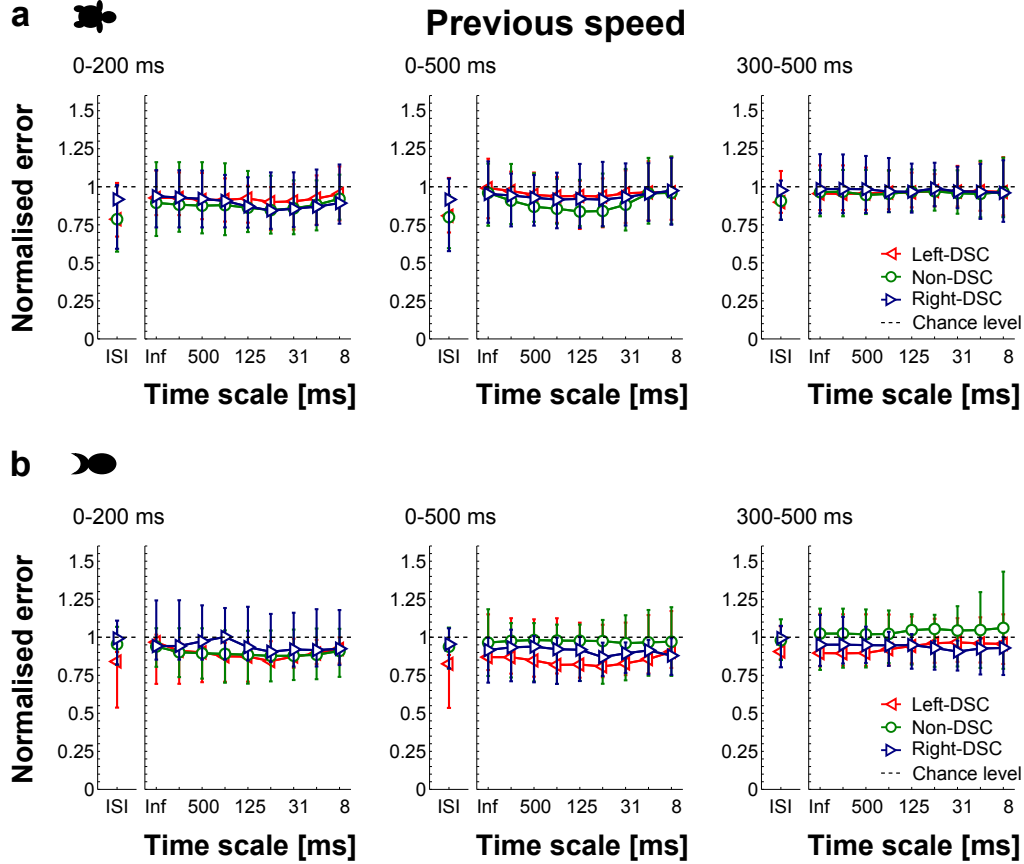
Figure 3.10: Absolute normalised error in the estimation of the motion speed of the moving stimulus before the instantaneous velocity changes. The estimation was carried out by applying spike cost-based metrics and ISI metrics on the activity of the selected RGC from all experiments within the three tested time intervals. Markers indicate the median, whereas error bars represent the range between maximum and minimum estimation performance. a) Turtle retinae: Three experiments; $n = 22$ Left-DSC, $n = 18$ Non-DSC and $n = 22$ Right-DSC. b) Fish retinae: Five experiments; $n = 9$ Left-DSC, $n = 14$ Non-DSC and $n = 7$ Right-DSC.

a qualitative improvement compared to the ones obtained for the spike cost-based metrics. Here, for the activity of the Left-DSC, the results obtained for the ISI metrics show a lower overestimation of the velocities in the anti-preferred direction and additionally, an improvement in the estimation of the velocities in the preferred direction. Moreover, the results for the Non-DSC show a lower overestimation of the absence of movement and an improvement in the estimation of the motion speed.

Figure 3.12 shows the histograms of the normalised occurrence frequency with which a time scale allowed the maximum estimation performance for a certain value of each of the previous motion features. As in Figure 3.6, these histograms reflect the results obtained by analysing the activity of all the tested turtle RGC ($n =$62) with the *spike cost-based metrics*. Here, it can be observed that medium and fine time scales are relevant for the encoding of this information. More specifically, for the 500 ms interval, the estimation performance for all motion velocity, speed and direction values, reached frequently its maximum for time scales 62 ms $\leq$ $1/q$ $\leq$ 250 ms. Conversely, for both 200 ms intervals, the maximum estimation performances for these motion features was frequently allowed by time scales 8 ms $\leq$ $1/q$ $\leq$ 125 ms (Figure 3.12).

Previous sections presented the results obtained for the estimation of the motion features of the moving stimulus without considering the stimulus history, i.e., without considering the previous motion velocity (pages 73-76). Therefore, in order to test if the information about the stimulus history would lead to better results, the motion features after the instantaneous velocity changes were estimated making this consideration. This additional analysis is motivated by the responses of RGC to different instantaneous velocity changes with a common posterior motion velocity (e.g., Figure 3.1). Here, for each of the velocity transitions, the transient period of the responses showed a similar temporal structure, which in turn showed some variability across velocity transitions. Therefore, it appears that the actual stimulus and the stimulus history have a strong influence in the temporal structure of the temporal structure of the transient period of RGC responses. In the next paragraphs, the motion features that were estimated considering the stimulus history are going to be referred with the prefix post.

Post velocity

Figure 3.13 shows the estimation performance for the post motion velocity, as well as the difference in the estimation performance when the stimulus history was not considered. Here, for both of the applied metrics, the estimation
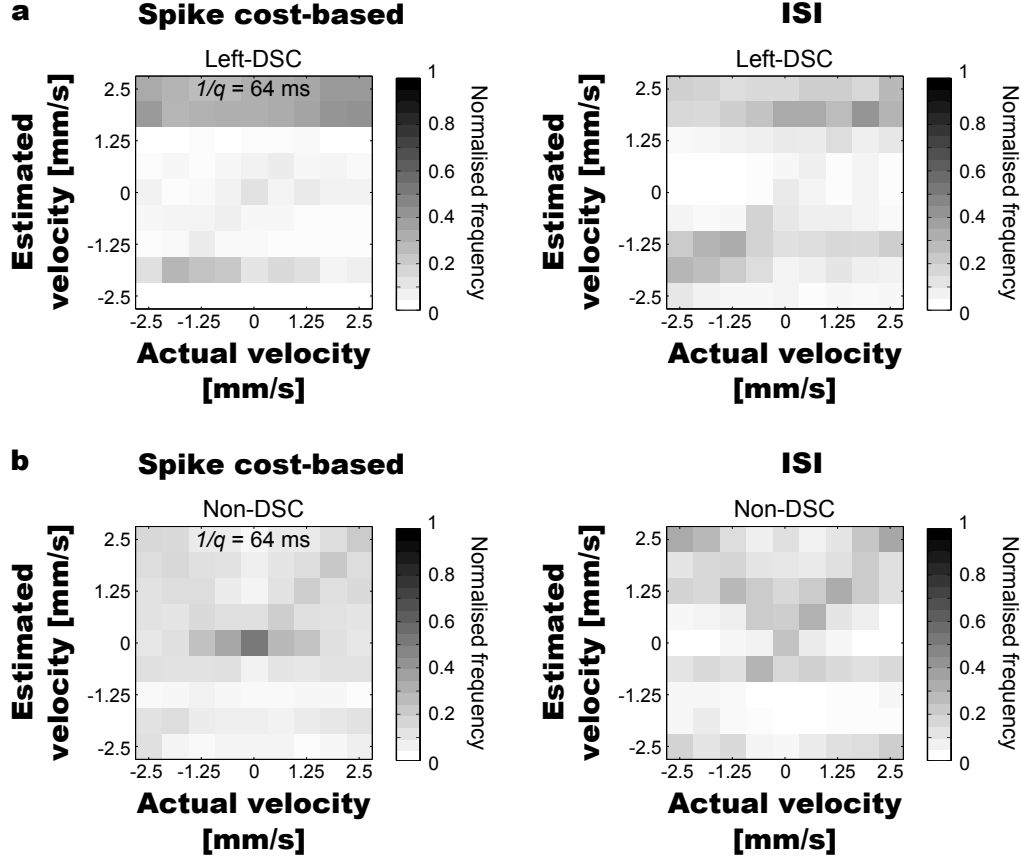
Figure 3.11: Distribution of the estimation performance for the nine motion velocities before the instantaneous velocity changes, obtained by applying the spike cost-based metrics and the ISI metrics on the activity of single turtle RGC within the 500 ms interval. In the case of the spike cost-based metrics, the time scale $1/q = 62$ ms allowed best estimation results for both of the displayed cells. In all cases, errors due to the assignment of adjacent velocities are observable. a) The activity of a Left-DSC allows better performance for velocities in the preferred direction but fails in the estimation of velocities in the anti-preferred direction. b) The activity of Non-DSC allows a good estimation of speed but fails in the estimation of the motion direction.
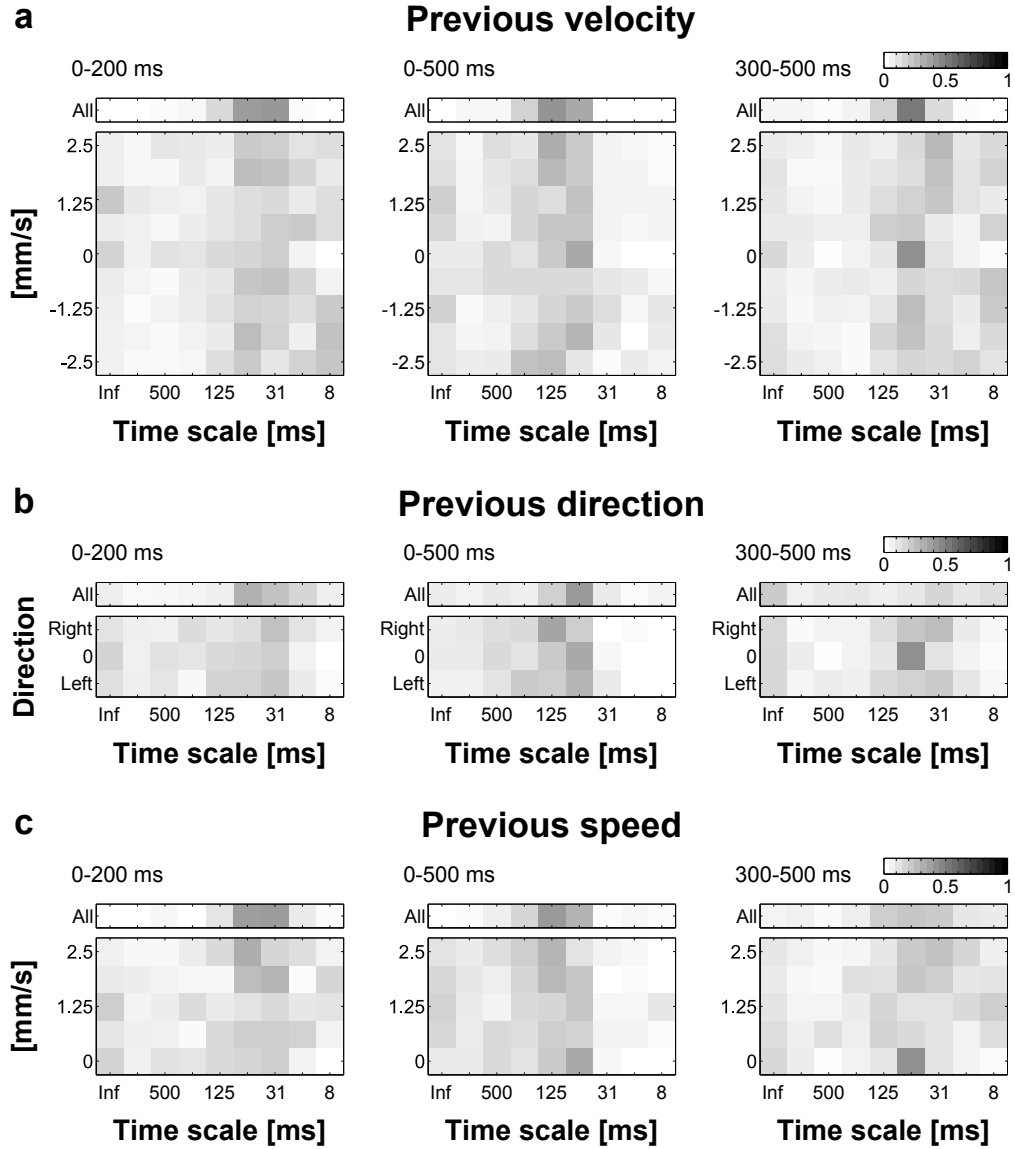
Figure 3.12: Histograms of the normalised occurrence frequency with which the tested time scales $(1/q)$ allowed the maximum estimation performance for a defined value of a stimulus motion feature. The histograms correspond to the activity of all the tested turtle RGC ($n =62$) within the three analysed time intervals. a) For each of the nine possible previous velocity values (bottom) and across all previous velocities (top). b) For each of the three possible previous direction values (bottom) and across all previous directions (top). c) For each of the five possible previous speeds values (bottom) and across all previous speeds (top).

differences were obtained individually for each of the tested RGC from both animal species. The maximum median in the estimation performance for the post velocity was yielded by the activity of RGC within the 500 ms interval for both animal species. Here, the time scale $1/q = 250$ ms led to estimation performances that reached 29.9% and 22.5% for single turtle and fish RGC, respectively.

In the case of the *spike cost-based metrics*, medium and fine time scales of the activity of the three tested classes of *turtle RGC* allowed a significant improvement in the estimation performance for the post motion velocity ($p < 0.005$). Moreover, this improvement led to estimation performances significantly better than those expected by chance for the three analysed time intervals ($p < 0.005$). In contrast, for the three tested classes of *fish RGC*, a significant estimation improvement was only observed for medium time scales of the activity within the 500 ms interval ($p < 0.05$).

Coarse time scales of the activity within the three analysed time intervals generally allowed similar estimation results for the motion velocity within and without the context of a stimulus transition. Thereby, for both animal species, coarse and medium time scales of the activity within the three analysed time intervals yielded better estimation results for the post motion velocity. In turn, these results were significantly above chance level for *turtle* and *fish RGC* ($p < 0.005$ and $p < 0.01$, respectively).

For the *ISI metrics*, the estimation results for the post motion velocity were not significantly different to those obtained for the estimation of velocity alone. Therefore, for the three tested time intervals, the estimation results for the post motion velocity were significantly above chance level for *turtle* and *fish RGC* ($p < 0.005$ and $p < 0.01$, respectively). The maximum estimation results for the post motion velocity, obtained for both of the applied metrics, are summarised in the table in page 264.

Post direction

For both animal species, the maximum median in the estimation performance for the post direction was obtained for the 500 ms interval. Here, the time scale $1/q = 500$ ms led to estimation performances up to 50% for single turtle RGC. In turn, the time scale $1/q = \infty$ led to estimation results up to 51.8% for single fish RGC.

For the *spike cost-based metrics*, medium and fine scales of the activity within the 500 ms and the first 200 ms intervals led to a significant improvement in the estimation of the post motion direction, compared to estimations not considering the stimulus history ($p < 0.05$). These results were obtained for the three tested RGC classes from both animal species (Figure 3.14).
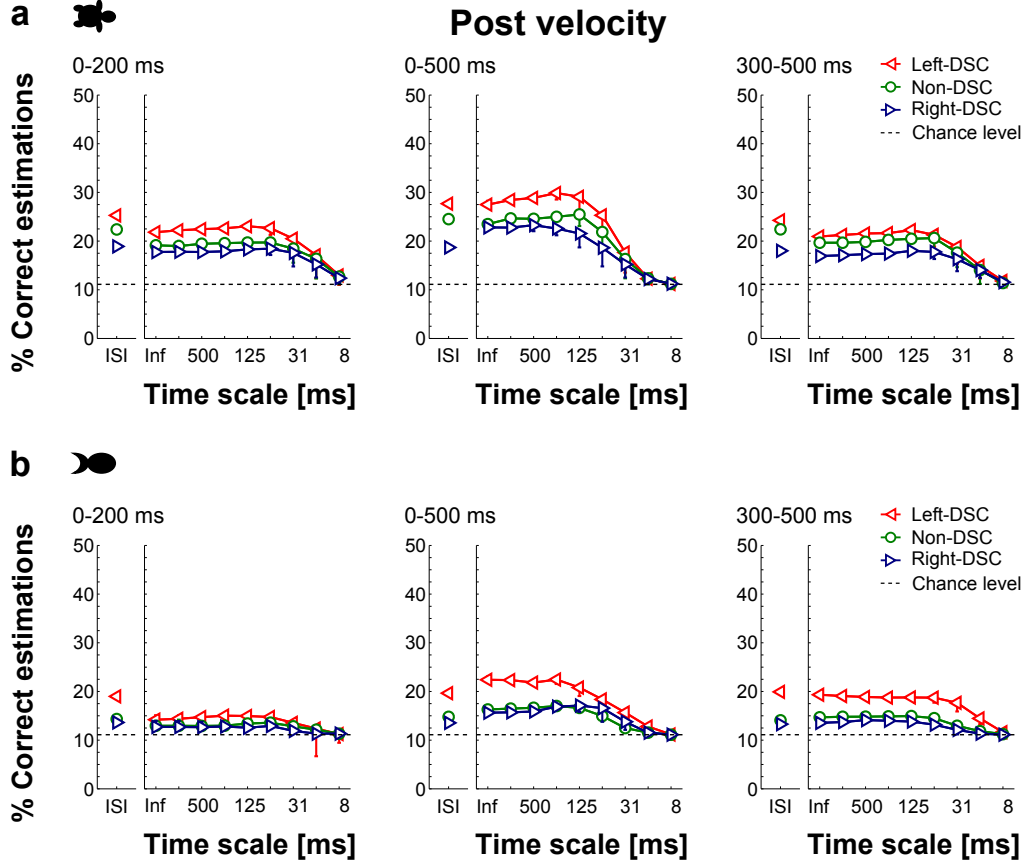
Figure 3.13: Estimation performance for the motion velocity of the moving stimulus after the instantaneous velocity changes. The estimation was carried out by applying spike cost-based metrics and ISI metrics on the activity of the selected RGC from all experiments within the three tested time intervals. Markers indicate the median of the estimation performance, whereas error bars represent the median of the differences in the estimation performance considering and disregarding the stimulus history. Downward bars indicate better estimation performance when the stimulus history is considered, while the opposite is true for upward bars. a) Turtle retinae: Three experiments; $n = 22$ Left-DSC, $n = 18$ Non-DSC and $n = 22$ Right-DSC. b) Fish retinae: Five experiments; $n = 9$ Left-DSC, $n = 14$ Non-DSC and $n = 7$ Right-DSC.

Nevertheless, in the case of *turtle RGC*, only coarse time scales of the activity of DSC within the 500 ms interval yielded estimation performances significantly above chance level ($p < 0.005$). In contrast, for *fish RGC*, estimation results significantly above chance level were only yielded by the activity of Left-DSC within the 500 ms interval ($p < 0.05$).

Applying the *ISI metrics* on the activity of RGC within the three analysed time intervals did not lead to significant differences in the estimation performance in favour of the post motion direction. These results were obtained for the three tested RGC classes of both animal species. Therefore, for *turtle* and *fish RGC*, the estimation performance for the post motion direction was not significantly above chance level. The maximum estimation results for the post motion direction, obtained for both of the applied metrics, are summarised in the table in page 265.

Post speed

For both animal species, the lowest median in the estimation errors for the post speed was obtained for the 500 ms interval. Here, the time scale $1/q = 1000$ ms led to normalised absolute errors that reached 0.57 for single turtle RGC. In turn, the time scale $1/q = 250$ ms led to estimation errors down to 0.66 for single fish RGC.

For the *spike cost-based metrics*, the reduction in the estimation errors for the post motion speed was generally allowed by medium and fine time scales of the activity of RGC within the three analysed time intervals (Figure 3.14). In turn, these reductions were significant for the three tested classes of *turtle RGC* ($p < 0.005$), whereas for *fish RGC*, significant reductions were only found for Left- and Non-DSC ($p < 0.05$). Moreover, for the 500 ms and the first 200 ms intervals, coarse and medium time scales of the activity of these cells led to estimation errors for the post motion speed that were significantly below chance level ($p < 0.005$ and $p < 0.05$ for turtle and fish, respectively).

For the *ISI metrics*, there were no significant differences between the obtained estimation errors for the post motion speed and speed alone. Moreover, these results were obtained for the activity of the three tested RGC classes of both animal species within the three analysed time intervals (Figure 3.14). Therefore, the activity of *turtle* Left- and Non-DSC was the only one that allowed estimation errors significantly below chance level for the three analysed time intervals ($p < 0.05$). In contrast, for *fish RGC*, only the activity of Left-DSC led to estimation errors significantly below chance level for the three analysed time intervals ($p < 0.05$). The lowest estimation errors for the post motion speed, obtained for both of the applied metrics,
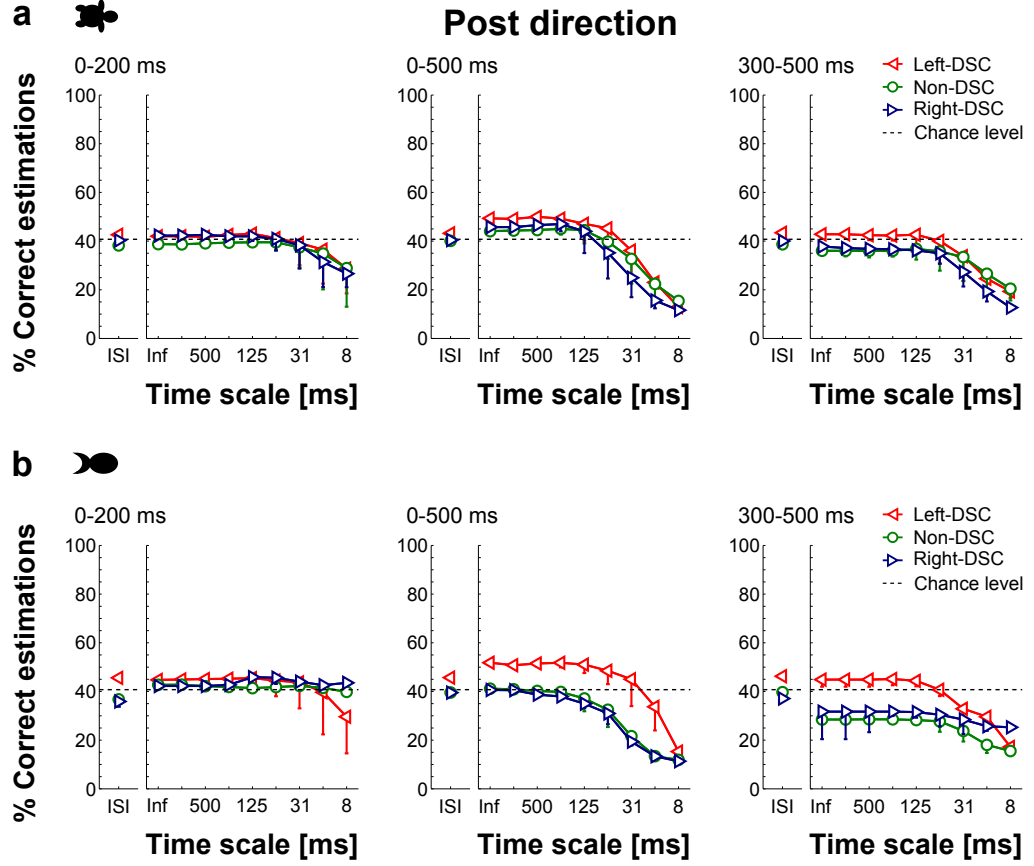
Figure 3.14: Estimation performance for the motion direction of the moving stimulus after the instantaneous velocity changes. The estimation was carried out by applying spike cost-based metrics and ISI metrics on the activity of the selected RGC from all experiments within the three tested time intervals. Markers indicate the median of the estimation performance, whereas error bars represent the median of the differences in the estimation performance considering and disregarding the stimulus history. Downward bars indicate better estimation performance when the stimulus history is considered, while the opposite is true for upward bars. a) Turtle retinae: Three experiments; $n = 22$ Left-DSC, $n = 18$ Non-DSC and $n = 22$ Right-DSC. b) Fish retinae: Five experiments; $n = 9$ Left-DSC, $n = 14$ Non-DSC and $n = 7$ Right-DSC.

are summarised in the table in page 266.

Analysis of estimation errors

The distribution of the estimation performances for the nine post motion velocities, obtained for both of the applied metrics, is shown in Figure 3.16. Here, the analyses were done considering the activity within the 500 ms interval from the same cells depicted in Figure 3.5 and 3.11. Comparing the estimation results for the motion velocities without considering the stimulus history (Figure 3.5), it can be observed that the results yielded by the *spike cost-based metrics* for the optimal time scales, show a reduction in the overestimation of the absence of movement (Figure 3.16). Moreover, for both of the displayed cells, there was an improvement in the estimation of slower motion velocities. On the other hand, in the case of the estimation results obtained for the *ISI metrics*, although the overestimation of the absence of movement for both cells was similar compared to the one obtained by disregarding the stimulus history, there was a slight improvement in the estimation of slower velocities.

For the *spike cost-based metrics*, the time scales that allowed the maximum performance for the estimation of the post motion features were variable across cells (Figure 3.17). In this sense, for the 500 ms interval, time scales $1/q \geq 250$ ms allowed frequently the maximum estimation performances for the fastest velocity and speed, as well as for the absence of movement. Furthermore, for the same time interval, the maximum estimation performance for the rest of the motion velocities and speeds was frequently allowed for time scales 62 ms $\leq 1/q \leq 250$ ms, and $1/q = \infty$. For the first 200 ms interval, time scales 16 ms $\leq 1/q \leq 250$ ms allowed frequently the maximum estimation performance for all velocities and speeds. Furthermore, for this time scale range, finer time scales showed to gain relevance for decreasing velocities and speed values. For the two fastest speeds, the time scale $1/q = \infty$ also allowed frequently the maximum estimation performance. In the case of the last 200 ms interval, the time scale $1/q = \infty$ allowed frequently the maximum estimation performance for the fastest velocities and speeds, whereas the range between 31 ms $\leq 1/q \leq 125$ ms did it for the rest of the velocities. Finally, for the absence of movement, time scales $1/q \geq 125$ ms allowed frequently maximum estimation performances for both 200 ms intervals.

In the case of the post motion direction, time scales $1/q \geq 125$ ms of the activity within the 500 ms interval frequently led to the maximum estimation performances for the different directions. In turn, for the first 200 ms inter-
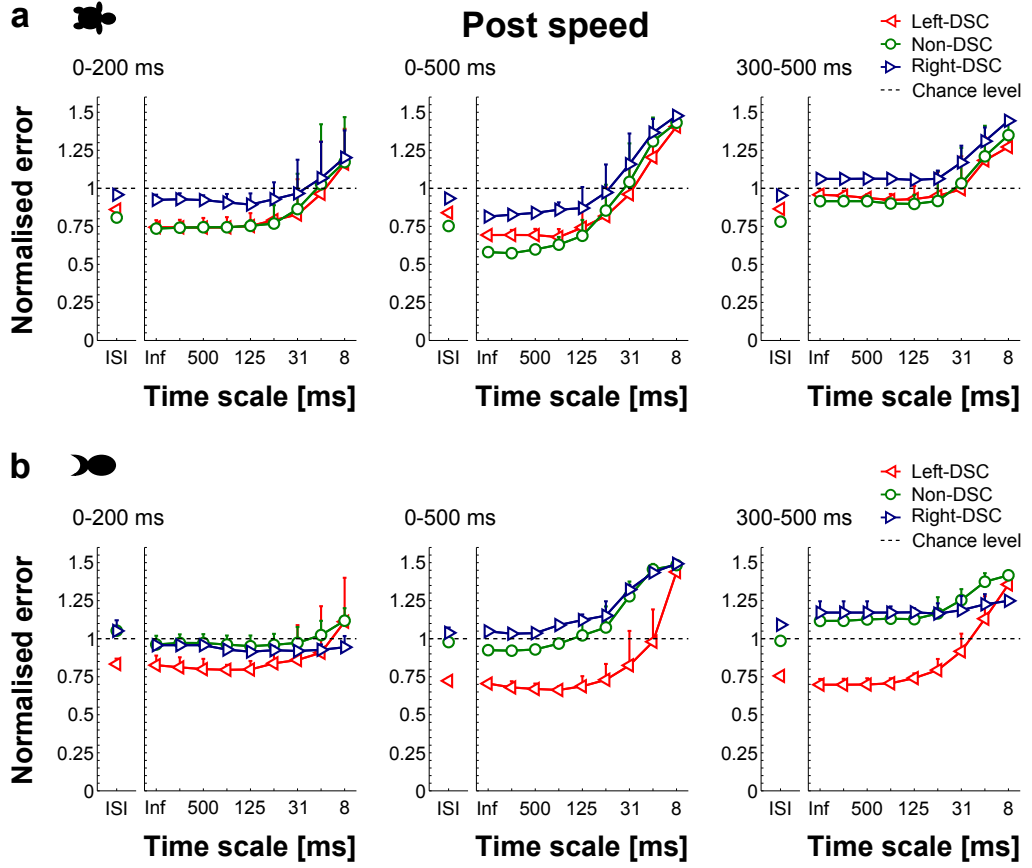
Figure 3.15: Absolute normalised estimation for the motion speed of the moving stimulus after the instantaneous velocity changes. The estimation was carried out by applying spike cost-based metrics and ISI metrics on the activity of the selected RGC from all experiments within the three tested time intervals. Markers indicate the median of the estimation performance, whereas error bars represent the median of the differences in the estimation performance considering and disregarding the stimulus history. Upward bars indicate lower estimation errors when the stimulus history is considered, while the opposite is true for downward bars. a) Turtle retinae: Three experiments; $n = 22$ Left-DSC, $n = 18$ Non-DSC and $n = 22$ Right-DSC. b) Fish retinae: Five experiments; $n = 9$ Left-DSC, $n = 14$ Non-DSC and $n = 7$ Right-DSC.
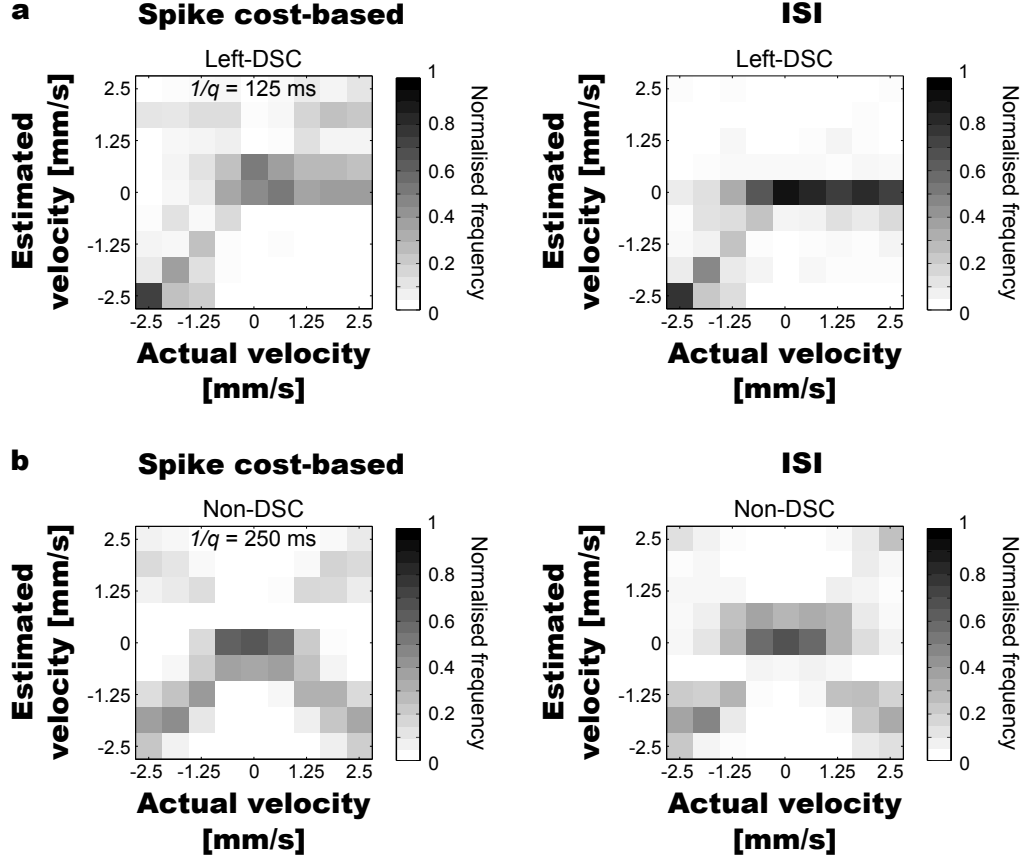
Figure 3.16: Distribution of the estimation performance for the nine motion velocities after the instantaneous velocity changes, obtained by applying the spike cost-based metrics and the ISI metrics on the activity of single turtle RGC within the 500 ms interval. In the case of the spike cost-based metrics, the time scales $1/q = 125$ ms and $1/q = 250$ ms allowed best estimation results for the Left-DSC and Non-DSC, respectively. In all cases, errors due to the assignment of adjacent velocities are observable. a) The activity of a Left-DSC allows better performance for velocities in the preferred direction but fails in the estimation of velocities in the anti-preferred direction. b) The activity of Non-DSC allows a good estimation of speed but fails in the estimation of the motion direction.

val, the maximum estimation performance for the different motion directions was frequently allowed by time scales $1/q \geq 31$ ms, whereas for the last 200 ms interval, maximum estimation performance was found for time scales $1/q \geq 62$ ms (Figure 3.17b).

Discrimination of motion feature changes

The results described in the previous sections indicate that based on the activity of some RGC, it is possible to estimate the motion velocity, and even the instantaneous velocity changes of a moving stimulus with a performance better than that expected by chance. However, this study also aimed at investigating if the activity of single RGC carries information about changes in the motion features of a moving stimulus. Thereby, because the instantaneous changes in motion velocity involve the change of at least one motion feature, it was tested if based on the activity of single RGC, it could be possible to discriminate the possible changes in the motion speed, motion direction, and the combination of changes in both features. Here, due to the design of the motion experiment protocol, the possible changes in the motion features can be individually divided by the following criteria:

Speed changes

- Increase in the motion speed regardless of the motion direction (frequency 32/72).

- Decrease in the motion speed regardless of the motion direction (frequency 32/72).

- No change in the motion speed, which implies the change of motion direction (frequency 8/72).

Direction changes

- Change in the motion direction regardless of the motion speed (frequency 32/72).

- Motion onset or motion arrest (frequency 16/72).

- No change in the motion direction, which implies the change of motion speed (frequency 24/72).
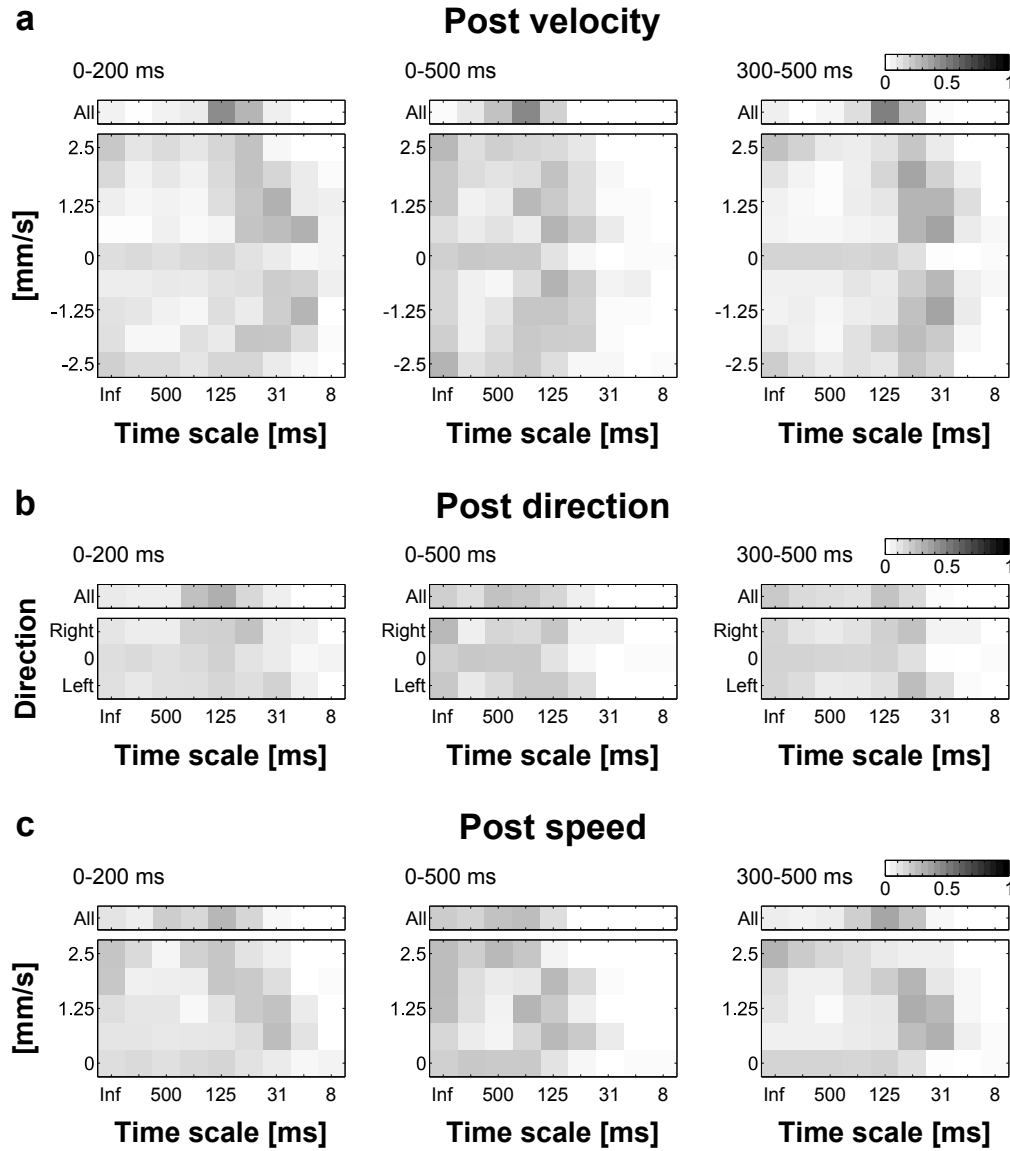
Figure 3.17: Histograms of the normalised occurrence frequency with which the tested time scales allowed the maximum estimation performance for a defined value of a stimulus motion feature. The histograms correspond to the activity of all the tested turtle RGC ($n = 62$) within the three analysed time intervals. a) For each of the nine possible post velocity values (bottom) and across all post velocities (top). b) For each of the three possible post direction values (bottom) and across all post directions (top). c) For each of the five possible post speeds values (bottom) and across all post speeds (top).

Combined speed and direction changes

- Increase in the motion speed combined with change in the motion direction (frequency 12/72).

- Increase in the motion speed combined with no change in the motion direction (frequency 12/72).

- Increase in the motion speed by motion onset (frequency 8/72).

- Decrease in the motion speed combined with change in the motion direction (frequency 12/72).

- Decrease in the motion speed combined with no change in the motion direction (frequency 12/72).

- Decrease in the motion speed by motion arrest (frequency 8/72).

- No change in the motion speed, which implies the change of motion direction (frequency 8/72).

Speed changes

For both animal species, the maximum median in the estimation performance for the three possible changes in motion speed was obtained for the 500 ms interval. Here, the time scale $1/q = 1000$ ms led to estimation performances that reached 62.6% for single turtle RGC. In turn, the ISI metrics led to estimation results up to 60.8% for single fish RGC.

The estimation results yielded by the *spike cost-based metrics* showed a tendency to be better for the 500 ms and the first 200 ms intervals (Figure 3.18). In turn, these results were found for the activity of the three tested classes of RGC from both animal species. Furthermore, for these two time intervals, coarse and medium time scales of the activity of *turtle RGC* led to estimation results significantly above chance level, i.e., 40.74% ($p < 0.005$). Although the estimation results for both animal species showed qualitative similarities, only medium and coarse time scales of the activity of *fish RGC* within the 500 ms interval allowed estimation results significantly above chance level ($p < 0.01$).

For the three analysed time intervals and both animal species, the estimation results obtained for the *ISI metrics* were quantitatively similar to the ones obtained by the spike cost-based metrics for the optimal time scales. Thus, the activity of RGC within the 500 ms and the first 200 ms intervals showed a slight tendency to allow better estimation results (Figure 3.18).

In the case of the three tested classes of *turtle RGC*, their activity within the three analysed time intervals led to estimation results significantly above chance level ($p < 0.005$). However, for *fish RGC*, estimation performances significantly above chance level for the three analysed time intervals were only yielded by the activity of Left- and Non-DSC ($p < 0.05$). The maximum estimation results for the possible changes in the motion speed, obtained for both of the applied metrics, are summarised in the table in page 267

Direction changes

For both animal species, the maximum median in the estimation performance for the three possible changes in motion direction was obtained for the 500 ms interval. Here, the time scale $1/q = 250$ ms led to estimation performances that reached 42.6% for single turtle RGC. In turn, the time scale $1/q = 1000$ ms led to estimation results up to 48.6% for single fish RGC.

With the exception of the activity of fish Left-DSC, the estimation performance obtained for the *spike cost-based metrics* was close to chance level, i.e., 35.8%. In turn, these results were found for the activity of single RGC of both animal species within the three analysed time intervals (Figure 3.19). However, for the three tested classes of *turtle RGC*, medium time scales of the activity within the 500 ms and the first 200 ms intervals allowed a slightly, but significantly better than chance estimation performance ($p < 0.05$). In contrast, for *fish RGC*, estimation results significantly above chance level for these two time intervals were only allowed by medium time scales of the activity of Left-DSC ($p < 0.05$).

The estimation results obtained for the *ISI metrics* showed quantitative similarities with the ones yielded by the optimal time scales for the spike cost-based metrics. However, only the activity of *turtle DSC* within the 500 ms and the first 200 ms intervals led to estimation performances that were slightly, but significantly above chance level ($p < 0.05$). In contrast, for the three analysed time intervals, the activity of the three tested classes of *fish RGC* classes did not led to estimation results significantly above chance level. The maximum estimation results for the possible changes in the motion direction, obtained for both of the applied metrics, are summarised in the table in page 268.

Combined speed and direction changes

For both animal species, the maximum median in the estimation performance for the seven possible combined changes in the motion speed and direction was obtained for the 500 ms interval. Here, the time scale $1/q = 250$ ms
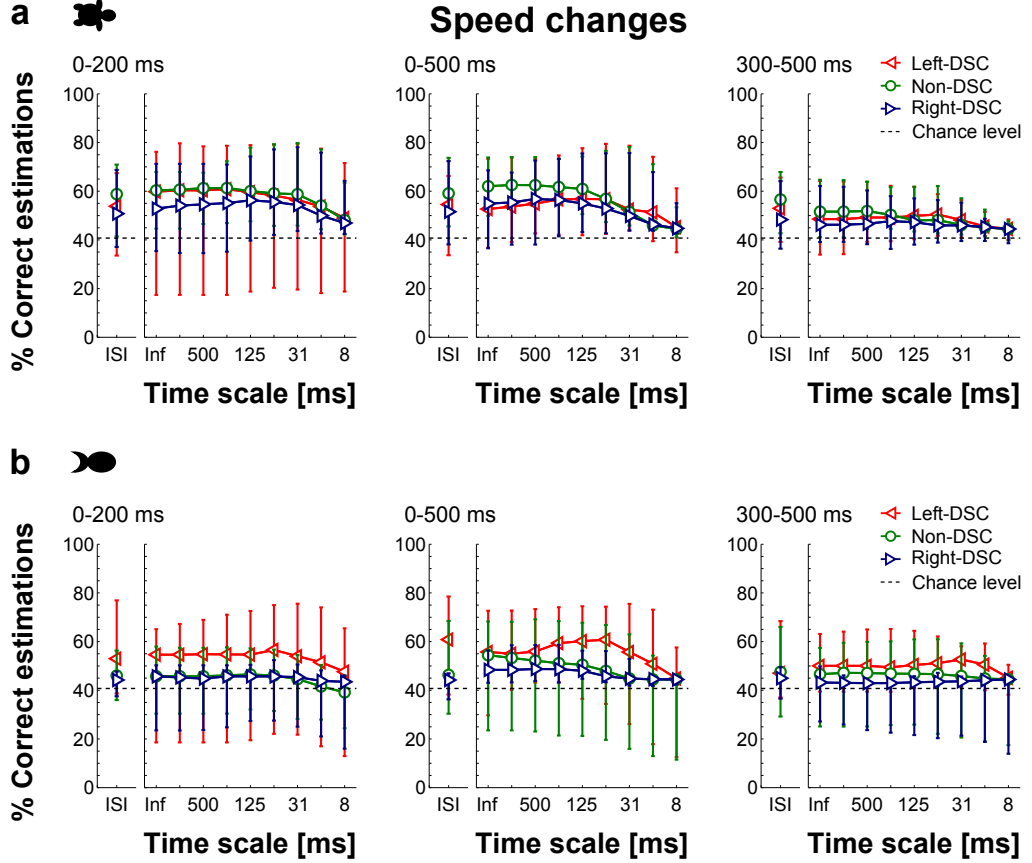
Figure 3.18: Estimation performance for the changes in the motion speed of the moving stimulus. The estimation was carried out by applying spike cost-based metrics and ISI metrics on the activity of the selected RGC from all experiments within the three tested time intervals. Markers indicate the median, whereas error bars represent the range between maximum and minimum estimation performance. a) Turtle retinae: Three experiments; $n = 22$ Left-DSC, $n = 18$ Non-DSC and $n = 22$ Right-DSC. b) Fish retinae: Five experiments; $n = 9$ Left-DSC, $n = 14$ Non-DSC and $n = 7$ Right-DSC.
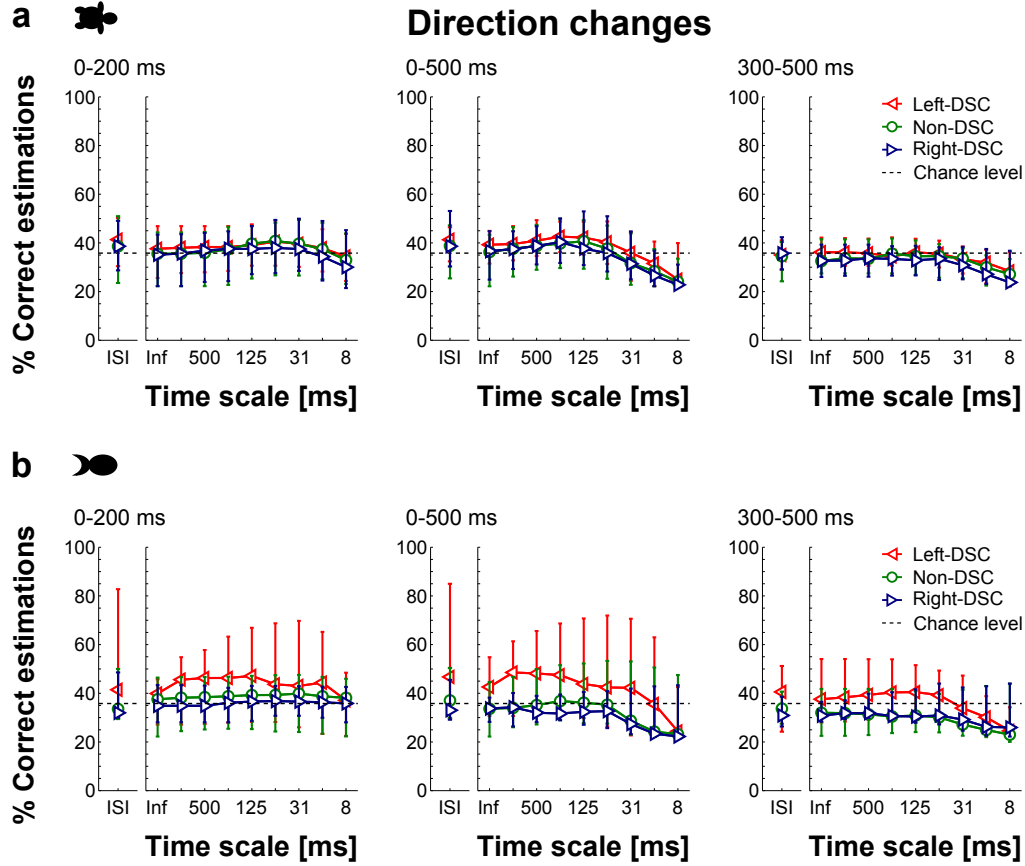
Figure 3.19: Estimation performance for the changes in the motion direction of the moving stimulus. The estimation was carried out by applying spike cost-based metrics and ISI metrics on the activity of the selected RGC from all experiments within the three tested time intervals. Markers indicate the median, whereas error bars represent the range between maximum and minimum estimation performance. a) Turtle retinae: Three experiments; $n = 22$ Left-DSC, $n = 18$ Non-DSC and $n = 22$ Right-DSC. b) Fish retinae: Five experiments; $n = 9$ Left-DSC, $n = 14$ Non-DSC and $n = 7$ Right-DSC.

led to estimation performances that reached 27.2% for single turtle RGC. In turn, the time scale $1/q = 125$ ms led to estimation results up to 28.3% for single fish RGC.

For the *spike cost-based metrics*, the estimation results for the seven possible combined changes in the motion speed and direction showed a tendency to be better for the 500 ms and the first 200 ms intervals. Moreover, for these two time intervals, medium time scales of the activity of RGC from both animal species appeared to be optimal for the encoding of information about the changes in motion features (Figure 3.20). Here, these time scales led to estimation results significantly above chance level, i.e., 14.8%, for *turtle* and *fish RGC* ($p < 0.005$ and $p < 0.05$, respectively).

The analysis by *ISI metrics* led to quantitatively similar estimation results as the ones obtained by the optimal time scales for the spike cost-based metrics. Therefore, for both animal species, the activity of RGC within the the 500 ms and the 200 ms intervals led estimation results which were better than the ones obtained for the last 200 ms interval. Moreover, for both animal species, the estimation results obtained for these two time intervals showed quantitative similarities for each of the tested classes of RGC. For the three tested classes of *turtle* and *fish RGC*, the estimation performance was significantly above chance level for the three analysed time intervals ($p < 0.005$ and $p < 0.05$, respectively). The maximum estimation results for the possible combined changes in the motion speed and direction, obtained for both of the applied metrics, are summarised in the table in page 269.

3.1.2   Joint Activity Coding

As mentioned in Section 1.2.4, there is some evidence supporting the conjecture that the combined activity of RGC encodes information about visual stimulus in a more efficient way than the activity of individual cells. Therefore, a further analysis in this study involved the estimation of motion features of a moving stimulus based on the activity of small populations of RGC. Here, in the case of the turtle experiments, three different joint activity coding hypothesis were tested; Pooled Population, Labelled Line and Functional Group (see Section 1.2.4). However, in the case of the fish experiments, due to the limited number of RGC recorded, only two joint activity coding hypotheses were tested; Pooled Population and Labelled Line. Thereby, Section 2.2.4 describes the procedure to combine the activity of RGC for each of the tested joint activity coding hypotheses.

Within the framework of multi-unit metrics, values of $k = 0$ correspond to the Pooled Population hypothesis. Here, all spikes are considered to be originated by the same neuron and thus, it is suggested that information
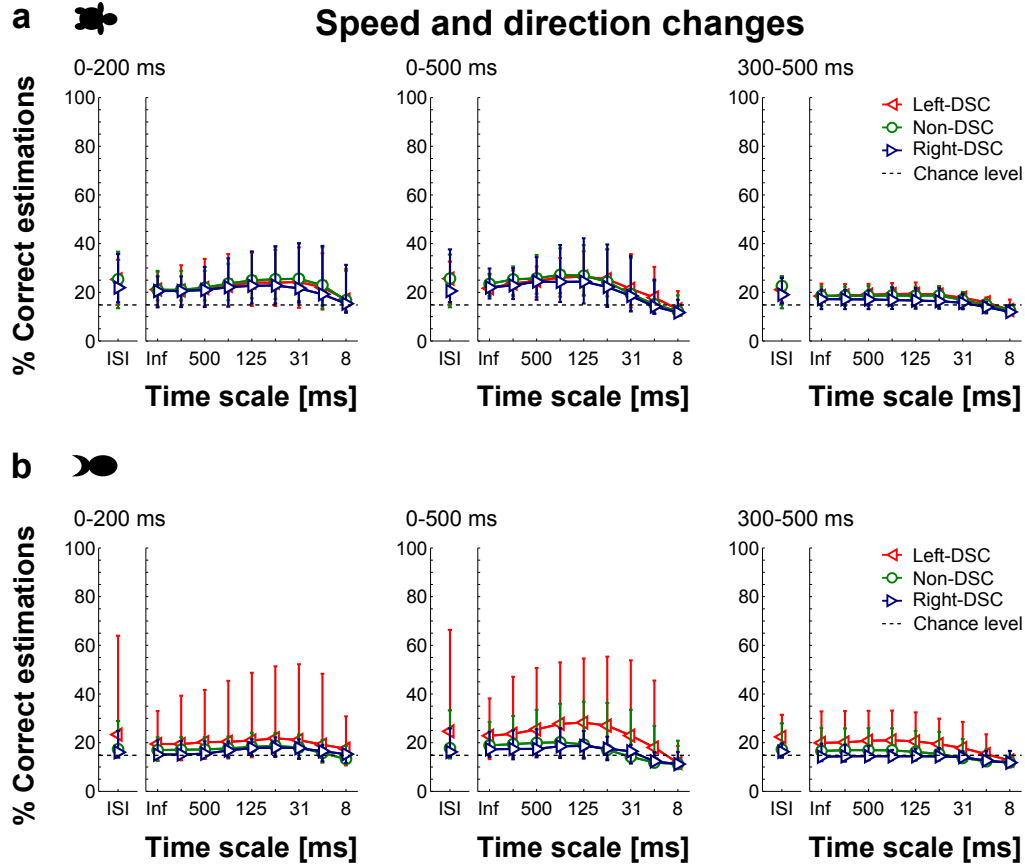
Figure 3.20: Estimation performance for the combined changes in the motion speed and direction of the moving stimulus. The estimation was carried out by applying spike cost-based metrics and ISI metrics on the activity of the selected RGC from all experiments within the three tested time intervals. Markers indicate the median, whereas error bars represent the range between maximum and minimum estimation performance. a) Turtle retinae: Three experiments; $n = 22$ Left-DSC, $n = 18$ Non-DSC and $n = 22$ Right-DSC. b) Fish retinae: Five experiments; $n = 9$ Left-DSC, $n = 14$ Non-DSC and $n = 7$ Right-DSC.

about the neuron of origin of each spike is irrelevant for the encoding of motion features. In contrast, for $k = 2$, information about the neuron of origin of each spike, either the exact neuron itself (Labelled Line hypothesis), or the neuron class (Functional Group hypothesis), is regarded as relevant for the encoding of motion features because the activity of each cell (or cell class) is considered to be independent and not interchangeable. For the spike cost-based metrics, an algorithm developed by Aronov (2003) allows to test values of $0 < k < 2$. Here, it would be assumed that spikes from different neurons are similar if their occurrence in time is sufficiently close. Nevertheless, due to the computational cost of the analysis for these values and the rather unclear interpretation of the results, the analyses shown in this section consider only values of $k = \{0, 2\}$.

For the multi-unit metrics analysis, a maximum of six cells of each class, i.e., Right-DSC, Left-DSC or Non-DSC, were considered to build the RGC ensembles. In turn, these cells were selected based on their velocity estimation performance (see Section 2.2.3). Furthermore, it has to be mentioned that the populations were built considering cells belonging to the same experiment. Thereby, for each of the turtle experiments ($n = 3$), ten ensembles of sizes $3 \leq n \leq 18$ were built, whereas for each of the fish experiments ($n = 5$), only one ensemble of size $n = 6$ was possible. With these ensembles, it was tested if the size of a RGC population has an effect on the encoding of information about motion. Moreover, because the populations consisted of the same number of RGC from each class, it was also explored if the combination of the activity of different RGC classes has an effect on the encoding of this information.

In this section, the results obtained for each of the tested hypotheses are shown separately. Thereby, for the representation of the estimation performance the following considerations were made:

- In addition to the RGC responses obtained for the entire 500 ms interval of stimulus presentation, the activity during the transient phase (first 200 ms) and the sustained phase (last 200 ms) were analysed separately.

- For each of the time intervals, figures display the results obtained by different time scales for the spike cost-based metrics (right), and the results obtained for the ISI metrics (left).

- The results correspond to populations that were built with the cells that were selected by the procedure described in Section 2.2.3.

- For each of the tested hypothesis, the results are individually represented for each of tested population sizes.

- For each of the population sizes, the estimation results allowed by the considered populations of all experiments were pooled together.

- With the exception of the post velocity, post direction and post speed (pages 142-155), the markers in the graphs correspond to the median, whereas the error bars depict the minimal and maximal estimation performances across all the populations of the same size from all experiments.

- For the post velocity, post direction and post speed, the markers in the graphs correspond to the median of the estimation performance, while the error bars depict the median of the estimation performance differences between the post motion features and the motion features alone.

- The Wilcoxon sum-rank-test, considering different values of α ($\alpha > p$), was applied to assess the significance of the results (see page 67).

Velocity

For both of the applied metrics and under the three tested joint activity coding hypotheses, the combined activity of RGC led to estimation performances for the motion velocity, that clearly surpassed the ones yielded by the activity of single RGC. Moreover, the estimation performance generally improved with larger populations of turtle RGC. However, this improvement became smaller for population sizes $n \geq 15$, being in some cases almost negligible. Generally, the 500 ms interval yielded the highest estimation performances, whereas both 200 ms intervals led frequently to similar estimation results. For the spike cost-based metrics, coarse time scales generally led to better estimation results for the the three tested joint activity coding hypotheses. In turn, the estimation of the motion velocity was qualitatively similar for both animal species under the Pooled Population hypothesis as well as under the Labelled Line hypothesis. For both animal species, the maximum median in the estimation performance was yielded by the time scale $1/q = \infty$ of the 500 ms interval. Here, the estimation performances under the Functional Group hypothesis reached 64.2% for turtle RGC. In turn, for fish RGC, the estimation results under the Labelled Line hypothesis reached 28.1%.

Pooled Population

For the *spike cost-based metrics*, fine time scales of the combined activity of RGC under the Pooled Population hypothesis generally led to poor es-

timation performances. However, the estimation performance improved for coarser time scales and appeared to reach a plateau for medium time scales. These results were observed for the three analysed time intervals and both animal species, but were more evident for turtle RGC (Figure 3.21). Furthermore, for all the tested population sizes, medium and coarse time scales of the activity of *turtle* and *fish RGC* led to estimation results significantly above chance level ($p < 0.005$ and $p < 0.05$, respectively). Although there was a tendency for larger turtle RGC populations to yield better estimation results, this improvement was almost negligible for populations $n > 12$.

For the 500 ms and the first 200 ms intervals, the estimation results obtained for the *ISI metrics* were quantitatively similar to those yielded by the optimal time scales for the spike cost-based metrics. In contrast, the last 200 ms interval led to lower estimation results for the ISI metrics. Moreover, for this time interval, the improvement in the estimation performance for larger turtle RGC populations was almost negligible. Nevertheless, for the three analysed time intervals, the estimation results for the motion velocity were significantly above change level for all the tested *turtle* and *fish RGC* populations ($p < 0.005$ and $p < 0.05$, respectively).

For both animal species, the 500 ms interval led to the maximum median in the estimation performance under the Pooled Population hypothesis. Here, the ISI metrics yielded estimation performances that reached 46.9% and 26% for turtle and fish RGC, respectively.

Labelled Line

For the *spike cost-based metrics*, the estimation performance for the motion velocity showed qualitative similarities for the activity of single RGC and populations built under the Labelled Line hypothesis. Thereby, under this hypothesis, the estimation performance yielded by fine time scales was close to that expected by chance. However, coarser time scales led to estimation performance improvement, which was in turn greater for fine time scales. Here, for all the tested RGC populations and the three analysed time intervals, the time scale $1/q = \infty$ appeared to be optimal for the encoding of information about the motion velocity (Figure 3.22). Coarse and medium time scales of the combined activity of *turtle* and *fish RGC* led to estimation performances that were significantly above chance level ($p < 0.005$ and $p < 0.05$, respectively). Here, although for the three analysed time intervals there was a tendency for larger turtle RGC populations to yield better estimation results, this improvement was more evident for the 500 ms interval.

For each of the tested RGC populations and in contrast to the spike cost-based metrics, the analysis with the *ISI metrics* led to estimation results
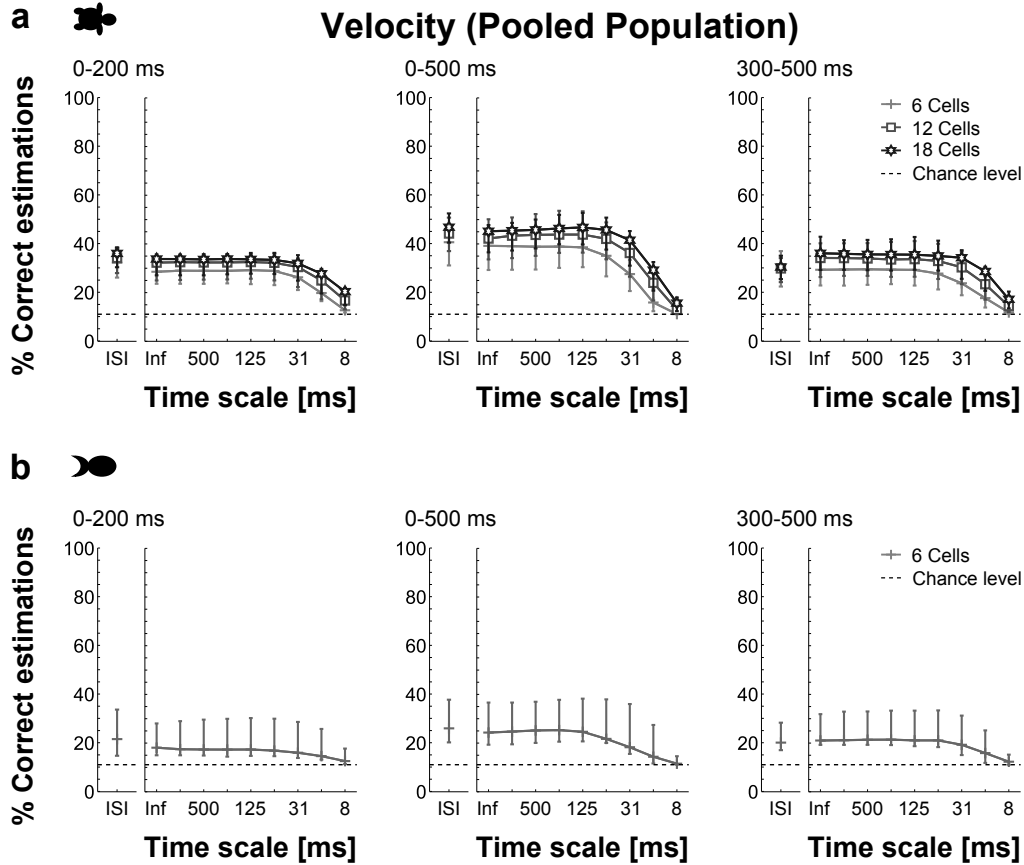
Figure 3.21: Estimation performance under the Pooled Population hypothesis, for the motion velocity of the moving stimulus. The estimation was carried out by applying spike cost-based metrics and ISI metrics on the combined activity of RGC within the three tested time intervals. Markers indicate the median, whereas error bars represent the range between maximum and minimum estimation performance. a) Turtle retinae, three experiments; $n = 10$ populations from each experiment and for each tested population size. b) Fish retinae five experiments; $n = 1$ population from each experiment.

that showed less variability across the three analysed time intervals. Thereby, for both animal species, the estimation results yielded by the ISI metrics clearly surpassed the ones obtained by the optimal time scales for the spike cost-based metrics for both 200 ms intervals. However, the opposite was found for the the 500 ms interval. Although the activity of larger turtle RGC populations led to better estimation results, these were significantly above change level for all the tested *turtle* and *fish RGC* populations ($p < 0.005$ and $p < 0.05$, respectively).

For turtle RGC, the 500 ms interval led to the maximum median in the estimation performance under the Labelled Line hypothesis. Here, the time scale $1/q = \infty$ yielded estimation performances that reached 60.2%.

Functional Group

As mentioned before, due to the limited number of recorded RGC from the fish experiments, the Functional Group hypothesis was only tested for the turtle experiments. In this sense, for the three analysed time intervals, the estimation performance obtained for the *spike cost-based metrics* was close to that expected by chance for the time scale $1/q = 8$ ms. Nonetheless, for all the tested population sizes, the estimation performance improved to values significantly above chance level for time scales $1/q \leq 31$ ms ($p < 0.005$). Furthermore, the estimation performance reached its maximum for $1/q = \infty$. In comparison to the other two tested hypotheses, the improvement in the estimation performance for larger turtle RGC populations was more evident for the Functional Group hypothesis (Figure 3.23).

For the *ISI metrics*, the activity of all the tested RGC populations led to estimation performances significantly above chance level for the three analysed time intervals ($p < 0.005$). Moreover, although for the three time intervals, the estimation performance improved for larger turtle RGC populations, this improvement was more evident for the 500 ms interval. The maximum estimation results for the motion velocity, obtained for both of the applied metrics under the three tested hypotheses, are summarised in the table in page 270.

For the three tested joint activity coding hypotheses, and as in the case of the activity of single RGC, the estimation of the stimulus motion velocity was further decomposed into the estimation of its motion direction and speed.

Direction

For both of the applied metrics and under the three tested joint activity coding hypotheses, the combined activity of RGC, in comparison to the ac-

Figure 3.22: Estimation performance under the Labelled Line hypothesis, for the motion velocity of the moving stimulus. The estimation was carried out by applying spike cost-based metrics and ISI metrics on the combined activity of RGC within the three tested time intervals. Markers indicate the median, whereas error bars represent the range between maximum and minimum estimation performance. a) Turtle retinae, three experiments; $n = 10$ populations from each experiment and for each tested population size. b) Fish retinae five experiments; $n = 1$ population from each experiment.
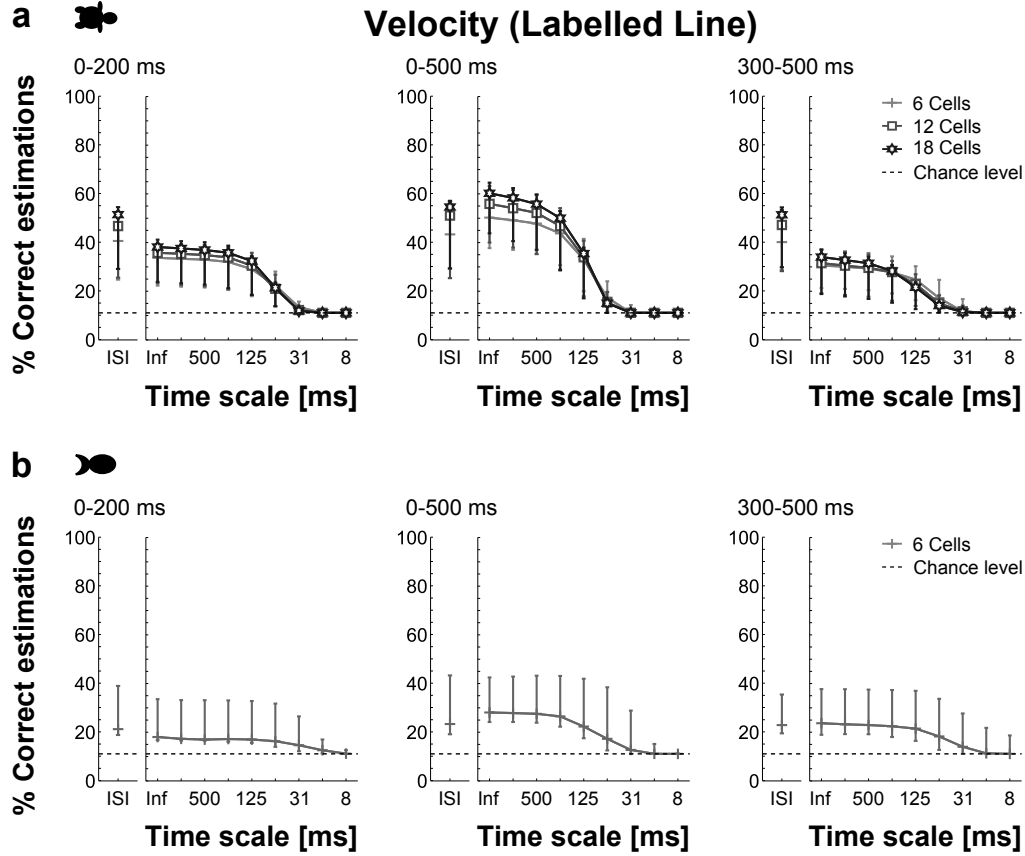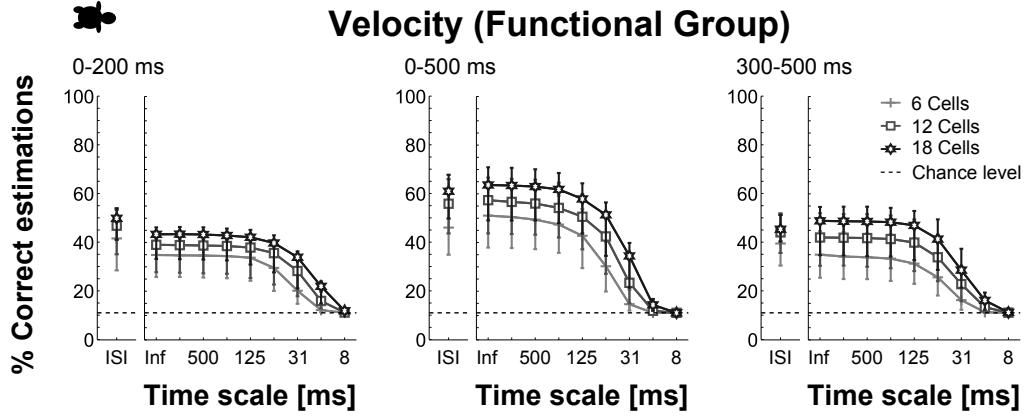
Figure 3.23: Estimation performance under the Functional Group hypothesis, for the motion velocity of the moving stimulus. The estimation was carried out by applying spike cost-based metrics and ISI metrics on the combined activity of turtle RGC within the three tested time intervals. Markers indicate the median, whereas error bars represent the range between maximum and minimum estimation performance. Three experiments; $n = 10$ populations from each experiment and for each tested population size.

tivity of single RGC, generally improved the estimation performance for the motion direction. Moreover, the activity of RGC within the 500 ms interval led to the maximum estimation performances. Nevertheless, in contrast to the estimation of the motion velocity, larger turtle RGC populations did not always lead to performance improvements. For the spike cost-based metrics, fine time scales generally led to estimation performances below chance level. These poor estimation performances were due to the over estimation of the absence of movement. However, coarser time scales improved the estimation performance, which in turn reached frequently its maximum for coarse time scales. The estimation of motion direction was quantitatively similar for both animal species under the Pooled Population hypothesis as well as under the Labelled Line hypothesis. For both animal species, the maximum median in the estimation performance was yielded by the time scale $1/q = \infty$ of the 500 ms interval. Here, the estimation performances under the Functional Group hypothesis reached 86% for turtle RGC. In turn, for fish RGC, the estimation results under the Labelled Line hypothesis reached 54.4%.

Pooled Population

For the *spike cost-based metrics*, the estimation performance for the motion direction was generally close or below chance level for the time scale $1/q = 8$ ms (Figure 3.24). Nonetheless, for the three analysed time intervals, medium and coarse time scales of the activity of *turtle RGC* led to estimation performances significantly above chance level ($p < 0.005$). Moreover, for the 500 ms and the first 200 ms intervals, larger populations of turtle RGC led to the improvement in the estimation performance for fine time scales. However, for these two time intervals, the improvement was absent for coarse time scales. In contrast, for last 200 ms interval, the activity of larger population sizes allowed better estimation results for all time scales. In the case of the combined activity of *fish RGC*, only coarse time scales within the 500 ms interval allowed estimation results significantly above chance level ($p < 0.05$).

With the exception of the last 200 ms interval for turtle RGC, and the first 200 ms interval for fish RGC, the estimation results obtained for the *ISI metrics* were quantitatively similar to the ones yielded by the optimal time scales for the spike cost-based metrics. Moreover, for each of the analysed time intervals, the estimation performance for the motion direction was similar across all the tested sizes of *turtle RGC* populations. Thereby, for three analysed time intervals, the activity of all the tested populations of turtle RGC led to estimation performances significantly above chance level ($p < 0.005$). In turn, although the median of the estimation performance for the three analysed time intervals was above chance level, only the combined activity of *fish RGC* within the 500 ms and the first 200 ms intervals allowed estimation results significantly above chance level ($p < 0.05$).

For both animal species, the 500 ms interval led to the maximum median in the estimation performance under the Pooled Population hypothesis. Here, the ISI metrics yielded estimation performances that reached 65.7% and 50.5% for turtle and fish RGC, respectively.

Labelled Line

For the *spike cost-based metrics*, the estimation performance for the motion direction under the Labelled Line hypothesis, showed qualitative similarities with the one yielded by the activity of single RGC. Thereby, for the three analysed time intervals, time scales $1/q \leq 62$ ms led to estimation performances much worse than those expected by chance. However, the estimation performance improved with coarser time scales and reached its maximum for time scales $1/q = \infty$ (Figure 3.25). For each of the three analysed time

Figure 3.24: Estimation performance under the Pooled Population hypothesis, for the motion direction of the moving stimulus. The estimation was carried out by applying spike cost-based metrics and ISI metrics on the combined activity of RGC within the three tested time intervals. Markers indicate the median, whereas error bars represent the range between maximum and minimum estimation performance. a) Turtle retinae, three experiments; $n = 10$ populations from each experiment and for each tested population size. b) Fish retinae five experiments; $n = 1$ population from each experiment.

intervals, similar estimation results were observed across all the tested sizes of *turtle RGC* populations. Here, coarse time scales of their activity led to estimation results significantly above chance level for the three analysed time intervals ($p < 0.005$). In contrast, for *fish RGC*, coarse time scales led estimation results significantly above chance level only for the 500 ms interval ($p < 0.05$).

Comparing the results obtained for both of the applied metrics, the *ISI metrics* led to estimation performances that were similar across the three analysed time intervals. Here, and in particular for the *turtle RGC*, the estimation results for both 200 ms intervals were better for the ISI metrics, whereas for the 500 ms interval, the opposite was observed. Furthermore, all the tested sizes of turtle RGC populations led to similar estimation performances, which were in turn significantly above chance level ($p < 0.005$). In contrast, although the combined activity of *fish RGC* led to estimation results whose median was above chance level, this difference was not significant for any of the three analysed time intervals.

For turtle RGC, the 500 ms interval led to the maximum median in the estimation performance under the Labelled Line hypothesis. Here, the time scale $1/q = \infty$ yielded estimation performances that reached 79%.

Functional Group

For the *spike cost-based metrics*, the estimation performance for the motion direction was generally below chance level for time scales $1/q \leq 16$ ms. However, for the three analysed time intervals, the activity of larger populations of turtle RGC allowed better estimation performance, which in turn reached its maximum for coarse time scales (Figure 3.26). Furthermore, for these time scales, the estimation performance for the motion direction was significantly above chance level ($p < 0.005$).

Comparing the results obtained for both of the applied metrics, the *ISI metrics* showed a tendency to allow better estimation performance for the first 200 ms interval. Furthermore, for the three analysed time intervals, the improvement in the estimation performance for larger turtle RGC populations was less evident for the ISI metrics (Figure 3.26). Nevertheless, for all of the tested population sizes, the estimation performance was significantly above chance level and for the three analysed time intervals ($p < 0.005$). The maximum estimation results for the motion direction, obtained by both of the applied metrics under the three tested hypotheses, are summarised in the table in page 271.
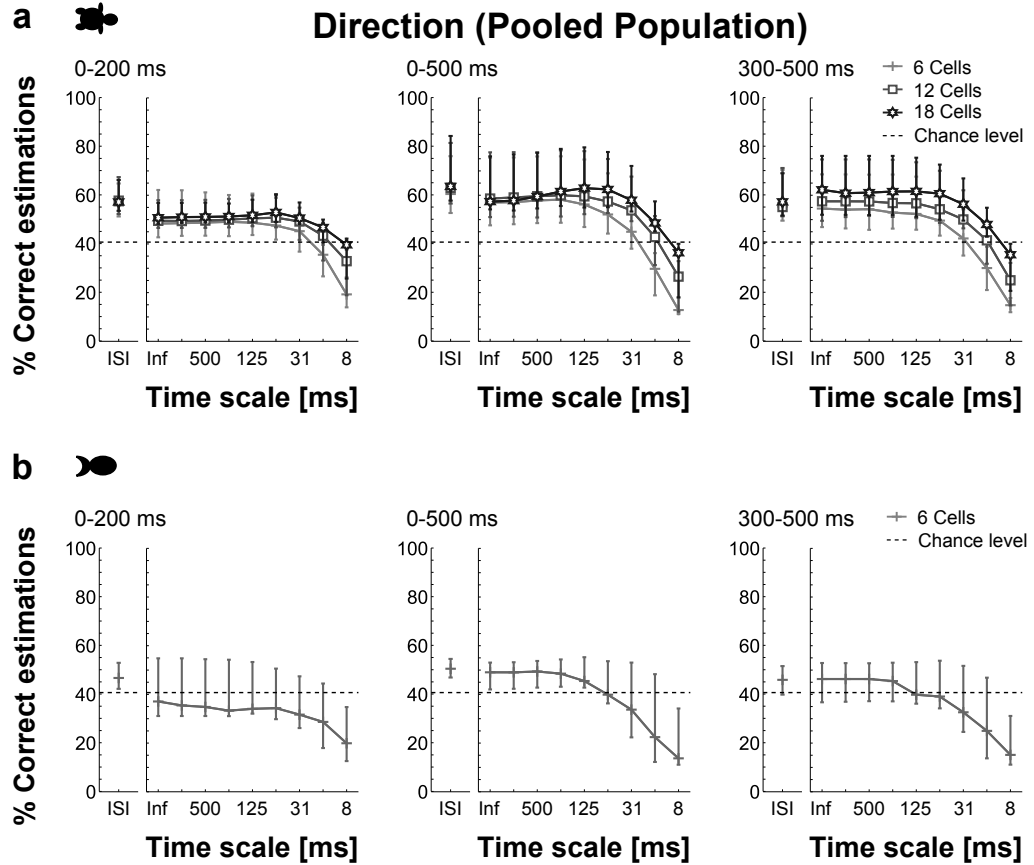
Figure 3.25: Estimation performance under the Labelled Line hypothesis, for the motion direction of the moving stimulus. The estimation was carried out by applying spike cost-based metrics and ISI metrics on the combined activity of RGC within the three tested time intervals. Markers indicate the median, whereas error bars represent the range between maximum and minimum estimation performance. a) Turtle retinae, three experiments; $n = 10$ populations from each experiment and for each tested population size. b) Fish retinae five experiments; $n = 1$ population from each experiment.
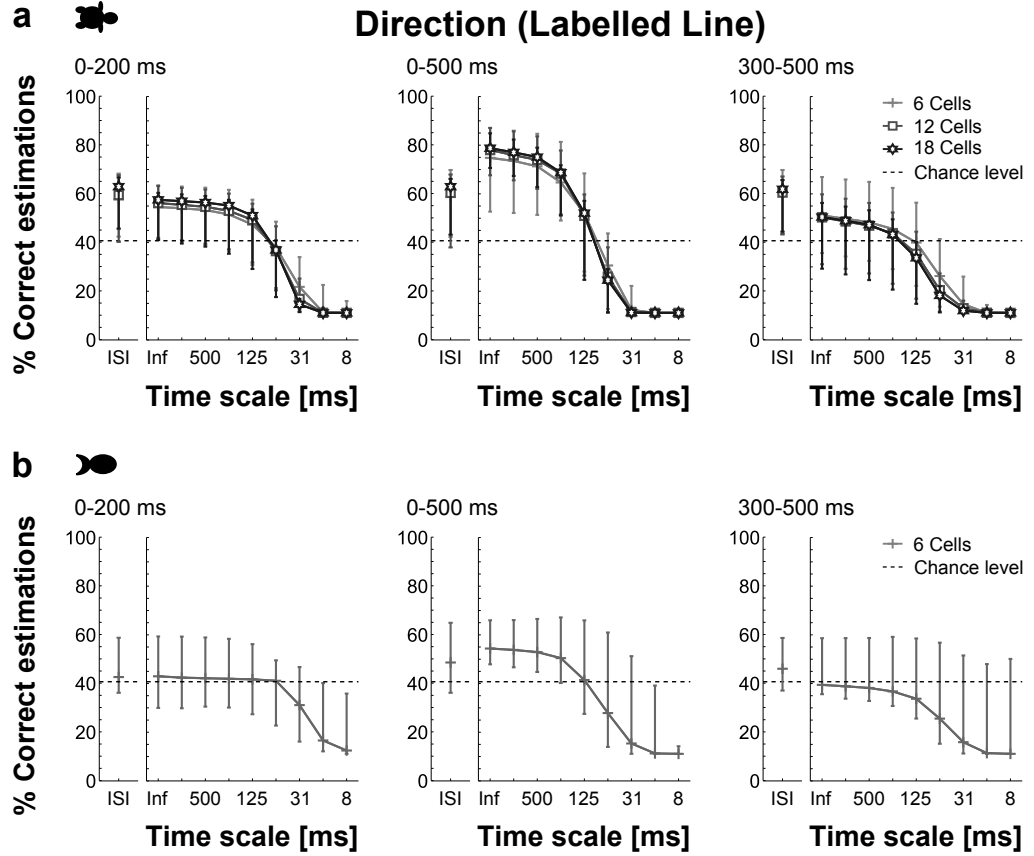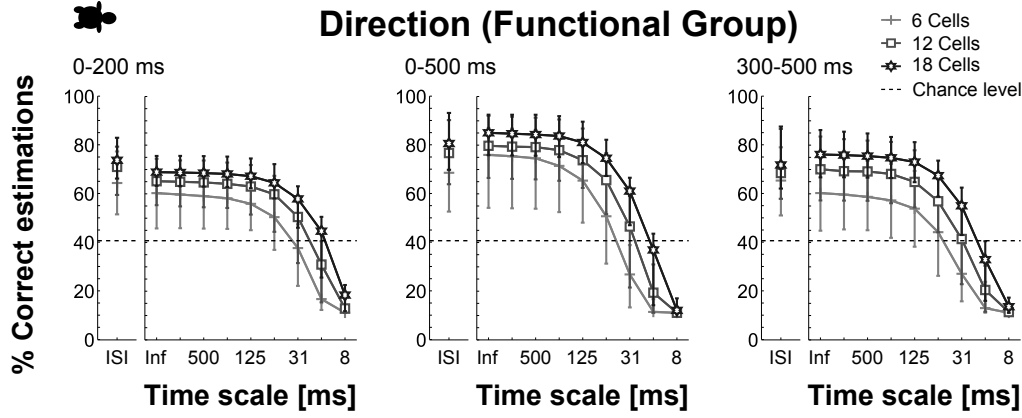
Figure 3.26: Estimation performance under the Functional Group hypothesis, for the motion direction of the moving stimulus. The estimation was carried out by applying spike cost-based metrics and ISI metrics on the combined activity of turtle RGC within the three tested time intervals. Markers indicate the median, whereas error bars represent the range between maximum and minimum estimation performance. Three experiments; $n = 10$ populations from each experiment and for each tested population size.

Speed

For the three analysed time intervals, the combined activity of RGC yielded lower estimation errors for the motion speed than the activity of single RGC. Here, the 500 ms interval generally led to the lowest estimation errors. Although the estimation errors showed a tendency to decrease for larger populations of turtle RGC, it was frequently observed that this reduction was almost negligible for population sizes $n \geq 12$. In turn, these results were obtained for both of the applied metrics and under the three tested joint activity coding hypotheses. For the spike cost-based metrics, fine time scales generally led to higher than chance estimation errors. In turn, these errors were provoked by the overestimation of the absence of movement. Nevertheless, coarser time scales led to the reduction of the estimation error, which frequently reached its minimum for coarse time scales. Qualitatively similar estimation errors for the motion speed were obtained for both animal species under the Pooled Population hypothesis as well as under the Labelled Line hypothesis. For both animal species, the lowest median in the estimation error was obtained for the 500 ms interval. Here, under the Functional Group hypothesis, the ISI metrics led to normalised absolute errors that reached 0.21 for turtle RGC. In turn, for fish RGC, the time scale $1/q = \infty$ under

the Labelled Line hypothesis led to estimation errors that reached 0.66.

Pooled Population

Generally, for the *spike cost-based metrics*, the reduction in the estimation errors for the motion speed appeared to reach a plateau for medium time scales (Figure 3.27). This observation was more evident for *turtle RGC*, for which the activity of larger population sizes led to lower estimation errors, especially for both 200 ms intervals. Nonetheless, for the 500 ms and the first 200 ms intervals, the reduction of the estimation errors for population sizes $n \geq 12$ was almost negligible. For the three analysed time intervals, medium and coarse time scales of the activity of all the tested sizes of turtle RGC populations yielded estimation errors significantly below chance level ($p < 0.005$). However, for *fish RGC*, coarse time scales led to significantly lower than chance estimation errors only for the 500 ms and the last 200 ms intervals ($p < 0.05$).

For the *ISI metrics*, the activity within the 500 ms intervals generally led to quantitative similar estimation errors as the ones obtained by the optimal time scales for the spike cost-based metrics. In contrast, for the last 200 ms interval, the errors obtained for the ISI metrics were slightly greater, especially for larger turtle RGC populations. However, for the three analysed time intervals, the error in the estimation of the motion speed was significantly below chance level for all the tested *turtle* and *fish RGC* populations ($p < 0.005$ and $p < 0.05$, respectively).

For both animal species, the 500 ms interval led to the lowest median in the estimation error under the Pooled Population hypothesis. Here, the time scale $1/q = \infty$ yielded estimation errors that reached 0.24 and 0.67 for turtle and fish RGC, respectively.

Labelled Line

For the *spike cost-based metrics*, the activity of single RGC and populations built under the Labelled Line hypothesis led to qualitatively similar estimation errors. Thereby, the error in the estimation of the motion speed was much worse than that expected by chance for time scales $1/q \leq 31$ ms, and appeared to reach its minimum at $1/q = \infty$ (Figure 3.28). In the case of *turtle RGC*, the estimation errors across the different tested population sizes did not show significant differences. Thus, for the optimal time scales, the estimation errors for turtle RGC were significantly below chance level for the three analysed time intervals ($p < 0.005$). In contrast, for *fish RGC*, coarse time scales led to estimation errors significantly below chance level

Figure 3.27: Absolute normalised estimation error under the Pooled Population hypothesis, for the motion speed of the moving stimulus. The estimation was carried out by applying spike cost-based metrics and ISI metrics on the combined activity of RGC within the three tested time intervals. Markers indicate the median, whereas error bars represent the range between maximum and minimum estimation performance. a) Turtle retinae, three experiments; $n = 10$ populations from each experiment and for each tested population size. b) Fish retinae five experiments; $n = 1$ population from each experiment.

only for the 500 ms interval ($p < 0.05$).

Comparing the results obtained for both of the applied metrics, the *ISI metrics* generally led to lower estimation errors for both 200 ms interval. In contrast, the opposite was observed for the 500 ms interval. For the combined activity of *turtle RGC*, the estimation error was similar across the three analysed time intervals, as well as across all the tested population sizes. Here, the estimation error was significantly below chance level ($p < 0.005$). Although the median of the estimation error was below chance level for the combined activity of *fish RGC*, this difference was not significant for any of the three analysed time intervals.

For turtle RGC, the 500 ms interval led to the lowest median in the estimation error under the Labelled Line hypothesis. Here, the time scale $1/q = \infty$ yielded estimation errors that reached 0.28.

Functional Group

For the *spike cost-based metrics*, the error in the estimation of the motion speed showed quantitative similarities for coarse time scales. Nonetheless, it appeared to reach its minimum at $1/q = \infty$. Although larger turtle RGC populations led to lower speed estimation errors for the three analysed time intervals, this finding was more evident for the last 200 ms interval (Figure 3.29). For the three analysed time intervals, medium and coarse time scales of the activity of all of the tested population sizes, led to significant lower than chance estimation errors ($p < 0.005$).

Comparing the results obtained for both of the applied metrics, the *ISI metrics* yielded lower estimation errors for the first 200 ms interval, whereas for the 500 ms and the last 200 ms intervals, the estimation errors were quantitatively similar to those yielded by the optimal time scales for the spike cost-based metrics. Moreover, for population sizes $n \geq 12$, the reduction in the estimation error was almost negligible. For all of the tested sizes of turtle RGC populations, the estimation error was significantly below chance level for the three analysed time intervals ($p < 0.005$). The lowest estimation errors for the motion speed, obtained for both of the applied metrics under the three tested hypotheses, are summarised in the table in page 272.

Velocity changes

For the instantaneous velocity changes, the combined activity of RGC generally led to better estimation performances than the activity of single RGC. Moreover, larger populations of turtle RGC improved the estimation performance. In turn, this improvement was greater for the 500 ms and the
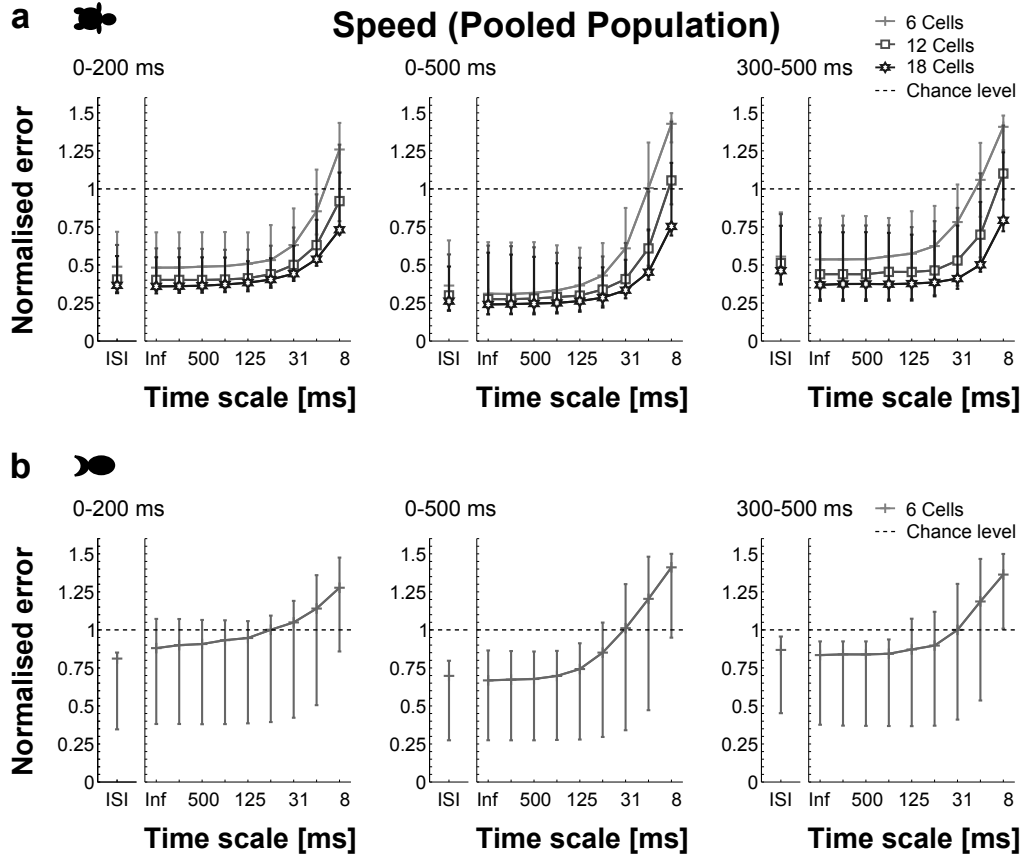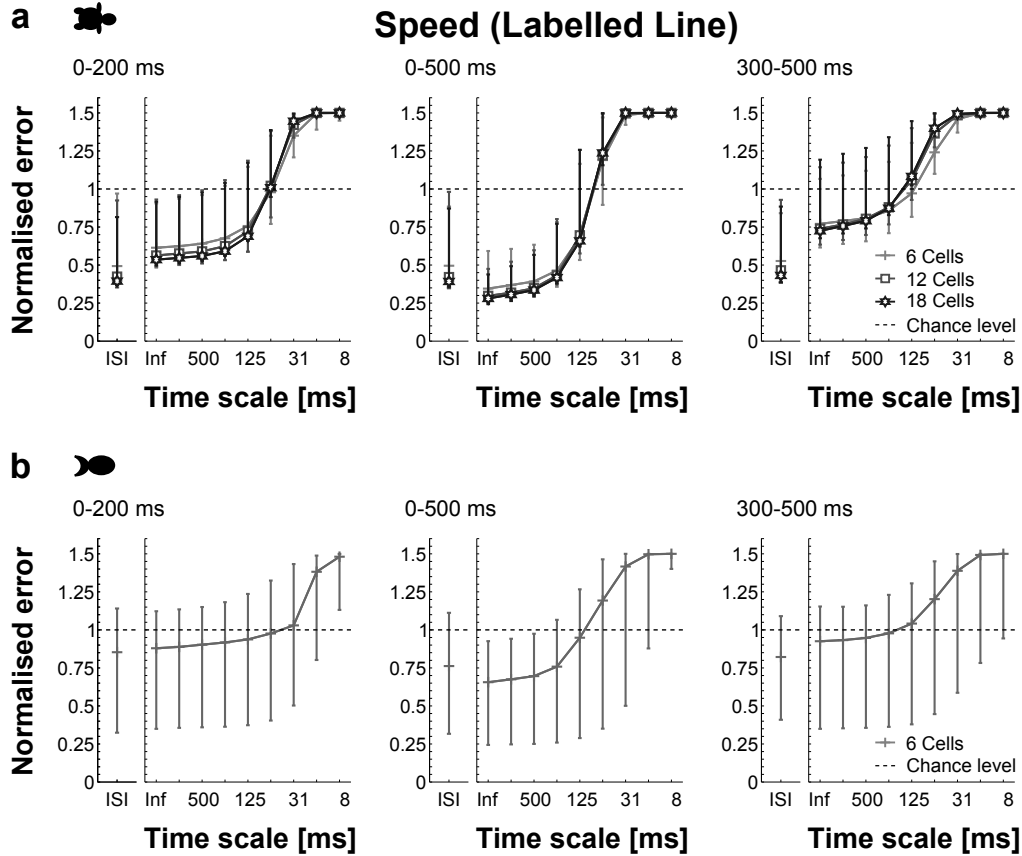
Figure 3.28: Absolute normalised estimation error under the Labelled Line hypothesis, for the motion speed of the moving stimulus. The estimation was carried out by applying spike cost-based metrics and ISI metrics on the combined activity of RGC within the three tested time intervals. Markers indicate the median, whereas error bars represent the range between maximum and minimum estimation performance. a) Turtle retinae, three experiments; $n = 10$ populations from each experiment and for each tested population size. b) Fish retinae five experiments; $n = 1$ population from each experiment.
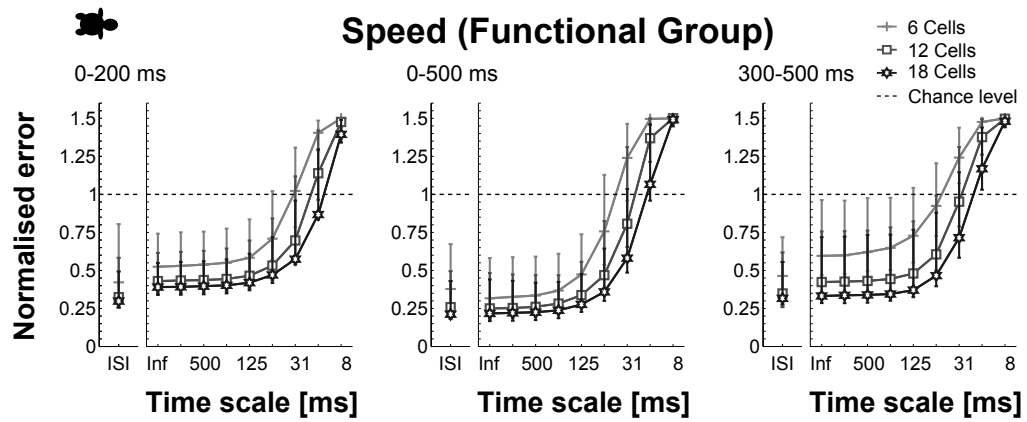
Figure 3.29: Absolute normalised estimation error under the Functional Group hypothesis, for the motion speed of the moving stimulus. The estimation was carried out by applying spike cost-based metrics and ISI metrics on the combined activity of turtle RGC within the three tested time intervals. Markers indicate the median, whereas error bars represent the range between maximum and minimum estimation performance. Three experiments; $n = 10$ populations from each experiment and for each tested population size.

first 200 ms intervals. Here, although these two time intervals yielded high estimation performances, the results obtained for the 500 ms interval were generally the highest. Conversely, the last 200 ms interval led generally to poor estimation performances. These results were obtained for both of the applied metrics and under the three tested joint activity coding hypotheses. For the spike cost-based metrics, the time scales that were optimal for the estimation of the instantaneous velocity changes varied across the three tested hypothesis. However, although the time scale $1/q = \infty$ showed to encode information about these changes, it did not lead to the highest estimation performances. Qualitatively similar estimation results for the instantaneous changes in motion velocity were obtained for both animal species under the Pooled Population hypothesis as well as under the Labelled Line hypothesis. For both animal species, the maximum median in the estimation performance was obtained for the 500 ms interval. Here, under the Functional Group hypothesis, the ISI metrics led to estimation performances that reached 41.6% for turtle RGC. In turn, for fish RGC, the estimation results under the Labelled Line hypothesis reached 9.1% for the time scale $1/q = 250$ ms.

Pooled Population

For the *spike cost-based metrics*, fine time scales of the activity within the 500 ms and the 200 ms intervals generally led to the highest estimation performances (Figure 3.30). Moreover, for these two time intervals, medium and fine time scales led to greater improvements in the estimation performance by larger populations of turtle RGC. However, for the three analysed time intervals, all the tested populations of *turtle* and *fish RGC* led to estimation results significantly above chance level ($p < 0.005$ and $p < 0.05$, respectively).

For the three analysed time intervals, the estimation results obtained for the *ISI metrics* were quantitatively similar to those yielded by the optimal time scales for the spike cost-based metrics. In turn, these results were obtained for all of the tested populations sizes from both animal species. Therefore, for the three analysed time intervals, the activity of all the tested populations of *turtle* and *fish RGC* led to estimation performances significantly above chance level ($p < 0.005$ and $p < 0.05$, respectively).

For both animal species, the 500 ms interval led to the maximum median in the estimation performance under the Pooled Population hypothesis. Here, the ISI metrics yielded estimation performances that reached 28.8% and 8.7% for turtle and fish RGC, respectively.

a

Velocity changes (Pooled Population)

b

Figure 3.30: Estimation performance under the Pooled Population hypothesis, for the instantaneous changes of the motion velocity of the moving stimulus. The estimation was carried out by applying spike cost-based metrics and ISI metrics on the combined activity of RGC within the three tested time intervals. Markers indicate the median, whereas error bars represent the range between maximum and minimum estimation performance. a) Turtle retinae, three experiments; $n = 10$ populations from each experiment and for each tested population size. b) Fish retinae five experiments; $n = 1$ population from each experiment.

Labelled Line

For the *spike cost-based metrics*, fine time scales of the activity within the three analysed time intervals generally led to estimation performances similar to those expected by chance. However, coarser time scales improved the estimation performance, which in turn, appeared to reach its maximum for time scales 125 ms $\leq 1/q \leq$ 500 ms. This improvement was greater for the 500 ms and the first 200 ms intervals (Figure 3.31). Moreover, for these two time intervals, medium and coarse time scales led to the largest improvements in the estimation performance for larger turtle RGC populations. However, for the three analysed time intervals, the estimation performance yielded by the optimal time scales was significantly above chance level for all the tested populations of *turtle* and *fish RGC* ($p < 0.005$ and $p < 0.05$, respectively).

The analysis with the *ISI metrics*, particularly for turtle RGC, led to estimation performances that clearly surpassed the ones yielded by the optimal time scales for the spike cost-based metrics. Moreover, for each of the tested sizes of turtle RGC populations, the estimation results obtained for the 500 ms and the first 200 ms intervals were quantitatively similar. Here, for all the tested population of *turtle* and *fish RGC*, the estimation results were significantly above chance level for the three analysed time intervals ($p < 0.005$ and $p < 0.05$, respectively).

For turtle RGC, the first 200 ms interval led to the maximum median in the estimation performance under the Labelled Line hypothesis. Here, the ISI metrics yielded estimation performances that reached 41.2%.

Functional Group

For the *spike cost-based metrics*, the time scale $1/q = 8$ ms led to the lowest estimation performances for turtle RGC. Nevertheless, coarser time scales improved the estimation performance. Thereby, for the 500 ms and the first 200 ms intervals, time scales 31 ms $\leq 1/q \leq$ 125 ms yielded the highest estimation performances. Moreover, these time scales yielded the largest improvements in the estimation performance for larger populations of turtle RGC (Figure 3.32). For all the tested populations of turtle RGC, the estimation results obtained for the optimal time scales were significantly above chance level for the three analysed time intervals ($p < 0.005$).

For the *ISI metrics*, the estimation results obtained for the 500 ms and first 200 ms intervals clearly outperformed the ones yielded by the optimal time scales for the spike cost-based metrics. However, for the last 200 ms interval, the estimation performance was qualitatively similar. Therefore, for the three analysed time intervals, the combined activity of all the tested
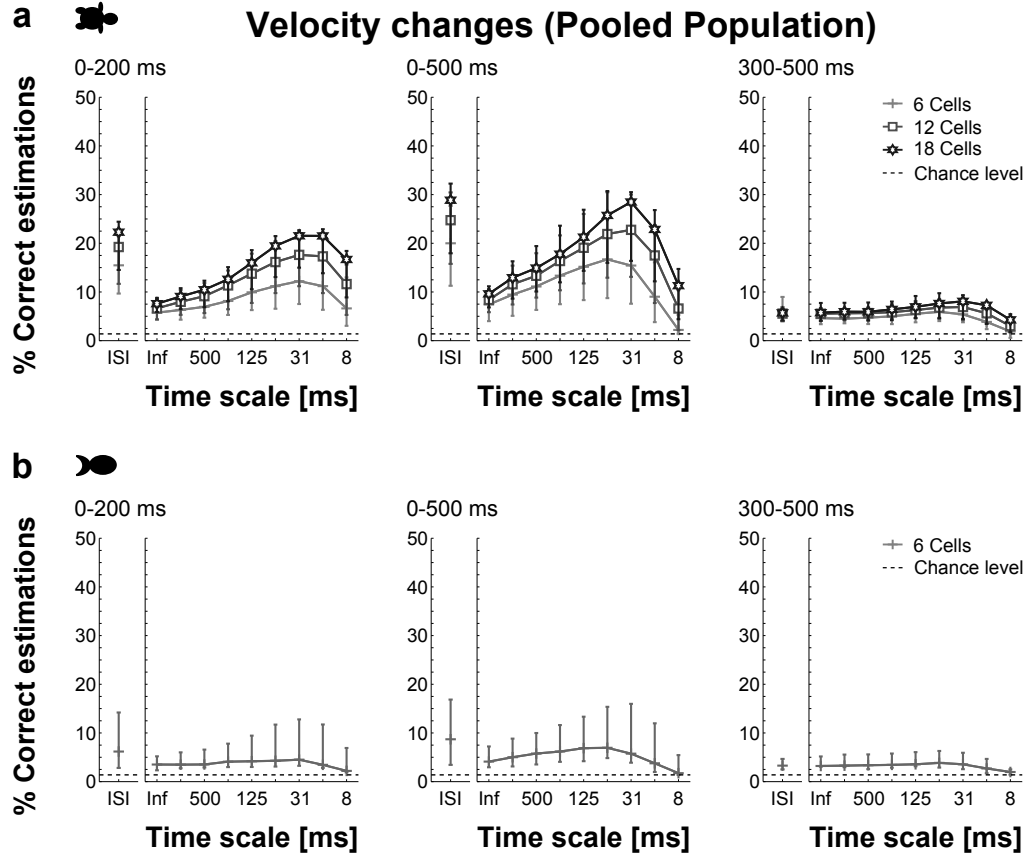
Figure 3.31: Estimation performance under the Labelled Line hypothesis, for the instantaneous changes of the motion velocity of the moving stimulus. The estimation was carried out by applying spike cost-based metrics and ISI metrics on the combined activity of RGC within the three tested time intervals. Markers indicate the median, whereas error bars represent the range between maximum and minimum estimation performance. a) Turtle retinae, three experiments; $n = 10$ populations from each experiment and for each tested population size. b) Fish retinae five experiments; $n = 1$ population from each experiment.
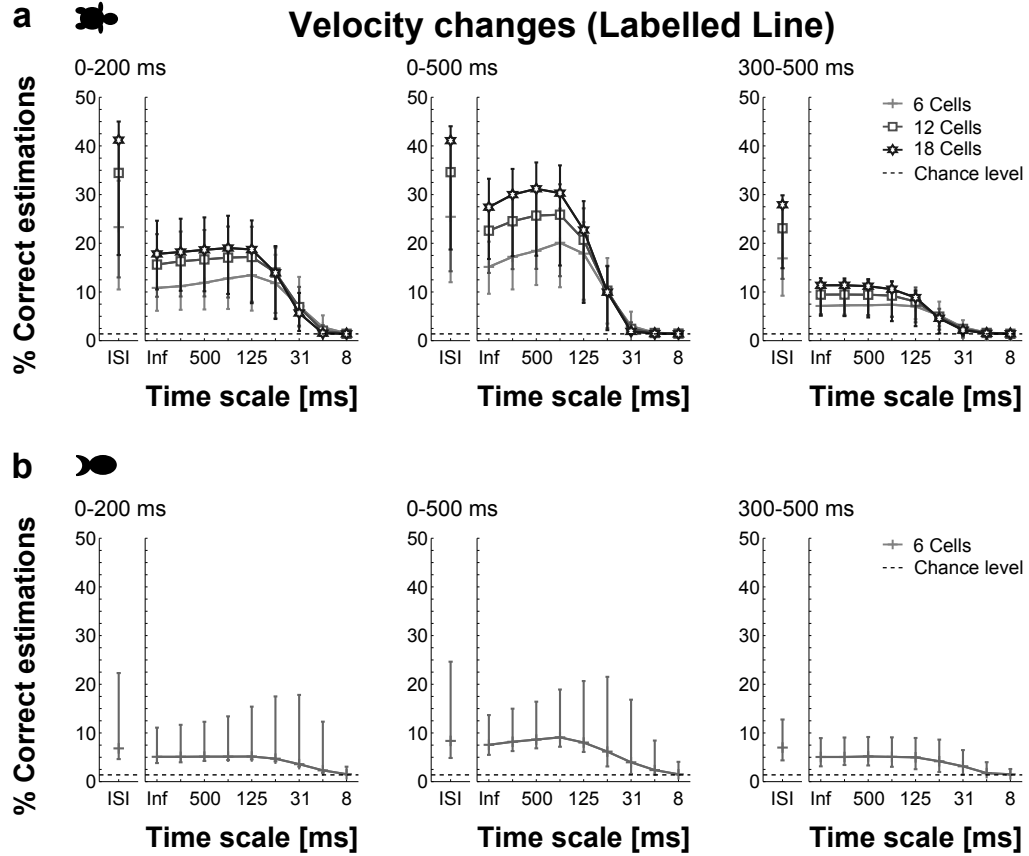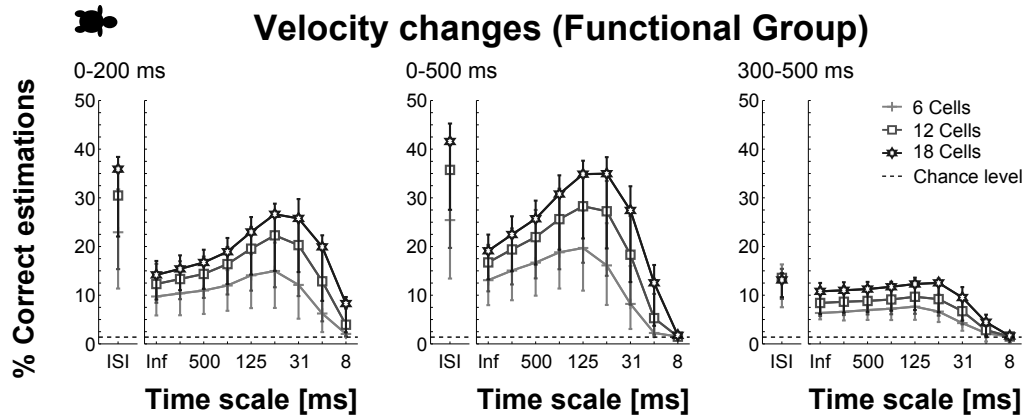
Velocity changes (Functional Group)

Figure 3.32: Estimation performance under the Functional Group hypothesis, for the instantaneous changes of the motion velocity of the moving stimulus. The estimation was carried out by applying spike cost-based metrics and ISI metrics on the combined activity of turtle RGC within the three tested time intervals. Markers indicate the median, whereas error bars represent the range between maximum and minimum estimation performance. Three experiments; $n = 10$ populations from each experiment and for each tested population size.

populations of turtle RGC led to estimation performances significantly above chance ($p < 0.005$). The maximum estimation results for the instantaneous velocity changes obtained for the both of the applied metrics and under the three tested hypotheses, are summarised in the table in page 273.

Previous velocity

Although the activity of RGC populations from both animal species led to better estimation results for the previous motion velocity, the improvement was more evident for turtle RGC. Here, although high estimation results were obtained for the 500 ms and the first 200 ms intervals, there was a slight tendency for the 500 ms interval to yield better estimation results. Moreover, for these time intervals, the estimation results improved for larger populations of turtle RGC. In contrast, the last 200 ms interval, for which the previous stimulus was already absent for 300 ms, led generally to estimation results similar to those expected by chance. These results were obtained for both of the applied metrics and under the three tested joint activity coding hypotheses. For the spike cost-based metrics, the time scales

that yielded the maximum estimation performances varied across the tested hypotheses. Moreover, these optimal time scales generally led to the greatest improvements in the estimation performance for larger populations of turtle RGC. Here, the Pooled Population hypothesis, as well as the Labelled Line hypothesis, led to qualitatively similar estimation performances for both animal species. Moreover, the ISI metrics led to the maximum median in the estimation performance for turtle and fish RGC. In turn, for the first 200 ms interval, the estimation performances under the Labelled Line hypothesis reached 49.3% for turtle RGC. In contrast, for fish RGC, the estimation results under the Pooled Population hypothesis reached 19.9% for the 500 ms interval.

Pooled Population

For the *spike cost-based metrics*, the time scales 16 ms $\leq 1/q \leq 31$ ms and 62 ms $\leq 1/q \leq 125$ ms, respectively, appeared to led to the optimal estimation results for *turtle* and *fish RGC* (Figure 3.33). In turn, these results were significantly above chance level ($p < 0.005$ and $p < 0.05$, for turtle and fish, respectively).

Generally, the estimation results obtained for the *ISI metrics* were quantitatively similar to those obtained by the optimal time scales for the spike cost-based metrics. However, small populations of turtle RGC led to slightly better estimation results for the ISI metrics. Therefore, for the 500 ms and the first 200 ms intervals, the combined activity of *turtle* and *fish RGC* led to estimation results significantly above chance level ($p < 0.005$ and $p < 0.05$, respectively).

For turtle RGC, the 500 ms interval led to the maximum median in the estimation performance under the Pooled Population hypothesis. Here, the ISI metrics yielded estimation performances that reached 36.5%.

Labelled Line

Generally, the estimation performance for the *spike cost-based metrics* was close to chance level for fine time scales. Nonetheless, the performance improved for coarser time scales and showed a tendency to reach its maximum for time scales 125 ms $\leq 1/q \leq 250$ ms. Moreover, these time scales allowed the maximum estimation performances for the 500 ms and the first 200 ms intervals, which were in turn significantly above chance level for *turtle* and *fish RGC* ($p < 0.005$ and $p < 0.05$, respectively).

For all of the tested *turtle RGC* populations, the estimation performance obtained for the *ISI metrics* clearly outperformed the one yielded by the

Figure 3.33: Estimation performance under the Pooled Population hypothesis, for the motion velocity of the moving stimulus before the instantaneous velocity changes. The estimation was carried out by applying spike cost-based metrics and ISI metrics on the combined activity of RGC within the three tested time intervals. Markers indicate the median, whereas error bars represent the range between maximum and minimum estimation performance. a) Turtle retinae, three experiments; $n = 10$ populations from each experiment and for each tested population size. b) Fish retinae five experiments; $n = 1$ population from each experiment.

optimal time scales for the spike cost-based metrics. In turn, these results were obtained for the three analysed time intervals. Furthermore, the 500 ms and the first 200 ms intervals led to similar estimation results for each of the tested turtle RGC populations. In contrast, for the *fish RGC*, the estimation results for both of the applied metrics were quantitatively similar. Therefore, for all the tested turtle and fish RGC populations, the estimation results were significantly above chance level ($p < 0.005$ and $p < 0.05$, respectively).

For fish RGC, the 500 ms interval led to the maximum median in the estimation performance under the Labelled Line hypothesis. Here, the time scale $1/q = 250$ ms yielded estimation performances that reached 20.8%.

Functional Group

For the *spike cost-based metrics*, the time scale $1/q = 8$ ms generally led to estimation results close to those expected by chance. Nevertheless, for the 500 ms and the first 200 ms intervals, the time scales 31 ms $\leq 1/q \leq 125$ ms allowed the improvement in the estimation performance, which in turn led to the highest estimation results for the previous motion velocity (Figure 3.35). Moreover, the estimation performances yielded by these time scales were significantly above chance level ($p < 0.005$).

For the *ISI metrics*, the estimation results for the 500 ms interval and especially for the first 200 ms one, showed a tendency to exceed the ones yielded by the optimal time scales for the spike cost-based metrics. Therefore, for these two time intervals, all of the tested populations of turtle RGC led to estimation performances significantly above chance level ($p < 0.005$). The maximum estimation results for the previous motion velocity, obtained for both of the applied metrics under the three tested hypotheses, are summarised in the table in page 274.

Previous direction

In comparison to the activity of single RGC, the estimation performance for the previous direction clearly improved for the combined activity of RGC. Moreover, the improvement was greater for the 500 ms and the first 200 ms intervals, which generally showed similar estimation performances. For these two time intervals, larger populations of turtle RGC led generally to estimation performance improvements. In contrast, for the last 200 ms interval, the estimation performance was generally close to that expected by chance. These results were obtained for both of the applied metrics and under the three tested joint activity coding hypotheses. For the spike cost-based metrics, the time scales that led to the maximum estimation performances var-
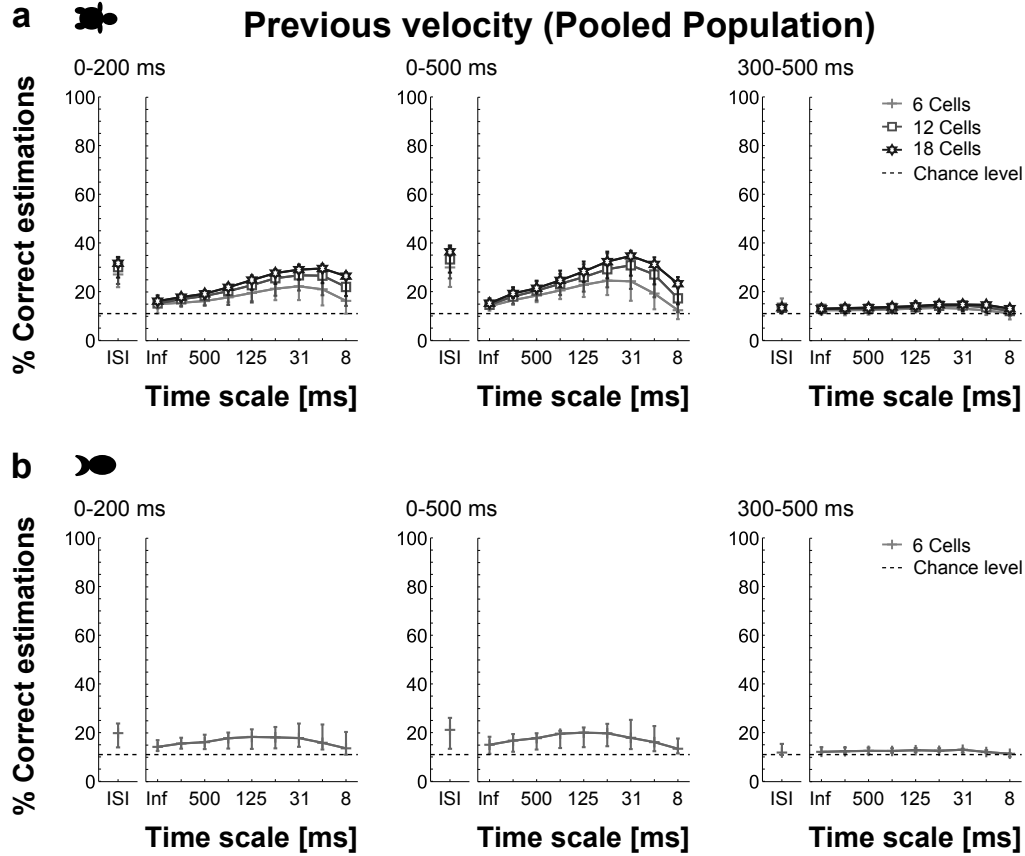
Figure 3.34: Estimation performance under the Labelled Line hypothesis, for the motion velocity of the moving stimulus before the instantaneous velocity changes. The estimation was carried out by applying spike cost-based metrics and ISI metrics on the combined activity of RGC within the three tested time intervals. Markers indicate the median, whereas error bars represent the range between maximum and minimum estimation performance. a) Turtle retinae, three experiments; $n = 10$ populations from each experiment and for each tested population size. b) Fish retinae five experiments; $n = 1$ population from each experiment.

Figure 3.35: Estimation performance under the Functional Group hypothesis, for the motion velocity of the moving stimulus before the instantaneous velocity changes. The estimation was carried out by applying spike cost-based metrics and ISI metrics on the combined activity of turtle RGC within the three tested time intervals. Markers indicate the median, whereas error bars represent the range between maximum and minimum estimation performance. Three experiments; $n = 10$ populations from each experiment and for each tested population size.

ied across the tested hypotheses. Here, these optimal time scales also led to greater improvements in the estimation performance for larger populations of turtle RGC. For the previous direction, qualitatively similar estimation results were obtained for both animal species under the Pooled Population hypothesis as well as under the Labelled Line hypothesis. For both animal species, the maximum median in the estimation performance was yielded by the ISI metrics for the 500 ms interval. Here, the estimation performances under the Functional Group hypothesis reached 73.4% for turtle RGC. In turn, for fish RGC, the estimation results under the Pooled Population hypothesis reached 52.7%.

Pooled Population

For the *spike cost-based metrics*, the time scales $16 \text{ ms} \leq 1/q \leq 62 \text{ ms}$ appeared to be optimal for the encoding of information about the previous motion direction(Figure 3.36). In turn, for these two time intervals, the estimation results yielded by the optimal time scales were significantly above chance level for *turtle* and *fish RGC* ($p < 0.005$ and $p < 0.05$, respectively).

Generally, the estimation results obtained for the *ISI metrics* were quantitatively similar to those obtained by the optimal time scales for the spike cost-based metrics. However, small populations of *turtle RGC* led to slightly better results for the ISI metrics. These results can be explained by the fact that for all three analysed time intervals, all the tested turtle RGC populations yielded similar estimation performances. Thereby, for 500 ms and the first 200 ms intervals, the estimation results for all the tested populations of turtle RGC were significantly above chance level ($p < 0.005$). In turn, although the median of the estimation performance for the 500 ms and the first 200 ms intervals was above chance level, only the activity of *fish RGC* within the first 200 ms interval led to estimation performances significantly above chance level ($p < 0.05$).

For turtle RGC, the 500 ms interval led to the maximum median in the estimation performance under the Pooled Population hypothesis. Here, the ISI metrics yielded estimation performances that reached 62.8%.

Labelled Line

For the *spike cost-based metrics*, fine time scales generally led to estimation results close to those expected by chance. Nevertheless, for the 500 ms and the first 200 ms intervals, the time scales $62 \text{ ms} \leq 1/q \leq 125 \text{ ms}$ appeared to be optimal for the encoding of information about the previous direction (Figure 3.37). Thereby, for these two time intervals, the estimation results
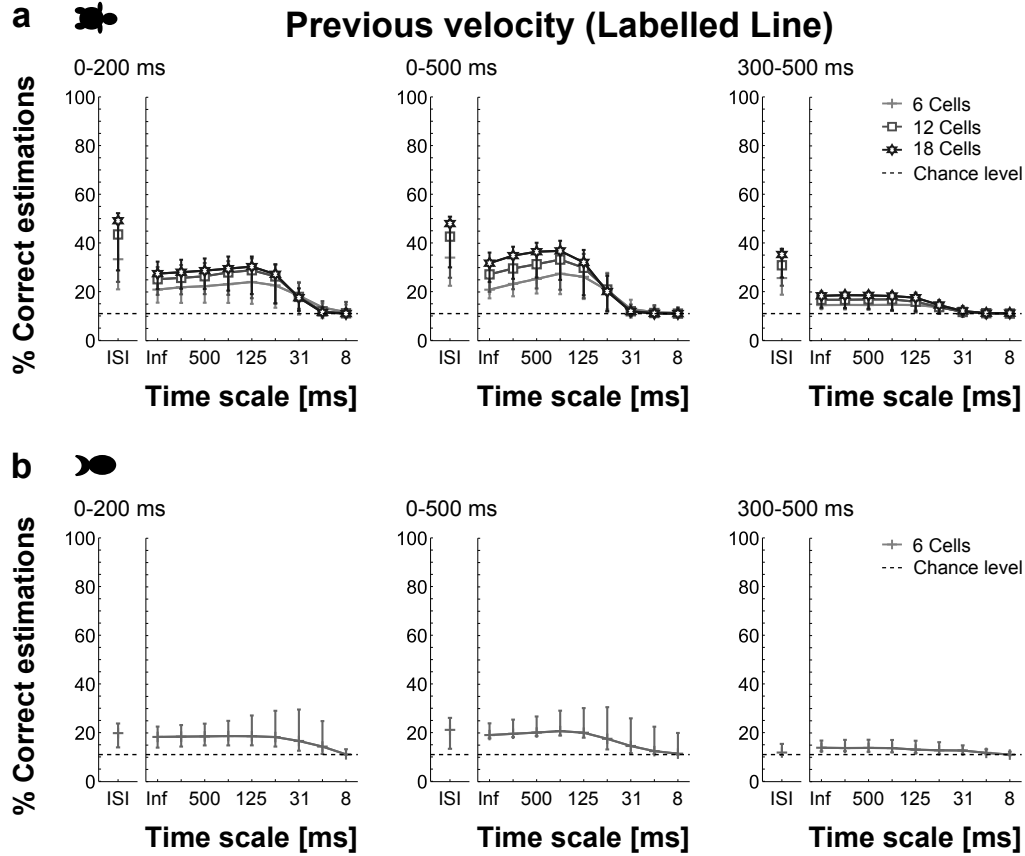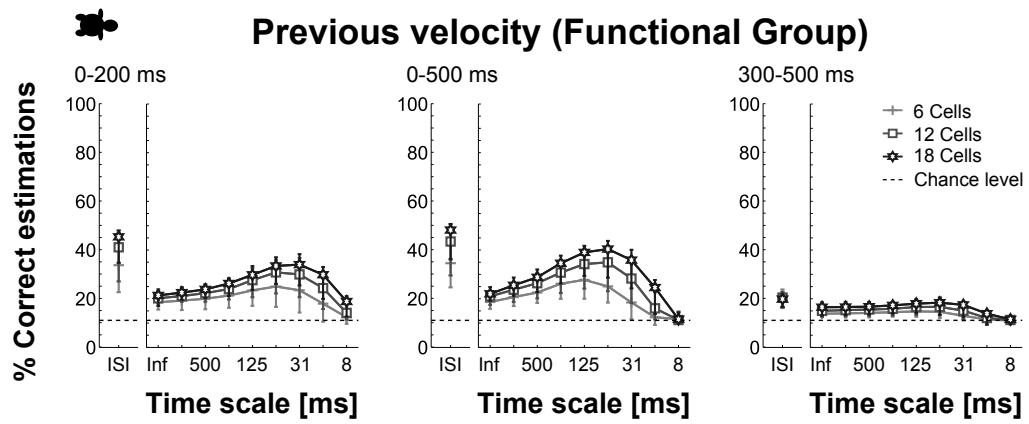
Figure 3.36: Estimation performance under the Pooled Population hypothesis, for the motion direction of the moving stimulus before the instantaneous velocity changes. The estimation was carried out by applying spike cost-based metrics and ISI metrics on the combined activity of RGC within the three tested time intervals. Markers indicate the median, whereas error bars represent the range between maximum and minimum estimation performance. a) Turtle retinae, three experiments; $n = 10$ populations from each experiment and for each tested population size. b) Fish retinae five experiments; $n = 1$ population from each experiment.

were significantly above chance level for all of the tested *turtle* and *fish RGC* populations ($p < 0.005$ and $p < 0.05$, respectively).

For the *ISI metrics*, the combined activity of *turtle RGC* led to estimation results that showed a tendency to exceed the ones yielded by the optimal time scales for the spike cost-based metrics. In contrast for *fish RGC*, the estimation results obtained for both of the applied metrics was similar. Thereby, and particularly for the 500 ms and the first 200 ms intervals, the estimation results for all the tested populations of turtle and fish RGC were significantly above chance level ($p < 0.005$ and $p < 0.05$, respectively).

For turtle RGC, the first 200 ms interval led to the maximum median in the estimation performance under the Labelled Line hypothesis. Here, the ISI metrics yielded estimation performances that reached 72%. In contrast, for fish RGC, the maximum estimation results were yielded by the time scale $1/q = 250$ ms of the 500 ms interval. Here, these results reached 52.6%.

Functional Group

For the *spike cost-based metrics*, the time scales 31 ms $\leq 1/q \leq 125$ ms within the 500 ms and the first 200 ms intervals, showed a tendency to be optimal for the encoding of information about the previous motion direction (Figure 3.38). Moreover, for these two time intervals, the estimation result yielded by these time scales were significantly above chance level for all of the tested population of turtle RGC ($p < 0.005$).

For the *ISI metrics*, and especially for small populations of turtle RGC, the obtained estimation results showed a tendency to exceed the ones yielded by the optimal time scales for the spike-cost based metrics. In turn, these results were obtained for the 500 ms and the first 200 ms intervals. Therefore, for these two time intervals, the estimation results yielded by all the tested populations of turtle RGC were significantly above chance level ($p < 0.005$). The maximum estimation results for the previous motion direction, obtained for both of the applied metrics under the three tested hypotheses, are summarised in the table in page 275.

Previous speed

In comparison to the activity of single RGC, and particularly for the 500 ms and the first 200 ms intervals, the combined activity of RGC clearly reduced the errors in the estimation of the previous motion speed. Here, the 500 ms interval generally led to the lowest estimation errors. Moreover, for the time intervals that led to the lower estimation errors, these errors showed to decrease for larger populations of turtle RGC. These results were obtained for
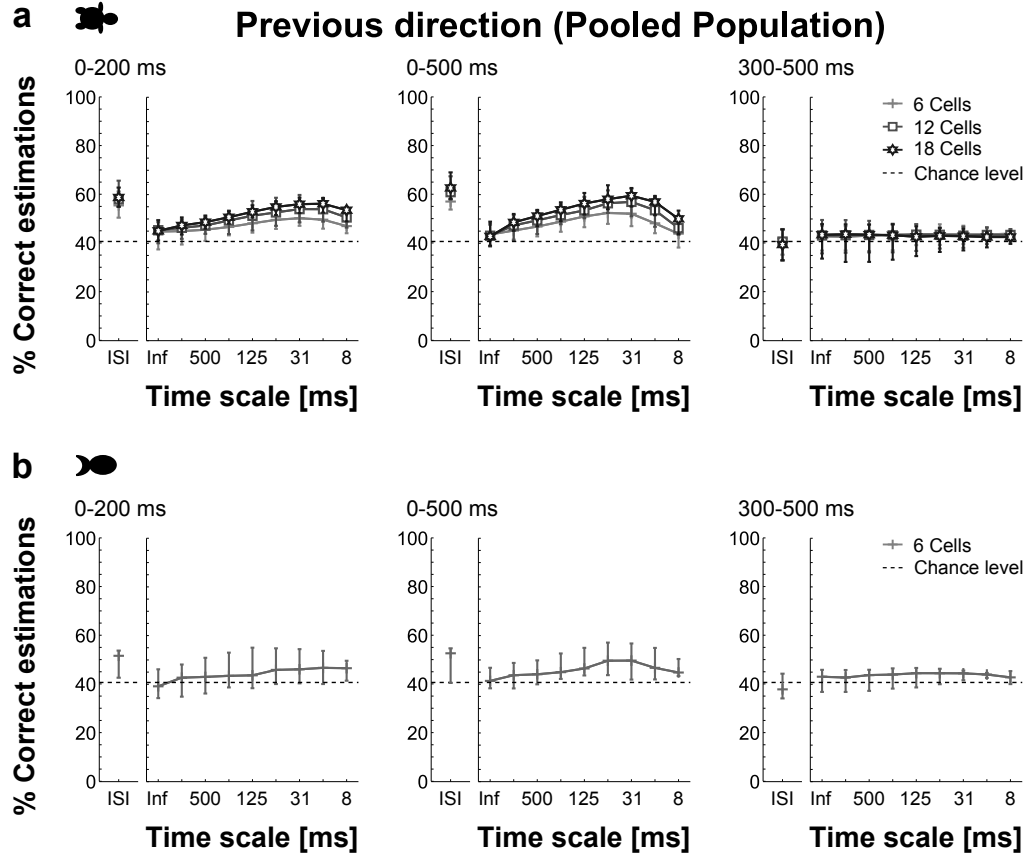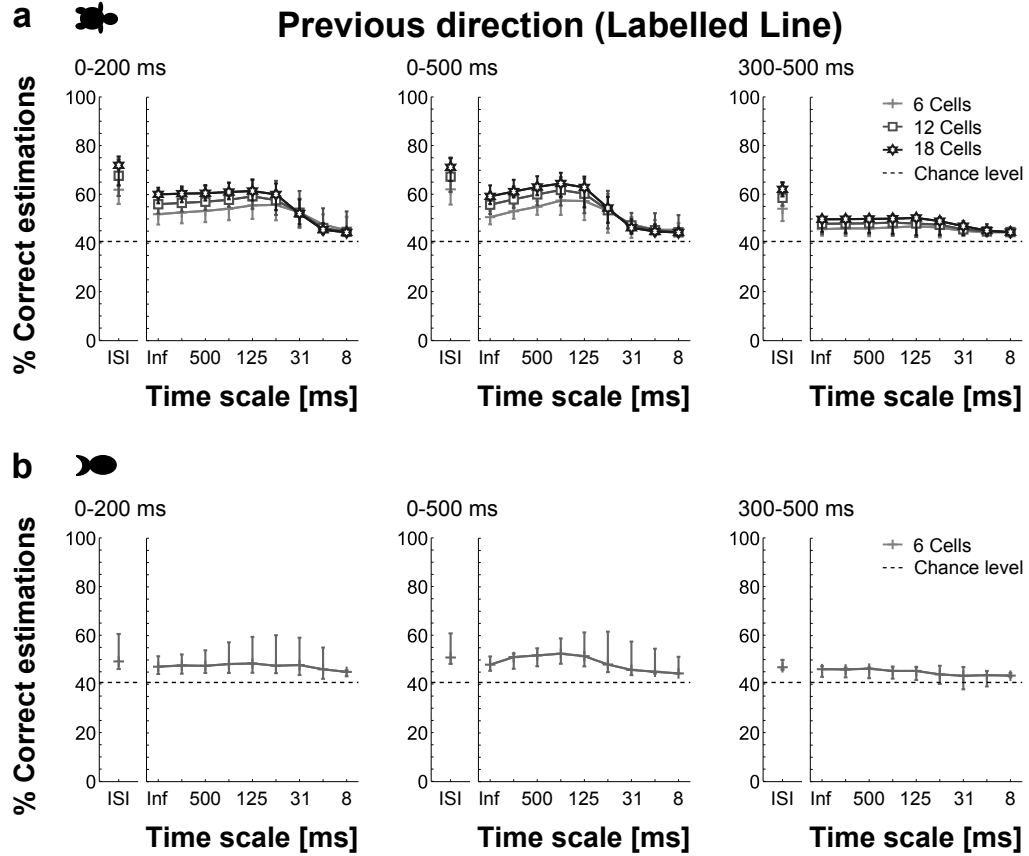
Figure 3.37: Estimation performance under the Labelled Line hypothesis, for the motion direction of the moving stimulus before the instantaneous velocity changes. The estimation was carried out by applying spike cost-based metrics and ISI metrics on the combined activity of RGC within the three tested time intervals. Markers indicate the median, whereas error bars represent the range between maximum and minimum estimation performance. a) Turtle retinae, three experiments; $n = 10$ populations from each experiment and for each tested population size. b) Fish retinae five experiments; $n = 1$ population from each experiment.

Previous direction (Functional Group)
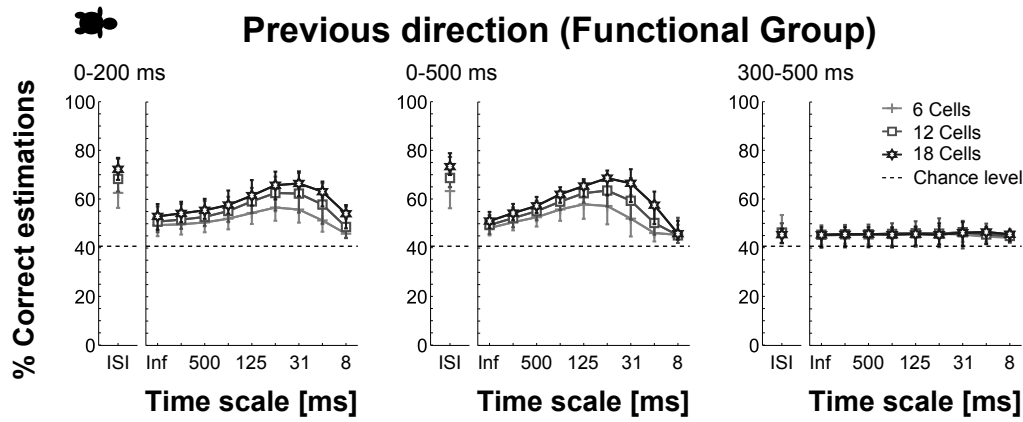
Figure 3.38: Estimation performance under the Functional Group hypothesis, for the motion direction of the moving stimulus before the instantaneous velocity changes. The estimation was carried out by applying spike cost-based metrics and ISI metrics on the combined activity of turtle RGC within the three tested time intervals. Markers indicate the median, whereas error bars represent the range between maximum and minimum estimation performance. Three experiments; $n = 10$ populations from each experiment and for each tested population size.

both of the applied metrics and under the three tested joint activity coding hypotheses. For the spike cost-based metrics, the time scales that led to the lowest estimation errors varied across the tested hypotheses. Furthermore, these optimal time scales also led to greater reductions in the estimation errors for larger populations of turtle RGC. Here, the Pooled Population hypothesis, as well as under the Labelled Line hypothesis, led to qualitative similar estimation errors for both animal species. For both animal species, the ISI metrics led to the lowest median in the estimation error. Here, for turtle RGC, the normalised absolute errors under the Functional Group hypothesis, reached 0.44 for the first 200 ms interval. In turn, for fish RGC, the estimation errors under the Labelled Line hypothesis reached 0.72 for the 500 ms interval.

Pooled Population

For the *spike cost-based metrics*, the time scales 16 ms $\leq 1/q \leq$ 62 ms within the 500 ms and first 200 ms intervals, appeared to be optimal for the encoding of information about the previous motion speed (Figure 3.39). Here, for the optimal time scales within these two time intervals, the estimation errors were significantly below chance level for all the tested *turtle RGC* populations ($p < 0.005$). In contrast, for the *fish RGC*, the optimal time scales led to errors significantly below chance level only for the 500 ms interval ($p < 0.05$).

For the 500 ms and first 200 ms intervals, the analysis with the *ISI metrics* showed a tendency to yield lower estimation errors than the optimal time scales for the spike cost-based metrics. Furthermore, for these two time intervals, the estimation errors were similar for each of the tested population sizes. Thereby, for the time intervals that led to the lower estimation errors, these were significantly below chance level for all the tested populations of *turtle* and *fish RGC* ($p < 0.005$ and $p < 0.05$, respectively).

For both animal species, the 500 ms interval led to the lowest median in the estimation error under the Pooled Population hypothesis. Here, the ISI metrics yielded estimation errors that reached 0.52 and 0.78 for turtle and fish RGC, respectively.

Labelled Line

For the *spike cost-based metrics*, fine time scales generally led to estimation errors close to those expected by chance. However, and particularly for turtle RGC, time scales 125 ms $\leq 1/q \leq$ 250 ms led to the lowest estimation errors for the 500 ms and the first 200 ms intervals (Figure 3.40). Furthermore,

Figure 3.39: Absolute normalised estimation error under the Pooled Population hypothesis, for the motion speed of the moving stimulus before the instantaneous velocity changes. The estimation was carried out by applying spike cost-based metrics and ISI metrics on the combined activity of RGC within the three tested time intervals. Markers indicate the median, whereas error bars represent the range between maximum and minimum estimation performance. a) Turtle retinae, three experiments; $n = 10$ populations from each experiment and for each tested population size. b) Fish retinae five experiments; $n = 1$ population from each experiment.

for these two time intervals, the estimation errors were significantly below chance level for all the tested populations of *turtle* and *fish RGC* ($p < 0.005$ and $p < 0.05$, respectively).

In the case of *turtle RGC*, the estimation errors obtained for the *ISI metrics* were generally lower than the ones yielded by the optimal time scales for the spike cost-based metrics. Moreover, for each of the tested turtle RGC populations, the estimation errors across the 500 ms and the first 200 ms interval were quantitatively similar. In contrast, for *fish RGC*, the estimation errors obtained for the ISI metrics were not lower than the ones yielded by the optimal time scales for the spike cost-based metrics. Furthermore, for fish RGC, the 500 ms interval showed a tendency to lead to the lowest estimation errors. Thereby, for the intervals that yielded the lowest estimation errors, these were significantly below chance level for all the tested populations of *turtle* and *fish RGC* ($p < 0.005$ and $p < 0.05$, respectively).

For turtle RGC, the first 200 ms interval led to the lowest median in the estimation error under the Labelled Line hypothesis. Here, the ISI metrics yielded estimation errors that reached 0.46.

Functional Group

For the *spike cost-based metrics*, the time scales 31 ms $\leq 1/q \leq$ 125 ms led to the lowest estimation errors for the the 500 ms and the first 200 ms intervals (Figure 3.41). Here, the estimation errors were significantly below chance level for all the tested populations of turtle RGC ($p < 0.005$).

For the *ISI metrics*, the estimation errors for each of the tested populations of turtle RGC were quantitatively similar for the 500 ms and the first 200 ms intervals. Moreover, these errors were lower than the ones yielded by the optimal time scales for the spike cost-based metrics. Therefore, for these two time intervals, the estimation errors were significantly below chance level for all of the tested turtle RGC populations ($p < 0.005$). The lowest estimation errors for the previous motion speed, obtained for both of the applied metrics under the three tested hypotheses, are summarised in the table in page 276.

Post velocity

For the estimation of the post velocity, i.e., considering the stimulus history, the combined activity of RGC generally led to better results than the ones yielded by the activity of single RGC. Here, in the case of turtle RGC, larger populations frequently led to better estimation results. Although the highest estimation performances were often found for the 500 ms interval,
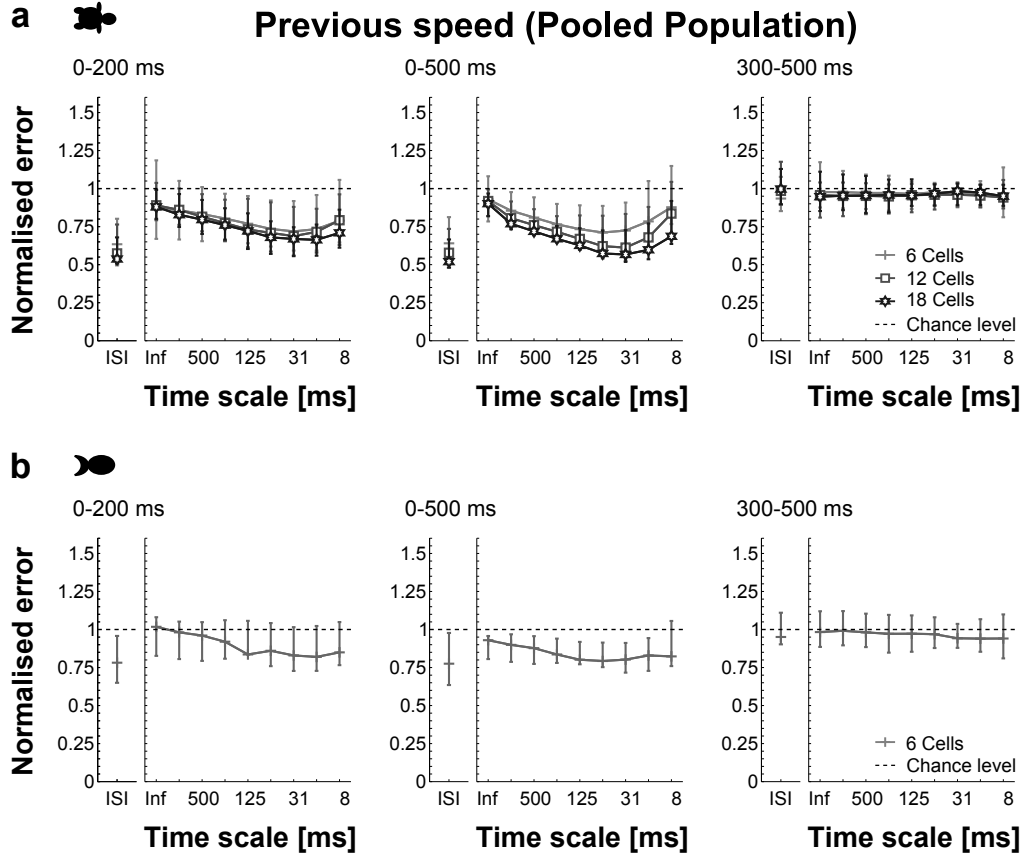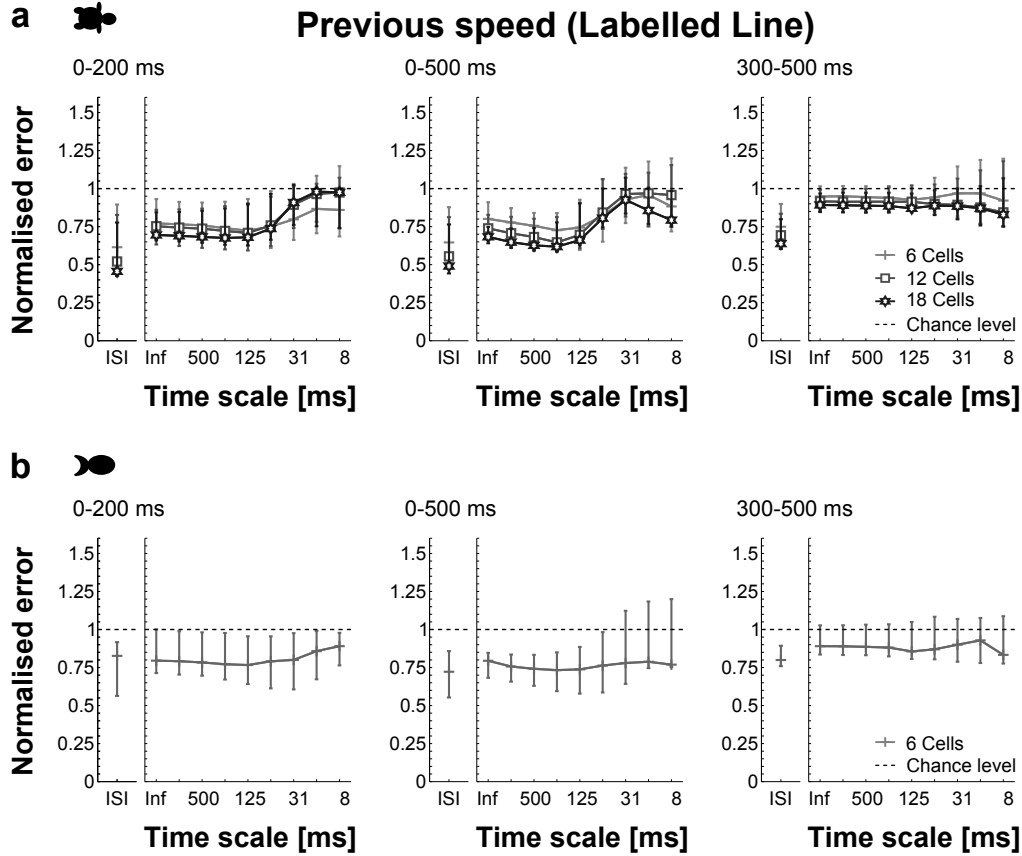
Figure 3.40: Absolute normalised estimation error under the Labelled Line hypothesis, for the motion speed of the moving stimulus before the instantaneous velocity changes. The estimation was carried out by applying spike cost-based metrics and ISI metrics on the combined activity of RGC within the three tested time intervals. Markers indicate the median, whereas error bars represent the range between maximum and minimum estimation performance. a) Turtle retinae, three experiments; $n = 10$ populations from each experiment and for each tested population size. b) Fish retinae five experiments; $n = 1$ population from each experiment.
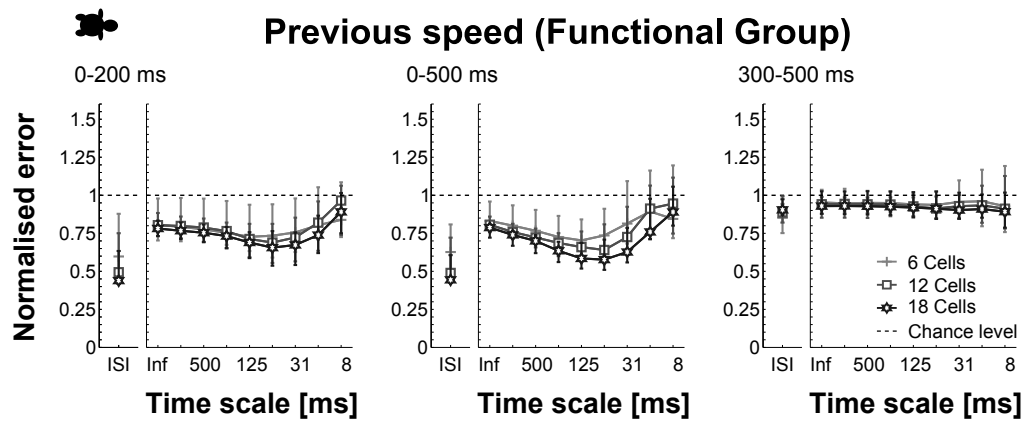
Figure 3.41: Absolute normalised estimation error under the Functional Group hypothesis, for the motion speed of the moving stimulus before the instantaneous velocity changes. The estimation was carried out by applying spike cost-based metrics and ISI metrics on the combined activity of turtle RGC within the three tested time intervals. Markers indicate the median, whereas error bars represent the range between maximum and minimum estimation performance. Three experiments; $n = 10$ populations from each experiment and for each tested population size.

the first 200 ms interval also allowed high estimation performances. These results were obtained for both of the applied metrics and under the three tested joint activity coding hypotheses. The difference in the estimation performance for the post velocity and the velocity alone, i.e., without considering the stimulus history, was more evident for the spike cost-based metrics. Here, the 500 ms and the first 200 ms intervals led to the largest estimation differences. Moreover, the time scales that led to the highest post velocity estimation performances, and the greater estimation improvements for larger turtle RGC populations, varied across the tested populations. Nevertheless, these time scales were frequently not the ones that yielded the larger estimation differences for the post velocity and the velocity alone. Qualitative similar estimation results were obtained for both animal species under the Pooled Population hypothesis as well as under the Labelled Line hypothesis. For both animal species, the maximum median in the estimation performance was obtained for the 500 ms interval. Here, for turtle RGC, the estimation performances under the Functional Group hypothesis reached 64.2% for the time scale $1/q = 250$ ms. In turn, for fish RGC, the estimation results under the Labelled Line hypothesis reached 29.2% for the time scale $1/q = 1000$ ms.

Pooled Population

For the *spike cost-based metrics* and especially for the 500 ms and the first 200 ms intervals, the highest estimation performance for the post velocity was yielded by time scales 31 ms $\leq 1/q \leq 125$ ms, which in turn, also led to large estimation differences between the post velocity and the velocity alone (Figure 3.42). Moreover, for *turtle* and *fish RGC* populations, these differences in the estimation performance were significant ($p < 0.005$ and $p < 0.05$, respectively). Together, these observations point out the increase in the relevance of fine and medium time scales for the encoding of information about the motion velocity when the stimulus history is considered. For the three analysed time intervals, the estimation results for the post motion velocity were significantly above chance level for all of the tested turtle and fish RGC populations ($p < 0.005$ and $p < 0.05$, respectively).

Generally, the estimation results obtained for the *ISI metrics* showed quantitative similarities with the ones yielded by the optimal time scales for the spike cost-based metrics. Therefore, for all the tested populations of *turtle* and *fish RGC*, the estimation results were significantly above chance level for the three analysed time intervals ($p < 0.005$ and $p < 0.05$, respectively). Moreover, the difference in the estimation performance for the post velocity and the velocity alone was only significant for populations of turtle RGC within the 500 ms and the first 200 ms intervals ($p < 0.005$).

For both animal species, the 500 ms interval led to the maximum median in the estimation performance under the Pooled Population hypothesis. Here, the ISI metrics yielded estimation performances that reached 52.5% and 28.1% for turtle and fish RGC, respectively.

Labelled Line

For the *spike cost-based metrics*, the greatest differences in the estimation performance for the post motion velocity and the velocity alone were generally yielded by the time scales 62 ms $\leq 1/q \leq$ 125 ms. However, the time scale $1/q = \infty$ led to the best estimation performances for the post motion velocity (Figure 3.43). Here, for the three analysed time intervals, the largest differences in the estimation performance for both velocities were significant for all the tested populations of *turtle* and *fish RGC* ($p < 0.005$ and $p < 0.05$, respectively). Moreover, for the optimal time scales, the estimation performance for the post velocity was significantly above chance level for the tested populations of turtle and fish RGC ($p < 0.005$ and $p < 0.05$, respectively).

For the *ISI metrics*, the estimation results for the 500 ms and the first 200 ms intervals were qualitatively similar for each of the tested RGC populations. Moreover, in comparison to the results yielded by the optimal time scales for the spike cost-based metrics, the ISI metrics generally yielded better estimation results for both 200 ms intervals, whereas for the 500 ms interval, the opposite happened (Figure 3.43). Thereby, for all the tested populations of *turtle* and *fish RGC*, the estimation performance for the post velocity was significantly above chance level for the three analysed time intervals ($p < 0.005$ and $p < 0.05$, respectively). Furthermore, the differences in the estimation performance for both velocities were frequently almost negligible.

For turtle RGC, the 500 ms interval led to the maximum median in the estimation performance under the Labelled Line hypothesis. Here, the time scale $1/q = \infty$ yielded estimation performances that reached 67.4%.

Functional Group

For the *spike cost-based metrics*, the differences in the estimation performance for both velocities were generally larger for medium and fine time scales. Here, and especially for the 500 ms and the first 200 ms intervals, time scales 16 ms $\leq 1/q \leq$ 62 ms yielded the greatest differences, which in turn were significant ($p < 0.005$). However, for these two time intervals, only medium time scales led to the highest estimation results for the post velocity. This finding points out the increase in the relevance of medium time scales

Figure 3.42: Estimation performance under the Pooled Population hypothesis, for the motion velocity of the moving stimulus after the instantaneous velocity changes. The estimation was carried out by applying spike cost-based metrics and ISI metrics on the combined activity of RGC within the three tested time intervals. Markers indicate the median of the estimation performance, whereas error bars represent the median of the differences in the estimation performance considering and disregarding the stimulus history. Downward bars indicate better estimation performance when the stimulus history is considered, while the opposite is true for upward bars. a) Turtle retinae, three experiments; $n = 10$ populations from each experiment and for each tested population size. b) Fish retinae five experiments; $n = 1$ population from each experiment.

a

Post velocity (Labelled Line)

b

Figure 3.43: Estimation performance under the Labelled Line hypothesis, for the motion velocity of the moving stimulus after the instantaneous velocity changes. The estimation was carried out by applying spike cost-based metrics and ISI metrics on the combined activity of RGC within the three tested time intervals. Markers indicate the median of the estimation performance, whereas error bars represent the median of the differences in the estimation performance considering and disregarding the stimulus history. Downward bars indicate better estimation performance when the stimulus history is considered, while the opposite is true for upward bars. a) Turtle retinae, three experiments; $n = 10$ populations from each experiment and for each tested population size. b) Fish retinae five experiments; $n = 1$ population from each experiment.
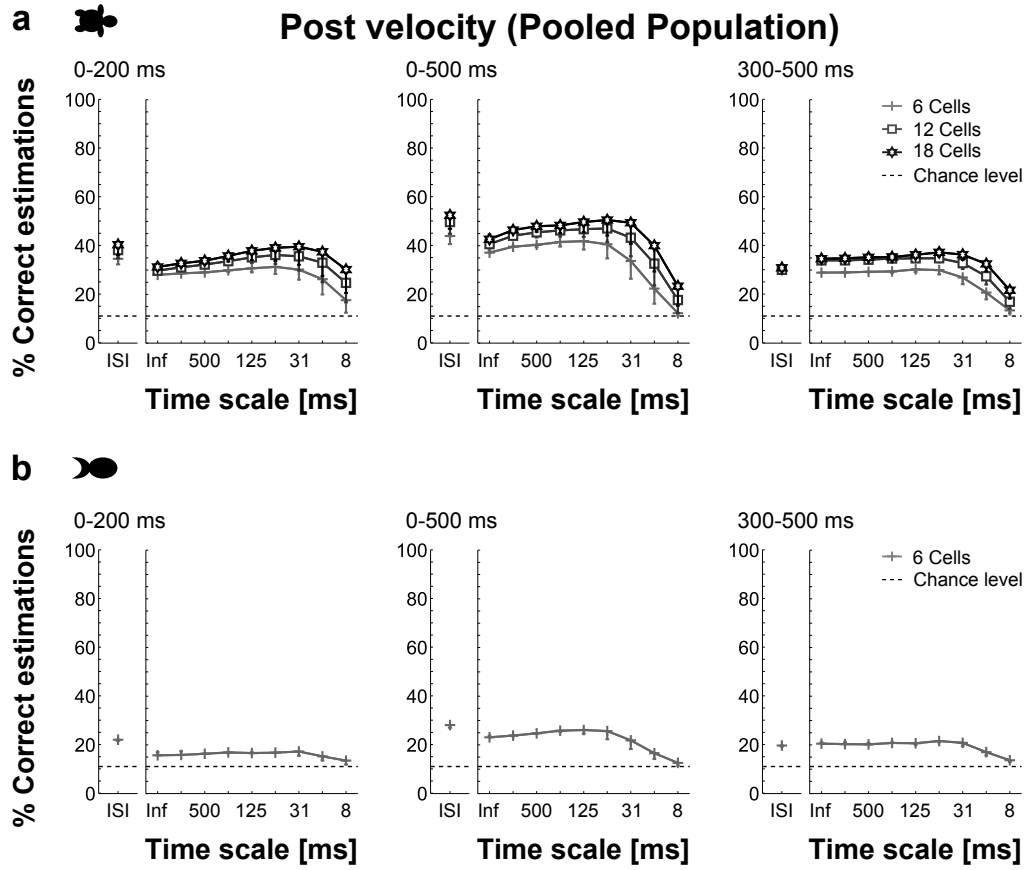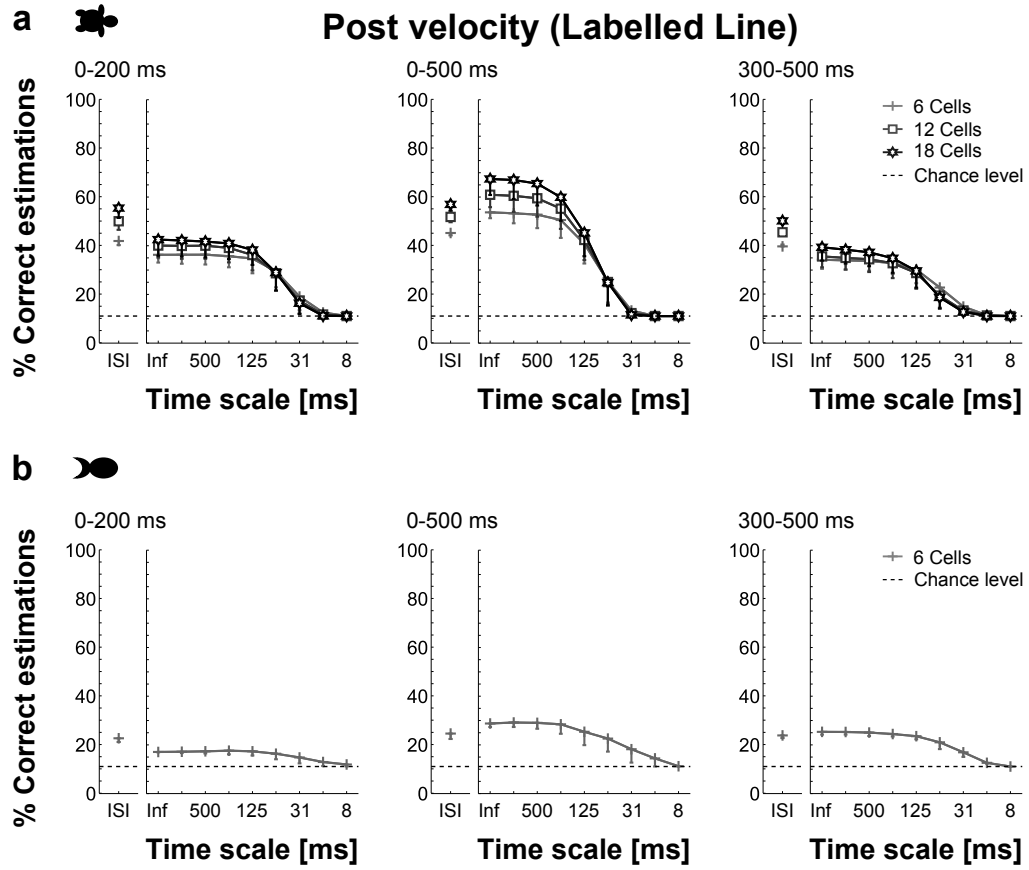
Figure 3.44: Estimation performance under the Functional Group hypothesis, for the motion velocity of the moving stimulus after the instantaneous velocity changes. The estimation was carried out by applying spike cost-based metrics and ISI metrics on the combined activity of RGC within the three tested time intervals. Markers indicate the median of the estimation performance, whereas error bars represent the median of the differences in the estimation performance considering and disregarding the stimulus history. Downward bars indicate better estimation performance when the stimulus history is considered, while the opposite is true for upward bars. Three experiments; $n = 10$ populations from each experiment and for each tested population size.

for the encoding of information about the motion velocity when the stimulus history is considered. For the three analysed time intervals, the estimation performance for the post velocity was significantly above chance level for all the tested populations of turtle RGC ($p < 0.005$).

For the first 200 ms interval, the results obtained for the *ISI metrics* generally exceeded those yielded by the optimal time scales for spike cost-based metrics. In contrast, for the 500 ms and the last 200 ms intervals, similar estimation performances were frequently found for both of the applied metrics. Therefore, for all the tested populations of turtle RGC, the estimation performance for the post velocity was significantly above chance level for the three analysed time intervals ($p < 0.005$). Moreover, the differences in the estimation performance between the two velocities were significant for the 500 ms and the first 200 ms intervals ($p < 0.005$). The maximum estimation results for the post motion velocity, obtained for both of the applied metrics under the three tested hypotheses, are summarised in the table in page 277.

Post direction

Generally, the estimation performance for the post direction was qualitatively similar to the one for the direction alone. Nevertheless, and especially for the spike cost-based metrics, the estimation of the post direction showed a tendency to yield better results. The combined activity of RGC led to better results for the estimation of the post direction than the ones yielded by the activity of single RGC. These results were found for the each corresponding joint activity coding hypotheses in both animal species. For both animal species, the maximum median in the estimation performance was for the 500 ms interval. Here, for turtle RGC, the estimation performances under the Functional Group hypothesis reached 88.3% for the time scale $1/q = 1000$ ms. In turn, for fish RGC, the estimation results under the Labelled Line hypothesis reached 59.3% for the time scale $1/q = \infty$.

Pooled Population

For the *spike cost-based metrics*, the greatest differences between the estimation of the post direction and the direction alone were observed for the 500 ms and the first 200 ms intervals. Here, these difference increased for finer time scales and were significant for turtle and fish RGC ($p < 0.005$ and $p < 0.05$, respectively). However, for these two time intervals, the maximum estimation performances for the post direction were frequently yielded by medium time scales (Figure 3.45). For three analysed time intervals, the estimation of the post direction, was significantly better than chance for all the tested *turtle RGC* populations ($p < 0.005$). However, for the tested populations of *fish RGC*, although the median of the estimation performance for the three analysed time intervals was above chance level, this difference was only significant for coarse time scales within the 500 ms interval ($p < 0.05$).

For *ISI metrics*, the estimation of the post direction and the direction alone showed slight differences. Nonetheless, these differences were significant for *turtle* and *fish RGC* ($p < 0.005$ and $p < 0.05$, respectively). Therefore, for the three analysed time intervals, the estimation performance for the post direction was significantly above chance level for all the tested populations of turtle and fish RGC ($p < 0.005$ and $p < 0.05$, respectively).

For both animal species, the 500 ms interval led to the maximum median in the estimation performance under the Pooled Population hypothesis. Here, the ISI metrics yielded estimation performances that reached 68.4% for turtle RGC. In turn, for fish RGC, the time scale $1/q = 250$ ms led to estimation results that reached 52.2%.
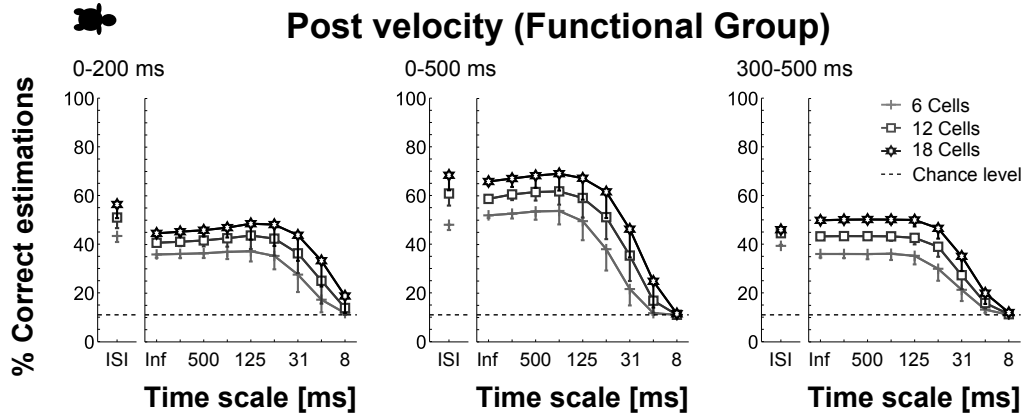
Figure 3.45: Estimation performance under the Pooled Population hypothesis, for the motion direction of the moving stimulus after the instantaneous velocity changes. The estimation was carried out by applying spike cost-based metrics and ISI metrics on the combined activity of RGC within the three tested time intervals. Markers indicate the median of the estimation performance, whereas error bars represent the median of the differences in the estimation performance considering and disregarding the stimulus history. Downward bars indicate better estimation performance when the stimulus history is considered, while the opposite is true for upward bars. a) Turtle retinae, three experiments; $n = 10$ populations from each experiment and for each tested population size. b) Fish retinae five experiments; $n = 1$ population from each experiment.

Labelled Line

For *spike cost-based metrics*, the greater differences in the estimation performance for the post direction and direction alone were observed for medium and coarse time scales. Moreover, these differences were found for the three analysed time intervals and were significant for all the tested populations of turtle and fish RGC ($p < 0.005$ and $p < 0.05$, respectively). Nevertheless, as in the case of the direction alone, the time scale $1/q = \infty$ led to the highest estimation results for the post direction for all cases (Figure 3.46). Thereby, the estimation results for the post direction for this time scale, and the three analysed time intervals, were significantly above chance level for all the tested *turtle RGC* populations ($p < 0.005$). However, for populations of *fish RGC*, this time scale led to significant results only for the 500 ms and the first 200 ms intervals ($p < 0.05$).

Generally, for the *ISI metrics*, the estimation results for the post direction and direction alone were similar for the tested populations of *turtle RGC*. Therefore, these results were significantly above chance level for the three three analysed time intervals ($p < 0.005$). In contrast, for populations of *fish RGC*, the estimation of the post direction led generally to significantly better results ($p < 0.05$). Nonetheless, these results were significantly above chance level for the two 200 ms intervals ($p < 0.05$).

For turtle RGC, the 500 ms interval led to the maximum median in the estimation performance under the Labelled Line hypothesis. Here, the time scale $1/q = \infty$ yielded estimation performances that reached 83.4%.

Functional Group

For the *spike cost-based metrics*, the greatest differences between the estimation performances for the post direction and the direction alone were generally yielded by fine time scales. Here, although these differences were significant ($p < 0.005$), coarse and medium time scales led to the maximum estimation performances for the post direction (Figure 3.47). In turn, for all the tested populations of turtle RGC, these performances were significantly above chance level ($p < 0.005$).

In the case of the *ISI metrics*, for all the tested turtle RGC populations, the estimation results for the post direction were similar to those for the direction alone. Thereby, for the three analysed time intervals, the estimation performance for the post direction was significantly above chance level ($p < 0.005$). The maximum estimation results for the post motion direction, obtained for both of the applied metrics under the three tested hypotheses, are summarised in the table in page 278.
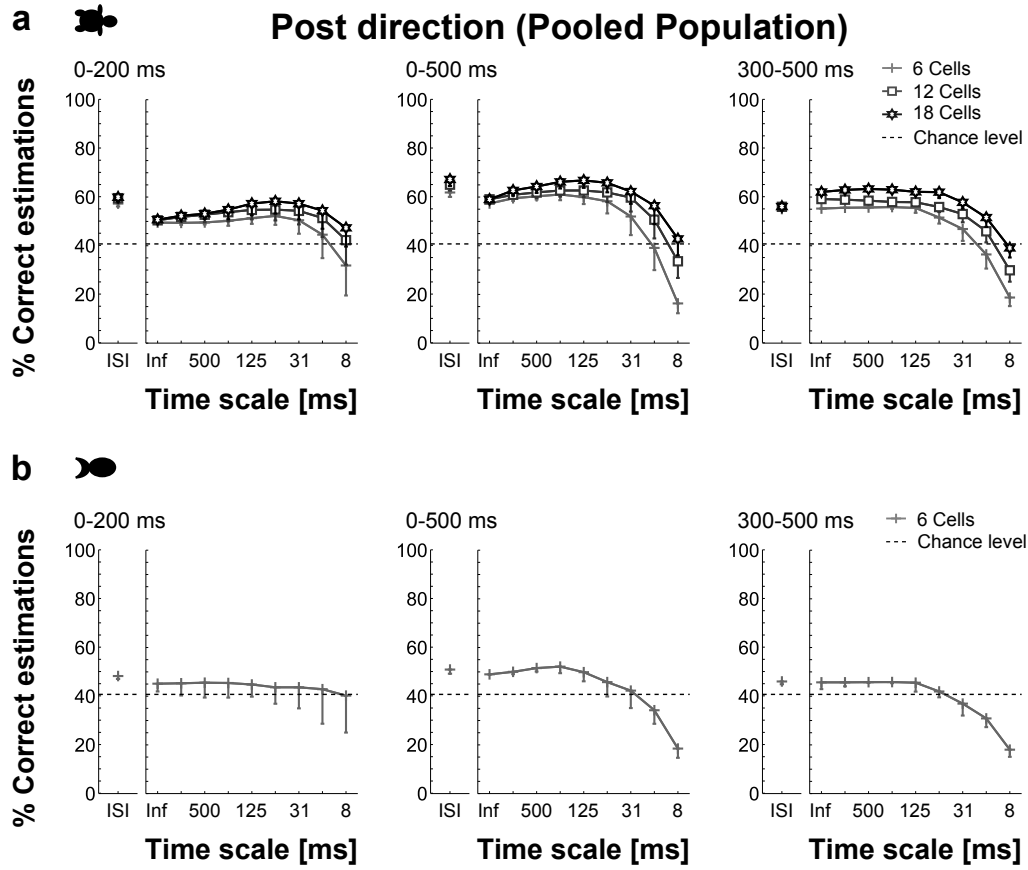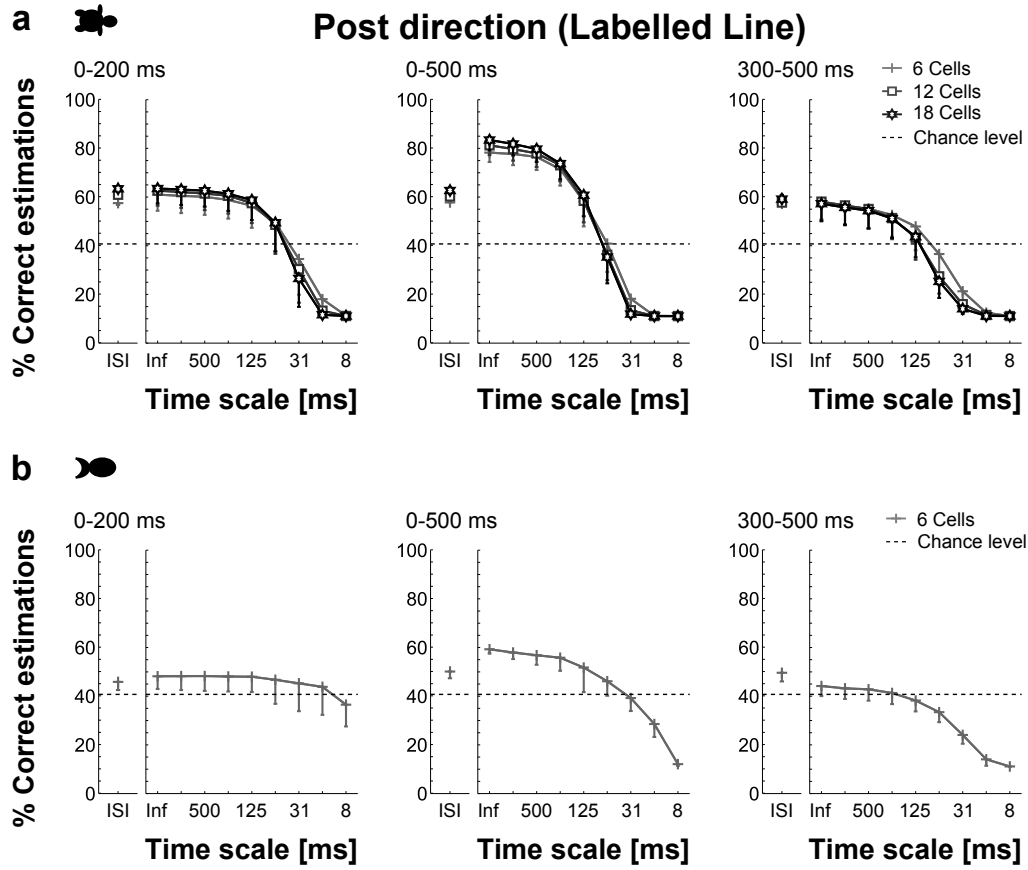
Figure 3.46: Estimation performance under the Labelled Line hypothesis, for the motion direction of the moving stimulus after the instantaneous velocity changes. The estimation was carried out by applying spike cost-based metrics and ISI metrics on the combined activity of RGC within the three tested time intervals. Markers indicate the median of the estimation performance, whereas error bars represent the median of the differences in the estimation performance considering and disregarding the stimulus history. Downward bars indicate better estimation performance when the stimulus history is considered, while the opposite is true for upward bars. a) Turtle retinae, three experiments; $n = 10$ populations from each experiment and for each tested population size. b) Fish retinae five experiments; $n = 1$ population from each experiment.

Figure 3.47: Estimation performance under the Functional Group hypothesis, for the motion direction of the moving stimulus after the instantaneous velocity changes. The estimation was carried out by applying spike cost-based metrics and ISI metrics on the combined activity of RGC within the three tested time intervals. Markers indicate the median of the estimation performance, whereas error bars represent the median of the differences in the estimation performance considering and disregarding the stimulus history. Downward bars indicate better estimation performance when the stimulus history is considered, while the opposite is true for upward bars. Three experiments; $n = 10$ populations from each experiment and for each tested population size.

Post speed

For the post speed, the combined activity of RGC generally led to lower estimation errors than the ones yielded by the activity of single RGC. Furthermore, the lowest estimation errors were frequently obtained for the 500 ms interval. In turn, comparing the estimation results for the post speed and the speed alone, almost no differences were found for the ISI metrics. These results were obtained for both animal species under the Pooled Population hypothesis as well as under the Labelled Line hypothesis. However, for the spike cost-based metrics, the estimation errors for the post speed were generally lower. Here, the Labelled Line hypothesis led to qualitatively similar estimation errors for the post speed and the speed alone. Nevertheless, although some similarities were found for the other two hypotheses, it was observed that fine and medium time scales gained relevance for the encoding of information about the post speed, especially for the 500 ms and the first 200 ms intervals. For both animal species, the lowest median in the estimation error was obtained for the 500 ms interval. Here, under the Functional Group hypothesis, the ISI metrics led to normalised absolute errors that reached 0.17 for turtle RGC. In turn, for fish RGC, the time scale $1/q = \infty$ under the Labelled Line hypothesis led to estimation errors that reached 0.6.

Pooled Population

For the *spike cost-based metrics*, the largest differences between the estimation performance for the post speed and the speed alone were observed for fine time scales within the 500 ms and the first 200 ms intervals (Figure 3.48). Furthermore, for all the tested *turtle* and *fish RGC* populations, these differences were significant ($p < 0.005$ and $p < 0.05$, respectively). In turn, the maximum estimation performance for these two time intervals was generally yielded by time scales 31 ms $\leq 1/q \leq$ 125 ms. This finding points out that when the stimulus history is considered, these time scales gain relevance for the encoding of information about the post speed. Thereby, for the three analysed time intervals, all the tested populations of *turtle* and *fish RGC* populations led to estimation errors for the post motion speed, that were significantly below chance level ($p < 0.005$ and $p < 0.05$, respectively).

As mentioned at the beginning of this section, the estimation results obtained for the *ISI metrics* were similar for the post speed and the speed alone. Thereby, all the tested *turtle* and *fish RGC* populations yielded estimation errors significantly below chance level for the three analysed time intervals ($p < 0.005$ and $p < 0.05$, respectively).

For both animal species, the 500 ms interval led to the lowest median in

the estimation error under the Pooled Population hypothesis. Here, the ISI metrics yielded estimation errors that reached 0.22 and 0.61 for turtle and fish RGC, respectively.

Labelled Line

For the *spike cost-based metrics*, time scales 31 ms $\leq 1/q \leq$ 62 ms led to the greatest differences between the estimation performance for the post speed and the speed alone. For the three analysed time intervals, these differences were significant for all the tested *turtle RGC* populations $p < 0.005$). In contrast, for the *fish RGC* populations, these differences were significant only for the 500 ms and the first 200 ms intervals ($p < 0.05$). In turn, the time scale $1/q = \infty$ generally yielded the lowest estimation errors for the post motion speed (Figure 3.49). Here, for all the tested turtle RGC populations, these errors were significantly below chance level for the three analysed time intervals ($p < 0.005$). Conversely, for the fish RGC populations, significant results were only found for the 500 ms and the first 200 ms intervals ($p < 0.05$).

For the *ISI metrics*, the estimation errors for the post motion speed and the speed alone were similar for all cases. Thereby, for all the tested *turtle RGC* populations, the estimation errors for the post motion speed was significantly below chance level for the three analysed time intervals ($p < 0.005$). Although for the three analysed time intervals the median of the estimation errors for the post speed was below chance level, this difference was not significant for the populations of *fish RGC*.

For turtle RGC, the 500 ms interval led to the lowest median in the estimation error under the Labelled Line hypothesis. Here, the time scale $1/q = \infty$ yielded estimation errors that reached 0.22.

Functional Group

For *spike cost-based metrics*, although fine time scales generally led to the greatest differences in the estimation performance for the post speed and speed alone, these differences were greater for the 500 ms and the first 200 ms intervals (Figure 3.50). Moreover, in all cases, these differences were significant ($p < 0.005$). Nevertheless, for the turtle RGC, medium time scales of their activity within the 500 ms and the first 200 ms intervals gained relevance with increasing population sizes. Furthermore, for the largest turtle RGC populations, these time scales generally led to the lowest estimation errors for the post speed. Thereby, the estimation error for the post motion speed, yielded by the combined activity of turtle RGC, was significantly

Figure 3.48: Absolute normalised estimation under the Pooled Population hypothesis, for the motion speed of the moving stimulus after the instantaneous velocity changes. The estimation was carried out by applying spike cost-based metrics and ISI metrics on the combined activity of RGC within the three tested time intervals. Markers indicate the median of the estimation performance, whereas error bars represent the median of the differences in the estimation performance considering and disregarding the stimulus history. Upward bars indicate lower estimation errors when the stimulus history is considered, while the opposite is true for downward bars. a) Turtle retinae, three experiments; $n = 10$ populations from each experiment and for each tested population size. b) Fish retinae five experiments; $n = 1$ population from each experiment.

Figure 3.49: Absolute normalised estimation under the Labelled Line hypothesis, for the motion speed of the moving stimulus after the instantaneous velocity changes. The estimation was carried out by applying spike cost-based metrics and ISI metrics on the combined activity of RGC within the three tested time intervals. Markers indicate the median of the estimation performance, whereas error bars represent the median of the differences in the estimation performance considering and disregarding the stimulus history. Upward bars indicate lower estimation errors when the stimulus history is considered, while the opposite is true for downward bars. a) Turtle retinae, three experiments; $n = 10$ populations from each experiment and for each tested population size. b) Fish retinae five experiments; $n = 1$ population from each experiment.
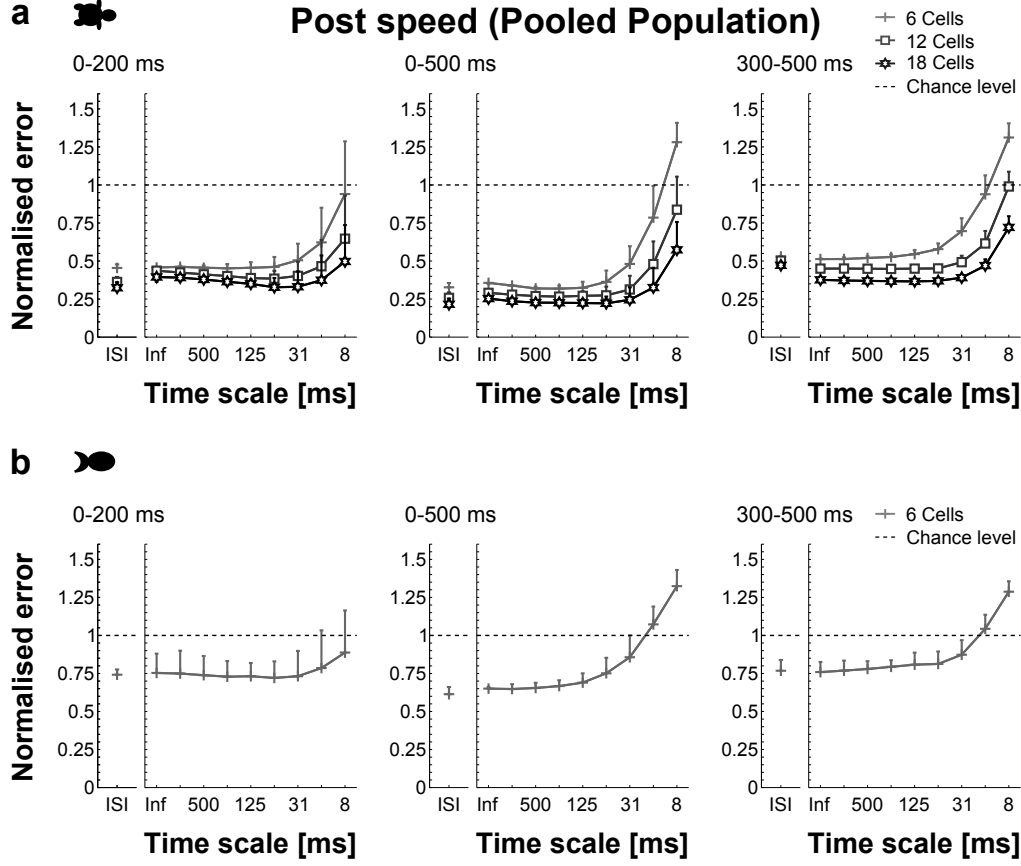
Figure 3.50: Absolute normalised estimation under the Functional Group hypothesis, for the motion speed of the moving stimulus after the instantaneous velocity changes. The estimation was carried out by applying spike cost-based metrics and ISI metrics on the combined activity of RGC within the three tested time intervals. Markers indicate the median of the estimation performance, whereas error bars represent the median of the differences in the estimation performance considering and disregarding the stimulus history. Upward bars indicate lower estimation errors when the stimulus history is considered, while the opposite is true for downward bars. Three experiments; $n = 10$ populations from each experiment and for each tested population size.

above chance level for the three analysed time intervals ($p < 0.005$).

For the *ISI metrics*, the errors in the estimation of the post speed and the speed alone were generally similar for all the tested turtle RGC populations. Therefore, for all the tested turtle RGC populations, the estimation errors for the post motion speed were significantly below chance level for the three analysed time intervals ($p < 0.005$). The lowest estimation errors for the post motion speed, obtained for both of the applied metrics under the three tested hypotheses, are summarised in the table in page 279.

Speed changes

For the estimation of the three possible changes in motion speed, the combined activity of RGC generally led to better estimation performances than the activity of single RGC. Moreover, in the case of turtle RGC, larger populations frequently improved the estimation performance, especially for the 500 ms and the first 200 ms intervals, for which the estimation results were

also the highest. Moreover, these two time intervals led frequently to similar estimation results. In contrast, the last 200 ms interval led generally to poor estimation performances. These results were obtained for both of the applied metrics and under the three tested joint activity coding hypotheses. For the spike cost-based metrics, the time scales that were optimal for the estimation of the instantaneous velocity changes varied across the three tested hypothesis. Furthermore, these time scales not always yielded the largest improvements for larger turtle RGC populations. Qualitatively similar estimation results were obtained for both animal species under the Pooled Population hypothesis as well as under the Labelled Line hypothesis. For turtle RGC, the maximum median in the estimation performance was yielded by the time scale $1/q = 16$ ms of the first 200 ms interval. Here, the estimation performances under the Pooled Population hypothesis reached 84%. In turn, for fish RGC, the maximum median in the estimation results was yielded by the time scale $1/q = 500$ ms of the 500 ms interval. Here, the estimation performances under the Labelled Line hypothesis reached 64.8%.

Pooled Population

Generally, for the *spike cost-based metrics*, the time scale $1/q = \infty$ showed to encode information about the changes in motion speed. Nonetheless, the estimation performance for the 500 ms and the first 200 ms intervals was generally the highest for time scales 8 ms $\leq 1/q \leq 31$ ms. Moreover, in the case of the turtle RGC, these time scales led to the largest improvements for larger populations (Figure 3.51). In turn, the estimation result yielded by these time scales within the 500 ms and the first 200 ms intervals, were significantly above chance level for all the tested populations of *turtle* and *fish RGC* ($p < 0.005$ and $p < 0.005$, respectively).

For the *ISI metrics*, and especially for the 500 ms and the first 200 ms intervals, the estimation performance obtained for all the tested populations of RGC was quantitatively similar to the one yielded by the optimal time scales for the spike cost-based metrics. Thereby, for these two time intervals, the estimation performance for all the tested *turtle* and *fish RGC* populations was significantly above chance level ($p < 0.005$ and $p < 0.05$, respectively).

For fish RGC, the 500 ms interval led the maximum median in the estimation performance under the Pooled Population hypothesis. Here, the time scale $1/q = 125$ ms yielded estimation performances that reached 64.7%.

Figure 3.51: Estimation performance under the Pooled Population hypothesis, for the changes in the motion speed of the moving stimulus. The estimation was carried out by applying spike cost-based metrics and ISI metrics on the combined activity of RGC within the three tested time intervals. Markers indicate the median, whereas error bars represent the range between maximum and minimum estimation performance. a) Turtle retinae, three experiments; $n = 10$ populations from each experiment and for each tested population size. b) Fish retinae five experiments; $n = 1$ population from each experiment.

Labelled Line

For the *spike cost-based metrics*, fine time scales led generally for estimation results close to those expected by chance, whereas the highest estimation performances were yielded by medium and coarse time scales. Moreover, in the case of the *turtle RGC*, all of the tested population sizes yielded similar estimation results for each of the analysed time intervals (Figure 3.52). Thereby, for the optimal time scales, and especially for the 500 ms and the first 200 ms intervals, the estimation performance was significantly above chance level for all the tested populations of turtle RGC ($p < 0.005$). In turn, for the tested *fish RGC* populations, coarse time scales led to estimation performances whose median was above chance level for the three analysed time intervals. However, this difference was significant only for the 500 ms and the last 200 ms intervals ($p < 0.05$).

For all the tested *turtle RGC* populations, and in the particular case of the 500 ms and the first 200 ms intervals, the estimation results obtained for the *ISI metrics* were quantitatively similar to those yielded by the optimal time scales for the spike cost-based metrics. Thus, these results were significantly above chance level for these two time intervals ($p < 0.005$). Moreover, the estimation results were also significantly above chance level for the tested *fish RGC* populations ($p < 0.05$). Nevertheless, these results were not as good as the maximum estimation results obtained for the spike cost-based metrics.

For turtle RGC, the first 200 ms interval led to the maximum median in the estimation performance under the Labelled Line hypothesis. Here, the ISI metrics yielded estimation performances that reached 80.2%.

Functional Group

For the *spike cost-based metrics*, the time scale $1/q = \infty$ generally led to good estimation results for the changes in motion speed. However, for the 500 ms and first 200 ms intervals, time scales $31 \text{ ms} \leq 1/q \leq 62 \text{ ms}$ led to the highest estimation results. Moreover, for time scales $1/q \leq 125 \text{ ms}$, the estimation performance improved with increasing sizes of the populations of turtle RGC (Figure 3.53). In this sense, for all the tested populations of turtle RGC, the estimation performance was significantly above chance level for the three analysed time intervals ($p < 0.005$)

Generally, in the case of the estimation results obtained for the *ISI metrics*, these were quantitatively similar to those yielded by the optimal time scales for the spike cost-based metrics. Therefore, the estimation performance for all the tested populations of turtle RGC was significantly above
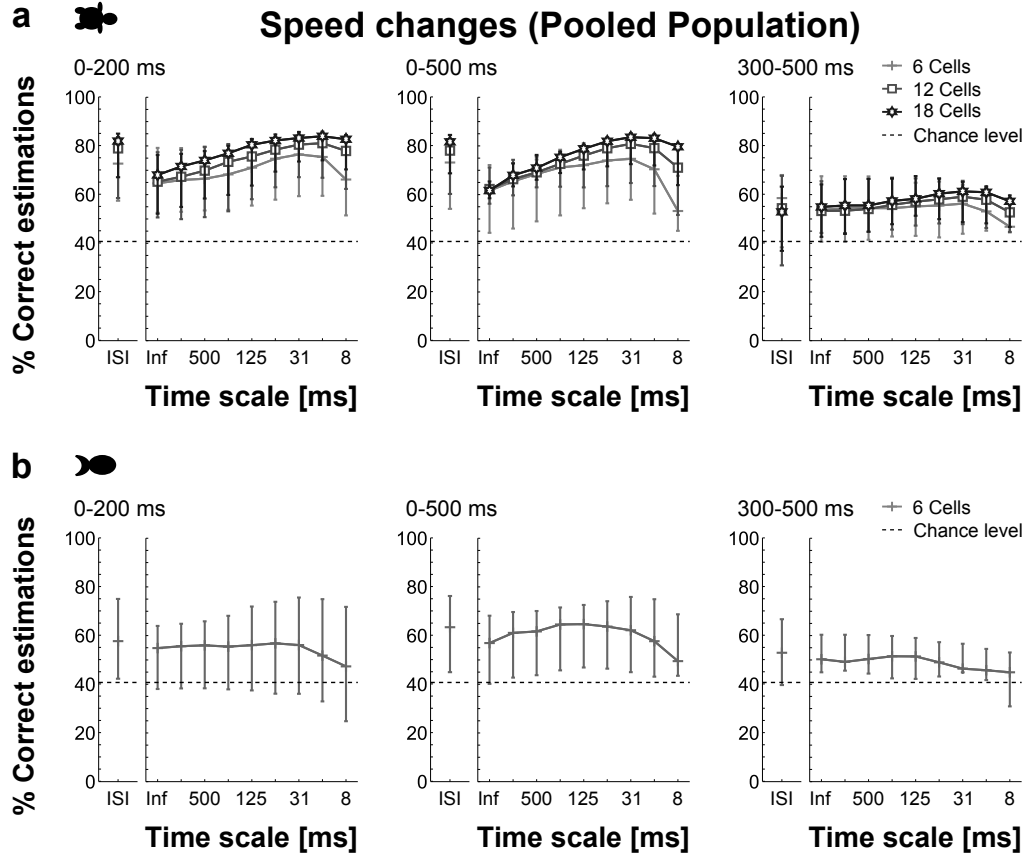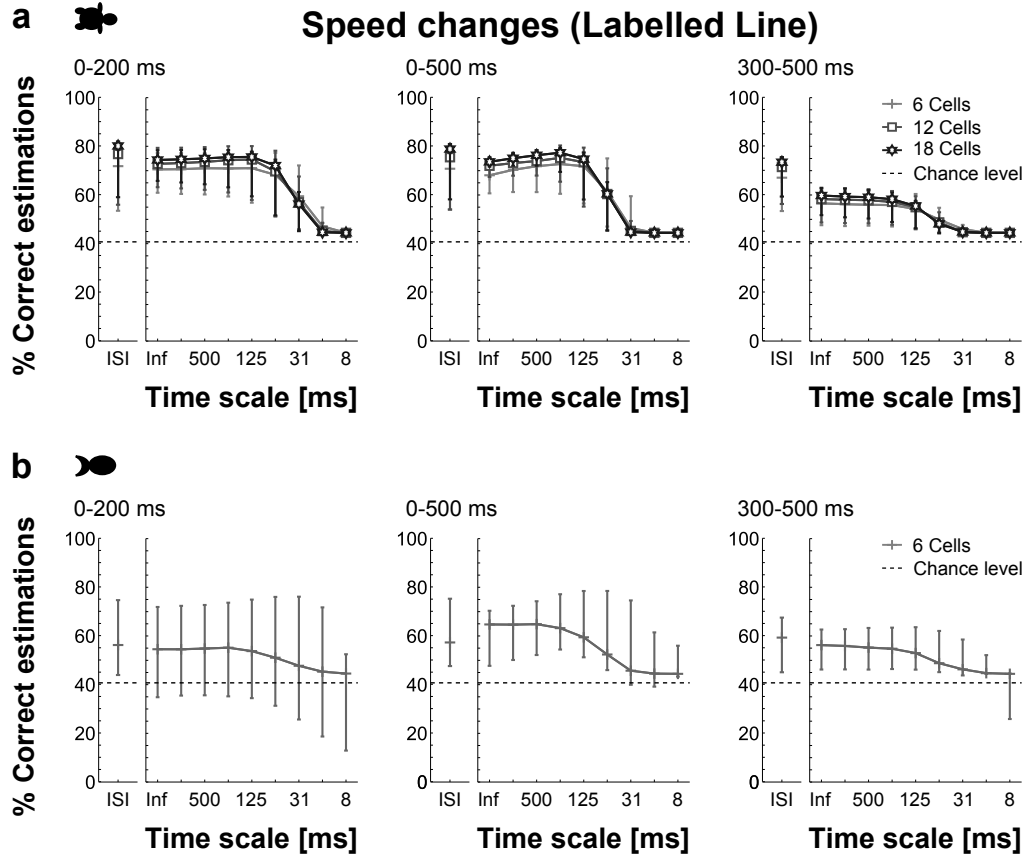
Figure 3.52: Estimation performance under the Labelled Line hypothesis, for the changes in the motion speed of the moving stimulus. The estimation was carried out by applying spike cost-based metrics and ISI metrics on the combined activity of RGC within the three tested time intervals. Markers indicate the median, whereas error bars represent the range between maximum and minimum estimation performance. a) Turtle retinae, three experiments; $n = 10$ populations from each experiment and for each tested population size. b) Fish retinae five experiments; $n = 1$ population from each experiment.
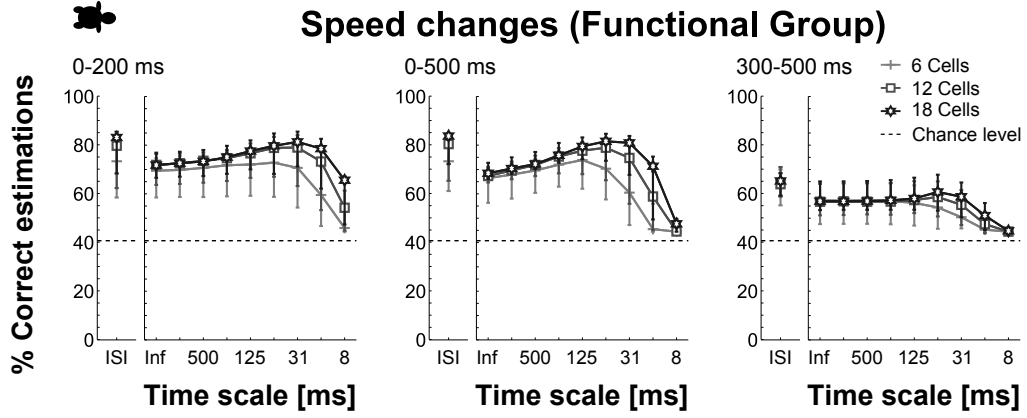
Figure 3.53: Estimation performance under the Functional Group hypothesis, for the changes in the motion speed of the moving stimulus. The estimation was carried out by applying spike cost-based metrics and ISI metrics on the combined activity of turtle RGC within the three tested time intervals. Markers indicate the median, whereas error bars represent the range between maximum and minimum estimation performance. Three experiments; $n = 10$ populations from each experiment and for each tested population size.

chance level for the three analysed time intervals ($p < 0.005$). The maximum estimation results for the changes in motion speed, obtained for both of the applied metrics under the three tested hypotheses, are summarised in the table in page 280.

The 500 ms interval led to the maximum median in the estimation performance under the Functional hypothesis. Here, the ISI metrics yielded estimation performances that reached 83.8%.

Direction changes

The estimation performance for the three possible changes in motion direction, allowed by the combined activity of RGC, generally showed qualitative similarities with the performance for the changes in motion speed. Nevertheless, and especially in the case of the results obtained for the spike cost-based metrics, some differences were also observed. For instance, fine time scales led some of the times to estimation results worse than those expected by chance. Furthermore, the differences in the estimation performance across the tested sizes of turtle RGC populations was slightly larger. Here, for

the three tested joint activity coding hypothesis, these differences were the largest for the time scales that led to the highest estimation performances. For both animal species, the maximum median in the estimation performance was obtained under the Pooled Population hypothesis for the 500 ms interval. Here, the ISI metrics led estimation performances that reached 75.9% and 55.% for turtle and fish RGC, respectively.

Pooled Population

For the *spike cost-based metrics*, and in the particular case of *turtle RGC*, time scales 31 ms $\leq 1/q \leq 62$ ms led to the highest estimation performances for the 500 ms and the first 200 ms intervals. In contrast, for *fish RGC* populations, time scales 31 ms $\leq 1/q \leq 250$ ms led to the highest estimation results for these two time intervals (Figure 3.54). Thereby, for the optimal time scales within the 500 ms and the first 200 ms intervals, the estimation performance was significantly above chance level for all the tested turtle and fish RGC populations ($p < 0.005$ and $p < 0.05$, respectively).

For the 500 ms and the first 200 ms intervals, the estimation results obtained for the *ISI metrics* generally exceeded the ones yielded by the optimal time scales for the spike cost-based metrics. Thus, for these two time intervals, the estimation results yielded by all the tested populations of *turtle* and *fish RGC* were significantly above chance level ($p < 0.005$ and $p < 0.05$, respectively).

Labelled Line

For the *spike cost-based metrics*, fine time scales generally led to estimation performances below chance level. However, time scales $1/q \geq 125$ ms led to the highest estimation results, particularly for the 500 ms and the first 200 ms intervals (Figure 3.55). In this sense, for the optimal time scales within the 500 ms and the first 200 ms intervals, the estimation results were significantly above chance level for all the tested populations of *turtle* and *fish RGC* ($p < 0.005$ and $p < 0.05$, respectively).

For the *ISI metrics*, the results obtained for both 200 ms intervals showed generally a tendency to exceed the ones yielded by the optimal time scales for the spike cost-based metrics. In contrast, for the 500 ms interval, the results obtained for both of the applied metrics were quantitatively similar. Therefore, for all the tested populations of *turtle* and *fish RGC*, the estimation performance was significantly above chance level ($p < 0.005$ and $p < 0.05$, respectively).

For turtle RGC, the first 200 ms interval led to the maximum median in

Figure 3.54: Estimation performance under the Pooled Population hypothesis, for the changes in the motion direction of the moving stimulus. The estimation was carried out by applying spike cost-based metrics and ISI metrics on the combined activity of RGC within the three tested time intervals. Markers indicate the median, whereas error bars represent the range between maximum and minimum estimation performance. a) Turtle retinae, three experiments; $n = 10$ populations from each experiment and for each tested population size. b) Fish retinae five experiments; $n = 1$ population from each experiment.

the estimation performance under the Labelled Line hypothesis. Here, the ISI metrics yielded estimation performances that reached 63.1%. In turn, for fish RGC, the 500 ms interval led to the maximum median in the estimation performance. Here, the time scale $1/q = 250$ ms yielded estimation performances that reached 51.7%.

Functional Group

For the *spike cost-based metrics* the time scale $1/q = 8$ ms led frequently to estimation performances below chance level. Nonetheless, coarser time scales led to better estimation results. Here, in the particular case of the 500 ms and the first 200 ms intervals, the estimation performance reached its maximum for time scales 31 ms $\leq 1/q \leq 125$ ms (Figure 3.56). Moreover, the optimal time scales within these two time intervals led to estimation performances significantly above chance level for all the tested populations of turtle RGC ($p < 0.005$).

For the 500 ms and the first 200 ms intervals, the estimation performance obtained for the *ISI metrics* was qualitatively similar to that obtained for the spike cost-based metrics. Nonetheless, it showed a tendency to exceed the estimation performance yielded by the optimal time scales for the spike cost-based metrics. Thus, for these two time intervals, the estimation performance was significantly above chance level for all the tested populations of turtle RGC ($p < 0.005$). The maximum estimation results for the changes in motion direction, obtained for both of the applied metrics under the three tested hypotheses, are summarised in the table in page 281.

The first 200 ms interval led to the maximum median in the estimation performance under the Functional hypothesis. Here, the ISI metrics yielded estimation performances that reached 75.8%.

Speed and direction changes

For the combined activity of RGC, the estimation performance for the seven possible combinations of changes in the motion speed and direction showed more qualitative similarities with the estimation performance for the changes in motion direction, than with the one for the changes in motion speed. For instance, in the case of the spike cost-based metrics, the time scales that led to the highest estimation performances also yielded the greater differences across the tested population sizes of turtle RGC. Furthermore, fine time scales led some of the times to estimation results below chance level. For both animal species, he ISI metrics led to the maximum median in the estimation performance. Here, for turtle RGC, the estimation performances under the
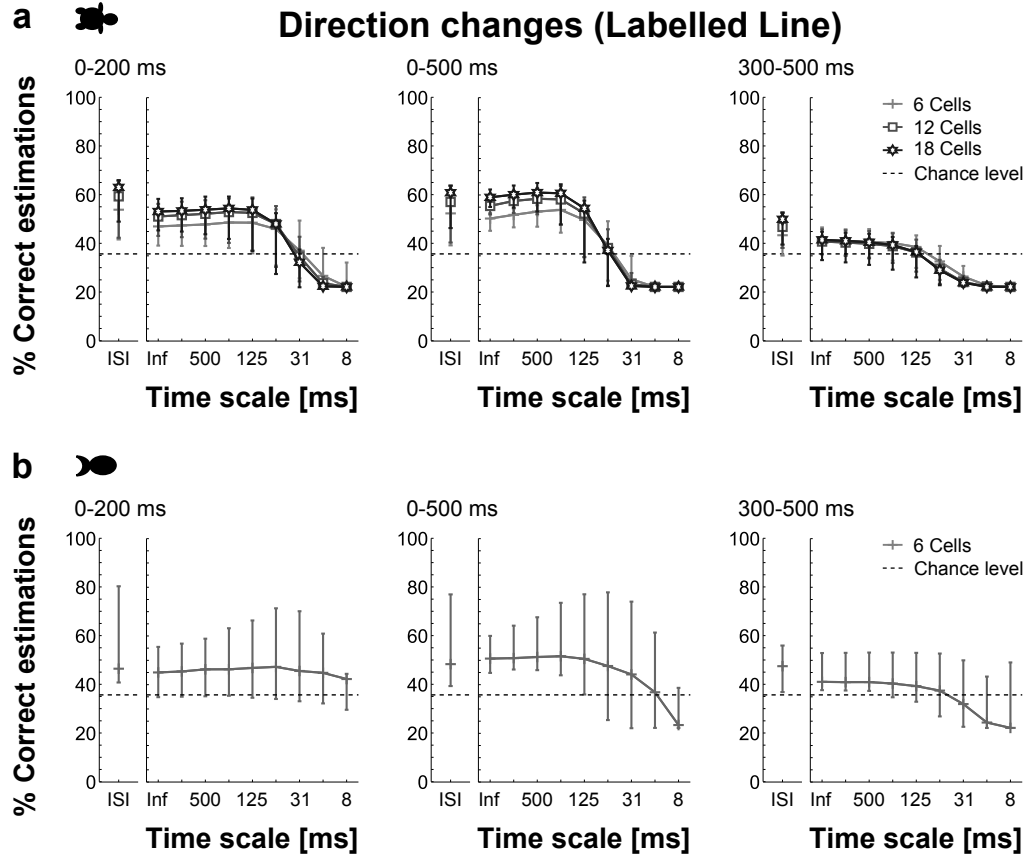
Figure 3.55: Estimation performance under the Labelled Line hypothesis, for the changes in the motion direction of the moving stimulus. The estimation was carried out by applying spike cost-based metrics and ISI metrics on the combined activity of RGC within the three tested time intervals. Markers indicate the median, whereas error bars represent the range between maximum and minimum estimation performance. a) Turtle retinae, three experiments; $n = 10$ populations from each experiment and for each tested population size. b) Fish retinae five experiments; $n = 1$ population from each experiment.
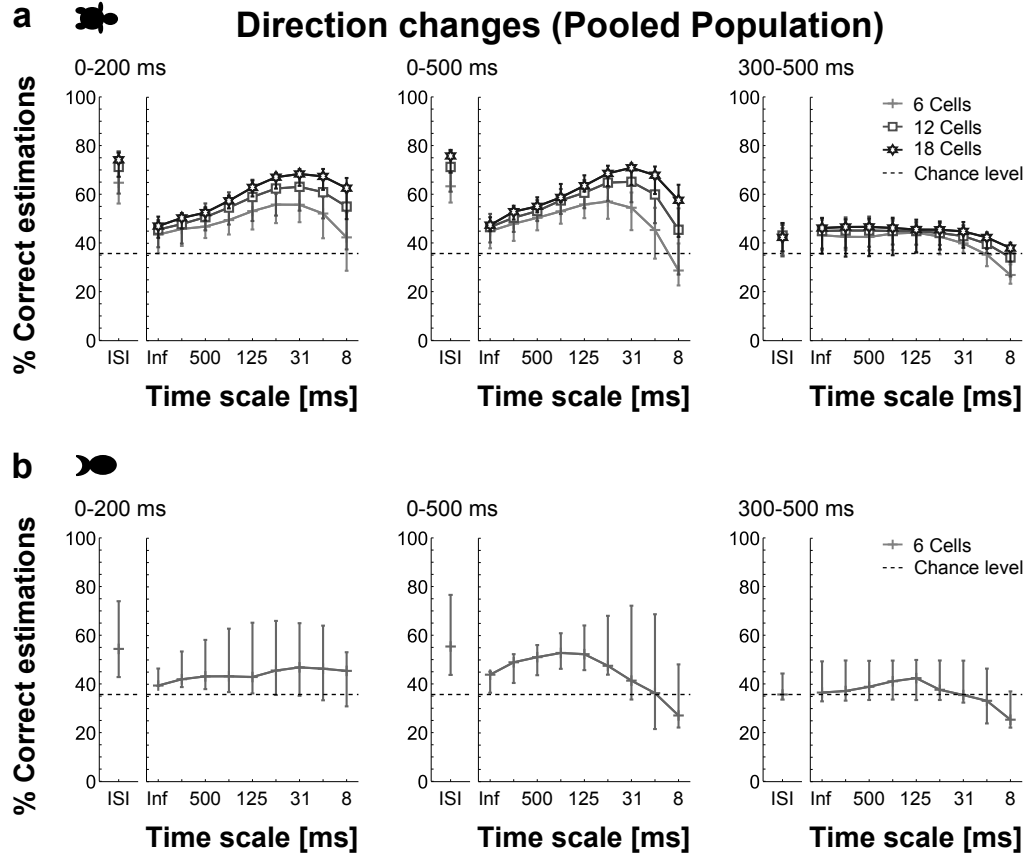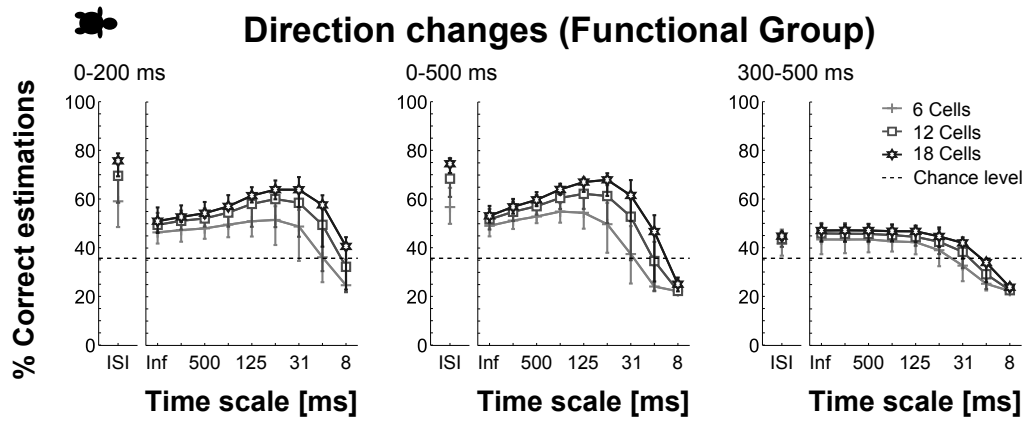
Figure 3.56: Estimation performance under the Functional Group hypothesis, for the changes in the motion direction of the moving stimulus. The estimation was carried out by applying spike cost-based metrics and ISI metrics on the combined activity of turtle RGC within the three tested time intervals. Markers indicate the median, whereas error bars represent the range between maximum and minimum estimation performance. Three experiments; $n = 10$ populations from each experiment and for each tested population size.

Functional Group hypothesis reached 65.1% for the first 200 ms interval.
In contrast, for fish RGC, the estimation performances under the Pooled
Population hypothesis reached 36.7% for the 500 ms interval.

Pooled Population

For the *spike cost-based metrics*, and particularly for *turtle RGC* popu-
lations, the estimation performance for the 500 ms and the first 200 ms
intervals was the highest for time scales 16 ms $\leq 1/q \leq$ 62 ms. In con-
trast, for these two time intervals, coarse and medium time scales led to the
maximum median of the estimation performances for $fish\ RGC$ populations
(Figure 3.57). Thereby, the optimal time scales within the 500 ms and the
first 200 ms interval led to estimation results significantly above chance level
for all the tested populations of turtle and fish RGC ($p < 0.005$ and $p < 0.05$,
respectively).

For the 500 ms and the first 200 ms intervals, the estimation results
obtained for the *ISI metrics* generally exceeded the ones yielded by the
optimal time scales for the spike cost-based metrics. Therefore, for these
two time intervals, all the tested populations of *turtle* and $fish\ RGC$ led to
estimation results significantly above chance level ($p < 0.005$ and $p < 0.05$,
respectively).

For turtle RGC, the 500 ms interval led to the maximum median in the
estimation performance under the Pooled Population hypothesis. Here, the
ISI metrics yielded estimation performances that reached 63.3%.

Labelled Line

For the *spike cost-based metrics*, the estimation performance yielded by
fine time scales was generally below chance level. However, and especially
for the 500 ms and the first 200 ms intervals, coarser time scales led to the
improvement in the estimation performance, which in turn appeared to reach
its maximum for time scales $1/q \geq$ 125 ms (Figure 3.58). Thereby, for all
the tested populations of *turtle* and $fish\ RGC$, the estimation results were
significantly above chance level ($p < 0.005$ and $p < 0.05$, respectively).

For the *ISI metrics*, the estimation results obtained for the 500 ms inter-
val were similar to those yielded by the optimal time scales for the spike cost-
based metrics. However, for both 200 ms intervals, the ISI metrics showed a
tendency to allow better estimation performances. Hence, and particularly
for the 500 ms and the first 200 ms intervals, the estimation performance was
significantly above chance level for all the tested populations of *turtle* and
$fish\ RGC$ ($p < 0.005$ and $p < 0.05$, respectively).
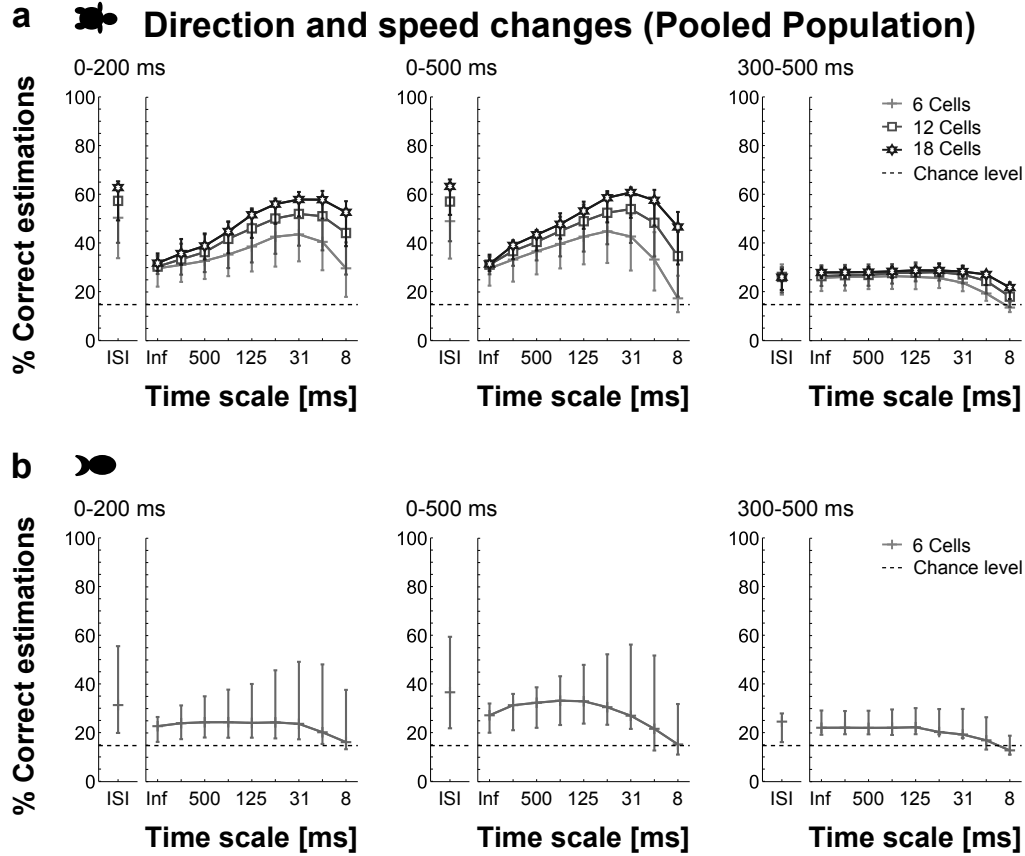
Figure 3.57: Estimation performance under the Pooled Population hypothesis, for the combined changes in the motion speed and direction of the moving stimulus. The estimation was carried out by applying spike cost-based metrics and ISI metrics on the combined activity of RGC within the three tested time intervals. Markers indicate the median, whereas error bars represent the range between maximum and minimum estimation performance. a) Turtle retinae, three experiments; $n = 10$ populations from each experiment and for each tested population size. b) Fish retinae five experiments; $n = 1$ population from each experiment.

For turtle RGC, the first 200 ms interval led to the maximum median in the estimation performance under the Labelled Line hypothesis. Here, the ISI metrics yielded estimation performances that reached 53.7%. In turn, for fish RGC, the 500 ms interval led to the maximum median in the estimation performance. Here, the time scale $1/q = 500$ ms yielded estimation performances that reached 33.1%.

Functional Group

Generally, for the *spike cost-based metrics*, the time scale $1/q = 8$ ms led to the poorest estimation performances. However, these performances improved for coarser time scales. Here, especially for the 500 ms and the first 200 ms intervals, the time scales 31 ms $\leq 1/q \leq$ 125 ms led to the highest estimation results (Figure 3.59). In turn, these time scales led to estimation performances significantly above chance level for all of the tested populations of turtle RGC ($p < 0.005$).

For the *ISI metrics* and particularly for the 500 ms and the first 200 ms intervals, the estimation results generally exceeded the ones yielded by the optimal time scales for the spike cost-based metrics. Thus, for all the tested turtle RGC populations, the estimation results were significantly above chance level ($p < 0.005$). The maximum estimation results for the combined changes in the motion speed and direction, obtained for both of the applied metrics under the three tested hypotheses, are summarised in the table in page 282.
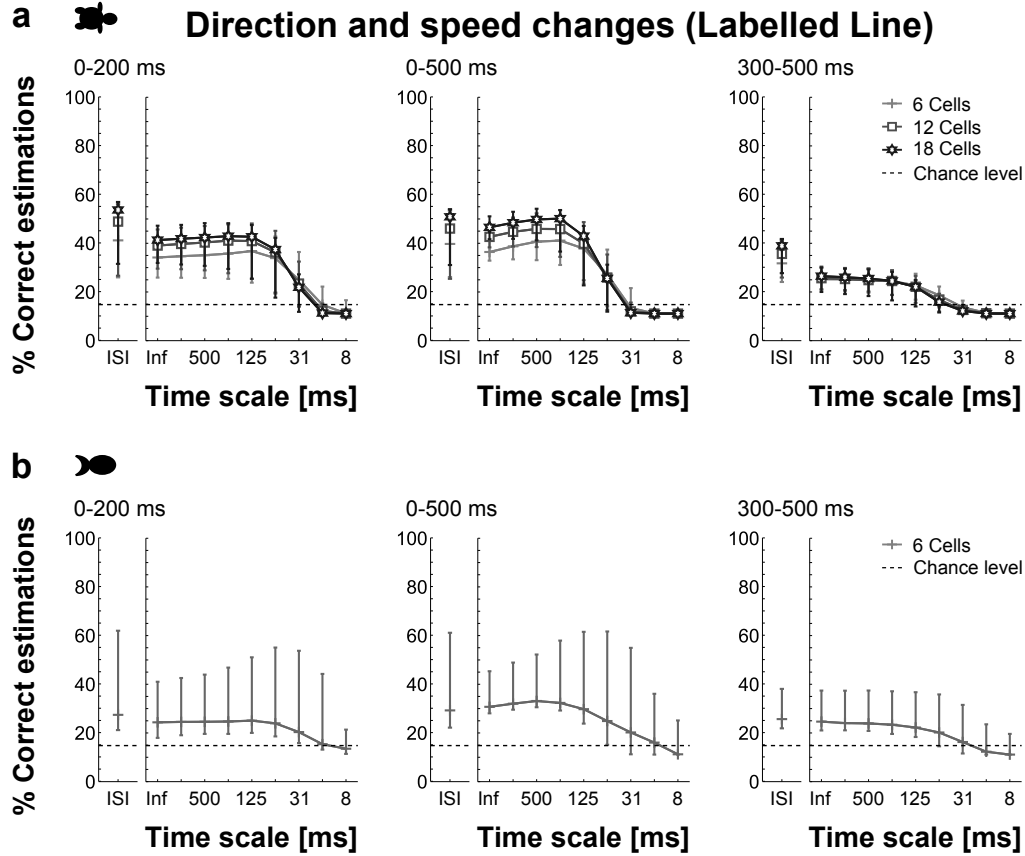
Figure 3.58: Estimation performance under the Labelled Line hypothesis, for the combined changes in the motion speed and direction of the moving stimulus. The estimation was carried out by applying spike cost-based metrics and ISI metrics on the combined activity of RGC within the three tested time intervals. Markers indicate the median, whereas error bars represent the range between maximum and minimum estimation performance. a) Turtle retinae, three experiments; $n = 10$ populations from each experiment and for each tested population size. b) Fish retinae five experiments; $n = 1$ population from each experiment.

Direction and speed changes (Functional Group)
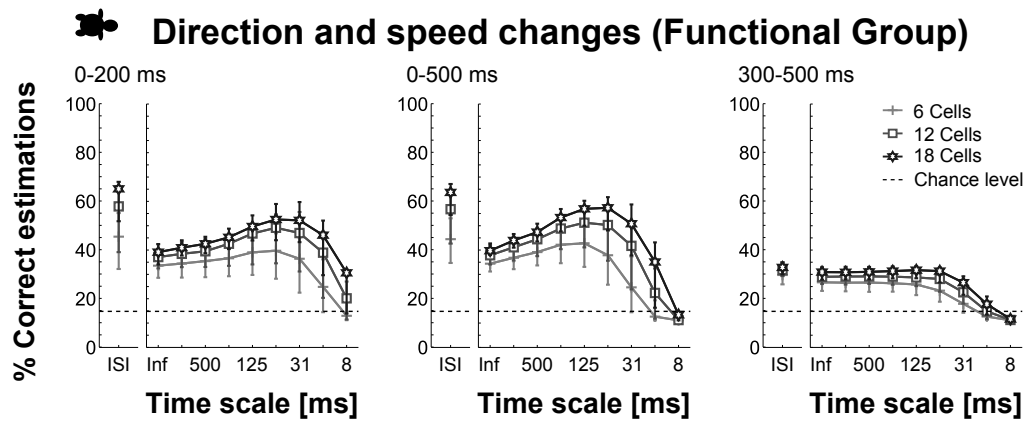
Figure 3.59: Estimation performance under the Functional Group hypothesis, for the combined changes in the motion speed and direction of the moving stimulus. The estimation was carried out by applying spike cost-based metrics and ISI metrics on the combined activity of turtle RGC within the three tested time intervals. Markers indicate the median, whereas error bars represent the range between maximum and minimum estimation performance. Three experiments; $n = 10$ populations from each experiment and for each tested population size.

3.2 Light-Motion Experiment

In a natural environment, the detection and estimation of motion have to be accomplished under dynamical light conditions. Therefore, an additional study explored how the activity of RGC encodes *simultaneously*, information about the light intensity and motion features of a visual stimulus. This study involved the design of a Light-Motion experiment protocol to record the responses of RGC to different light intensities and motion velocities. A detailed description of this experiment protocol can be found in Section 2.1.2. Briefly, the Light-Motion experiment protocol considered as visual stimulus the moving pattern of squares that was used in the Motion Experiment protocol. Furthermore, the protocol included different light intensities with which the pattern of squares was projected onto the retina. Four different light intensities and five different motion velocities comprised the experiment protocol. Here, the light intensity and motion velocity were instantaneously changed in periods of 500 ms in an alternate way.

For the Light-Motion experiment protocol, the activity of RGC from one retina of carp (*cyprinus carpio*) was recorded. After spike sorting, 114 RGC were identified (see Figure 2.4). Moreover, based on the visual inspection of the spike rate probability distributions of the recorded RGC, it was found that several RGC tuned their activity to the different light intensities and motion velocities of the stimulus. Here, the number of cells whose responses showed light intensity sensitivity, clearly exceeded the number of cells that exhibited motion sensitive responses. Figure 3.60 shows the spike firing rate probability distributions of the responses of a fish RGC to different light intensities under constant motion velocities (Figure 3.60a), and the probability distributions of the same RGC to different velocities under constant background luminance (Figure 3.60b). Here, it can be observed that the response properties of the depicted fish RGC depend on the combination of both stimulus features in a non-linear way.

A further characterisation of the responses of the fish RGC, can be observed in Figure 3.61. Here, the responses to the instantaneous changes of one of the visual stimulus features are represented. Thereby, the first two columns to the left in Figure 3.61 depict changes in the light intensity with which the pattern of squares is projected onto the retina. Here, for the stimulus transitions presented in these columns, the motion velocity of the pattern of squares was kept constant. Conversely, the last two columns depict changes in the motion velocity with a constant background luminance. For the changes in light intensity, the raster plots show a strong transient in the activity within the first milliseconds after the stimulus transition (Figure 3.61b). These transients are captured in the large activity peaks after the stimulus transition
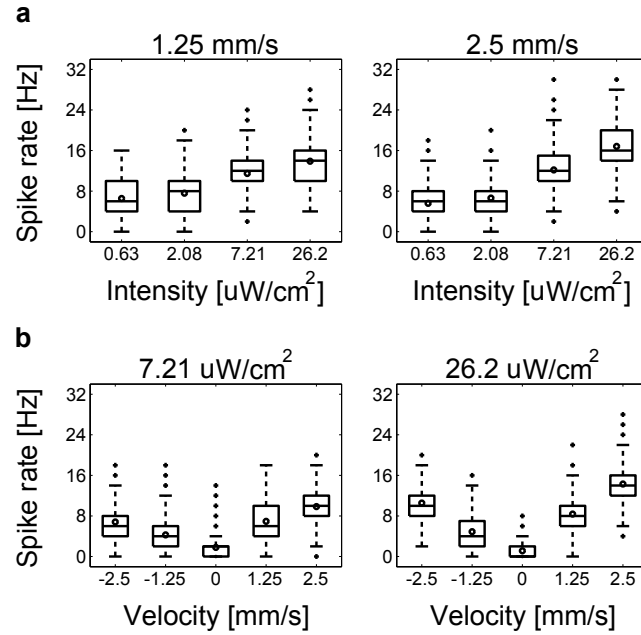
Figure 3.60: Firing rate probability distributions of one of the recorded fish RGC. Each box plot corresponds to each of the light intensities or velocities utilised in the experiment protocol. For the cell shown, the central mark within the box plots depicts the median, whereas the edges of the box plots refer to the 25th and 75th percentiles of the spike firing rate. In turn, whiskers extend to the most extreme spike firing rates which are not considered outliers. Finally, the circles depict the mean firing rate. a) Probability distributions for different light intensities under constant motion velocities. b) Probability distributions for different motion velocities under constant background light intensities.

depicted by the PSTH (Figure 3.61c). Nevertheless, although the change in light intensity is the same for both cases, the motion velocities of the moving stimulus yield different '*background*' or '*baseline*' activity. These differences can be observed in the late period of the responses depicted by the raster plots and the PSTH as well as in the shift of the spike count probability distribution (Figure 3.61d). In contrast, for identical motion velocity transitions with different background luminance, the responses of the fish RGC showed clearer differences (two right-most columns in Figure 3.61b and c). Here, the transients in the activity of the RGC were only evident for the brightest intensity of the projection light, whereas for the darkest intensity, the activity of the RGC remained relatively constant for the period in which the stimulus was presented. This phenomenon is captured by the difference in the probability distribution of the ISI (Figure 3.61d). Furthermore, it can be observed that the transients in the activity evoked by motion velocity changes for all background light intensities were weaker and slower than the ones evoked by changes in light intensity regardless of the motion velocity of the pattern of squares.

The characterisations shown in Figures 3.60 and 3.61, suggest that the activity of single fish RGC could in fact encode information about different stimulus features simultaneously. In this sense, by inspecting the spike rate probability distributions for light intensities and motion velocity of the depicted RGC, it can be observed that the strength of the responses to the different light intensities and motion velocities, is affected by the background motion and luminance conditions, respectively (Figure 3.60). Moreover, for the stimulus transitions shown in Figure 3.61, changes in light intensity provoke fast and strong transients in the activity of RGC, but have little effect in the sustained activity. In contrast, changes in the motion velocity provoke slower and weaker transients in the activity of RGC. However, constant motion velocities appear to have some effect in the sustained activity of RGC.

In order to explore more in detail the findings described in the previous paragraph, the activity of the recorded fish RGC was analysed using the spike cost-based metrics to estimate different features of the visual stimulus. Here, as in the case of the Motion Experiment protocol, the analysis was carried out within three time intervals; the 500 ms with constant stimulus features, the first 200 ms after the instantaneous change of a stimulus feature, and the last 200 ms before the next feature change. Furthermore, the results shown in this section were obtained considering the activity of single, as well as one population of $n = 18$ RGC. Here, the RGC considered for the analysis and therefore, to build the population, were selected by the visual inspection of the probability distribution of their spike firing rate to the different light projection intensities and motion velocities, e.g., Figure 3.60. Thereby, the
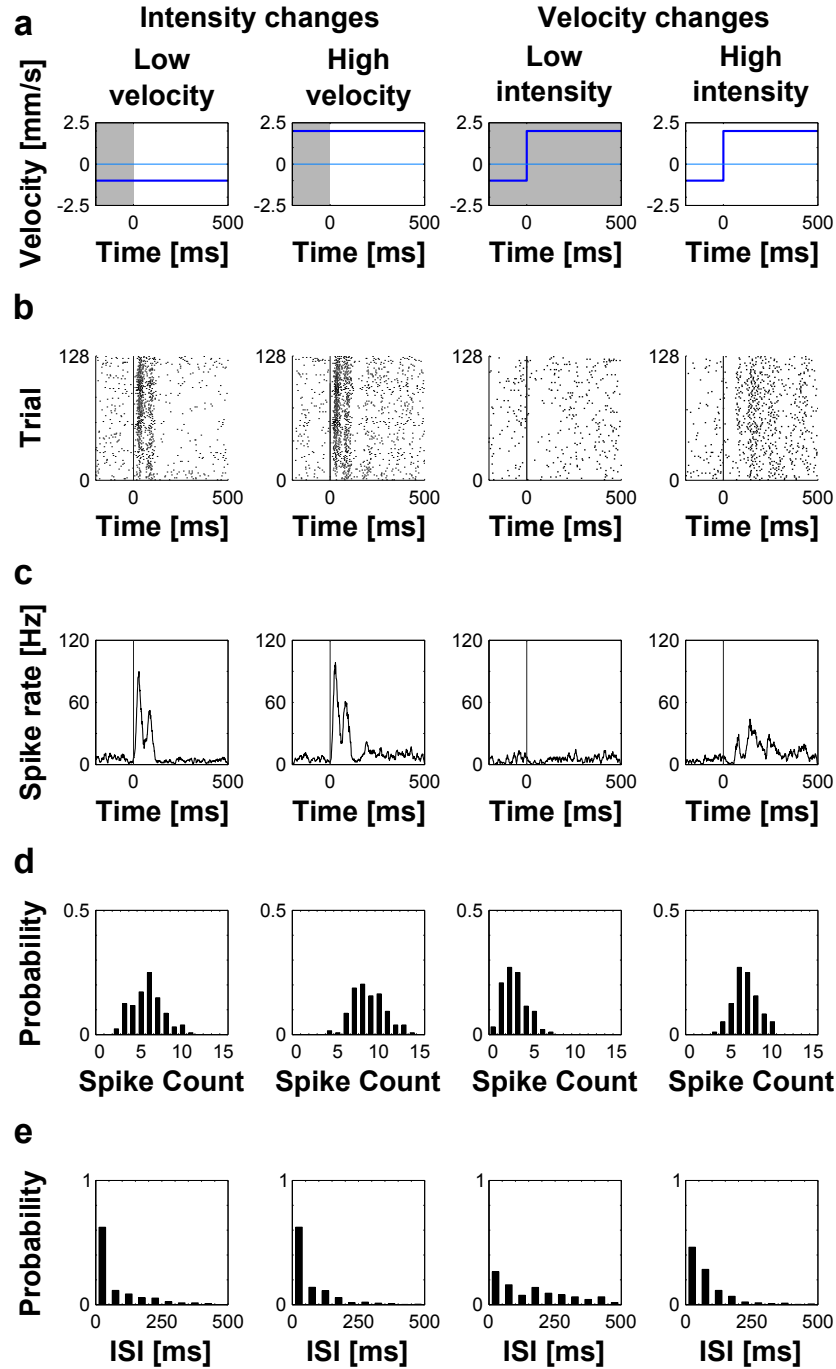
Figure 3.61: Characterisation of the responses of a fish RGC to a moving stimulus with changing background luminance. a) Instantaneous changes of light intensity or motion velocity. b) Raster plot of the responses of the RGC for each of the trials. c) PSTH with a time resolution of 1 ms. The spike rate has been averaged across trials and smoothed with a rectangular sliding window of 10 ms. d) Spike count probability measured over the 500 ms interval considering bins of 1 spike. e) Interspike time interval probability measured over the 500 ms interval considering bins of 50 ms.

RGC that showed clear differences in their spike firing rate for the different intensity and velocity values were considered for the analysis. Furthermore, for this experimental protocol, two joint activity coding hypotheses were tested; Pooled Population and Labelled Line.

The results described in this section should allow to gain more knowledge about which features of the responses of RGC are relevant for the encoding of visual information. Thereby, within the framework of the spike cost-based metrics, the parameter q allowed the assessment of the relevance of the spike firing rate and different time scales of the temporal structure of RGC responses (see Section 2.3.1). Hence, in the following paragraphs, some of the times the description of the results is going to be made based in a rough classification of the time scales. Like before, the time scales in the range between 8 ms $\leq 1/q \leq 31$ ms are going to be referred to as fine time scales, whereas the ones in the range between 62 ms $\leq 1/q \leq 250$ ms, are going to be referred to as medium time scales. Finally, coarse time scales will be the ones falling in the range between 500 ms $\leq 1/q \leq \infty$. Furthermore, the representation of the estimation results obtained by the spike cost-based metrics was done making the following considerations:

- In addition to the RGC responses obtained for the entire 500 ms interval of stimulus presentation, the activity during the transient phase (first 200 ms) and the sustained phase (last 200 ms) were analysed separately.

- In the case of the activity of single RGC, the depicted results correspond to the cells that were selected by the visual inspection of their spike firing rate probability distributions, i.e., $n = 18$.

- In the case of the activity of populations of RGC, the depicted results correspond to the population built with the selected cells.

- The results are individually represented for each of the three stimulus conditions considered for the analysis; changes in the light intensity with constant motion velocity, changes in the motion velocity with constant light intensity, and changes in the light intensity or motion velocity.

- For each of the three conditions considered, the estimation results allowed by the activity of the considered single RGC were pooled together. The procedure to assess the estimation performance is described in Section 2.3.4.

- The markers in the graphs correspond to the median, whereas the error bars depict the minimal and maximal estimation performances across the considered single RGC.

- The Wilcoxon sum-rank-test, considering different values of α ($\alpha > p$), was applied to assess the significance of the results (see page 67).

3.2.1   Constant Features

This section describes the results in the estimation of the possible projection light intensities and motion velocities of the visual stimulus utilised in this protocol. Here, the described results refer to the estimation of each individual feature and the combination of both features. Here, three conditions were considered for the estimation task; a) Changes in the light intensity with constant motion velocity. b) Changes in the motion velocity with constant light intensity. c) Changes in the light intensity or motion velocity.

Light intensity

Figure 3.62 shows the results obtained for the estimation of the four possible light intensities. Here, it can be observed that for the three analysed time intervals and the three tested stimulus conditions, the two tested joint activity coding hypotheses led to estimation results which were better than the median of the estimation performance yielded by the activity of single RGC. Moreover, the time scales that led to the highest estimation performances were different for single RGC and the two tested joint activity population hypothesis. Generally, the estimation performance was better for the 500 ms interval. Furthermore, for the 500 ms and the first 200 ms interval, the estimation performance showed quantitative and qualitative differences across the three tested stimulus conditions. Here, better results in the estimation of the light intensity were obtained in the context of light intensity changes. In contrast, for the last 200 ms interval, the estimation performance was similar across the three tested stimulus conditions.

With the exception of the time scales $1/q = 8$ ms, which generally led to estimation results close to those expected by chance, the estimation results yielded by the activity of *single RGC* were significantly above chance level, i.e., 25 % ($p \leq 0.005$). Here, time scales $1/q > 16$ ms improved the estimation performance, which frequently appeared to reach a plateau for time scales $1/q \geq 125$ ms. Exceptions to this finding were observed for the 500 ms and the first 200 ms intervals in the context of light intensity changes.

Here, medium time scales showed a tendency to led to the highest estimation results. Furthermore, within the context of light intensity changes, the maximum median in the estimation performance reached 46.7 %, and it was found for the 500 ms interval.

Generally, qualitative similarities were observed between the estimation performance obtained under the *Pooled Population* hypothesis, and the best estimation performance yielded by a single RGC (upper limit of the error bars in Figure 3.62). Therefore, for this hypothesis, better estimation results were frequently observed for coarse and medium time scales. However, the maximum estimation performance for this hypothesis was yielded by the time scale $1/q = 8$ ms within the context of light intensity changes, reaching 70.8 % for the first 200 ms interval.

Under the *Labelled Line* hypothesis, the time scale $1/q = 8$ ms led generally to estimation performances close to chance level. Moreover, for the time scales $1/q \leq 62$ ms, the estimation performance obtained under this hypothesis was worse than the best estimation performance yielded by a single RGC (upper limit of the error bars in Figure 3.62). Nevertheless, for this hypothesis, coarser time scales improved the estimation performance, which frequently reached its maximum for the time scale $1/q = \infty$. For this time scale, the estimation performance allowed by the Labelled Line hypothesis frequently exceeded the best estimation performance yielded by a single RGC. However, the highest estimation performance for this hypothesis was yielded by the time scale $1/q = 31$ ms within the context of light intensity changes, reaching 69.7 % for the first 200 ms interval.

Velocity

Figure 3.63 shows the results obtained for the estimation of the five possible motion velocities. Here, it can be observed that for the three analysed time intervals and the three tested stimulus conditions, the estimation results obtained under the two tested joint activity coding hypotheses were better than the median of the estimation performance yielded by the activity of single RGC. Moreover, the time scales that led to the highest estimation performances were different for single RGC and the two tested joint activity coding hypotheses. Generally, the 500 ms interval led to the highest estimation performances. Moreover, for the 500 ms and the first 200 ms intervals, the estimation performance for the motion velocity was better when changes in this stimulus feature were present. In contrast, for the other two stimulus conditions involving changes in light intensity, the estimation of motion velocity, particularly for the first 200 ms interval, was impaired. This effect was not observed for the last 200 ms interval, for which the estimation
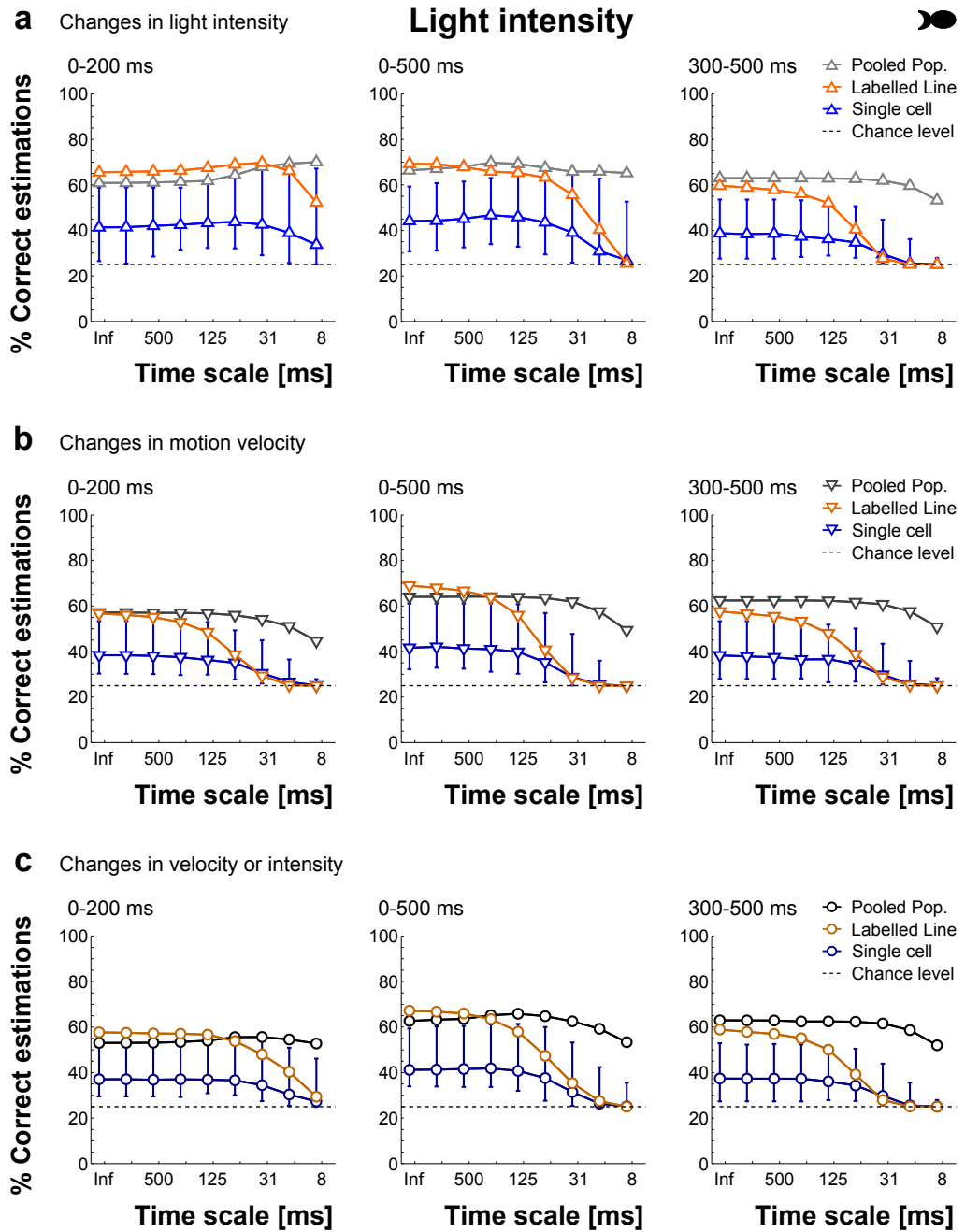
Figure 3.62: Estimation performance for the projection light intensity of the moving stimulus. The estimation was carried out by applying spike cost-based metrics on the activity of RGC within the three tested time intervals. In the case of the estimation allowed by the activity of single RGC, markers indicate the median, whereas error bars represent the range between maximum and minimum estimation performance. Three conditions were considered for the estimation; a) Changes in the light intensity with constant motion velocity. b) Changes in the motion velocity with constant light intensity. c) Changes in the light intensity or motion velocity.

performance was similar across the three tested stimulus conditions.

With the exception of the time scales $1/q = 8$ ms, the estimation results yielded by the activity of *single RGC* were significantly above chance level, i.e., 20 % ($p \leq 0.005$). Generally, the estimation performance reached a plateau for time scales $1/q \geq 125$ ms. Furthermore, for the 500 ms interval and within the context of motion velocity changes, the time scale $1/q = \infty$ led to the highest median in the estimation performance, which reached 28.9 %. Additionally, under this stimulus condition, it was also found that for time scales $1/q \geq 125$ ms within the 500 ms and the last 200 ms intervals, the best estimation performance yielded by a single RGC exceeded the estimation performance obtained under the two tested joint activity coding hypothesis.

In the context of motion velocity changes, the estimation performance under the *Pooled Population* hypothesis was very stable performance across the tested time scales. Here, while the time scale $1/q = 8$ ms showed a tendency to lead to the lowest estimation performances, the range 31 ms $\leq 1/q \leq 62$ ms appeared to be optimal for the encoding of information about motion velocity, allowing estimation performances up to 34.7 % for the 500 ms interval.

Under the *Labelled Line* hypothesis, time scales $1/q \leq 31$ ms led to estimation performances that were generally worse than the best estimation performance yielded by a single RGC. Nevertheless, the estimation performance for the Labelled Line hypothesis improved with coarser time scales. Furthermore, within the context of motion velocity changes, the time scale $1/q = \infty$ led to the highest estimation performances, which reached up to 35.6 % for the 500 ms interval.

Light intensity and velocity

The estimation results for the 20 possible combinations of light intensities and motion velocities are shown in Figure 3.64. Here, it can be observed that for the three analysed time intervals and the three tested stimulus conditions, the estimation results obtained for the two joint activity coding hypotheses generally outperformed the estimation performance yielded by all of the single RGC. Moreover, the results show clear differences between the best estimation performance yielded by a single RGC and the estimation results obtained for the combined activity of RG. Here, the time scales that led to the highest estimation performances were different for single RGC and the two tested hypotheses. Generally, the highest estimation results were obtained for the 500 ms interval. Furthermore, for the 500 ms and the first 200 ms intervals, changes in only one stimulus feature led to higher estimation results. Moreover, comparing the estimation performance obtained within the context of changes in one stimulus feature for these two time intervals, it

a Changes in light intensity

b Changes in motion velocity

c Changes in velocity or intensity
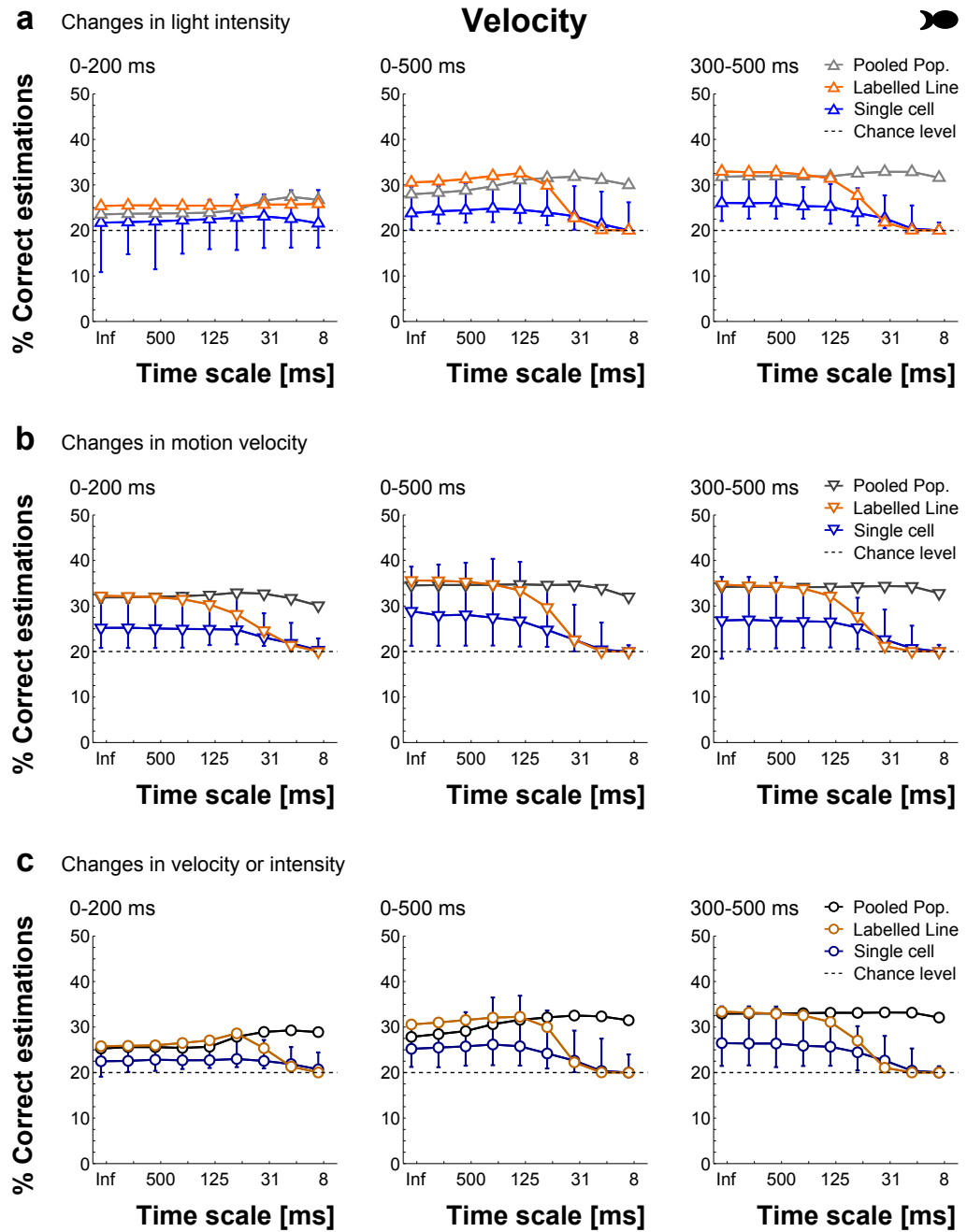
Figure 3.63: Estimation performance for the motion velocity of the moving stimulus. The estimation was carried out by applying spike cost-based metrics on the activity of RGC within the three tested time intervals. In the case of the estimation allowed by the activity of single RGC, markers indicate the median, whereas error bars represent the range between maximum and minimum estimation performance. Three conditions were considered for the estimation; a) Changes in the light intensity with constant motion velocity. b) Changes in the motion velocity with constant light intensity. c) Changes in the light intensity or motion velocity.

was observed that finer time scales led frequently to better estimation results when light intensity changes were present. In contrast, the estimation performance was similar across the three tested stimulus conditions for the last 200 ms interval.

With the exception of the time scales $1/q \leq 16$ ms, which led generally to estimation results close to those expected by chance, the estimation results obtained for *single RGC* were significantly above chance level, i.e., 5 % ($p \leq 0.005$). For the 500 ms and the first 200 ms intervals and when changes in only one stimulus feature were present, the estimation performance appeared to reach its maximum for medium time scales. Moreover, for these stimulus conditions, medium time scales led to the maximum in the median of the estimation performance, which was between 12 % and 13.4 % for the 500 ms interval.

Under the *Pooled Population* hypothesis and within the context of light intensity changes, fine time scales led generally to the highest estimation performances for the 500 ms and the first 200 ms intervals. In contrast, when motion velocity changes were present, time scales 31 ms $\leq 1/q \leq 62$ ms of these two time intervals appeared to be optimal for the estimation task. The maximum estimation performances were obtained for the 500 ms interval when changes in one stimulus feature occurred. Here, the optimal time scales yielded results that ranged between 28.9 % and 30.7 %.

Under the *Labelled Line* hypothesis, time scales $1/q \leq 31$ ms led to the lowest estimation performances. Nevertheless, the estimation performance for the this hypothesis improved with coarser time scales. Here, for the 500 ms and the first 200 ms intervals, medium time scales led generally to the highest estimation performances within the context of light intensity changes. In contrast, within the context of motion velocity changes, coarse time scales led generally to the highest estimation results for these two time intervals. Thereby, the highest estimation performance was obtained for the 500 ms interval when changes in one stimulus feature were present. Here, the estimation performance yielded by the optimal time scales ranged between 33.5.9 % and 38.6 %.

3.2.2 Features Changes

This section describes the estimation results for the instantaneous changes in the projection light intensity and the motion velocity of the visual stimulus utilised in this protocol. Additionally, the results described in this section include the estimation performance for all the possible instantaneous changes of the stimulus features. Finally, it was tested if based on the activity of fish RGC, it could be possible to discriminate between changes in the light

Figure 3.64: Estimation performance for the projection light intensity and the motion velocity of the moving stimulus. The estimation was carried out by applying spike cost-based metrics on the activity of RGC within the three tested time intervals. In the case of the estimation allowed by the activity of single RGC, markers indicate the median, whereas error bars represent the range between maximum and minimum estimation performance. Three conditions were considered for the estimation; a) Changes in the light intensity with constant motion velocity. b) Changes in the motion velocity with constant light intensity. c) Changes in the light intensity or motion velocity.

intensity and changes in the motion velocity of the presented stimulus.

Light intensity changes

Due to the fact that for the Light-Motion experiment protocol four different light intensities were utilised, 12 instantaneous changes of light intensity are possible. However, because five different motion velocities were included in the experiment protocol, there are 60 possible combinations of light intensity changes and background motion velocity. Thereby, the results described below comprise the estimation of the light intensity changes under constant motion velocities.

Figure 3.65 shows the estimation results for the combinations of light intensity changes and constant background motion velocity. Here, it can be observed that generally, the estimation results obtained for the two tested joint activity coding hypotheses surpassed the ones yielded by the activity of single RGC. Moreover, the 500 ms and the first 200 ms intervals led to much higher estimation performances in comparison to the last 200 ms interval.

For *single RGC*, the maximum median in the estimation performance was obtained for time scales 31 ms $\leq 1/q \leq$ 62 ms within the 500 ms and the first 200 ms intervals, reaching up to 6.9 % for the 500 ms interval. Moreover, excepting the time scales $1/q \leq$ 16 ms of the last 200 ms interval, the estimation results yielded by the activity of single RGC were significantly above chance level, i.e., 1.66% ($p \leq 0.005$).

Under the *Pooled Population* hypothesis, the time scale $1/q = \infty$ led to the lowest estimation results. However, finer time scales within the 500 ms and the first 200 ms intervals improved the estimation performance, which appeared to be optimal for time scales 16 ms $\leq 1/q \leq$ 31 ms. Here, the maximum estimation results reached up to 29.3% for the 500 ms interval. In contrast, under the *Labelled Line* hypothesis, fine time scales led generally to low estimation results, which nonetheless improved for coarser time scales. Here, for the 500 ms and the first 200 ms intervals, time scales 125 ms $\leq 1/q \leq$ 250 ms were optimal for the estimation task, allowing results up to 31.4% for the 500 ms interval.

Velocity changes

Because five different velocities were utilised in this experiment protocol, 20 different instantaneous velocity changes are possible. Nevertheless, due to the fact that the experiment protocol considered four different projection light intensities, the estimation procedure considered 80 possible combinations of instantaneous velocity changes and background luminance. In this sense, the

Figure 3.65: Estimation performance for the changes in projection light intensity of the moving stimulus. The estimation was carried out by applying spike cost-based metrics on the activity of RGC within the three tested time intervals. In the case of the estimation allowed by the activity of single RGC, markers indicate the median, whereas error bars represent the range between maximum and minimum estimation performance.

results described below refer to the estimation of the velocity changes under constant background light intensities.

In Figure 3.66 the estimation results for the combination of instantaneous velocity changes and constant background light intensity are shown. Here, it can be observed that generally, the estimation results obtained for the two tested joint activity coding hypotheses exceeded the ones yielded by the activity of single RGC. Moreover, the estimation performances for the 500 ms and the first 200 ms intervals were much better than the ones yielded by the last 200 ms interval.

Although the activity of *single RGC* allowed poor estimation results for the three analysed time intervals, with the exception of time scales $1/q \leq 31$ ms within the last 200 ms interval, these results were significantly above chance level, i.e., 1.25%, ($p \leq 0.005$). In turn, the time scale $1/q = 125$ ms within the 500 ms led to the maximum median in the estimation performance, which reached 4.3%.

Under the *Pooled Population* hypothesis, the lowest estimation results were yielded by the time scale $1/q = \infty$. Nevertheless, finer time scales within the 500 ms and the first 200 ms intervals improved the estimation performance, which appeared to be optimal for time scales 16 ms $\leq 1/q \leq 31$ ms. Here, the maximum estimation results reached 19.4% for the 500 ms interval.
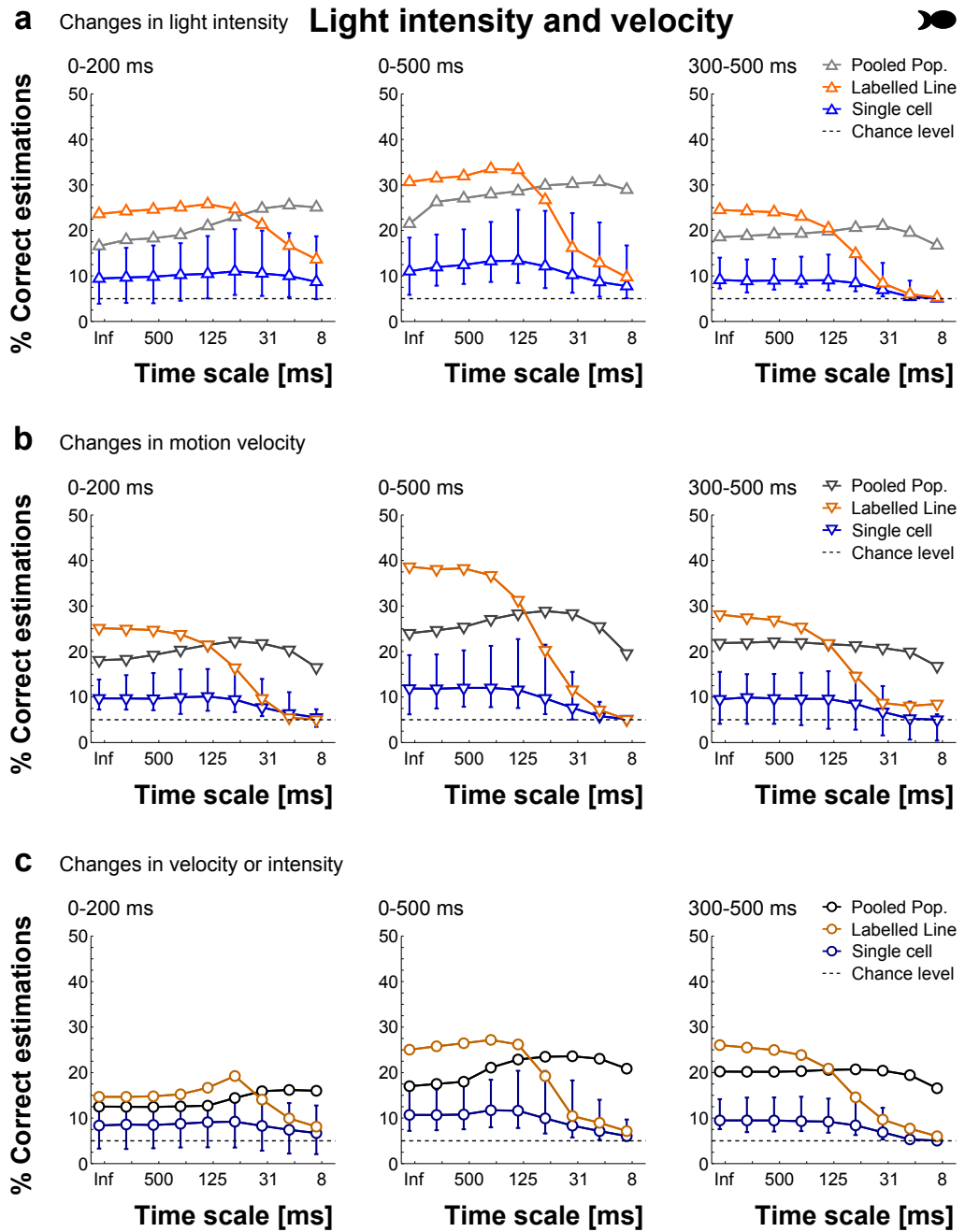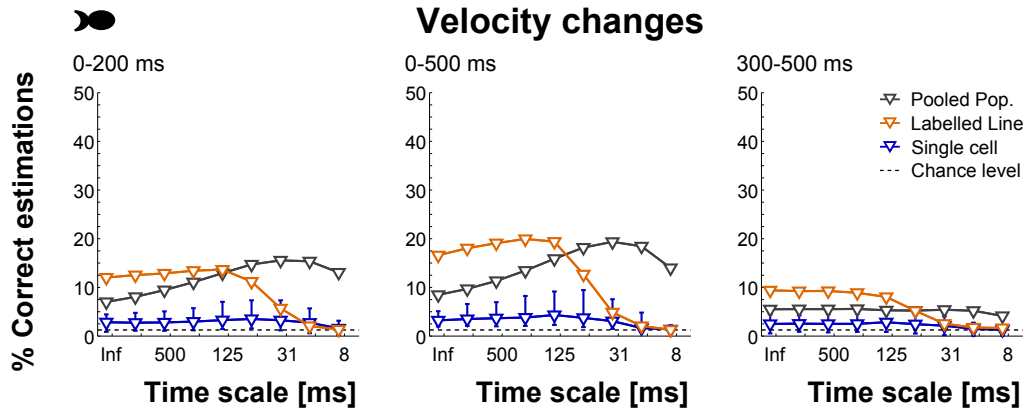
Figure 3.66: Estimation performance for the changes in motion velocity of the moving stimulus. The estimation was carried out by applying spike cost-based metrics on the activity of RGC within the three tested time intervals. In the case of the estimation allowed by the activity of single RGC, markers indicate the median, whereas error bars represent the range between maximum and minimum estimation performance.

In contrast, under the *Labelled Line* hypothesis, fine time scales led generally to the lowest estimation results, which nonetheless improved for coarser time scales. Here, for the 500 ms and the first 200 ms intervals, time scales $125\,\text{ms} \le 1/q \le 250\,\text{ms}$ were optimal for the estimation task, allowing results up to 20% for the 500 ms interval.

Light intensity/velocity changes

As mentioned before, for the Light-Motion experiment protocol, there were 60 possible instantaneous light intensity changes and 80 possible instantaneous motion velocity changes. Therefore, the total number of possible changes of the stimulus features was 140. Thereby, the results obtained for the estimation of these instantaneous changes are described below.

Figure 3.67 shows the estimation results for the instantaneous velocity and light intensity changes. Here, it can be observed that as in the case of the estimation of the instantaneous changes of one of the stimulus features, the estimation results obtained for the two tested joint activity coding hypotheses exceeded the ones yielded by the activity of single RGC. Moreover, the estimation performances for the 500 ms and the first 200 ms intervals were much better than the ones yielded by the last 200 ms interval.
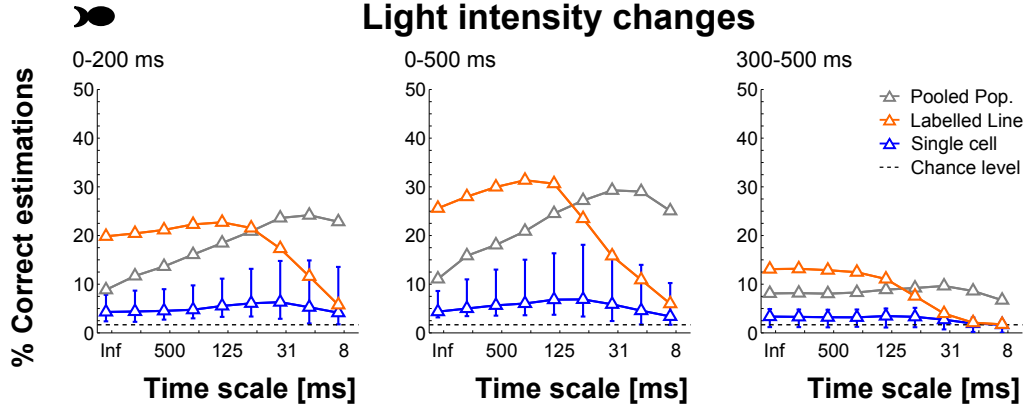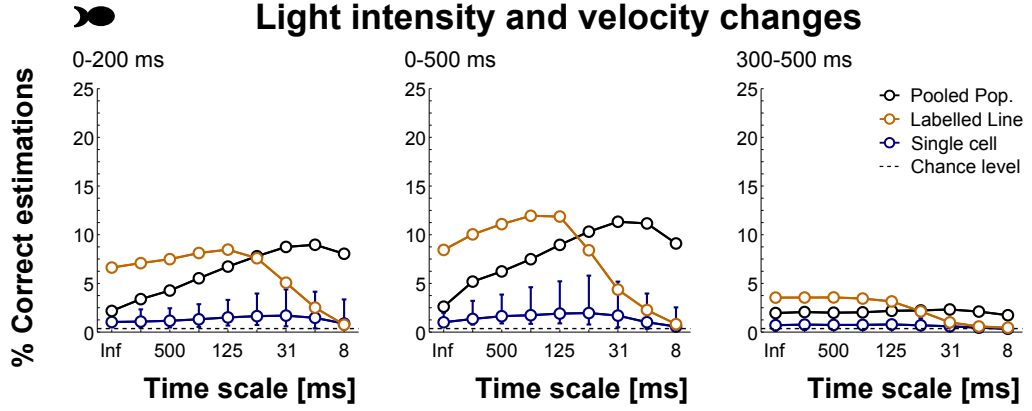
Figure 3.67: Estimation performance for the changes in projection light in-
tensity or motion velocity of the moving stimulus. The estimation was carried
out by applying spike cost-based metrics on the activity of RGC within the
three tested time intervals. In the case of the estimation allowed by the activ-
ity of single RGC, markers indicate the median, whereas error bars represent
the range between maximum and minimum estimation performance.

Although the activity of *single RGC* allowed poor estimation results for
the three analysed time intervals, with the exception of time scales $1/q \leq 16$ ms
within the last 200 ms interval, these results were significantly above chance
level, i.e., 0.71%, ($p \leq 0.005$). Here, the time scale $1/q = 62$ ms within the
500 ms led to the maximum median in the estimation performance, which
reached 3.9%.

Under the *Pooled Population* hypothesis, the lowest estimation results
were yielded by the time scale $1/q = \infty$. Nonetheless, for the the 500 ms and
the first 200 ms intervals, finer time scales improved the estimation perfor-
mance, which appeared to be optimal for time scales 16 ms $\leq 1/q \leq 31$ ms.
Here, the maximum estimation results reached 22.7% for the 500 ms inter-
val. In contrast, under the *Labelled Line* hypothesis, fine time scales led
generally to low estimation results, which nonetheless improved for coarser
time scales. Here, for the 500 ms and the first 200 ms intervals, time scales
125 ms $\leq 1/q \leq 250$ ms were optimal for the estimation task, yielding results
up to 23.9% for the 500 ms interval.

Feature change discrimination

Finally, because this experiment protocol involved alternate changes in the intensity of the projection light and the motion velocity of the moving stimulus, it was tested if the information encoded in the activity of fish RGC is enough to allow the discrimination of the stimulus feature that changed.

Figure 3.68 shows the results for the discrimination of the stimulus feature that has changed. Here, it can be observed that for the 500 ms and the first 200 ms intervals, the estimation results obtained for the two tested joint activity coding hypotheses clearly exceeded the ones yielded by the activity of single RGC. Moreover, the estimation performances for these two time intervals were quantitatively similar and much better than the ones yielded by the last 200 ms interval, for which the estimation results were close to those expected by chance.

With the of the last 200 ms interval, the activity of *single RGC* led to estimation results that were significantly above chance level, i.e., 50%, ($p \leq 0.005$). Moreover, medium time scales within the 500 ms and the first 200 ms intervals appeared to be optimal for the discrimination task. Here, the time scale $1/q = 125$ ms within the 500 ms led to the maximum median in the estimation performance, which reached 69.7%.

Under the *Pooled Population* hypothesis, the lowest estimation results were yielded by the time scale $1/q = \infty$. However, for the the 500 ms and the first 200 ms intervals, finer time scales improved the estimation performance, which appeared to be optimal for the time scale $1/q = 16$ ms. Here, the maximum estimation results reached 91.4% for the 500 ms interval. In contrast, under the *Labelled Line* hypothesis, fine time scales led generally to low estimation results, which nevertheless improved for coarser time scales. Here, for the 500 ms and the first 200 ms intervals, time scales 62 ms $\leq 1/q \leq 125$ ms were optimal for the discrimination task, yielding performances up to 92.8% for the 500 ms interval.
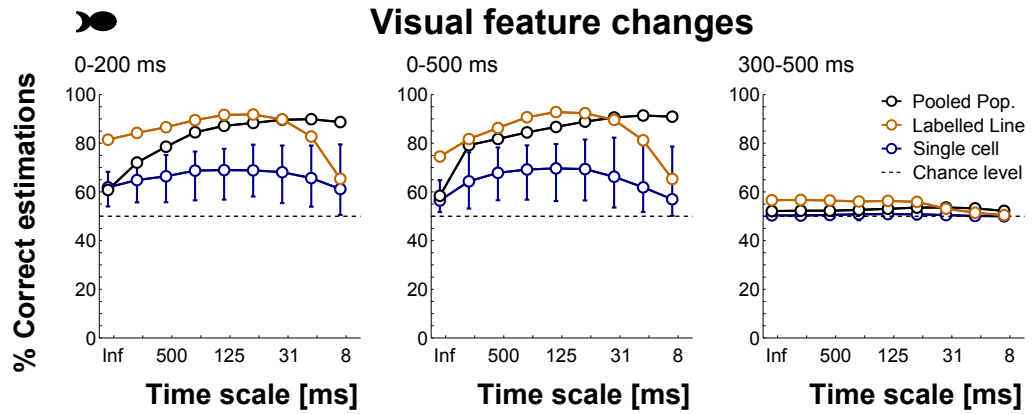
Figure 3.68: Estimation performance for the stimulus feature that changed. The estimation was carried out by applying spike cost-based metrics on the activity of RGC within the three tested time intervals. In the case of the estimation allowed by the activity of single RGC, markers indicate the median, whereas error bars represent the range between maximum and minimum estimation performance.

Chapter 4

Discussion

The present study was dedicated to explore how the information about motion features of a visual stimulus is encoded by the activity of retinal ganglion cells (RGC). Therefore, the responses of RGC to a moving stimulus were recorded extracellularly using a multi-electrode array. The recordings were performed on two animal species; turtle (*traquemys scripta elegans*) and carp (*cyprinus carpio*).

For both animal species and under constant luminance conditions, it was found that the responses of single RGC carry information about the motion features of a moving stimulus. Moreover, it was observed that the encoded information was enhanced by the combined activity of RGC. These results were more evident for the analyses carried out in the turtle retina. Additionally, it has been found that for the encoding of information about motion features, the spike firing rate of the responses of RGC, as well as their temporal structure, are plausible coding strategies. Furthermore, for the activity of single RGC, as well as for the three tested joint activity coding hypotheses, it was observed that the relevance of the spike firing rate and the temporal structure for encoding tasks show some differences. In turn, these differences were more evident for combined activity of RGC. Nevertheless, the spike firing rate appears to be more involved in the encoding of motion features under constant stimulus conditions, e.g., constant velocities, whereas the temporal structure of the responses allows to enhance the encoding of information under dynamic conditions, e.g., instantaneous velocity changes.

An additional study within the scope of this study aimed to explore how the activity of RGC could simultaneously encode information about the luminance and motion features of a visual stimulus. For this study, the activity of RGC from a carp retina was analysed. Here, it was found that the activity of several of the recorded RGC tuned their activity to both stimulus features. Furthermore, the degree in which the activity of the RGC is modulated by

193

a stimulus feature is affected by the complementary stimulus feature in a non-linear way. A deeper analysis allowed to explore the role of the spike firing rate and the temporal structure of the responses of RGC. The obtained results show that for the activity of single RGC and small cell populations, both response properties carry information about luminance and motion features. However, for the encoding of these two stimulus features, the relevance of the spike firing rate and the temporal structure of the responses of RGC showed some differences. Here, when changes of light intensity were present, finer time scales improved the estimation results for either stimulus feature, particularly for the time intervals containing the transient activity period. Furthermore, it was found that the activity of small RGC populations is more efficient than the activity of single RGC, especially for the simultaneous encoding of luminance and motion features, as well as stimulus feature changes.

4.1   Spike Train Metrics

Two analysis methods were employed in this study to explore the relevance of the spike firing rate and the temporal structure of the responses of RGC for the encoding of information about different features of visual stimuli. Here, the spike cost-based metrics and the ISI metrics offer a formal mathematical framework to assess the similarity between pairs of spike trains. Thereby, the quantification of the similarity or dissimilarity between spike trains has proved to be an important tool for decoding strategies that in turn, are used to estimate the stimuli that have evoked these spike trains. Moreover, based on the obtained estimation results, it is possible to gain insights into the role of neuronal response properties for the encoding of visual information (refer to Victor (2005) for a review).

The *spike cost-based metrics* is a time scale parametric method. Here, by means of the parameter q, it is possible to explore the relevance of the spike firing rate, as well as different time scales for the encoding of information (section 2.3.1). Thereby, by comparing the information retrieved by each value of q, the spike cost-based metrics assesses the role of individual time scales, i.e., $1/q$, as a possible component of the neural code. Therefore, the primary advantage of the spike cost-based metrics is that it allows to narrow down the possible time scales that can be involved in the encoding task (Samonds and Bonds, 2005).

However, the interpretation of the time scales that are optimal for the encoding of neural information is not always straightforward (Paiva et al., 2010; Chicharro et al., 2011). Here, in the case of decoding tasks, it has been

observed that the time scales that allow the highest stimulus estimation performances are the result of a non-trivial interplay of the different sources of information contained in the spike trains. Thus, the optimal time scales could be interpreted as a balance between different response properties that allow best stimulus estimation performances, e.g., spike firing rate, spike timing, and interspike time intervals (Samonds and Bonds, 2005; Chicharro et al., 2011). For instance, in studies in gustatory cells of rat (Di Lorenzo and Victor, 2003) and V1 visual cells of macaques (Victor and Purpura, 1998), the authors have found that finer time scales maximised the retrieved information about the applied stimulus when the transient period of the neuronal responses was analysed. In contrast, when the sustained period was included in the analysis, coarser time scales began to gain relevance.

Thereby, the interpretation of the optimal time scales for two different scenarios has been addressed in studies that involved analyses with the spike cost-based metrics. The first scenario is when successive time scales, comprising the spike firing rate and the temporal structure lead to the highest estimation performances. Here, it is not easy to identify which, the spike firing rate or the temporal structure, has more relevance for information encoding tasks. For this situation, Samonds and Bonds (2005) and Roussin et al. (2008) have suggested that besides the spike firing rate, patterns in the temporal structure or modulations of the spike firing rate could be relevant for the encoding of neuronal information. The second scenario is when the range of the optimal time scales does not include the spike firing rate. Here, Huetz et al. (2006) have proposed that for stimulus estimation, the finer time scales in the range indicate the precision at which regularities in the spike trains occur. This proposal agrees in some degree with the earlier hypothesis of Reich et al. (2001b), which suggested that the temporal precision limit for sensory information encoding is given by the time scale that allows half of the best estimation performance for decoding tasks. Additionally, Huetz et al. (2006) suggested that the coarser time scales in the range indicate the length of the time window that is necessary for stimulus estimation. In turn, it has been suggested that this time window performs an estimation of the spike firing rate (Paiva et al., 2010). An additional scenario would be when the spike firing rate led to the maximum estimation performances. Therefore, it can be suggested, under the analysis of the spike cost-based metrics, that this coding mechanism predominates over the remained tested time scales (Chicharro et al., 2011). However, this situation not necessarily rules out the suitability of a coding mechanism based in the temporal structure of the responses, as observed in some of the results obtained under the Labelled Line hypothesis (see discussion in page 206).

Within the framework of this study, the time scales that have been tested

by means of the spike cost-based metrics were grouped in three classes; fine time scales (8 ms $\leq 1/q \leq$ 31 ms), medium time scales (62 ms $\leq 1/q$ $\leq$ 250 ms) and coarse time scales (500 ms $\leq 1/q \leq$ 1000 ms). Generally, the results are discussed making reference to a range of time scales that showed to be relevant for the encoding of stimulus features. Moreover, in order to test if the spike firing rate or the temporal structure of the responses predominate as neuronal coding strategy, the comparison of the estimation results obtained for both of the applied metrics is discussed.

The *ISI metrics*, in contrast to the spike cost-based metrics, is a parameter free method that has been proposed as a complementary tool to assess spike train synchrony (Kreuz et al., 2007). Thereby, for the measurement of the synchrony between two spike trains, i.e., similarity, the ISI metrics utilise the interspike time interval (ISI) as the basic element of comparison. Here, based on the ISIs, the ratio of the instantaneous firing rates is evaluated (section 2.3.2). The ISI metrics has been mostly applied to measure the variability across spike trains generated by neuronal models (Dodla and Wilson, 2009; Ying and Qi-Shao, 2010; Ying et al., 2010; Du et al., 2010), as well as spike trains recorded from neurons in the ampullary receptors of weakly electric fish (Engelmann et al., 2010), neurons of the entorhinal cortex of rats (Haas et al., 2010) and neurons in the mechanosensory lateral line of goldfish (Goulet et al., 2012). Furthermore, based on simulated neuronal responses, Kreuz et al. (2007) tested the performance of the ISI metrics for clustering tasks, and compared it with the one yielded by the optimal time scales for the spike cost-based metrics. The authors found similar estimation performances and proposed that the main advantage of the ISI metrics it that is self-adaptive. Therefore, if for instance, regular spiking and bursting occurs in the same spike train, the ISI metrics will have the ability to identify automatically the optimal time scales for clustering tasks and adjust them continuously during each response trace. In this sense, the ISI metrics allows to test the general relevance of the temporal structure of spike trains for the encoding of neuronal information. Nevertheless, it does not provide further details on the time scales that are relevant for the encoding task.

The *multi-unit metrics* approach followed in this study is the one proposed in Aronov et al. (2003) and Aronov (2003). Here, by means of the parameter k, it is tested how important it is for the encoding of neuronal information, to distinguish spikes that are fired by different neurons. Thereby, the extreme values that k could adopt allow to test directly two joint activity coding hypotheses; Pooled Population ($k = 0$), and Labelled Line ($k = 2$) (see page 57). The multi-unit metrics has been applied to analyse the joint activity of simple and complex neurons from the V1 area of macaque mon-

keys Aronov et al. (2003). In this study, the authors found that the joint activity of two simple cells with different phase tuning encoded more information about spatial phase when the spikes coming from each of the neurons were totally ($k = 2$) or partially ($0 < k < 2$) distinguished. Moreover, these results were also obtained for a pair of complex cells. In contrast, for a pair of simple cells with similar phase tuning, the distinction of spikes did not show to be relevant. However, the joint activity of all cell pairs allowed to encode more information than the individual activity of each cell. Thereby, the results presented in the study suggest that the joint activity of neurons could in fact encode more efficiently neuronal information, especially if the neurons exhibit different tuning for the same stimulus. Nonetheless, the efficiency of the encoding task depends on the weighted combination of this activity, i.e., k. Besides the Pooled Population and the Labelled Line hypotheses, an additional hypothesis has been introduced in this study; the Functional Group hypothesis. This hypothesis suggests that it is not important to distinguish spikes coming from different individual neurons, but rather, to distinguish spikes coming from different neuron classes ($k = 0$ across neurons of the same class and $k = 2$ across cell classes).

4.2 Motion Experiment

The first part of this study involved the analysis of responses of turtle and fish RGC to a moving stimulus under constant luminance conditions. In turn, the experiment protocol consisted in a pseudo-random sequence of 500 ms periods, for which the stimulus moved with a constant motion velocity (refer to section 2.1.2 for more details).

As first step, the responses of single RGC were analysed with the spike cost-based metrics and the ISI metrics to investigate if they encode information about the motion features of the moving stimulus. The next step involved the analysis of the activity of small populations of RGC ($6 \leq n \leq 18$). Here, the focus of the analysis was to test three different joint activity coding hypotheses, which differed in how the activity of RGC was combined. Thereby, for the experiments performed in the turtle retina, three different hypotheses were tested; Pooled Population, Labelled Line and Functional Group. However, in the case of fish, the number of recorded cells allowed the test of only the first two hypotheses. If not stated otherwise, the discussion in the following paragraphs refers to the results obtained for the RGC of both animal species. Moreover, the analysed time intervals are going to be addressed as containing solely the transient activity period (first 200 ms), solely the sustained activity period (last 200 ms), or both periods (500 ms).

4.2.1   General Findings

For the activity of single RGC, as well as for the three tested joint activity coding hypotheses, the activity within the three tested time intervals allowed the estimation of constant motion features. Here, while the time interval containing the transient and the sustained activity periods led generally to the highest estimation results, the time intervals containing either the transient or the sustained activity period, led to similar estimation performances. Furthermore, for the estimation of the motion features before the instantaneous velocity changes, as well as the discrimination of the changes in the motion features, the time intervals that contained the transient period activity were the only ones that allowed good performances. Here, the time intervals containing solely the transient activity period or including also the sustained period, led to similar performances for these cases. In contrast, while the time intervals containing the transient activity period were the ones that yielded good estimation performances for the instantaneous velocity changes, the estimation performance for these changes was further improved by the sustained activity.

Generally, for the spike cost-based metrics, fine time scales led to estimation results for the motion direction and speed that were much worse than those expected by chance. This effect can be explained on the one hand, by the design of the experiment protocol. Here, the absence of movement occurs less frequently than the movement in either direction or with either speed. Therefore, a bias in the estimation of the absence of movement will lead to estimation performances lower than those expected by chance for these two motion features.

On the other hand, the overestimation of the absence of movement is provoked by the procedure with which the spike cost-based metrics calculates the similarity between two spike trains. Here, for two spike trains S_a and S_b with few or no coincident spikes, the distance obtained for decreasing $1/q$ will increase monotonically until the limit $n_{S_a} + n_{S_b}$, with n being the number of spikes for each spike train. Therefore, because the high spike time precision of the responses of RGC appears to have no relevance for the encoding of constant motion features, for spike trains evoked by the same stimulus motion feature and with similar number of spikes, the cost of shifting a spike in time for high q values is greater than deleting and inserting a spike in the correct time position. In turn, the minimal cost for relocating each spike in the correct time position for the transformation of the spike trains equals two. In contrast, because spike trains evoked by either motion stimulus feature generally contain more spikes than spike trains evoked by the absence of movement, the transformation procedure will involve only the deletion or

insertion of spikes. This situation leads to a lower total transformation cost, i.e., distance, which in turn provokes the overestimation of the absence of movement for all motion velocities for fine time scales.

Moreover, regarding the estimation results yielded by the spike cost-based metrics for the motion direction and speed before and after the instantaneous velocity changes, it is necessary to discuss more in detail why fine time scales led to close to chance level estimation performance for the previous motion features, and to worse than chance estimation performance for the post motion features. This effect is in part explained by the fact that the estimation of instantaneous velocity changes involved the correct estimation of the previous and post motion features. Moreover, this estimation was performed based on RGC responses that correspond to the time interval where the post motion features were present. Therefore, a bias to estimate the post motion features will arise. In turn, if there is an overestimation of the absence of movement for the post velocity, the estimated previous velocity will always be different to velocity zero. Here, a bias in the estimation of a movement with either direction or speed, will lead to estimation performances close to those expected by chance.

As in the case of the activity of single RGC, the worse than chance estimation performance for the motion direction and speed is due to the overestimation of the absence of movement. Here, the overestimation present at the single cell level is preserved at a population level because under the Labelled Line hypothesis, the activity of the RGC that comprise the populations is regarded individually. Therefore, for a population of RGC, the sum of the distance matrices of the individual RGC will enhance in a weighted form the pairwise distances of the spike trains. Here, the weight will increase for larger distances.

4.2.2 Single Cell Coding

The estimation results obtained by analysing the responses of RGC with spike cost-based metrics and ISI metrics, suggest that the spike firing rate, as well as the temporal structure of the responses of single cells, encode information about all the analysed motion features. Nevertheless, the relevance of these two response properties for the encoding of information depends on the nature of the motion feature as well as on the analysed response time interval.

For the encoding of information about *constant motion features*, i.e., the ones that remained constant for the 500 ms intervals, the spike firing rate and the temporal structure showed to be suitable coding strategies for

single RGC. This affirmation is based on the estimation results obtained for the spike cost-based metrics, which were similar for medium and coarse time scales, as well as for the time scale $1/q = \infty$, i.e., spike firing rate. Moreover, additional evidence for the relevance of the temporal structure was yielded by the results allowed by the ISI metrics, which were often similar to those yielded by the optimal time scales for the spike cost-based metrics (pages 73-76).

In this context, while the temporal structure of the responses of single RGC has shown to be relevant in the encoding of information about constant motion features, due to the low estimation results yielded by fine time scales for the spike-cost based metrics, it appears that a high precision of the spike occurrence is not relevant for encoding. Moreover, comparing the estimation results obtained for both of the applied metrics, the spike cost-based metrics led to greater differences in the estimation performance between the long and the two short time intervals. This finding indicates that for the encoding of stimulus information based on a spike firing rate strategy, longer time windows are necessary for the integration of the firing rate. Nevertheless, because this response property did not led to perfect estimation performances, it can be asserted that it does not account for the encoding of all the information about constant motion features.

A deeper analysis showed that the estimation results for the motion direction yielded by the activity of turtle direction selective cells (DSC), were only significant for coarse time scales within the 500 ms interval (pages 74). Moreover, as in the case of the estimation of motion speed, there was not a clear tendency for a cell class to yield the highest estimation performance for the motion direction.

For DSC, the significance of the direction estimation observed only for coarse time scales and the 500 ms interval, can be in part explained by the fact that the classification of the RGC was based on their spike firing rate probability distributions. In turn, these distributions were calculated considering the 500 ms interval (Section 2.2.2). Moreover, it was also observed that not all the cells that were classified as DSC showed a strong tuning of their responses.

Further errors in the estimation of motion direction and speed by DSC are provoked by the fact that for the preferred direction, DSC tune their activity to the different speed values, whereas for the anti-preferred direction, they remain most of the time silent as in the case of the absence of movement. The similarities between the responses of DSC to the absence of movement and movements in the anti-preferred direction lead to an overestimation of the absence of movement and therefore, to errors in the estimation of the stimulus motion direction and speed.

On the other hand, while *Non-DSC* show some tuning of their activity to the different speeds, they fire relative few spikes in response to slow speeds. Therefore, the responses to slow speed exhibit similarities to those elicited by the absence of movement, provoking thus an overestimation of the absence of movement and therefore, errors in the speed estimation. Furthermore, the tuning of the activity of Non-DSC is independent of the direction of movement and this in turn, provokes additional errors in the estimation of motion direction.

As mentioned before, the estimation results for the *instantaneous velocity changes* were better for the time intervals containing the transient activity period. In turn, these results made evident that for the encoding of information about velocity changes, the temporal structure of single RGC responses has a higher relevance than the spike firing rate. This affirmation is based on the one hand, on the results obtained for the spike cost-based metrics, which were significantly above chance level for the spike firing. However, these results were surpassed by the ones obtained for medium and fine time scales. On the other hand, the ISI metrics led also to estimation results better than the ones allowed by the spike firing rate (page 81). Based on these observations and because the time intervals containing the transient activity period led to the highest estimation results, it can be suggested that the information about velocity changes is encoded in the spike firing rate of this period, but especially, in its temporal structure.

Because for the correct estimation of the instantaneous velocity changes, the motion features before and after the transitions have to be rightly estimated, the estimation results for the *previous motion features*, i.e., the features before the instantaneous velocity changes, stressed the relevance of the temporal structure of the transient activity period for the encoding of information about velocity changes. Here, for the spike cost-based metrics, the highest estimation performances for the previous motion velocity were yielded by medium time scales of the time intervals containing the transient activity period. Furthermore, for these time intervals, the ISI metrics led to estimation results that were similar to those yielded by the optimal time scales for the spike cost-based metrics ((pages 83-88)). Thus, based on these observations, it can be suggested that temporal structure of the transient activity period carries information about the stimulus history. Furthermore, the close to chance estimation performance for the motion features previous to the instantaneous velocity changes for all time intervals, especially for sustained activity, accounts for most of the errors in the estimation of the instantaneous velocity changes.

Although the spike firing rate showed to be the relevant coding mechanism

for the *post motion features*, i.e., the features after the instantaneous velocity changes considering the stimulus history, the obtained estimation results showed that the temporal structure of the transient activity period gained relevance for the encoding of information about these features. Here, in comparison to the results obtaining without considering the stimulus history, the estimation yielded by medium time scales for the spike cost-based metrics showed a slight but significant tendency to allow better performances for post the motion features. In contrast, the ISI metrics did not led to significant differences in these estimation results ((pages 90-95)). These findings indicate that some of the information about the post motion features is available in the temporal structure of the activity transient when the stimulus history is considered.

Moreover, the superior performance yielded by fine and medium time scales of the transient activity period for the estimation of the instantaneous velocity changes, can be explained by the combined effects provoked by these time scales. On the one hand, the better estimation performance for the previous motion features and on the other hand, the improvement in the estimation performance for the post motion features.

In this study it was also tested if the activity of single RGC carries information about changes of motion features of a moving stimulus that could have more relevance for survival tasks. For instance, the information about these changes would allow the animal to detect either a change in the motion direction, or a change in the motion speed, or the combined changes of both motion features of a prey or a predator.

The obtained results for the *discrimination of motion feature changes* indicated that the transient activity period encodes most of this information. This affirmation is based on the close to chance estimation performances yielded by the sustained activity, as well as the similar estimation results observed for the time intervals containing the transient activity period. Here, for the spike cost-based metrics, coarse and medium time scales led to better performances for the discrimination of motion feature changes. Moreover, because the ISI metrics led to similar discrimination results as the one yielded by the optimal time scales for the spike cost-based metrics, it can be suggested that the information about the changes in the motion features of the moving stimulus is encoded by both, the spike firing rate and the temporal structure the activity transient period (pages 102-103).

Regarding the spike cost-based metrics, and as closing remark for this section, it has to be mentioned that the time scales that led to the maximum estimation results varied across the RGC analysed and displayed in this study as well as across the motion features of the moving stimulus (see

Figures 3.6, 3.12 and 3.17). This finding points out that although certain time scales are relevant for the encoding of specific motion features, RGC use different time scales to encode information about the same motion feature. In turn, this point is going to gain relevance when discussing the difference in the estimation results for the motion features obtained for both of the applied metrics under the Labelled Line hypothesis.

4.2.3 Joint Activity Coding

In comparison to the activity of single RGC, the combined activity of small population of RGC ($6 \leq n \leq 18$) showed to improve the estimation performance for the motion features of a moving stimulus. In turn, this improvement was greater for larger population sizes. As in the case of the activity of single RGC, the relevance of the spike firing rate and the temporal structure was defined by the nature of the motion features that were encoded. Moreover, the variability in the relevance of these response properties was observed across the three tested joint activity coding hypotheses. However, the results obtained for the spike cost-based metrics and the ISI metrics show that the spike firing rate, as well as the temporal structure of the combined activity of RGC, carry information about all the analysed motion features.

Pooled Population hypothesis

The activity of populations of RGC was first analysed under the Pooled Population hypothesis. Here, the hypothesis makes the assumption that for the encoding of information about motion features of a moving stimulus, the information about the neuron of origin of each spike has a low relevance. Therefore, like in an integrate-and-fire model, a post-synaptic neuron is assumed to drive its membrane potential towards threshold by integrating at its dendrites the responses of many pre-synaptic individual neurons in a not weighted form. Thereby, the Pooled Population hypothesis proposes that the encoding of information about motion features is carried out by integrating the activity of several single RGC in one spike train. Here, the information would be encoded by the spike firing rate and the temporal structure.

The results obtained for the estimation of *constant motion features* indicate that the spike firing rate and the temporal structure are suitable coding strategies. However, the temporal structure appears to have more relevance for the time intervals that include the transient activity period, especially for larger population sizes. Here, for the spike cost-based metrics the spike firing rate and coarse time scales showed to encode most of the information about

the motion features. However, for increasing population sizes, there was a tendency for medium time scales to enhance the information, especially for motion velocity and motion direction. Here, this effect of the medium time scales appeared to be only present for the intervals containing the transient activity period, since it was not present for the sustained activity. Additionally, for the time intervals containing the transient period, the estimation results for the ISI metrics were similar to those yielded by the optimal time scales for the spike cost-based metrics, whereas for the sustained activity, the spike firing rate led to the higher estimation results. Moreover, while the estimation results for the constant motion features improved with increasing population sizes, the performance showed to reach a saturation point for larger population sizes, which suggests that the estimation improvement was not linearly related to the size of the populations (pages 109-120).

The estimation performances for the *instantaneous velocity changes* indicate that the spike firing rate of the transient activity period encodes some information about these changes. Nevertheless, most of this information is encoded by the temporal structure of this activity period. These affirmations are based on the one hand, on the results obtained for the spike cost-based metrics. Here, the spike firing rate allowed results that were significantly above chance level for the three analysed time intervals. However, a clear enhancement in the information about these instantaneous changes was yielded by fine and medium time scales of the activity of increasing population sizes, especially for the time intervals including the transient activity period. On the other hand, the estimation results obtained for the ISI metrics were similar to those yielded by the optimal time scales for the spike-cost based metrics. Furthermore, for the two time intervals containing the transient activity period, it was found that their differences in estimation performance were more evident for their temporal structure. Thus, it can be suggested that the temporal structure of the sustained activity enhances the information encoded by the transient activity period. Nevertheless, based on the low estimation results found for the interval containing solely the sustained activity, it seems that this activity alone fails to encode information about the instantaneous velocity changes. For the time intervals containing the transient activity period, it appeared that the limit in the estimation performance for the instantaneous velocity changes was not reached for the largest population sizes analysed in this study, i.e., $n = 18$, therefore, it can be suggested that even larger population sizes would further improve the estimation results (page 125).

As in the case of the single RGC, the estimation results for the *previous motion features* pointed out that the information about the stimulus history

is only present in the transient activity period, where its temporal structure encodes most of this information. Here, similar estimation performances were obtained for the time intervals containing the transient activity period. Moreover, for these time intervals, the estimation results yielded by coarse time scales for the spike cost-based metrics were significantly better than those expected by chance. However, medium and especially fine time scales allowed a clear improvement in the estimation performance, which further increased for larger population sizes. In turn, the similar estimation results obtained for the ISI metrics and the optimal time scales for the spike cost-based metrics stress the relevance of the temporal structure of the transient activity period for the encoding of information about the stimulus history. Furthermore, the improvement in the estimation performance for increasing population sizes for the time intervals containing the transient activity period, as well as the close to chance estimation performances found for the sustained activity, account for the estimation results obtained for the instantaneous velocity changes (pages 130-140).

For the estimation of the *post motion features*, the spike firing rate appears to be the relevant coding mechanism. However, the temporal structure of transient activity showed to enhance the information encoded by the spike firing rate. Here, for the spike cost-based metrics and in comparison to the results obtained without considering the stimulus history, similar estimation results were obtained for coarse time scales. However, the estimation performance for the post motion velocity and post motion direction was clearly improved by fine and medium time scales of the time intervals containing the transient activity period. Moreover, the improvement in the estimation performance was also found for the ISI metrics, especially for the activity of turtle RGC. Here, because the sustained activity led to similar estimation result for the motion features considering and disregarding the stimulus history, it can be suggested that the information about the post motion features is mostly encoded by the spike firing rate of the combined transient and sustained activity periods. In contrast, the temporal structure of the transient activity period appears to be modulated by the stimulus history (pages 145-155).

The results obtained for the *discrimination of motion feature changes* indicated that the transient activity period encodes most of this information. Here, fine and medium time scales of this period appear to be relevant for the discrimination task. For the spike cost-based metrics, fine and medium time scales of the time intervals containing the transient activity period led to the highest discrimination performances, which in turn, improved for larger turtle RGC populations. Furthermore, the estimation results obtained for the ISI

metrics were similar to those yielded by the optimal time scales for the spike cost-based metrics. Additionally, because similar estimation performances were obtained for the time intervals containing the transient activity period, it can be suggested that the sustained activity does not contribute for the discrimination of motion feature changes (pages 160-170).

Labelled Line hypothesis

In contrast to the Pooled Population hypothesis, the Labelled Line hypothesis proposes that the information about motion features of a moving stimulus is not encoded by the integrated activity of single RGC, but rather by their differentiated combined activity. Here, the information about the neuron of origin of each spike is always available. Thus, this hypothesis proposes that additionally to the spike firing rate and the temporal structure of the combined responses of RGC, the knowledge about the cell of origin of neuronal activity is relevant for the encoding of information about motion features. More precisely, under the Labelled Line hypothesis, it is considered that for the encoding of information about motion features, this information is first encoded by the activity of single RGC on independent channels and then, the information coming from each channel is integrated. In terms of the metric methods applied in this study, the Labelled Line hypothesis involves the calculation of the distance matrices for the responses of each of the cells comprising the populations and then, the sum of these matrices (Aronov et al., 2003).

Based on the estimation results for the *constant motion features*, it can be suggested on the one hand, that the spike firing rate of the transient activity carries more information about these features, than the spike firing rate of the sustained activity. However, the individual contribution by the optimal time scales of the transient and sustained activity from each of the RGC building the populations, allows to enhance the encoded information. On the other hand, the spike firing rate appears to be the relevant coding mechanism for the combination of the transient and sustained activity periods. Here, for the spike cost-based metrics, the estimation performance showed qualitative similarities to the one obtained based on the activity of single RGC. Consequently, the spike firing rate and coarse time scales yielded the best estimation results, whereas fine time scales led to the lowest estimation results. In the case of the ISI metrics, the estimation performances for time intervals containing solely the transient or the sustained activity period surpassed the ones yielded by the optimal time scales for the spike cost-based metrics. In contrast, for the time interval containing both the transient and

the sustained activity periods the opposite happened (pages 110-120).

A possible explanation for the better estimation performance obtained for the ISI metrics for time intervals containing solely the transient or the sustained activity period could be given by the histograms shown in Figure 3.6. There, it can be observed that the time scales that encode information about the features of a moving stimulus, show variations across the values of the motion features as well as across the RGC analysed in this study. Therefore, the spike cost-based metrics will fail to find the optimal time scale if greater variations across RGC are present. Conversely, if the temporal structure of the activity of RGC is relevant for the encoding of motion features, the ISI metrics would find automatically the optimal time scale for each of the RGC that build the analysed population. However, if the spike firing rate has a higher relevance for the encoding of motion features, which is the case of time interval containing both the transient and the sustained activity periods, then the ISI metrics will fail to register this phenomenon.

Moreover, it was observed that for the spike cost-based metrics, the length of the time interval considered for the analysis has a greater influence on the estimation performance than the size of the population, especially for the spike firing rate and coarse time scales. Therefore, it can be suggested the integration of the spike firing rate by longer periods, rather than larger population sizes, allows the enhancement of encoded information about constant motion features.

The estimation results for the *instantaneous velocity changes* pointed out, that the transient activity encoded the information about these changes. Here, the temporal structure appeared to be the relevant coding mechanism. However, the spike firing rate was also a suitable coding mechanisms. Here, for this response property, the encoded information was enhanced for larger integration windows. Moreover, it was found that the temporal structure of the sustained activity does not contribute to enhance the encoded information. Here, for the spike cost-based metrics, the spike firing rate led to high estimation performances for the time intervals containing the transient activity period. In turn, these performances further improved for coarse time scales. Moreover, the time interval containing both the transient and the sustained activity period, led to better estimation results. In contrast, for the ISI metrics, the time intervals containing the transient activity period led to similar estimation results, which in turn clearly outperformed the ones yielded by the optimal time scales for the the spike cost-based metrics. Moreover, for both of the applied metrics and in contrast to the constant motion features, the obtained results showed a tendency to improve with increasing population sizes (pages 127).

The estimation performance for the *previous motion features* suggested that the temporal structure of the transient activity encoded most of the information about the stimulus history. This is because for both of the applied metrics, the time interval containing the transient activity led to similar estimation results. Here, although for the spike cost-based metrics the spike firing rate led to high estimation performances, medium time scales yielded the maximum results. Moreover, these results were clearly outperformed by the ones obtained for the ISI metrics (pages 130-140).

Based on the estimation results obtained for the *post motion features*, it can be suggested that when the stimulus history is considered, the spike firing rate and the temporal structure of the transient activity allow to enhance the information about these features. This affirmation is based on the finding that these two response properties are modulated by the stimulus history. Here, for the spike cost-based metrics and in comparison to the results obtained without considering the stimulus history, medium time scales yielded the greatest improvements in favour of the post motion features for all the analysed time intervals. In contrast, for the ISI metrics, the estimation improvement was only present for the time intervals containing the transient activity period (pages 146-156).

The results for the *discrimination of motion feature changes* suggested that the temporal structure of the transient activity encodes most of this information, and that the sustained activity does not contribute to enhance the encoded information. This affirmation is based on the similar discrimination results obtained for the time intervals containing the transient activity period, as well as the poor results yielded by the sustained activity for both of the applied metrics. Here, for the spike cost-based metrics, the spike firing rate but also coarse time scales of the time intervals containing the transient activity period led to the highest discrimination performances. Moreover, the results obtained for the ISI metrics were similar to those obtained for the optimal time scales for the spike cost-based metrics (pages 162-170).

As a closing remark for the Labelled Line hypothesis, it has to be stressed that the improvement in the estimation performance with increasing population sizes was more evident for the instantaneous changes of motion velocity, the motion features before the instantaneous changes, and to a lesser degree for the changes of motion features.

Functional Group hypothesis

The last of the tested hypothesis about how the combined activity of RGC could encode information about a moving stimulus was the Functional Group

hypothesis. However, due to the limited number of recorded fish RGC, this hypothesis could only be tested for the activity of turtle RGC. The Functional Group hypothesis is a combination of the Pooled Population hypothesis and the Labelled Line hypothesis. Here, it is assumed that the information about the motion features of a moving stimulus is first encoded by the integrated activity of RGC of the same class on independent pathways and then, the information coming from the different pathways is integrated. In this sense, the Functional Group hypothesis states that for the encoding of motion features, besides the spike firing rate and the temporal structure of the responses of RGC, it is relevant to know to which class belongs the neuron that fired each spike. In terms of the analysis carried out in this study, the responses of RGC belonging to the same class were first pooled together. Then, the distance matrices for the responses of each of the cell classes were calculated and finally, the matrices were summed together.

The results obtained for the estimation of *constant motion features* suggested that the spike firing rate and the temporal structure are suitable coding strategies. Here, larger population sizes and longer time windows allow to enhance the encoded information about these features. Furthermore, for the transient activity, the temporal structure appears to have more relevance than the spike firing rate. For the spike cost-based metrics, the spike firing rate as well as medium and coarse time scales led to the maximum estimation performances. Moreover, qualitatively similar estimation results were obtained for all of the tested population sizes. Here, in contrast to the other two tested hypotheses, there was a clear improvement in the estimation performance with increasing population sizes. This improvement was also observed for the estimation results yielded by the ISI metrics. Furthermore, for the transient activity, the results obtained for the ISI metrics exceeded the ones yielded by the optimal time scales for the spike cost-based metrics (pages 112-122).

The estimation performance for the *instantaneous velocity changes* suggest that the temporal structure of the transient activity has a higher relevance than the spike firing rate for the encoding of information about these changes. Here, it appears that larger population sizes allow the enhancement of the encoded information. These suggestions are based in part on the similar estimation results obtained for the time intervals containing the transient activity period. Moreover, although for spike cost-based metrics the spike firing rate led to high estimation results, medium time scales yielded the maximum performances, which in turn, improved with increasing population sizes. However, these results were surpassed by the ones obtained for the ISI metrics (page 127).

For the *previous motion features* the obtained results indicate that the temporal structure of the transient activity carries more information about the stimulus history than the spike firing rate. Furthermore, larger populations allow to enhance this information. These affirmation is based on the similar estimation results obtained for the time intervals containing the transient activity period. Here, the spike firing rate led to high estimation results for spike cost-based metrics: However, the maximum performances were yielded by medium time scales. Furthermore, the results obtained for the ISI metrics exceeded the ones yielded by the optimal time scales for the spike cost-based metrics. Additionally, due to the fact that the sustained activity led to estimation performances close to chance level, it can be suggested that the information about the stimulus history is absent in this activity period (pages 132-142).

For the estimation of the *post motion features*, the spike firing rate appears to have a high relevance. Nevertheless, medium time scales of the transient activity showed to enhance the information encoded by the spike firing rate. For the spike cost-based metrics, and in comparison to the results obtained without considering the stimulus history, fine and medium time scales of the time intervals that contained the transient activity period, led to improvements in the estimation performance for post motion features. Here, the estimation results yielded by medium time scales were similar to those obtained for the ISI metrics (pages 146-156).

The results for the *discrimination of motion feature changes*, indicated that this information is mostly encoded in the temporal structure of the transient activity. This affirmation is supported on the fact that for both of the applied metrics, similar estimation results were obtained for the time intervals containing the transient activity period. Here, although the spike firing rate led to discrimination performances that were significantly above chancel for the spike cost-based metrics, these performances were improved for finer time scales, especially for increasing population sizes. Moreover, the estimation results obtained for the ISI metrics were generally better than the ones yielded by the optimal time scales for the spike cost-based metrics. Additionally, because the sustained activity led to poor estimation results for both of the applied metrics, it can be also suggested that the information about motion feature changes is almost absent in this activity period (pages 162-172).

4.2.4 Coding Strategies

In the previous sections, based on the results obtained for the estimation of the different motion features, it was discussed whether the spike firing rate or the temporal structure of RGC responses encodes information about a moving stimulus. This discussion was done individually for the activity of single RGC as well as for the three tested joint activity coding hypotheses. However, in order to offer a more comprehensive overview, this section discusses the comparison of the tested coding strategies, i.e., spike firing rate vs. temporal structure (Figure 4.1), as well as the explored coding hypotheses, i.e., single cell coding, Pooled Population, Labelled Line and Functional Group Figure 4.2. Here, in order to simplify the discussion, only the comparison for the motion velocity, the instantaneous velocity changes and the changes in motion features is going to be addressed. These motion features comprise respectively, the estimation of constant stimulus conditions, the estimation of instantaneous changes in stimulus conditions and the discrimination of motion feature changes. Although qualitative similarities were found for both of the analysed animal species, the figures in this section correspond to the results obtained for the turtle experiments.

Figure 4.1 shows the comparison of the coding strategies for the single cell coding and the three tested joint activity coding hypotheses. The comparison was done by calculating the ratio between the estimation performance allowed by the temporal structure of the responses of RGC and the spike firing rate. Thereby, as a first step for the spike cost-based metrics, the maximum estimation performances for fine, medium and coarse time scales were determined. Then, these values were divided by the estimation performance yielded by the spike firing rate. Furthermore, the comparison also included the ratio for the estimation performances yielded by the ISI metrics. In this sense, ratios equal to one indicate similar estimation performances for the spike firing rate and the temporal structure of RGC responses. Conversely, ratios above and below one indicate better estimation performances yielded either by the temporal structure or the spike firing rate, respectively.

In turn, Figure 4.2 shows the comparison of the tested joint activity coding hypotheses. Here, for each of the three hypotheses, the plots correspond to the median estimation performance allowed by population sizes $n = 18$. Additionally, the median of the estimation performance allowed by the activity of all the analysed single cells ($n = 62$) is plotted as reference.

Constant motion features

Generally, for the *spike cost-based metrics*, the temporal structure of RGC responses, as well as the spike firing rate, showed to be equally suitable to encode information about constant motion features (Figure 4.1a). Thereby, for the activity of single RGC, medium and coarse time scales yielded similar estimation results as the spike firing rate. In turn, these results were also found for the Pooled Population and the Functional Group hypotheses. Nevertheless, in the case of the Labelled Line hypothesis, only coarse time scales led to estimation results similar to those obtained for the spike firing rate.

In the case of the *ISI metrics*, the spike firing rate and the temporal structure of RGC responses showed to have the same relevance for single cells, as well as for two of the tested joint activity coding hypotheses; the Pooled Population and the Functional Group. In contrast, great ratios in favour of the ISI metrics were observed under the Labelled Line hypothesis for both 200 ms intervals. Because these results were not observed for the other joint activity coding hypotheses, it can be suggested that for the transient and sustained periods of RGC responses, the information about motion features is present in different time scales of the activity of single RGC. Thus, by utilising simultaneously different time scales, the differentiated activity of RGC would be able to encode more information.

Based on these observations, it can be suggested that the spike firing rate and the temporal structure of RGC responses encode information about constant motion features. Nevertheless, the way in which RGC interact has an effect in the relevance of these two responses properties for the encoding task. Here, in the case of the spike firing rate, the Functional Group hypothesis appears to utilise this coding strategy more efficiently, where longer integration time windows allow to enhance the encoded information. In contrast, the results allowed by the ISI metrics show that the temporal structure of the activity of RGC populations is more efficiently utilised by the Functional Group and the Labelled Line hypotheses. However, under the Labelled Line hypothesis, longer integration time windows do not enhance the encoded information as they do under the Functional Group hypothesis (Figure 4.2a).

All together, the findings described in the previous paragraph indicate that under the Functional Group hypothesis, the integration of the activity of RGC of the same class has a positive effect on the encoding of information about the motion velocity of a stimulus by the spike firing rate. In turn, this positive effect would allow to encode information in shorter time windows, which explains in part the better estimation results obtained under the Functional Group hypothesis for both 200 ms intervals. Additionally, and in

contrast to the Pooled Population hypothesis, the knowledge of the class to which the cells that fire spikes belongs prevents the loss of information about motion direction. Therefore, it can be proposed that for the spike firing rate, the integrated activity of RGC, either belonging to the same class or not, contributes to enhance the encoded information about the magnitude of motion features, i.e., motion speed, while the knowledge of the class to which the cell that fires spikes belong contributes to encode information about qualitative motion features, i.e., motion direction.

Changing motion features

In the case of the estimation of the instantaneous velocity changes and the discrimination of motion feature changes, the temporal structure of the responses of RGC generally allowed better results than the spike firing rate (Figure 4.1b and c). Moreover, the improvement in the estimation results was more evident for the activity within the 500 ms and the first 200 ms intervals, for which the greatest ratios in favour of the temporal structure were found for both of the applied metrics.

More in detail, for the *spike cost-based metrics*, finer time scales gained relevance for the encoding of information about changing motion features with increasing activity integration. Thus, for the Pooled Population hypothesis, for which the activity of the RGC is pooled together, fine time scales are more relevant than medium or coarse time scales. In contrast, for the Labelled Line hypothesis, the activity of RGC is regarded independently and therefore, coarse time scales have more relevance than medium and fine time scales.

Comparing the ratios yielded by the *ISI metrics* and the optimal time scales for the spike cost-based metrics, it was observed that the difference in ratios in favour to the ISI metrics decreased with increasing activity integration. This effect could be explained by the fact that for the ISI metrics, the optimal time scales are individually obtained for each of the analysed single or group of RGC. In turn, these observations offer additional evidence to suggest that information about motion features, especially about instantaneous changes, is encoded simultaneously by different time scales of the activity of single or small groups of RGC.

For the three tested joint activity coding hypotheses, the temporal structure of RGC activity shows to encode most of the information about changes in motion features. However, the increase of information about the origin of the spikes, either the exact cell or the cell class, enhanced the relevance of the spike firing rate for the encoding this information. Moreover, the efficiency in the encoding of information about motion feature changes varies across the

three tested joint activity coding hypotheses. Here, these variations depend on the nature of the information to be encoded.

Based on the estimation results obtained for the *instantaneous velocity changes* by the spike cost-based metrics, medium time scales of the activity of RGC under the Functional Group hypothesis appeared to be optimal for the estimation of these changes. This finding was more evident for the 500 ms and the first 200 ms intervals, which in turn, yielded the highest estimation performances. Nevertheless, the results obtained for the ISI metrics pointed out the fact that the temporal structure of the activity of RGC under the Labelled Line hypothesis allows a more efficient encoding of this information (Figure 4.2b). Moreover, in contrast to the Functional Group hypothesis, for which the estimation performance improved with longer integration time windows, the estimation results yielded by the activity of RGC under the Labelled Line hypothesis were not significantly different for the 500 ms and the first 200 ms interval. These observations suggest that for the optimal time scales, all the available information about the instantaneous velocity changes is encoded in the temporal structure of the transient period of the differentiated activity of RGC. Here, the knowledge about the origin of each spike, either the exact cell or just the type, seems to play a relevant role in the encoding task.

In contrast, for the *discrimination of motion feature changes*, the results obtained for the spike cost-based metrics show that fine time scales of the activity of RGC under the Pooled Population hypothesis allow significantly better results than the optimal time scales for the other two tested hypotheses ($p \leq 0.005$). These results were found for the 500 ms and the first 200 ms intervals, which in turn yielded the best discrimination performance for the three tested joint activity coding hypotheses. Furthermore, for these two time intervals, the Functional Group and the Pooled Population hypotheses yielded the best estimation results for the ISI metrics. Here, for the Pooled Population hypothesis, the results obtained for the ISI metrics were similar to the ones allowed by the optimal time scales for the spike cost-based metrics (Figure 4.2c). This finding indicates that in contrast to the instantaneous velocity changes, the integration of RGC activity allows the temporal structure to encode more efficiently information about sudden changes in the motion features, where the knowledge of the cell of origin of each spike has a low relevance for the encoding task. Moreover, the temporal structure of the transient period of the integrated activity appears to encode most of this information.
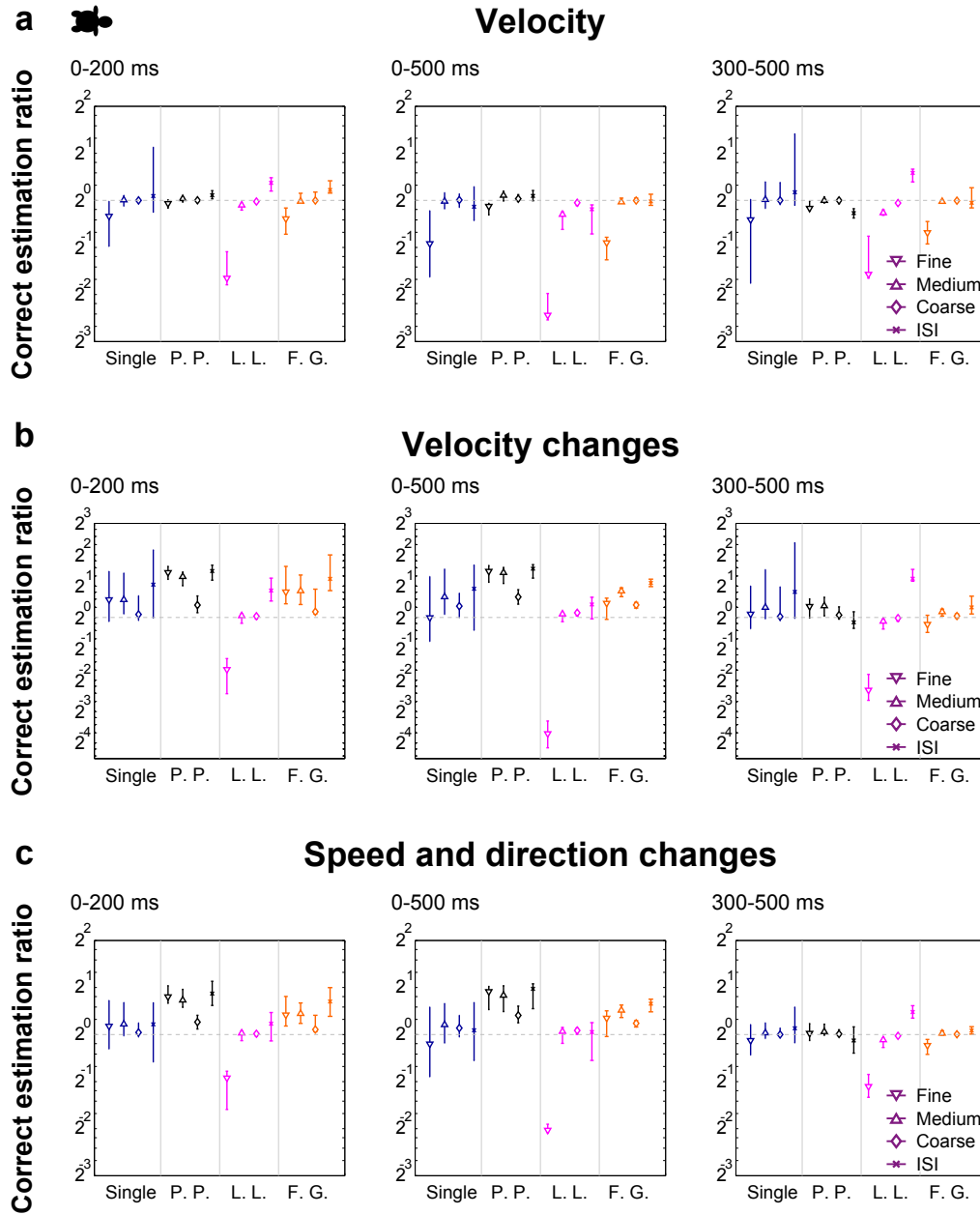
Figure 4.1: Ratio of the estimation performance yielded by the temporal structure of RGC responses and their spike firing rate. The ratio was calculated for fine, medium and coarse time scales, as well as for the results obtained by the ISI metrics. Ratios equal one indicate equal estimation performance for the temporal structure and the spike firing rate. Ratios above and below one indicate better estimation performance for the temporal structure or the spike firing rate, respectively. Markers indicate the median, whereas error bars represent the range between maximum and minimum estimation performance ratios. a) Estimation of motion velocity. b) Estimation of instantaneous velocity changes. c) Estimation of changes in the motion features.
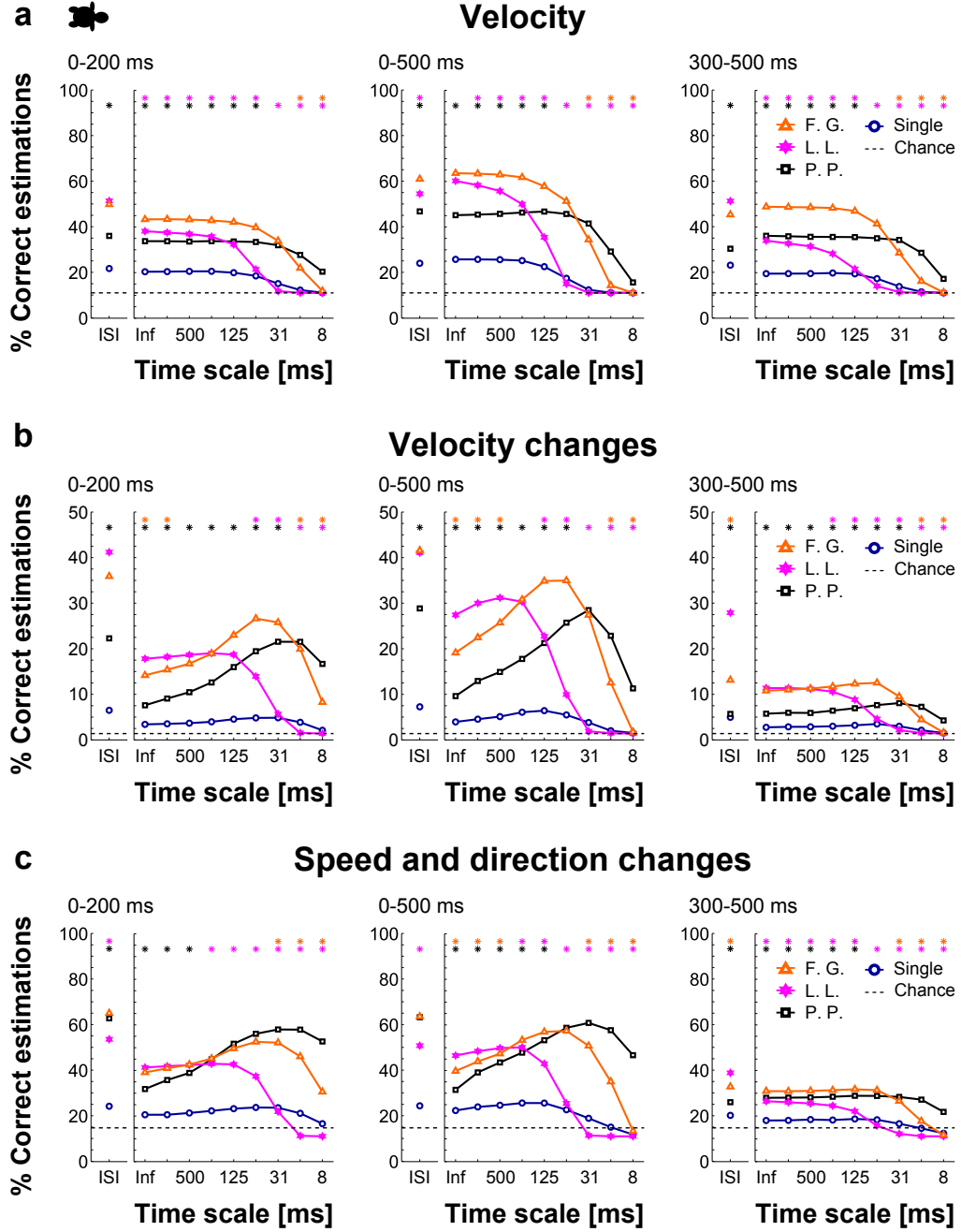
Figure 4.2: Comparison of the median estimation performance for the motion features of the moving stimulus. The estimation was carried out by applying spike cost-based metrics and ISI metrics on the activity of turtle RGC within the three tested time intervals. For both metrics, the estimation allowed by the activity of single RGC is plotted as reference. For the three tested hypotheses, the results correspond to the ones allowed by RGC populations $n = 18$. Star symbols at the top of the plots indicate significant differences between the hypothesis that allowed maximum estimation performance and the other two hypotheses ($p < 0.005$). In the legend P.P.: Pooled Population, L.L.: Labelled Line and F.G.: Functional Group a) Estimation of motion velocity. b) Estimation of instantaneous velocity changes. c) Estimation of changes in the motion features.

4.3 Light-Motion Experiment

The second part of this study tested if the activity of fish RGC encodes simultaneously information about the motion features of a moving stimulus and its background luminance. Thus, the experiment protocol comprised a pseudo-random sequence for which the motion velocity and the luminance were kept constant for periods of 500 ms. At the end of these periods, one of the stimulus features was instantaneously changed (refer to section 2.1.2 for more details).

For this study, the responses of RGC from one fish retina were analysed with the spike cost-based metrics in order to explore if the spike firing rate or the temporal structure of their responses carried information about the motion features and the light intensities. Here, the activity of single RGC, as well as two joint activity coding hypotheses were tested, i.e., Pooled Population and Labelled Line. Moreover, the hypotheses were tested on one population built with $n = 18$ RGC.

4.3.1 Constant Features

For the constant light intensities and motion velocities of the moving stimulus, it was observed that information about these features was present in the activity within the three tested time intervals. Furthermore, comparing the estimation performances for both stimulus features, it was observed that generally, the estimation of light intensities was more robust. This affirmation is based on the estimation results allowed for the first 200 ms interval for both stimulus features. Here, it was observed that changes in the complementary stimulus feature had a stronger influence on the estimation of motion velocities than on the estimation of light intensities. In turn, this influence provoked that the estimation of the motion velocity was strongly impaired by the light intensity changes. Moreover, it was found that for the encoding of information about motion features in the transient period, the relevance of the spike firing rate, as well as the temporal structure, is determined by the stimulus history. Here, it was observed that when changes in light intensity occurred, the temporal structure gained relevance for the encoding of information about motion features. In contrast, when changes in the motion velocity were present, the spike firing rate led to the maximum estimation performances. Therefore, it can be suggested that the temporal structure of the transient period could be utilised as a cue to estimate which stimulus features has changed. The combined activity of RGC led to estimation performances for the light intensity and the motion velocity that surpassed the median estimation performance found for single RGC. Moreover, for both

of the tested hypotheses, the estimation results for each of the stimulus features were qualitatively similar. However, when the two stimulus features were simultaneously estimated, the combined activity of RGC led to results that clearly outperformed the ones obtained for single RGC. These results suggest that although the activity of single RGC encode information about single stimulus features, it fails to encode simultaneously information about additional features. Here, this deficit is coped by the combined activity of RGC.

Single cell coding

For the three analysed time intervals, the spike firing rate of the activity of single RGC showed to encode information about the light intensity and the motion velocities. Furthermore, the spike firing rate showed also to be suitable for the simultaneous encoding of these two stimulus features. However, for the 500 ms and the first 200 ms intervals, and especially when changes in the light intensity were present, medium time scales showed a tendency to improve the estimation performances. Therefore, it can be suggested that most of the information about constant stimulus features is encoded by the spike firing rate of the transient and sustained periods of the activity of single RGC. Moreover, for the encoding of information about motion features, longer integration windows allow the enhancement of the encoded information. However, the temporal structure of the transient period could be used as a cue to estimate which stimulus feature has changed.

Joint activity coding

For the *Pooled Population* hypothesis, the spike firing rate of the sustained activity showed to encode information about the light intensities and the motion velocities. Moreover, it also showed to be suitable for the simultaneous encoding of both stimulus features. However, for the time intervals that included the transient period, the temporal structure showed to gain relevance, especially for the encoding of information about motion velocity and the simultaneous encoding of both stimulus features. Therefore, it can be suggested that information about the light intensity is robustly encoded in the firing rate of the combined activity of RGC under the Pooled Population hypothesis. However, in the transient period, the encoding of information about the motion features and the simultaneous encoding of both stimulus features, is more efficient for the temporal structure. Here, fine time scales appear to be more relevant when light intensity changes occur. In turn, when motion velocity changes occur, medium time scales gain relevance.

For the *Labelled Line* hypothesis, the spike firing rate showed to encode robustly the information about the light intensities and the motion velocities. Moreover, it also showed to be suitable for the simultaneous encoding of both stimulus features. Here, for the time intervals including the sustained activity period, the spike firing rate of the differentiated activity of RGC, showed to be the most efficient strategy for the simultaneous encoding of both stimulus features. However, when changes in the light intensity occurred, medium time scales of the temporal structure of the transient period, encoded more efficiently the information about the motion features and also allowed a better performance in the simultaneous encoding of both stimulus features.

4.3.2 Changing Features

For each of the three analysed time intervals, the estimation results across the changes in stimulus features were qualitatively similar for the activity of single RGC, as well as for each of the tested joint activity coding hypotheses. Thereby, it appears that the combined activity of RGC allows to encode more information about the instantaneous changes in the stimulus features, than the activity of single RGC. Furthermore, it can be proposed that most of the information about the instantaneous changes in light intensity and motion velocity is present in the transient period of the responses of RGC. This affirmation is based on the fact that for the activity of single RGC and the two tested joint activity coding hypotheses, better estimation results were obtained for the 500 ms and the first 200 ms intervals. Here, for these two time intervals, the estimation performance reached its maximum for fine and medium time scales. While the time intervals that included the transient period led to the highest estimation results, the interval containing only the sustained period led to the poorest estimation performances. Therefore, it can be suggested that the temporal structure of the transient period encodes information about both, the stimulus history and the stimulus features after the instantaneous changes. In contrast, the information about the instantaneous changes in the stimulus features is almost absent in the sustained period. Nevertheless, the spike firing rate of the sustained period seems to encode information about the post stimulus features, which in turn represents additional information about the stimulus changes to the one encoded by the transient period.

Single cell coding

Aside from the last 200 ms interval, the spike firing rate of the activity of single RGC showed to encode information about the instantaneous changes

in the stimulus features. However, for the 500 ms and the first 200 ms intervals, fine and medium time scales of the temporal structure enhanced the encoded information. Thus, it can be suggested that for the activity of single RGC, the spike firing rate of the transient period encodes information about the stimulus changes. However, the temporal structure of this period has a higher relevance for the encoding task.

Joint activity coding

For the *Pooled Population* hypothesis, the spike firing rate of the responses within the 500 ms and the first 200 ms intervals, showed to have a low relevance for the encoding of information about changes in the stimulus features. In contrast, fine time scales of these responses showed to be the ones involved in the encoding task. Therefore, it can be proposed that under this hypothesis, the available information about changes in the stimulus features is encoded in the temporal structure of the transient period.

For the *Labelled Line* hypothesis, the spike firing rate showed to have a high relevance for the encoding of information about changes in the stimulus features. Moreover, the information about stimulus changes showed to be almost absent in the fine time scales of the combined activity of RGC under this hypothesis. Nevertheless, and particularly for the 500 ms and the first 200 ms intervals, medium time scales were optimal for the encoding of this information. Thus, it can be proposed that under this hypothesis, the spike firing rate of the transient period carries much of the information about stimulus changes but nonetheless, the information is enhanced by the temporal structure of this period.

4.3.3   Feature Change Discrimination

For the single RGC as well as for the two tested joint activity coding hypotheses, it was found that the transient period of the neuronal responses carries information that allows to discriminate which stimulus feature has changed. Moreover, the sustained period does not contribute for the encoding of additional information. These claims are supported on the fact that the highest estimation performances for the discrimination of changes in the stimulus features, were yielded by the 500 ms and the first 200 ms intervals. Here, these two time intervals led to similar estimation results for single RGC and each of the two tested joint activity coding hypotheses. Furthermore, the last 200 ms interval led to estimation results that were close to those expected by chance. The relevance of the spike firing rate and the temporal structure for the discrimination of stimulus features changes showed differences between

the single RGC and the two tested joint activity coding hypotheses. However, in all cases, the temporal structure appears to encode more efficiently information about the stimulus feature that has changed.

Single cell coding

For the activity of single RGC, the spike firing rate of the transient period allows the discrimination of stimulus feature changes. Nevertheless, medium time scales contribute to the improvement in the discrimination performance. Thus, it can be proposed that information about which stimulus feature has changed is more efficiently encoded in the temporal structure of the transient period.

Joint activity coding

For the *Pooled Population* hypothesis, the spike firing rate of the transient period showed to have a low relevance for the discrimination of stimulus feature changes. In contrast, fine time scales within this period showed to be the ones involved in the discrimination task. Thus, it can be suggested that under this hypothesis, the discrimination of stimulus feature changes is mediated by a high precision temporal structure of the transient period.

For the *Labelled Line* hypothesis, the spike firing rate showed to have a high relevance for discrimination of stimulus feature changes. However, medium time scales of the transient period were optimal for the discrimination task. Therefore, it can be proposed that under this hypothesis, the spike firing rate of the transient period allows the discrimination of stimulus feature changes but nevertheless, the task is more efficiently mediated by the temporal structure of this period.

4.4 Behavioural Implications

In primates, it has been suggested that the processing of visual motion starts in the primary visual cortex (Blake et al., 2003). Here, models have been developed to estimate motion features, e.g., direction, based on the activity of ensembles of RGC (Chichilnisky and Kalmar, 2003). Moreover, it has been found that is not until the MT area of primates, where some neurons tune their spike firing rate to the motion speed of an image (Lisberger and Movshon, 1999). Here, it has been suggested that pooling the activity of these cells could allow to encode information about motion acceleration (Cao et al., 2004). In contrast, the responses of some RGC in other animal species

like rabbits, cats, turtles and fish, have proved to encode information about motion features like direction (Barlow and Hill, 1963; Barlow et al., 1964; Ammermüller and Kolb, 1996; Tsvilling et al., 2012), velocity (Oyster et al., 1972; Ariel and Adolph, 1985) and accelerations (Thiel et al., 2007). In this sense, the results obtained in this study are in accordance with these previous studies. Therefore, for the animal species examined, i.e., turtle and carp, it has been shown that visual motion processing occurs already in the retina. In turn, this finding has implications in the velocity with which the visual stimulus is processed. For instance, in the archer fish, it has been proposed that their fast responses for hunting manoeuvres are mediated by the retinal identification of motion direction (Tsvilling et al., 2012).

4.4.1   Relevance of Visual Motion Processing

For many animal species, the information delivered by the visual system about their environment has a great influence on their behaviour. Accordingly, the detection and estimation of motion features of natural visual scenes allow to gain information about their environment and in turn, perform the adequate correction tasks if necessary (Hengstenberg et al., 1986; Lisberger and Movshon, 1999; Berry II et al., 1999; Thiel et al., 2007), enhancing in this way, the animal's chance of survival. Thereby, the processing of motion information by the visual system is necessary for the detection and location of external moving objects and the estimation of self motion-parameters (Dellen and Wessel, 2009; Dellen et al., 2010). Here, the estimation of the motion velocities plays an important role in pursuit eye movements, which allow to keep the visual image in the foveal region of the retina (Yamasaki and Wurtz, 1991). Moreover, self-motion generates patterns of optic flow, which in turn, induce the perception of motion of the whole visual field. Therefore, these optic flow patterns have to be analysed by the visual system to allow compensation that ensures optimal visual acuity and velocity discrimination (Laughlin, 1999; Crowder et al., 2003). Additionally, the detection of changes in motion features of external objects have a great relevance for survival. Here, the estimation of changes in motion trajectory or velocity play an important role in avoiding collisions, catching a prey or escaping from a predator, breaking camouflage, or detecting threats (Laughlin, 1999; Thiel et al., 2007; Dellen and Wessel, 2009). Based on these facts, it can be observed that the visual motion processing is a complex task. Nevertheless, the results obtained in this study show that the primary stages for visual motion processing are already undertaken in the retina of turtle and carp.

An additional aspect that has to be considered in visual motion processing is that scenes of natural environments generally include several visual

features such as luminance, wavelength, texture and shape. Nevertheless, in order to ensure correct behaviour, a robust estimation of motion features has to be performed independently of other visual attributes, e.g., luminance. This mechanism for independent coding of motion features has already been observed in the avian tectum (Dellen and Wessel, 2009). However, in the case of the carp, the results obtained in this study suggest that this independent coding takes place already in the retina.

4.4.2   Relevant Time Scales

It has been proposed that in the visual system, the spike firing rate and different time scales of neuronal responses could carry information that allow to distinguish stimulus features (Oram et al., 2002). Moreover, it could be possible that individual spike trains encode information about several stimulus features in a temporally multiplexed fashion. Here, the relevance of the time scales for encoding tasks would be dependent on the stimulus features (Victor and Purpura, 2010). Evidence to support these claims have been found in the responses of neurons in the primary visual cortex of monkeys and cats (Richmond et al., 1987; Optican and Richmond, 1987; Tovee et al., 1993; Samonds et al., 2003; Samonds and Bonds, 2004)

Visual motion can be defined as spatio-temporal changes of light intensity of an image (Dellen and Wessel, 2009), where the motion velocity describes the rate or frequency in which these changes take place. Since it has been observed that the visual system responds mainly to changes (Greschner et al., 2002), in this study it was not surprising to find that after a transient period, the responses often showed stronger sustained activity to constant velocities than to constant light intensities. Moreover, one of the findings in this study was that for scenarios with constant stimulus conditions, e.g., constant light intensity or constant motion velocity, the spike firing rate, as well as the temporal structure of RGC responses, encodes information that allows the estimation of the stimulus features. In contrast, once changes in the stimulus conditions were involved, the temporal structure of the responses, especially in the transient period, gained relevance for the estimation of the stimulus changes. In this context, it has been proposed that for the visual tracking of a moving stimulus, the size of time scales that are relevant for motion estimation are bound to the speed required for behavioural responses (Theunissen and Miller, 1995; Gautrais and Thorpe, 1998).

In this study, the spike firing rate has proved to encode information about constant stimulus features. Nonetheless, this coding strategy may be too slow to ensure correct behaviour for survival tasks. Here, the temporal structure of the responses could help to cope with this problem. According to Oram

et al. (2002), Samonds and Bonds (2005) and Roussin et al. (2008), besides the spike firing rate, temporal patterns in the neuronal responses could be involved in the encoding of information about stimulus features. Moreover, these patterns could have a structure, which cannot be anticipated from the spike firing rate, e.g., latency or ISI. Despite the possibility that these temporal patterns may not provide additional information, their temporal structure could be utilised by simple synaptic mechanisms to decode information in a more efficient way than a spike firing rate code would allow (Victor, 2000). In the case of the results obtained for the spike cost-based metrics in this study, the time scales within the range that led to the highest estimation performances should be regarded as averages across the entire response (Victor and Purpura, 2010; Chicharro et al., 2011). Here, these time scales could be interpreted as the time window necessary to update the estimation of the response properties that contain information about a stimulus feature (Paiva et al., 2010), or the spike firing precision of the responses that allow the maximum discrimination across stimulus features (Reich et al., 2001b; Huetz et al., 2006).

In agreement with the proposal that the spike firing rate as coding strategy may be too slow to process sensory information (Gautrais and Thorpe, 1998; Van Rullen et al., 2005), the spike firing rate lost relevance for the encoding of information about stimulus changes. Here, medium and fine time scales showed to be optimal for the encoding of this information. Furthermore, for changes in the motion velocity and light intensity, it was not observed that different time scales were involved in the information encoding tasks for each of the stimulus features. However, it was observed that for the estimation of the stimulus features after a stimulus change, fine time scales gained relevance when changes in the light intensity occurred, whereas for changes in motion velocity this effect was observed for medium time scales. Therefore, as proposed by Victor and Purpura (1998) and Oram et al. (2002) for the visual system, it could be possible that different time scales of RGC activity encode simultaneously different stimulus features.

Thiel et al. (2007) have found that in turtle retina, the decoding of motion velocity and accelerations can be achieved by updating the instantaneous firing rate of a population of RGC with a time window of ∼86 ms (i.e., medium time scale). The approach followed by Thiel et al. (2007) cannot be directly compared with the analysis in this study. However, there are similarities with the Labelled Line hypothesis tested here. For instance, in both studies, the activity of each single RGC contributed individually to the encoding of information by the population. However, in the approach of Thiel et al. (2007), the instantaneous firing rate was the response property suggested to encode information. In contrast, for the spike cost-based metrics, the spike

timing, an estimation of the spike firing rate, or both response properties could be involved in the encoding tasks (Huetz et al., 2006; Paiva et al., 2010). Furthermore, in the study by Thiel et al. (2007), the calculation of the time scale was not done individually for constant motion velocities and velocity changes. Despite these differences, the optimal time scale found by Thiel et al. (2007) falls in the range of the relevant time scales found for the Labelled Line hypothesis in this study.

The absolute latency, i.e., the time difference between the stimulus onset and the first spike, is an additional coding strategy that was not directly tested in this study. Here, this response property was indirectly tested by analysing the transient period of the RGC responses. Cerquera and Freund (2011) tested this response property together with the two following ISI in populations of turtle RGC. Here, the authors assessed the performance of these response properties for the estimation of motion velocities and instantaneous velocity changes. They found that the absolute latency alone encoded enough information to allow the estimation of the motion velocity and the velocity changes. Thus, it is possible that fine time scales encode information about motion features. Here, this suggestion is supported on the fact that the latency is associated with the firing events after a stimulus onset, i.e., stimulus change, and these firing events have been found to be highly precise in time (Berry et al., 1997).

An aspect that has to be addressed is the fact that information about the stimulus history is present in the temporal structure of the transient period. Here, it not suggested that this observation implies that the RGC have a memory mechanism. Instead, this finding could be explained by the fact that RGC respond mainly to stimulus changes (Greschner et al., 2002), where the stimulus history plays an important role in shaping the transient period of the responses. This effect has been observed since the first recordings of RGC responses to changes in light intensity (Hartline, 1938). Here, the transient burst of On- and Off-cell responses after light intensity changes is in part defined by the stimulus history (Berry et al., 1997; Greschner et al., 2006). Moreover, as observed for the estimation of the motion features considering the stimulus history, the temporal structure of the transient activity allowed to improve the estimation performances. In this direction, it has been suggested that the temporal correlation of spikes enhances the encoded information about visual stimulus (Jacobs et al., 2009). In the case of the turtle retina, it has been found that the activity of RGC encode information about motion acceleration (Thiel et al., 2007). Here, the encoding of this information would not be possible if information about the stimulus history, as well as the present stimulus, were not present in the

temporal structure of the transient period. Moreover, as closing remark for this section, it is worth stressing that the results for the post motion features in this study did not considered the a priori knowledge of the previous motion features. However, it is very probable that by making this consideration, the performance in the estimation for the post motion features would increase significantly.

4.4.3   Ensemble and Population Coding

The discussion in the previous paragraphs addressed the general findings in this study regarding the relevance of time scales. Nonetheless, additionally to the stimulus features, the relevance of the spike firing rate and the temporal structure was also related with the way in which the activity of RGC was combined. Moreover, the time scales that showed to be relevant for the encoding of stimulus features varied across the three tested coding hypotheses for joint activity.

According to the definition of population and ensemble coding proposed by Theunissen and Miller (1995) and Lestienne (2001), the Pooled Population hypothesis appears to fit in the definition of population coding, where each neuron in the population contributes with its firing rate for the encoding task. Here, this affirmation is more evident for the encoding of information about constant motion features. Furthermore, although the temporal structure showed to be more relevant than the spike firing rate for the estimation of stimulus changes, the temporal structure of each cell does not contribute to the encoding task. This affirmation is supported on the fact that for the Pooled Population hypothesis, there is no distinction across the spikes coming from each of the neurons comprising the population. Therefore, the temporal structure in the activity of the population is a product of the spike firing rate from each neuron.

In contrast, the Labelled Line hypothesis seems to fit into the definition of ensemble coding. Here, although for constant motion features the spike firing rate led to the highest estimation results for the spike cost-based metrics, these results were outperformed by the ones obtained for the ISI metrics. Here, these results were particularly found for the time intervals containing only the transient or the sustained activity period. Thereby, the results obtained for the ISI metrics indicate that for the encoding of information about stimulus features, different time scales are utilised by each of the neurons building the population and most importantly, that the temporal structure of each neuron contributes to the encoding task. These results are more evident for the encoding of information about stimulus changes, where for both of the applied metrics, the highest estimation performances

were yielded by the temporal structure of the time intervals containing the transient period.

The Functional Group hypothesis lies between the definitions of population coding and ensemble coding because the temporal structure of each cell group building the population, i.e., cell class, contributes for the encoding of information of constant stimulus features as well as stimulus changes. Nevertheless, the temporal structure of each group is, as in the case of the Pooled Population hypothesis, the result of the spike firing rate contributions from each of the neurons building these groups.

Based on the results obtained for the three tested joint activity coding hypothesis, it seems that all of them are suited to encode information about the features of a visual stimulus. Moreover, it could be possible that the three proposed joint activity coding strategies are utilised by the visual system. For instance, in the direction of this study, it has been proposed that for the detection of stimulus onsets, the information from a large population of neurons should be pooled together (Pooled Population hypothesis) (Knight, 1972; van Vreeswijk and Sompolinsky, 1996; Gerstner, 2000). However, after the stimulus onset, i.e., stimulus change, coding strategies involving specific responses of single cells could be optimal for the estimation of the stimulus features (Labelled Line hypothesis). The combination of these two strategies has been proposed for cat's lateral geniculate neurons and fish's retinal ganglion cells (Wörgötter et al., 1999; Vasserman et al., 2010). Furthermore, coding strategies similar to the Pooled Population and the Labelled Line are found within the retina. Here, the rod system exhibits a greater degree of cell interconnection convergence in comparison to the cone system. Thereby, the pathway from rods to amacrine cells involve that several rods contact one rod bipolar cell and in turn, that several rod bipolar cells contact a given amacrine cell. This convergence (Pooled Population) makes the rod system a better detector of light at the expense of acuity. In contrast, and particularly in the fovea region, the one to one connection between cones, bipolar cells and RGC (Labelled Line) accounts for the high visual acuity at the expense of light sensitivity (Purves et al., 2001).

The proposals by Wörgötter et al. (1999) and Vasserman et al. (2010) are in accordance with the findings in this study. Here, it has been observed that the Pooled Population hypothesis, and to a lesser degree the Functional Group hypothesis, led to the highest performances for the discrimination of changes in the stimulus features. Nevertheless, the best estimation results for the stimulus features were yielded by the Labelled Line hypothesis, followed closely by the Functional group hypothesis. Again, as in the the definitions proposed by Theunissen and Miller (1995) and Lestienne (2001), the Pooled Population hypothesis and the Labelled Line hypothesis lie on

the extremes. Nevertheless, the Functional Group hypothesis shows to meet a compromise between both joint activity coding strategies. Here, it is also plausible that this strategy is utilised by the visual system. For instance, it has been found that at early stages of visual processing in mammals, cortical areas are retinotopically organized, where cells with similar functional properties are grouped together into functional streams. Moreover, it has also been observed that along the processing stages, there is a extensive interaction across these functional areas (Engel et al., 1992; Singer and Gray, 1995). Similar observations have been reported for the encoding of tactile stimulus in different cortical areas of primates (Nicolelis et al., 1998). In this direction, it has been found that for DSC in the turtle, there is a direct connection pathway to the the basal optic nucleus, which is the primary nucleus of the turtle accessory optic system (Rosenberg and Ariel, 1991).

The correlated activity of RGC is a suitable ensemble coding mechanism that was not tested in this study. The main reason for this is the multi electrode array utilised for the recordings of the extracellular activity for this study. Here, due to the distance between electrodes, it was very unlikely that the activity of neighbouring cells was registered. Nevertheless, correlations in the activity of neighbouring retinal ganglion cells have been reported in cats and monkeys (Mastronarde, 1989; Shlens et al., 2009). In turn, these correlations, appear to reflect the interaction of the neighbouring cells, and rather than introducing redundancy, it has been proposed that they provide additional sensory information to the visual circuits in the brain (Bair, 1999; Meister and Berry II, 1999; Pillow et al., 2008).

An important advantage of the ensemble coding over the population coding lies on the proposal that neurons could encode information about different stimulus features utilising different time scales. Here, the temporal patterns of the activity of single cells could be used as symbols. Therefore, if the temporal structure of single cells contributes individually to the encoding of information, more symbols will be available to encode different stimulus features for the ensemble coding (Theunissen and Miller, 1995; Victor and Purpura, 1998). In turn, this coding mechanism will help to minimise the number of necessary neurons for encoding tasks (Oram et al., 2002). In this direction, Kjaer et al. (1994) found that single complex cells from the V1 area of monkeys are not specialized for encoding information about one stimulus feature, but instead, they encode simultaneously information about different stimulus features. Moreover, they found that the joint activity of several cells allowed to enhance the encoded information about a single stimulus feature. Similar results were obtained in this study for both experimental protocols. Here, single neurons encoded information about a single stimulus

feature such as motion velocity or light intensity. However, the joint activity of the analysed RGC enhanced significantly the information about motion velocity or light intensity and particularly, the simultaneous encoding of both stimulus features.

In the last two sections of this chapter, the relevance of the information encoding mechanism tested in this study were discussed. In summary, based on the results obtained in this study and due to the integrative properties of the brain in space and time, as well as the chemical properties such as facilitation and depression (Samonds and Bonds, 2005), the spike firing rate, the latency, the interspike time interval and the spike timing, appear to be plausible coding strategies for retinal ganglion cells. Moreover, these response features could convey information about different aspects of a visual scene, enhancing in this way, the encoding efficiency. This assumption is reinforced by the fact that neurons are not specialised in conveying only one stimulus feature, but rather, they encode simultaneously information about several aspects of sensory stimuli Kjaer et al. (1994). In this direction, retinal ganglion cells could use a multiplexing mechanism based in different time scales to encode simultaneously these features. Here, the increasing complexity of the stimulus features to encode, would require the combination of encoding symbols from several retinal ganglion cells. In this sense, the three tested joint activity coding hypotheses tested in this study have been reported in different sensory systems including the visual system. Therefore, it is possible that turtle and fish retinal ganglion cells utilise these three joint activity coding strategies for the processing of visual motion and the simultaneous encoding of stimulus features. For instance, while a similar coding mechanism as the Pooled Population hypothesis could serve for the fast detection of changes in stimulus features, finer details of the stimulus could be encoded by a Labelled Line or Functional Group similar mechanism.

Chapter 5

Conclusions

Based on the results in this study, it can be stated that for turtle and carp, the processing of visual motion starts already in the retina. Moreover, the activity of carp retinal ganglion cells simultaneously encode information about about motion features and light intensities. The spike firing rate and the different time scales of the temporal structure of retinal ganglion cell responses encode information about constant motion features. However, the temporal structure gains relevance as coding mechanism when changes in the stimulus conditions are present. The combined activity of retinal ganglion cells allows to enhance the efficiency of visual information encoding. In turn, different interactions of the activity of retinal ganglion cells can for instance, allow to make fast discriminations of stimulus features changes or to obtain detailed information about a visual scene.

All together, it seems that while retinal ganglion cells are not specialised to encode one stimulus feature, they make use of different symbols, i.e., mechanisms, for the simultaneous encoding of several stimulus features. Furthermore, the efficiency of these symbols is boosted by the joint activity of these cells.

Bibliography

Abbott, L. F., 1994. Decoding neuronal firing and modelling neural networks. Quarterly Reviews of Biophysics Vol. 27 (Issue 3), [291–331].

Abeles, M., 1982. Role of the cortical neuron: Integrator or coincidence detector? Israel Journal of Medical Sciences Vol. 18 (Issue 1), [83–92].

Abeles, M., Prut, Y., 1996. Spatio-temporal firing patterns in the frontal cortex of behaving monkeys. Journal of Physiology-Paris Vol. 90 (Issues 3-4), [249–250].

Adrian, E. D., Matthews, R., September 1927. The action of light on the eye. part i. the discharge of impulses in the optic nerve and its relation to the electric changes in the retina. The Journal of Physiology Vol. 63 (Issue 4), [378–414].

Adrian, E. D., Matthews, R., June 1928. The action of light on the eye. part iii. the iteraction of retinal neurones. The Journal of Physiology Vol. 65 (Issue 3), [273–298].

Adrian, E. D., Zotterman, Y., April 1926a. The impulses produced by sensory nerve endings. part ii. the response of a sengle end-organ. The Journal of Physiology Vol. 61 (Issue 2), [151–171].

Adrian, E. D., Zotterman, Y., August 1926b. The impulses produced by sensory nerve endings. part iii. impulses set up by touch and pressure. The Journal of Physiology Vol. 61 (Issue 4), [465–483].

Ammermüller, J., Ithhaki, A., Weiler, R., I., P., May 1998. Uv-sensitive input to horizontal cells in the turtle retina. European Journal of Neuroscience Vol. 10 (Issue 5), [1544–1552].

Ammermüller, J., Kolb, H., 1995. The organization of the turtle inner retina. i. on- and off-center pathways. The Journal of Comparative Neurology Vol. 358 (Num. 1), [1–34].

Ammermüller, J., Kolb, H., 1996. Functional architecture of the turtle retina. Progress in Retinal and Eye Research Vol. 15 (Num. 2), [393–433].

Ammermüller, J., Muller, J. F., Kolb, H., 1995. The organization of the turtle inner retina. ii. analysis of color-coded and directionally selective cells. The Journal of Comparative Neurology Vol. 358 (Num. 1), [35–62].

Arabzadeh, E., Panzeri, S., Diamond, M. E., September 2006. Deciphering the spike train of a sensory neuron: Counts and temporal patterns in the rat whisker pathway. The Journal of Neuroscience Vol. 26 (Num. 36), [9216–9226].

Ariel, M., Adolph, A. R., November 1985. Neurotransmitter inputs to directionally sensitive turtle retinal ganglion cells. Journal of Neurophysiology Vol. 54 (Num. 5), [1123–1143].

Arkadir, D., Morris, G., Vaadia, E., Bergman, H., 2004. Independent coding of movement direction and reward prediction by single pallidal neurons. The Journal of Neuroscience Vol. 24 (Num. 45), [10047–10056].

Aronov, D., 2003. Fast algorithm for the metric-space analysis of simultaneous responses of multiple single neurons. Journal of Neuroscience Methods Vol. 124, [175–179].

Aronov, D., Reich, D. S., Mechler, F., Victor, J. D., June 2003. Neural coding of spatial phase in v1 of the macaque monkey. Journal of Neurophysiology Vol. 89 (Num. 6), [3304–3327].

Atick, J. J., Redlich, A. N., 1992. What does the retina know about natural scenes? Neural Computation Vol. 4 (Num. 2), [196–210].

Attneave, F., 1954. Some informational aspects of visual perception. Pshychological Review Vol. 61 (Num. 3), [183–193].

Averbeck, B. B., Lee, D., August 2003. Neural noise and movement-related codes in the macaque supplementary motor area. The Journal of Neuroscience Vol. 23 (Num. 20), [7630–7641].

Baccus, S. A., Ölveczky, B. P., Manu, M., Meister, M., July 2008. A retinal circuit that computes object motion. The Journal of Neuroscience Vol. 28 (Num. 27), [6807–6817].

Bair, W., 1999. Spike timing in the mammalian visual system. Current Opinion in Neurobiology Vol. 9 (Issue 4), [447–453].

Barlow, H. B., January 1953. Summation and inhibition in the frog's retina. The Journal of Physiology Vol. 119 (Issue 1), [69–88].

Barlow, H. B., 1961. Possible principles undelying the transformation of sensory messages. Sensory Communication Vol. 1, [217–234].

Barlow, H. B., Hill, R. M., February 1963. Selective sensitivity to direction of movement in ganglion cells of the rabbit retina. Science Vol. 139 (Num. 3553), [412–414].

Barlow, H. B., Hill, R. M., Levick, W. R., September 1964. Retinal ganglion cells responding selectively to direction and speed of image motion in the rabbit. The Journal of Physiology Vol. 173 (Issue 3), [377–407].

Berényi, A., Benedek, G., Nagy, A., October 2007. Double sliding-window technique: A new method to calculate the neuronal response onset latency. Brain Research Vol. 1178, [141–148].

Berry, M. J., Warland, D. K., Meister, M., May 1997. The structure and precision of retinal spike trains. Proceedings of the National Academy of Sciences of the United States of America Vol. 94 (Num. 10), [5411–5416].

Berry II, M. J., Brivanlou, I. H., Jordan, T. A., Meister, M., March 1999. Anticipation of moving stimuli by the retina. Nature Vol. 398 (Num. 6725), [334–338].

Bialek, W., Rieke, F., de Ruyter van Steveninck, R. R., Warland, D., June 1991. Reading a neural code. Science Vol. 252 (Num. 5014), [1854–1857].

Bizley, J. K., Walker, K. M. M., King, A. J., Schnupp, J. W. H., April 2010. Neural ensemble codes for stimulus periodicity in auditory cortex. The Journal of Neuroscience Vol. 30 (Num. 14), [5078–5091].

Blake, R., Sekuler, R., Grossman, E., July 2003. The Primate Visual System, 1st Edition. CRC Press, Ch. Motion Processing in Human Visual Cortex, pp. [311–345].

Bloomfield, A. S., September 1992. Relationship between receptive and dendritic field size of amacrine cells in the rabbit retina. Journal of Neurophysiology Vol. 68 (Num. 3), [711–725].

Borkholder, D. A., Bao, J., Maluf, N. I., Perl, E. R., Kovacs, G. T. A., November 1997. Microelectrode arrays for stimulation of neural slice preparations. Journal of Neuroscience Methods Vol. 77 (Issue 1), [61–66].

Borst, A., Theunissen, F. E., November 1999. Information theory and neural coding. Nature Neuroscience Vol. 2 (Num. 11), [947–957].

Boycott, B. B., Wässle, H., July 1974. The morphological types of retinal ganglion cells of the domestic cat's retina. The Journal of Physiology Vol. 240 (Issue 2), [397–419].

Bridge, P. D., Sawilowsky, S. S., March 1999. Increasing physicians' awareness of the impact of statistics on research outcomes: Comparative power of the t-test and wilcoxon rank-sum test in small samples applied research. Journal of Clinical Epidemiology Vol. 52 (Issue 3), [229–235].

Briggman, K. L., Helmstaedter, M., Denk, W., March 2011. Wiring specificity in the direction-selectivity circuit of the retina. Nature Vol. 471 (Issue 7337), [183–188].

Brown, P. K., George, W., October 1963. Visual pigments in human and monkey retinas. Nature Vol. 200 (Issue 4901), [37–43].

Brown, P. K., George, W., April 1964. Visual pigments in single rods and cones of the human retina. Science Vol. 144 (Num. 3614), [45–52].

Buck, L. B., November 2004. Olfactory receptors and odor coding in mammals. Nutrition Reviews Supplement Issue Vol. 62 (Issue S3), [S184–S188].

Cao, P., Gu, Y., Wang, S.-R., September 2004. Visual neurons in the pigeon brain encode the acceleration of stimulus motion. The Journal of Neuroscience Vol. 24 (Num. 35), [7690–7698].

Carmena, J. M., Lebedev, M. A., Crist, R. E., O'Doherty, J. E., Santucci, D. M., Dimitrov, D. F., Patil, P. G., Henriquez, C. S., Nicolelis, M. A. L., November 2003. Learning to control a brain-machine interface for reaching and grasping by primates. PLoS Biology Vol. 1 (Issue 2), [1–16].

Cerquera, A., Freund, J., 2011. Fast estimation of motion from selected populations of retinal ganglion cells. Biological Cybernetics Vol. 104, [53–64].

Cerquera, A. E., Greschner, M., Freund, J., October 2008. Classifying the motion of visual stimuli from the spike response of a population of retinal ganglion cells. Conference Proceedings of the International Conference of IEEE Engineering in Medicine and Biology Society Vol. 2008, [4082–4085].

Chapin, J. K., Moxon, K. A., Markowitz, R. S., Nicolelis, M. A. L., 1999. Real-time control of a robot arm using simultaneously recorded neurons in the motor cortex. Nature Neuroscience Vol. 2 (Num. 7), [664–670].

Chase, S. M., Young, E. D., April 2006. Spike-timing codes enhance the representation of multiple simultaneous sound-localization cues in the inferior colliculus. The Journal of Neuroscience Vol. 26 (Num. 15), [3889–3898].

Chase, S. M., Young, E. D., March 2007. First-spike latency information in single neurons increases when referenced to population onset. Proceedings of the National Academy of Sciences of the United States of America Vol. 104 (Num. 12), [5175–5180].

Chase, S. M., Young, E. D., April 2008. Cues for sound localization are encoded in multiple aspects of spike trains in the inferior colliculus. Journal of Neurophysiology Vol. 99 (Num. 4), [1672–1682].

Chicharro, D., Kreuz, T., Andrzejak, R. G., July 2011. What can spike train distances tell us about the neural code? Journal of Neuroscience Methods Vol. 199 (Issue 1), [146–165].

Chichilnisky, E. J., Kalmar, R. S., 2003. Temporal resolution of ensemble visual motion signals in primate retina. The Journal of Neuroscience Vol. 23 (Num. 17), [6681–6689].

Cohen, B., Matsuo, V., Raphan, T., September 1977. Quantitative analysis of the velocity characteristics of optokinetic nystagmus and optokinetic after-nystagmus. The Journal of Physiology Vol. 270 (Issue 2), [321–344].

Crowder, N. A., Lehmann, H., Parent, M. B., Wylie, D. R. W., August 2003. The accessory optic system contributes to the spatio-temporal tuning of motion-sensitive pretectal neurons. Journal of Neurophysiology Vol. 90 (Num. 2), [1140–1151].

Crowe, P. R., 1933. The analysis of rainfall probability. a graphical method and its application to european data. Scottish Geographical Magazine Vol. 49 (Num. 2), [73–91].

Dacheux, R. F., 1982. Connections of the small bipolar cells with the photoreceptors in the turtle. an electron microscope study of golgi-impregnated, gold-toned retinas. The Journal of Comparative Neurology Vol. 205, [55–62].

Dellen, B. K., Wessel, R., 2009. Encyclopedia of Neuroscience. Vol. Vol. 10. Oxford: Academic Press, Ch. Visual Motion Detection, pp. [291–295].

Dellen, B. K., Wessel, R., Clark, J. W., Wörgötter, F., 2010. Motion processing with wide-field neurons in the retino-tecto-rotundal pathway. Journal of Computaional Neuroscience Vol. 28 (Issue 1), [47–64].

Demb, J. B., Zaghloul, K., Peter, S., November 2001. Cellular basis for the response to second-order motion cues in y retinal ganglion cells. Neuron Vol. 32 (Issue 4), [711–721].

DeVries, S. H., December 2000. Bipolar cells use kainate and ampa receptors to filter visual information into separate channels. Neuron Vol. 28 (Issue 3), [847–856].

Di Lorenzo, P., Victor, J. D., September 2003. Taste response variability and temporal coding in the nucleus of the solitary tract of the rat. Journal of Neurophysiology Vol. 90 (Num. 3), [1418–1431].

Di Lorenzo, P. M., Chen, J.-Y., Victor, J. D., July 2009. Quality time: Representation of a multidimensional sensory domain through temporal coding. The Journal of Neuroscience Vol. 29 (Num. 29), [9227–9238].

Dodla, R., Wilson, C., February 2009. Asynchronous response of coupled pacemaker neurons. Physical Review Letters Vol. 102 (Issue 6), 068102.

Dong, C.-J., Werblin, F. S., April 1998. Temporal contrast enhancement via gabac feedback at bipolar terminals in the tiger salamander retina. Journal of Neurophysiology Vol. 79 (Num. 4), [2171–2180].

Dong, D. W., Atick, J. J., January 1995a. Temporal decorrelation: A theory of lagged and nonlagged responses in the lateral geniculate nucleus. Network: Computation in Neural Systems Vol. 6 (Num. 2), [159–178].

Dong, Dawei, W., Atick, J. J., January 1995b. Statics of natural time-varying images. Network: Computation in Neural Systems Vol. 6 (Num. 3), [345–358].

Dowling, J. E., 1987. The Retina: An Approachable Part of the Brain. Cambridge, MA: Harvard University Press.

Dowling, J. E., Ripps, H., 1970. Visual adaptation in the retina of the skate. The Journal of General Physiology Vol. 56, [491–520].

Du, Y., Lu, Q., Wang, R., September 2010. Using interspike intervals to quantify noise effects on spike trains in temperature encoding neurons. Cognitive Neurodynamics Vol. 4 (Num. 3), [199–206].

Eggermont, J. J., October 1998. Azimuth coding in primary auditory cortex of the cat. ii. relative latency and interspike interval representation. Journal of Neurophysiology Vol. 80 (Num. 4), [2151–2161].

Ellaway, P. H., August 1978. Cumulative sum technique and its application to the analysis of peristimulus time histograms. Electroencephalography and Clinical Neurophysiology Vol. 45 (Issue 2), [302–304].

Engel, A. K., König, P., Kreite, A. K., Shillen, T. B., Singer, W., June 1992. Temporal coding in the visual cortex: New vistas on integration in the nervous system. Trends in Neurosciences Vol. 15 (Issue 6), [218–226].

Engelmann, J., Gertz, S., Goulet, J., Schuh, A., von der Emde, G., October 2010. Coding of stimuli by ampullary afferents in gnathonemus petersii. Journal of Neurophysiology Vol. 104 (Num. 4), [1955–1968].

Enroth-Cugell, C., Robson, J. G., December 1966. The contrast sensitivity of retinal ganglion cells of the cat. The Journal of Physiology Vol. 187 (Issue 3), [517–522].

Falzett, M., Moore, R. K., Petry, H. M., Powers, M. K., November 1985. A method for determinig threshold from single-unit neural activity. Brain Research Vol. 347 (Issue 1), [127–131].

Famiglietti, E. V., June 1987. Starburst amacrine cells in cat retina are associated with bistratified, presumed directionally selective, ganglion cells. Brain Research Vol. 413 (Issue 2), [404–408].

Famiglietti, E. V., July 1991. Synaptic organization of starburst amacrine cells in rabbit retina: Analysis of serial thin sections by electron microscopy and graphic reconstruction. The Journal of Comparative Neurology Vol. 309 (Issue 1), [40–70].

Famiglietti Jr, E. V., Kaneko, A., Tachibana, M., December 1977. Neuronal architecture of on and off pathways to ganglion cells in carp retina. Science Vol. 198 (Num. 4323), [1267–1269].

Fernandez, E., Ferrandez, J. M., Ammermüller, J., Normann, R. A., 2000. Population coding in spike trains of simultaneously recorded retinal ganglion cells. Brain Research Vol. 887, [222–229].

Ferrandez, J. M., Bongard, M., Garcia de Quiros, F., Bolea, J. A., Fernandez, E., 2002. Neural coding analysis in retinal ganglion cells using information theory. Lecture Notes In Computer Science; Proceedings of the International Conference on Artificial Neural Networks Vol. 2415, [174–179].

Ferrández, J. M., Bolea, J. A., Ammermüller, J., Normann, R. A., Fernández, E., 1999. A neural network approach for the analysis of multineural

recordings in retinal ganglion cells. Lecture Notes in Computer Science Vol. 1607, [289–298].

Ferster, D., Spruston, N., November 1995. Cracking the neuronal code. Science Vol. 270 (Num. 5237), [756–757].

Field, D. J., December 1987. Relations between the statistics of natural images and the response properties of cortical cells. Journal of the Optical Society of America A Vol. 4 (Num. 12), [2379–2394].

Fontaine, B., Peremans, H., 2009. Bat echolocation processing using first-spike latency coding. Neural Networks Vol. 22 (Issue 10), [1372–1382].

Frechette, E. S., Sher, A., Grivich, M. I., Petrusca, D., Litke, A. M., Chichilnisky, E. J., December 2005. Fidelity of the ensemble code for visual motion in primate retina. Journal of Neurophysiology Vol. 94 (Num.), [119–135].

Gautrais, J., Thorpe, S. J., 1998. Rate coding versus temporal oder coding: A theoretical approach. BioSystems Vol. 48, [57–65].

Gawne, T. J., Kjaer, T. W., Richmond, B. J., August 1996. Latency: Another potential code for feature binding in striate cortex. Journal of Neurophysiology Vol. 76 (Num. 2), [1356–1360].

Georgopoulos, A. P., Schwartz, A. B., Ketiner, R. E., September 1986. Neuronal population coding of movement direction. Science Vol. 233 (Num. 4771), [1416–1419].

Gerstner, W., January 2000. Population dynamics of spiking neurons: Fast transients, asynchronous states, and locking. Neural Computation Vol. 12 (Issue 1), [43–89].

Gerstner, W., Kistler, W. M., August 2002. Spiking Neuron Models Single Neurons, Populations, Plasticity. Cambridge University Press.

Gollisch, T., February 2009. Throwing a glance at the neural code: Rapid information transmission in the visual system. HFSP Journal Vol. 3 (Num. 1), [36–46].

Gollisch, T., Meister, M., February 2008. Rapid neural coding in the retina with relative spike latencies. Science Vol. 319 (Num. 5866), [1108–1111].

Goulet, J., van Hemmen, J. L., Jung, S. N., Chagnaud, B. P., Scholze, B., Engelmann, J., May 2012. Temporal precision and reliability in the velocity regime of a hair-cell sensory system: The mechanosensory lateral line of goldfish, carassius auratus. Journal of Neurophysiology Vol. 107 (Num. 10), [2581–2593].

Granda, A. M., Fulbrook, J. E., 1989. Classification of turtle retinal ganglion cells. Journal of Neurophysiology Vol. 62 (Num. 3), [723–737].

Greschner, M., Bongard, M., Rujan, P., Ammermüller, J., 2002. Retinal ganglion cell synchronization by fixational eye movements improves feature estimation. Nature Neuroscience Vol. 5 (Num. 4), [341–347].

Greschner, M., Thiel, A., Kretzberg, J., Ammermüller, J., 2006. Complex spike-event pattern of transient on-off retinal ganglion cells. Journal of Neurophysiology Vol. 96 (Num. 6), [2845–2856].

Grewe, J., Kretzberg, J., Warzecha, A.-K., Egelhaaf, M., November 2003. Impact of photon noise on the reliability of a motion-sensitive neuron in the fly's visual system. The Journal of Neuroscience Vol. 23 (Num 34), [10776–10783].

Haas, J. S., Kreuz, T. K., Torcini, A., Politi, A., Abarbanel, H. D. I., December 2010. Rate maintenance and resonance in the entorhinal cortex. European Journal of Neuroscience Vol. 32 (Issue 11), [1930–1939].

Habermann, C. J., O'Brien, Brendan J., W. H., Protti, D. A., July 2003. Aii amacrine cells express l-type calcium channels at their output synapses. The Journal of Neuroscience Vol. 23 (Num. 17), [6904–6913].

Hartline, H. K., 1938. The response of single optic nerve fibers of the vertebrate eye to illumination of the retina. American Journal of Physioloy Vol. 121, [400–415].

Hartveit, E., 1999. Reciprocal synaptic interactions between rod bipolar cells and amacrine cells in the rat retina. Journal of Neurophysiology Vol. 81 (Num. 6), [2923–2936].

Hengstenberg, R., Sandeman, D. C., Hengstenberg, B., May 1986. Compensatory head roll in the blowfly calliphora during flight. Proceedings of the Royal Society of London. Series B, Biological Sciences Vol. 227 (Num. 1249), [455–482].

Hodgkin, A. L., Huxley, A. F., August 1952. A quantitative description of membrane current and its application to conduction and excitation in nerve. The Journal of Physiology Vol. 117 (Issue 4), [500–544].

Hollander, M., Wolfe, D. A., 1999. Nonparametric Statistical Methods, 2nd Edition. New York: John Wiley & Sons.

Hubel, D. H., Wiesel, T. N., December 1960. Receptive fields of optic nerve fibers in the spider monkey. The Journal of Physiology Vol. 154 (Issue 3), [572–580].

Hubel, D. H., Wiesel, T. N., January 1962. Receptive fields, binocular interaction and functional architecture in the cat's visual cortex. The Journal of Physiology Vol. 160 (Issue 1), [106–154].

Hubel, D. H., Wiesel, T. N., May 1977. Functional architecture of macaque monkey visual cortex. Proceedings of the Royal Society of London. Series B, Biological Sciences Vol. 198 (Num. 1130), [1–59].

Huetz, C., Del Negro, C., Lebas, N., Tarroux, P., Edeline, J.-M., August 2006. Contribution of spike timing to the information transmitted by hvc neurons. European Journal of Neuroscience Vol. 24 (Issue 4), [1091–1108].

Hunter, J. D., Milton, J. G., July 2003. Amplitude and frequency dependence of spike timing: Implications for dynamic regulation. Journal of Neurophysiology Vol. 90 (Num. 1), [387–394].

Jacobs, A. L., Fridman, G., Douglas, R. M., Alama, N. M., Latham, P. E., Prusky, G. T., Nirenberg, S., April 2009. Ruling out and ruling in neural codes. Proceedings of the National Academy of Sciences of the United States of America Vol. 106 (Num. 14), [5936–5941].

Johansson, R. S., Birznieks, I., February 2004. First spikes in ensembles of human tactile afferents code complex spatial fingertip events. Nature Neuroscience Vol. 7 (Num. 2), [170–177].

Junek, S., Kludt, E., Wolf, F., Schild, D., September 2010. Olfactory coding with patterns of response latencies. Neuron Vol. 67 (Issue 5), [872–884].

Kaneko, A., 1971. Physiological studies of single retinal cells and their morphological identification. Vision Research Vol. 11 (Supplement 3), [17–26].

Kaneko, A., 1979. Physiology of the retina. Annual Review of Neuroscience Vol. 2, [169–191].

Kaneko, A., Stuart, A. E., February 1984. Coupling between horizontal cells in the carp retina revealed by diffusion of lucifer yellow. Neuroscience Letters Vol. 47, [1–7].

Kara, P., Reinagel, P., Reid, R. C., September 2000. Low response variability in simultaneously recorded retinal, thalamic, and cortical neurons. Neuron Vol. 27 (Issue 3), [635–646].

Kersten, D., December 1987. Predicatability and redundancy of natural images. Journal of the Optical Society of America A Vol. 4 (Num. 12), [2395–2400].

Kjaer, T. W., Hertz, J. A., Richmond, B. J., 1994. Decoding cortical neuronal signals: Network models, information estimation and spatial tuning. Journal of Computational Neuroscience Vol. 1 (Num. 1-2), [109–139].

Knight, B. W., June 1972. The relationship between the firing rate of a single neuron and the level of activity in a population of neurons: Experimental evidence for resonant enhancement in the population response. The Journal of General Physiology Vol. 59 (Num. 6), [767–778].

Koch, K., McLean, J., Berry, M. J., Sterling, P., Balasubramanian, V., Freed, M. A., September 2004. Efficiency of information transmission by retinal ganglion cells. Current Biology Vol. 14 (Issue 17), [1523–1530].

Kolb, H., 1979. The inner plexiform layer in the retina of the cat: Electron microscopic observations. Journal of Neurocytology Vol. 8, [298–329].

Kolb, H., 1997. Amacrine cells of the mammalian retina: Neurocircuitry and functional roles. Eye Vol. 11, [904–923].

Kolb, H., January 2003. How the retina works. American Scientist Vol. 91, [28–35].

Kolb, H., Nelson, R., Marini, A., 1981. Amacrine cells, bipolar cells and ganglion cells of the cat retina: A golgi study. Vision Research Vol. 21, [1081–1114].

Kretschmer, V., Kretschmer, F., Ahlers, M. T., Ammermüller, J., 2012. High speed coding for velocity by archerfish retinal ganglion cells. BMC Neuroscience Vol. 13, Art. 69.

Kreuz, T., Haas, J. S., Morelli, A., Abarbanel, H. D. I., Politi, A., 2007. Measuring spike train synchrony. Journal of Neuroscience Methods Vol. 165, [151–161].

Kuffler, S. W., 1953. Discharge patterns and functional organization of mammalian retina. Journal of Neurophysiology Vol. 16 (Num. 1), [37–68].

Lamb, T. D., Collin, S. P., Pugh Jr., E. N., December 2007. Evolution of the vertebrate eye: Opsins, photoreceptors, retina and eye cup. Nature Reviews Neuroscience Vol. 8 (Num. 12), [960–976].

Lamb, T. D., Pugh Jr., E. N., May 2004. Dark adaptation and the retinoid cycle of vision. Progress in Retinal and Eye Research Vol. 23 (Issue 3), [307–380].

Land, M. F., Collet, T. S., December 1974. Chasing behaviour of houseflies (*Fannia canicularis*): A description and analysis. Journal of Comparative Physiology A: Neuroethology, sensory, Neural, and Behavioral Physiology Vol. 89 (Num. 4), [331–357].

Lapicque, L. M., 1907. Recherches quantitatives sur l'excitation électrique des nerfs traitée comme une polarization. Journal de Physiologie et de Pathologie Générale Vol. 9, [620–635].

Larson, J., Wong, D., Lynch, G., March 1986. Patterned stimulation at the theta frequency is optimal for the induction of hippocampal long-term potentiation. Brain Research Vol. 368 (Issue 2), [347–350].

Laughlin, S., September-October 1981. A simple coding procedure enhances a neuron's information capacity. Zeitschrift für Naturforschung. Section C: Bioscences Vol. 36 c (Num. 9-10), [910–912].

Laughlin, S. B., January 1999. Visual motion: Dendritic integration makes sense of the world. Current Biology Vol. 9 (Num. 1), [R15–R17].

Leibovic, K. N., 1990. Science of Vision. Springer-Verlag.

Lemon, C. H., Katz, D. B., September 2007. The neural processing of taste. BMC Neuroscience Vol. 8 (Supplement 3), S5.

Lestienne, R., 2001. Spike timing, synchronization and information processing on the sensory side of the central nervous system. Progress in Neurobiology Vol. 65, [545–591].

Lestienne, R., Strehler, B. L., December 1987. Time structure and stimulus dependence of precisely replicating patterns in monkey cortical neuronal spike trains. Brain Research Vol. 437 (Issue 2), [214–238].

Lestienne, R., Strehler, B. L., 1988. Differences between monkey visual cortex cells in triplet and ghost doublet informational symbols relationships. Biological Cybernetics Vol. 59 (Num. 4-5), [337–352].

Levick, W. R., April 1973. Variation in the response latency of cat retinal ganglion cells. Vision Research Vol. 13 (Issue 4), [837–853].

Lewen, G. D., Bialek, W., de Ruyter van Steveninck, R. R., 2001. Neural coding of naturalistic motion stimuli. Network: Computation in Neural Systems Vol. 12, [317–329].

Lisberger, S. G., Movshon, J. A., March 1999. Visual motion analysis for pursuit eye movements in area mt of macaque monkeys. The Journal of Neuroscience Vol. 19 (Num. 6), [2224–2246].

Lorente de Nó, R., September 1939. Transmission of impulses through cranial motor neuclei. Journal of Neurophysiology Vol. 2 (Num. 5), [402–464].

Machens, C. K., Schuetze, H., Franz, A., Kolesnikova, O., Stemmler, M. B., Ronacher, A., Herz, A. V. M., April 2003. Single auditory neurons rapidly discriminate conspecific communication signals. Nature Neuroscience Vol. 6 (Num. 4), [341–342].

MacKay, D. M., McCulloch, Warren, S., 1952. The limiting information capacity of neuronal link. Bulletin of Mathematical Biophysics Vol. 14 (Num. 2), [127–135].

Marks, W. B., May 1965. Visual pigments of single goldfish cones. The Journal of Physiology Vol. 178 (Issue 1), [14–32.1].

Marks, W. B., Dobelle, W. H., MacNichol Jr., E. F., March 1964. Visual pigments of single primate cones. Science Vol. 143 (Num. 3611), [1181–1182].

Mastronarde, D. N., 1989. Correlated firing of retinal ganglion cells. Trends in Neuroscience Vol. 12 (Issue 2), [75–80].

Mechler, F., Reich, D. S., Victor, J. D., July 2002. Detection and discrimination of relative spatial phase by v1 neurons. The Journal of Neuroscience Vol. 22 (Num. 14), [6129–6157].

Mechler, F., Victor, J. D., Purpura, K. P., Shapley, R., August 1998. Robust temporal coding of contrast by v1 neurons for transient but not for steady-state stimuli. The Journal of Neuroscience Vol. 18 (Num. 16), [6583–6598].

Meister, M., Berry II, M. J., March 1999. The neural code of the retina. Neuron Vol. 22 (Issue 3), [435–450].

Meister, M., Pine, J., Baylor, D. A., January 1994. Multi-neuronal signals from the retina: Acquisition and analysis. Journal of Neuroscience Methods Vol. 51 (Issue 1), [95–106].

Middlebrooks, J. C., Clock, A. E., Xu, L., Green, D. M., May 1994. A panoramic code for sound location by cortical neurons. Science Vol. 264 (Num. 5160), [842–844].

Miles, L. K., Katarzyna, K., Lumsden, J., Macrae, C. N., May 2010. The meandering mind: Vection and mental time travel. PLoS ONE Vol. 5 (Issue 5), e10825.

Müller, J., 1826. Zur vergleichenden Physiologie des Gesichtssinnes des Menschen und der Thiere: nebst einem Versuch über die Bewegungen der Augen und über den menschlichen Blick. C. Cnobloch.

Nelson, R., Famiglietti, E. V., Kolb, H., March 1978. Intracellular staining reveals different levels of stratification for on- and off-center ganglion cells in cat retina. Journal of Neurophysiology Vol. 41 (Num. 2), [472–483].

Nicolelis, M. A. L., Ghazanfar, A. A., Stambaugh, C. R., Oliveira, L. M. O., Laubach, M., Chapin, J. K., Nelson, R. J., Kaas, J. H., November 1998. Simultaneous encoding of tactile information by three primate cortical areas. Nature Neuroscience Vol. 1 (Num. 7), [621–630].

Nirenberg, S., Carcieri, S. M., Jacobs, A. L., Latham, P. E., June 2001. Retinal ganglion cells act largely as independent encoders. Nature Vol. 411 (Issue 6838), [698–701].

Nordhausen, C. T., Maynard, E. M., Normann, R. A., July 1996. Single unit recording capabilities of a 100 microelectrode array. Brain Research Vol. 726 (Issue 1-2), [129–140].

Norrsell, U., Finger, S., Lajonchere, C., March 1999. Cutaneous sensory spots and the "law of specific nerve energies": History and development of ideas. Brain Research Bulletin Vol. 48 (Issue 5), [457–465].

O'Keefe, J., Recce, M. L., July 1993. Phase relationship between hippocampal place units and the eeg theta rhythm. Hippocampus Vol. 3 (Num. 3), [317–330].

Optican, L. M., Richmond, B., January 1987. Temporal encoding of two-dimensional patterns by single units in primate inferior temporal cortex. iii. information theoretic analysis. Journal of Neurophysiology Vol. 57 (Num. 1), [162–178].

Oram, M. W., Xiao, D., Dritschel, B., Payne, K. R., August 2002. The temporal resolution of neural codes: Does response latency have a unique role? Philosophhical Transactions of The Royal Society of London Series B-Biological Sciences Vol. 357 (Num. 1424), [987–1001].

Oyster, C. W., Takahashi, E., Collewijn, H., February 1972. Direction-selective retinal ganglion cells and control of optokinetic nystagmus in the rabbit. Vision Research Vol. 12 (Issue 2), [183–193].

Oyster, C. W., Takahashi, E. S., Hurst, D. C., December 1981. Density, soma size and regional distribution of rabbit retinal ganglion cells. The Journal of Neuroscience Vol. 1 (Num. 12), [1331–1346].

Paiva, A. R. C., Park, I., Príncipe, J. C., April 2010. A comparison of binless spike train measures. Neural Computing and Applications Vol. 19 (Issue 3), [405–419].

Peichl, L., Wässle, H., August 1983. The structural correlate of the receptive field centre of α ganglion cells in the cat retina. The Journal of Physiology Vol. 341 (Issue 1), [309–324].

Perkel, D. H., Gerstein, G. L., Moore, G. P., July 1967. Neuronal spike trains and stochastic point processes i. the single spike train. Biophysical Journal Vol. 7 (Issue 4), [391–418].

Pillow, J. W., Paninski, L., Uzzell, V. J., Simoncelli, E. P., Chichilnisky, E. J., November 2005. Prediction and decoding of retinal ganglion cell responses with a probabilistic spiking model. The Journal of Neuroscience Vol. 25 (Num. 47), [11003–11013].

Pillow, J. W., Shlens, J., Paninski, L., Sher, A., Litke, A. M., Chichilnisky, E. J., P, S. E., August 2008. Spatio-temporal correlations and visual signalling in a complete neuronal population. Nature Vol. 454 (Issue 7207), [995–999].

Polyak, S. L., 1941. The Retina. University of Chicago Press.

Prothero, J. D., Hoffman, H. G., Parker, D. E., Furness, T. A., Wells, M. J., 1995. Foreground/background manipulations affect presence. In: Proceedings of Human Factors and Ergonomics Society.

Puchalla, J. L., Schneidman, E., Harris, R. A., Berry, M. J., May 2005. Redundancy in the population code of the retina. Neuron Vol. 46 (Issue 3), [493–504].

Purves, D., Augustine, G. J., Fitzpatrick, D., Katz, L. C., LaMantia, A.-S., McNamara, J. O., Williams, S. M. (Eds.), 2001. Neuroscience, 2nd Edition. Sinauer Associates.

Ramón y Cajal, S., 1892. The Structure of the Retina. Charles C. Thomas.

Ramón y Cajal, S., 1894. Die Retina der Wirbel Thiere: Untersuchungen mit der Golgi-Cajal'schen Chromsilbermethode und der Ehrlich'schen Methylenblaufärbung. Bergmann.

Reich, D. S., Mechler, F., Victor, J. D., January 2001a. Formal and attribute-specific information in primary visual cortex. Journal of Neurophysiology Vol. 85 (Num. 1), [305–318].

Reich, S. D., Mechler, F., Victor, J. D., 2001b. Temporal coding of contrast in primary visual cortex: When, what, and why. Journal of Neurophysiology Vol. 85 (Num.), [1039–1050].

Reuter, T., November 2011. Fifty years of dark adaptation 1961-2011. Vision Research Volume 51 (Issue 21-22), [2243–2262].

Reyes, A. D., June 2003. Synchrony-dependent propagation of firing rate in iteratively constucted networks in vitro. Nature Neuroscience Vol. 6 (Num. 6), [593–599].

Richmond, B., Optican, L. M., Podell, M., Spitzer, H., January 1987. Temporal encoding of two-dimensional patterns by single units in primate inferior temporal cortex. i. response characteristics. Journal of Neurophysiology Vol. 57 (Num. 1), [132–146].

Richmond, B., Optican, L. M., Spitzer, H., August 1990. Temporal encoding of two-dimensional patterns by single units in primate primary visual cortex. i. stimulus-response relations. Journal of Neurophysiology Vol. 64 (Num. 2), [351–369].

Rieke, F., Warland, D., de Ruyter van Steveninck, R. R., Bialek, W., 1999. Spikes Exploring the Neural Code. The MIT Press.

Ripps, H., Dowling, J. E., 1990. Structural features and adaptive properties of photoreceptors in the skate retina. The Journal of Experimental Zoology

Supplement: Vision in Elasmobranchs: A Comparative and Ecological Perspective Vol. 256 (Issue S5), [46–54].

Rosenberg, A. F., Ariel, M., May 1991. Electrophysiological evidence for a direct projection of direction-sensitive retinal ganglion cells to the turtle's accessory optic system. Journal of Neurophysiology Vol. 65 (Num. 5), [1022–1033].

Roska, B., Werblin, F. S., June 2003. Rapid global shifts in natural scenes block spiking in specific ganglion cell types. Nature Neuroscience Vol. 6 (Num. 6), [600–608].

Roussin, A. T., Victor, J. D., Chen, J.-Y., Di Lorenzo, P. M., February 2008. Variability in responses and temporal coding of tastants of similar quality in the nucleus of the solitary tract of the rat. Journal of Neurophysiology Vol. 99 (Num. 2), [644–655].

Ruderman, D. L., 1994. The statistics of natural images. Network: Computation in Neural Systems Vol. 5 (Num. 4), [517–548].

Ruderman, D. L., Cronin, T. W., Chiao, C.-C., August 1998. Statistics of cone responses to natural images: Implications for visual coding. Journal of the Optical Society of America A Vol. 15 (Num. 8), [2036–2045].

Saal, H. P., Vijayakumar, S., Johansson, R. S., June 2009. Information about complex fingertip parameters in individual human tactile afferent neurons. The Journal of Neuroscience Vol. 29 (Num. 25), [8022–8031].

Sachsa, A. J., Khayata, P. S., Niebergalla, R., Martínez-Trujillo, J., January 2011. A metric-based analysis of the contribution of spike timing to contrast and motion direction coding by single neurons in macaque area mt. Brain Research Vol. 1368, [163–184].

Samonds, J. M., Allison, J. D., Brown, H. A., Bonds, A. B., March 2003. Cooperation between area 17 neuron pairs enhances fine discrimination of orientation. The Journal of Neuroscience Vol. 23 (Num. 6), [2416–2425].

Samonds, J. M., Bonds, A. B., November 2004. From another angle: Differences in cortical coding between fine and coarse discrimination of orientation. Journal of Neurophysiology Vol. 91 (Num.), [1193–1202].

Samonds, J. M., Bonds, A. B., November 2005. Cooperative and temporally structured information in the visual cortex. Signal Processing Vol. 85 (Issue 11), [2124–2136].

Savur, S. R., June 1937. Use of the median in tests of significance. Proceedings of the Indian Academy of Sciences, Section A Vol. 5, [564–576].

Schiller, P. H., October 2010. Parallel information processing channels created in the retina. Proceedings of the National Academy of Sciences of the United States of America Vol. 107 (Num. 40), [17087–17094].

Schreiber, S., Fellous, J. M., Whitmer, D., Tiesinga, P. H. E., Sejnowski, T. J., 2003. A new correlation-based measure of spike timing reliability. Neurocomputing Vol. 52 (Num. 54), [925–931].

Segev, R., Goodhouse, J., Puchalla, J., Berry II, M. J., October 2004. Recording spikes from a large fraction of the ganglion cells in a retinal patch. Nature Neuroscience Vol. 7 (Num. 10), [1155–1162].

Segev, R., Schneidman, E., Goodhouse, J., Berry II, M. J., September 2007. Role of eye movements in the retinal code for a size discrimination task. Journal of Neurophysiology Vol. 98 (Num 3), [1380–1391].

Sestokas, A. K., Lehmkuhle, S., Kratz, K. E., 1991. Relationship between response latency and amplitude for ganglion and geniculate x- and y-cells in the cat. International Journal of Neuroscience Vol. 60 (Num. 1), [59–64].

Shadlen, M. N., Newsome, W. T., August 1994. Noise, neural codes and cortical organization. Current Opinion in Neurobiology Vol. 4 (Issue 4), [569–579].

Shadlen, M. N., Newsome, W. T., April 1995. Is there a signal in the noise? Current Opinion in Neurobiology Vol. 5 (Issue 2), [248–250].

Shenoy, P., Rao, R. P. N., 2004. Dynamic bayesian networks for brain-computer interfaces. Advances in Neural Information Processing Systems Vol. 17, [1–8].

Shlens, J., Fled, G. D., Gauthier, J. L., Greschner, M., Sher, A., Litke, A. M., Chichilnisky, E. J., April 2009. The structure of large-scale synchronized firing in primate retina. The Journal of Neuroscience Vol. 29 (Num. 15), [5022–5031].

Simoncelli, E. P., Olshausen, B. A., 2001. Natural image statistics and neural representation. Annual Review of Neuroscience Vol. 24, [1193–1216].

Singer, W., Gray, C. M., March 1995. Visual feature integration and the temporal correlation hypothesis. Annual Review of Neuroscience Vol. 18, [555–586].

Softky, W., January 1994. Sub-millisecond coincidence detection in active dendritic trees. Neuroscience Vol. 58 (Issue 1), [13–41].

Softky, W. A., Koch, C., January 1993. The highly irregular firing of cortical cells is inconsistent with temporal integration of random epsps. The Journal of Neuroscience Vol. 13 (Num. 1), [334–350].

Softky, W. R., April 1995. Simple codes versus efficient codes. Current Opinion in Neurobiology Vol. 5 (Issue 2), [239–247].

Srinivasan, M. V., Laughlin, S. B., Dubs, A., November 1982. Predictive coding: A fresh view of ihnhibitionin the retina. Proceedings of the Royal Society of London. Series B, Biological Sciences Vol. 216 (Num. 1205), [427–459].

Stell, W. K., Lightfoot, D. O., 1975. Color-specific interconnections of cones and horizontal cells in the retina of the goldfish. The Journal of Comparative Neurology Vol. 159 (Issue 4), [473–502].

Stone, J., Fabian, M., May 1966. Specialized receptive fields of the cat's retina. Science Vol. 152 (Num. 726), [1277–1279].

Stone, J., Fukuda, Y., July 1974. Properties of cat retinal ganglion cells: A comparison of w-cells with x- and y-cells. Journal of Neurophysiology Vol. 37 (Num. 4), [722–748].

Stone, J., Hoffman, K.-P., August 1972. Very slow-conducting ganglion cells in the cat's retina: a major, new functional type? Brain Research Vol. 43 (Issue 2), [610–616].

Stoppini, L., Duport, S., Corrèges, P., March 1997. A new extracellular multirecording system for electrophysiological studies: Application to hippocampal organotypic cultures. Journal of Neuroscience Methods Vol. 72 (Issue 1), [23–33].

Strehler, B. L., 1969. Information handling in the nervous system: An analogy to molecular-genetic coder-decoder mechanisms. Perspectives in Biology and Medicine Vol. 12 (Num. 4), [584–612].

Strehler, B. L., Lestienne, R., December 1986. Evidence on precise time-coded symbols and memory patterns in monkey cortical neuronal spike trains. Proceedings of the National Academy of Sciences of the United States of America Vol. 83 (Num. 24), [9812–9816].

Svaetichin, G., MacNichol Jr., E. F., November 1959. Retinal mechanisims for chromatic and achromatic vision. Annals of the New York Academy of Sciences Vol. 74 (Issue 2), [385–404].

Tachibana, M., Kaneko, A., 1988. Retinal bipolar cells receive negative feedback input from gabergic amacrine cells. Visual Neuroscience Vol. 1, [297–305].

Taylor, W. R., Vaney, D. I., July 2003. New directions in retinal research. Trends in Neurosciences Vol. 26 (Num. 7), [379–385].

Theunissen, F., Miller, J. P., June 1995. Temporal encoding in nervous systems: A rigorous definition. Journal of Computational Neuroscience Vol. 2 (Num. 2), [149–162].

Thiel, A., Greschner, M., Ammermüller, J, 2006. The temporal structure of transient on/off ganglion cell responses and its relation to intra-retinal processing. Journal of Computational Neuroscience Vol. 21, [131–151].

Thiel, A., Greschner, M., Eurich, C. W., Ammermüller, J., Kretzberg, J., 2007. Contribution of individual retinal ganglion cell responses to velocity an acceleration encoding. Journal of Neurophysiology Vol. 98 (Num. 4), [2285–2296].

Thomson, E. E., Kristan, W. B., July 2006. Encoding and decoding touch location in the leech cns. The Journal of Neuroscience Vol. 26 (Num. 30), [8009–8016].

Thorpe, S. J., 1990. Parallel Processing in Neural Systems and Computers. Elsevier science Publishers B.V. (North-Holland), Ch. Spike Arrival Times: A highly Efficient Coding Scheme For Neural Networks, pp. [91–94].

Thorpe, S. J., Delorme, A., Van Rullen, R., 2001. Spike-based satrategies for rapid processing. Neural Networks Vol. 14, [715–725].

Thorpe, S. J., Fize, D., Marlot, C., June 1996. Speed of processing in the human visual system. Nature Vol. 381 (Issue 6582), [520–520].

Thorpe, S. J., Imbert, M., 1989. Connectionism in Perspective. North-Holland, Ch. Biological Constraints on Connectionist Modelling, pp. [63–92].

Tomita, T., Kaneko, A., Murakami, M., Pautler, E. L., 1967. Spectral response curves of single cones in the carp. Vision Research Vol. 7, [519–531].

Tovee, M. J., T, R. E., adn Bellis R P, T. A., August 1993. Information encoding and the responses of single neurons in the primate temporal visual cortex. Journal of Neurophysiology Vol. 70 (Num. 2), [640–654].

Tsvilling, V., Donchin, O., Shamir, M., Segev, R., February 2012. Archer fish fast hunting maneuver may be guided by directionally selective retinal ganglion cells. European Journal of Neuroscience Vol. 35 (Issue 3), [436–444].

Twig, G., Levy, H., Perlman, I., January 2003. Color opponency in horizontal cells of the vertebrate retina. Progress in Retinal and Eye Research Vol. 22 (Issue 1), [31–68].

Uzzell, V. J., Chichilnisky, E. J., August 2004. Precision of spike trains in primate retinal ganglion cells. Journal of Neurophysiology Vol. 92 (Num. 2), [780–789].

van Rossum, M. C. W., April 2001. A novel spike distance. Neural Computation Vol. 13 (Issue 4), [751–763].

van Rossum, M. C. W., Turrigiano, Gina G.and Nelson, S. B., March 2002. Fast propagation of firing rates through layered networks of noisy neurons. The Journal of Neuroscience Vol. 22 (Num. 5), [1956–1966].

Van Rullen, R., Guyonneau, R., Thorpe, S. J., 2005. Spike times make sense. Trends in Neurosciences Vol. 28 (Num. 1), [1–4].

Van Rullen, R., Thorpe, S. J., 2001. Rate coding versus temporal order coding: What the retinal ganglion cells tell the visual cortex. Neural Computation Vol. 13, [1255–1283].

van Vreeswijk, C., Sompolinsky, H., December 1996. Chaos in neuronal networks with balanced excitatory and inhibitory activity. Science Vol. 274 (Num. 5293), [1724–1726].

Vaney, D. I., Young, H. M., January 1988. Gaba-like immunoreactivity in cholinergic amacrine cells of the rabbit retina. Brain Research Vol. 438 (Issue 1-2), [369–373].

Vasserman, G., Shamir, M., Ben Simon, A., Segev, R., November 2010. Coding what and when in the archer fish retina. PLoS Computational Biology Vol. 6 (Issue 11), e1000977.

Victor, J. D., 1999. Temporal aspects of neural coding in the retina and lateral geniculate. Network: Computation in Neural Systems 10 (Num. 4), [1–66].

Victor, J. D., December 2000. How the brain uses time to represent and process visual information. Brain Research Vol. 886 (Issues 1-2), [33–46].

Victor, J. D., 2002. Binless strategies for estimation of information from neural data. Physical Review E Vol. 66 (Num. 5), [1–15].

Victor, J. D., 2005. Spike train metrics. Current Opinion in Neurobiology Vol. 15, [585–592].

Victor, J. D., Purpura, K. P., August 1996. Nature and precision of temporal coding in visual cortex: A metric-space analysis. Journal of Neurophysiology Vol. 76 (Num. 2), [1310–1326].

Victor, J. D., Purpura, K. P., 1997. Metric-space analysis of spike trains: Theory, algorithms and application. Network: Computation in Neural Systems Vol. 8, [127–164].

Victor, J. D., Purpura, K. P., August 1998. Spatial phase and the temporal structure of the response to gratings in v1. Journal of Neurophysiology Vol. 80 (Num. 2), [554–571].

Victor, J. D., Purpura, K. P., 2010. Analysis of Parallel Spike Trains. Springer Series in Computational Neuroscience 7. Springer Science Business Media, Ch. Spike Metrics, pp. [129–156].

von Békésy, G., Wever, E. G., 1960. Experiments in Hearing. McGraw-Hill.

von Helmholtz, H. L. F., 1863. Die Lehre von den Tonempfindungen als physiologische Grundlage für die Theorie der Musik. F. Vieweg und Sohn.

Warland, D. K., Reinagel, P., Meister, M., November 1997. Decoding visual information from a population of retinal ganglion cells. Journal of Neurophysiology Vol. 78 (Num. 5), [2336–2350].

Wilcoxon, F., December 1945. Individual comparisons by ranking methods. Biometrics Bulletin Vol. 1 (Num. 6), [80–83].

Wilke, S. D., Thiel, A., Greschner, M., Bongard, M., Ammermüller, J., Schwegler, H., 2001. Population coding of motion patterns in the early visual system. Journal of Comparative Physiology Vol. 187, [549–558].

Wörgötter, F., Suder, K., Funke, K., 1999. The dynamic spatio-temporal behavior of visual responses in thalamus and cortex. Restorative Neurology and Neuroscience Vol. 15 (Num. 2-3), [137–152].

Wässle, H., October 2004. Parallel processing in the mammalian retina. Nature Neuroscience Vol. 5, [1–11].

Yamasaki, D. S., Wurtz, R. H., September 1991. Recovery of function after lesions in the superiro temporal sulcus in the monkey. Journal of Neurophysiology Vol. 66 (Num. 3), [651–673].

Ying, D., Qi-Shao, L., February 2010. Noise effects on temperature encoding of neuronal spike trains in a cold receptor. Chinese Physics Letters Vol. 27 (Num. 2), 020503.

Ying, D., Qi-Shao, L., Wang, R., 2010. Using interspike intervals to quantify noise effects on spike trains in temperature encoding neurons. Cognitive Neurodynamics Vol. 4 (Num. 3), [199–206].

Zhang, K., Ginzburg, I., McNaughton, B. L., Sejnowski, T. J., 1998. Interpreting neuronal population activity by reconstruction: Unified framework with application to hippocampal place cells. Journal of Neurophysiology Vol. 79 (Num.), [1017–1044].

Zhou, Z. J., Fain, G. L., July 1996. Starburst amacrine cells change from spiking to nonspiking neurons during retinal revelopment. Proceedings of the National Academy of Sciences of the United States of America Vol. 93 (Num. 15), [8057–8062].

Zohar, O., Shackleton, T. M., Nelken, I., Palmer, A. R., Shamir, M., June 2011. First spike latency code for interaural phase difference discrimination in the guinea pig inferior colliculus. The Journal of Neuroscience Vol. 31 (Num. 25), [9192–9204].

Appendix

Time interval	Animal	Metrics	Left-DSC	Non-DSC	Right-DSC
0-200 ms	Turtle	Cost-based	23% $1/q=\infty$	19.8% $1/q=125$ms	19.2% $1/q=\infty$
		ISI	24.6%	20.8%	18.6%
	Fish	Cost-based	17.3% $1/q=\infty$	14.1% $1/q=1000$ms	14% $1/q=\infty$
		ISI	17.8%	14.7%	13.7%
0-500 ms	Turtle	Cost-based	28.5% $1/q=\infty$	23.8% $1/q=\infty$	23% $1/q=\infty$
		ISI	26.4%	24.3%	19.3%
	Fish	Cost-based	23.5% $1/q=\infty$	17.1% $1/q=500$ms	15.8% $1/q=\infty$
		ISI	19.1%	14.6%	13.3%
300-500 ms	Turtle	Cost-based	21.3% $1/q=500$ms	19.3% $1/q=\infty$	18% $1/q=125$ms
		ISI	24.5%	22.2%	18.3%
	Fish	Cost-based	19.5% $1/q=1000$ms	15.3% $1/q=250$ms	14.2% $1/q=250$ms
		ISI	19.9%	14.3%	13.7%

Table 5.1: Highest median of estimation results for the motion velocity of the moving stimulus, obtained by applying spike cost-based metrics and ISI metrics on the activity of single RGC within the three tested time intervals.

STIMULUS FEATURE	TIME INTERVAL	METRICS	LEFT-DSC	NON-DSC	RIGHT-DSC
0-200 ms	Turtle	Cost-based	39.1% $1/q=$ 250ms	38.7% $1/q=$ 250ms	39.2% $1/q=\infty$
		ISI	42.8%	37.7%	40.5%
	Fish	Cost-based	45.9% $1/q=$ 125ms	41% $1/q=$ 125ms	46.5% $1/q=$125ms
		ISI	45.6%	36%	33.6%
0-500 ms	Turtle	Cost-based	48.2% $1/q=$1000ms	44.2% $1/q=\infty$	50.7% $1/q=$1000ms
		ISI	45.3%	41.7%	41%
	Fish	Cost-based	42.7% $1/q=\infty$	34.7% $1/q=$500ms	42.1% $1/q=$1000ms
		ISI	45.9%	34.9%	35.5%
300-500 ms	Turtle	Cost-based	37.3% $1/q=\infty$	32.3% $1/q=\infty$	35.9% $1/q=$250ms
		ISI	44.9%	40.5%	41.6%
	Fish	Cost-based	43.9% $1/q=$250ms	25.8% $1/q=\infty$	29.7% $1/q=\infty$
		ISI	46.8%	36.3%	37.7%

Table 5.2: Highest median of estimation results for the motion direction of the moving stimulus, obtained by applying spike cost-based metrics and ISI metrics on the activity of single RGC within the three tested time intervals.

STIMULUS FEATURE	TIME INTERVAL	METRICS	LEFT-DSC	NON-DSC	RIGHT-DSC
0-200 ms	Turtle	Cost-based	0.82 $1/q$=500ms	0.82 $1/q$=∞	0.91 $1/q$=∞
		ISI	0.87	0.87	0.95
	Fish	Cost-based	1.01 $1/q$=∞	1.01 $1/q$=125ms	0.9 $1/q$=125ms
		ISI	0.96	1.01	1.14
0-500 ms	Turtle	Cost-based	0.65 $1/q$=∞	0.6 $1/q$=∞	0.84 $1/q$=∞
		ISI	0.81	0.73	0.93
	Fish	Cost-based	0.7 $1/q$=∞	1.03 $1/q$=1000ms	1.09 $1/q$=500ms
		ISI	0.82	1.01	1.12
300-500 ms	Turtle	Cost-based	1.03 $1/q$=1000ms	0.92 $1/q$=∞	1.04 $1/q$=∞
		ISI	0.87	0.81	0.91
	Fish	Cost-based	% $1/q$=125ms	% $1/q$=250ms	% $1/q$=∞
		ISI	0.72	1.02	1.08

Table 5.3: Lowest median of absolute normalised estimation errors for the motion speed of the moving stimulus, obtained by applying spike cost-based metrics and ISI metrics on the activity of single RGC within the three tested time intervals.

STIMULUS FEATURE	TIME INTERVAL	METRICS	LEFT-DSC	NON-DSC	RIGHT-DSC
0-200 ms	Turtle	Cost-based	5.5% $1/q$=62ms	5.4% $1/q$=62ms	4.5% $1/q$=31ms
		ISI	8.1%	6.8%	5.5%
	Fish	Cost-based	3.5% $1/q$=125ms	2.5% $1/q$=62ms	2.3% $1/q$=125ms
		ISI	5.6%	2.3%	2.6%
0-500 ms	Turtle	Cost-based	7.3% $1/q$=125ms	6.8% $1/q$=125ms	5.1% $1/q$=125ms
		ISI	10.1%	7.3%	5.4%
	Fish	Cost-based	5.9% $1/q$=125ms	3.3% $1/q$=125ms	4.4% $1/q$=125ms
		ISI	6.7%	2.9%	2.9%
300-500 ms	Turtle	Cost-based	3.9% $1/q$=62ms	3.4% $1/q$=62ms	2.9% $1/q$=62ms
		ISI	5.9%	5.3%	4.1%
	Fish	Cost-based	3.5% $1/q$=62ms	2.2% $1/q$=250ms	2% $1/q$=125ms
		ISI	4.6%	2.2%	2.8%

Table 5.4: Highest median of estimation results for the instantaneous velocity changes of the moving stimulus, obtained by applying spike cost-based metrics and ISI metrics on the activity of single RGC within the three tested time intervals.

STIMULUS FEATURE	TIME INTERVAL	METRICS	LEFT-DSC	NON-DSC	RIGHT-DSC
0-200 ms	Turtle	Cost-based	15.3% $1/q$=62ms	15.3% $1/q$=62ms	14.9% $1/q$=62ms
		ISI	18.4%	17.9%	16.8%
	Fish	Cost-based	18.2% $1/q$=31ms	13.9% $1/q$=31ms	13.5% $1/q$=62ms
		ISI	16.2%	13.1%	12.8%
0-500 ms	Turtle	Cost-based	16% $1/q$=62ms	15.9% $1/q$=125ms	15% $1/q$=125ms
		ISI	20.4%	18.4%	17.3%
	Fish	Cost-based	18.2% $1/q$=250ms	14.2% $1/q$=125ms	14.1% $1/q$=125ms
		ISI	19%	13.3%	13.7%
300-500 ms	Turtle	Cost-based	12.6% $1/q$=62ms	12.2% $1/q$=62ms	12.2% $1/q$=62ms
		ISI	15.7%	14.9%	14.3%
	Fish	Cost-based	12.4% $1/q$=62ms	12.2% $1/q$=∞	12.2% $1/q$=250ms
		ISI	14%	12.9%	12.8%

Table 5.5: Highest median of estimation results for the motion velocity of the moving stimulus before the instantaneous velocity changes, obtained by applying spike cost-based metrics and ISI metrics on the activity of single RGC within the three tested time intervals.

STIMULUS FEATURE	TIME INTERVAL	METRICS	LEFT-DSC	NON-DSC	RIGHT-DSC
0-200 ms	Turtle	Cost-based	46.4% $1/q$=31ms	45.2% $1/q$=31ms	46.5% $1/q$=31ms
		ISI	49.6%	46.8%	48.5%
	Fish	Cost-based	45.6% $1/q$=62ms	44.5% $1/q$=16ms	44.5% $1/q$=31ms
		ISI	47.1%	44.8%	45.6%
0-500 ms	Turtle	Cost-based	47.1% $1/q$=31ms	44.7% $1/q$=31ms	46.8% $1/q$=31ms
		ISI	49.9%	46.2%	47.8%
	Fish	Cost-based	45.6% $1/q$=32ms	45% $1/q$=32ms	44.5% $1/q$=16ms
		ISI	47.8%	45.7%	44.9%
300-500 ms	Turtle	Cost-based	45% $1/q$=∞	44.4% $1/q$=8ms	43.9% $1/q$=8ms
		ISI	45.5%	42.6%	45.8%
	Fish	Cost-based	44.4% $1/q$=8ms	44.3% $1/q$=16ms	44.2% $1/q$=16ms
		ISI	42.4%	43.7%	44.6%

Table 5.6: Highest median of estimation results for the motion direction of the moving stimulus before the instantaneous velocity changes, obtained by applying spike cost-based metrics and ISI metrics on the activity of single RGC within the three tested time intervals.

STIMULUS FEATURE	TIME INTERVAL	METRICS	LEFT-DSC	NON-DSC	RIGHT-DSC
0-200 ms	Turtle	Cost-based	0.9 $1/q$=62ms	0.85 $1/q$=62ms	0.84 $1/q$=62ms
		ISI	0.79	0.79	0.92
	Fish	Cost-based	0.84 $1/q$=62ms	0.88 $1/q$=62ms	0.9 $1/q$=62ms
		ISI	0.84	0.95	0.99
0-500 ms	Turtle	Cost-based	0.94 $1/q$=62ms	0.84 $1/q$=125ms	0.92 $1/q$=250ms
		ISI	0.81	0.8	0.92
	Fish	Cost-based	0.81 $1/q$=62ms	0.96 $1/q$=31ms	0.87 $1/q$=62ms
		ISI	0.83	0.94	0.95
300-500 ms	Turtle	Cost-based	0.95 $1/q$=1000ms	0.95 $1/q$=500ms	0.96 $1/q$=8ms
		ISI	0.9	0.91	0.98
	Fish	Cost-based	0.89 $1/q$=1000ms	1.02 $1/q$=500ms	0.91 $1/q$=31ms
		ISI	0.91	0.98	0.99

Table 5.7: Lowest median of absolute normalised estimation errors for the motion speed of the moving stimulus before the instantaneous velocity changes, obtained by applying spike cost-based metrics and ISI metrics on the activity of single RGC within the three tested time intervals.

STIMULUS FEATURE	TIME INTERVAL	METRICS	LEFT-DSC	NON-DSC	RIGHT-DSC
0-200 ms	Turtle	Cost-based	23% $1/q$=125ms	19.7% $1/q$=62ms	18.4% $1/q$=62ms
		ISI	25.3%	22.4%	18.9%
	Fish	Cost-based	15% $1/q$=250ms	13.6% $1/q$=m32s	12.9% $1/q$=32ms
		ISI	19%	14.3%	13.6%
0-500 ms	Turtle	Cost-based	29.9% $1/q$=250ms	25.5% $1/q$=125ms	23.3% $1/q$=500ms
		ISI	27.7%	24.5%	18.7%
	Fish	Cost-based	22.4% $1/q$=250ms	17% $1/q$=250ms	17.1% $1/q$=125ms
		ISI	19.7%	14.8%	13.6%
300-500 ms	Turtle	Cost-based	22.3% $1/q$=125ms	20.6% $1/q$=62ms	18% $1/q$=125ms
		ISI	24.3%	22.4%	18%
	Fish	Cost-based	19.3% $1/q$=∞	14.9% $1/q$=125ms	14.1% $1/q$=500ms
		ISI	19.9%	14%	13.3%

Table 5.8: Highest median of estimation results for the motion velocity of the moving stimulus after the instantaneous velocity changes, obtained by applying spike cost-based metrics and ISI metrics on the activity of single RGC within the three tested time intervals.

Stimulus Feature	Time Interval	Metrics	Left-DSC	Non-DSC	Right-DSC
0-200 ms	Turtle	Cost-based	43% $1/q$=125ms	39.5% $1/q$=62ms	42.6% $1/q$=500ms
		ISI	45.6%	38.2%	40.3%
	Fish	Cost-based	45.5% $1/q$=125ms	42.8% $1/q$=1000ms	45.9% $1/q$=125ms
		ISI	45.6%	36.8%	35.9%
0-500 ms	Turtle	Cost-based	50% $1/q$=500ms	45% $1/q$=250ms	47% $1/q$=250ms
		ISI	43.2%	40%	40.4%
	Fish	Cost-based	51.8% $1/q$=∞	41.1% $1/q$=∞	40.6% $1/q$=∞
		ISI	45.7%	39.6%	39.5%
300-500 ms	Turtle	Cost-based	42.8% $1/q$=∞	36.8% $1/q$=125ms	37.8% $1/q$=∞
		ISI	43.4%	38.7%	40%
	Fish	Cost-based	45.1% $1/q$=250ms	28.6% $1/q$=500ms	31.7% $1/q$=∞
		ISI	46.3%	39.7%	37.1%

Table 5.9: Highest median of estimation results for the motion direction of the moving stimulus after the instantaneous velocity changes, obtained by applying spike cost-based metrics and ISI metrics on the activity of single RGC within the three tested time intervals.

STIMULUS FEATURE	TIME INTERVAL	METRICS	LEFT-DSC	NON-DSC	RIGHT-DSC
0-200 ms	Turtle	Cost-based	0.74 $1/q$=500ms	0.74 $1/q$=∞	0.89 $1/q$=125ms
		ISI	0.86	0.81	0.96
	Fish	Cost-based	0.8 $1/q$=250ms	0.95 $1/q$=125ms	0.91 $1/q$=125ms
		ISI	0.83	1.05	1.05
0-500 ms	Turtle	Cost-based	0.68 $1/q$=250ms	0.57 $1/q$=1000ms	0.81 $1/q$=∞
		ISI	0.84	0.75	0.93
	Fish	Cost-based	0.66 $1/q$=250ms	0.92 $1/q$=1000ms	1.03 $1/q$=1000ms
		ISI	0.72	0.98	1.04
300-500 ms	Turtle	Cost-based	0.92 $1/q$=250ms	0.9 $1/q$=125ms	1.06 $1/q$=125ms
		ISI	0.86	0.78	0.95
	Fish	Cost-based	0.7 $1/q$=∞	1.12 $1/q$=∞	1.16 $1/q$=62ms
		ISI	0.75	0.99	1.09

Table 5.10: Lowest median of absolute normalised estimation errors for the motion speed of the moving stimulus after the instantaneous velocity changes, obtained by applying spike cost-based metrics and ISI metrics on the activity of single RGC within the three tested time intervals.

STIMULUS FEATURE	TIME INTERVAL	METRICS	LEFT-DSC	NON-DSC	RIGHT-DSC
0-200 ms	Turtle	Cost-based	60.8% $1/q$=250ms	61.3% $1/q$=250ms	56.3% $1/q$=125ms
		ISI	53.8%	58.8%	50.8%
	Fish	Cost-based	56.6% $1/q$=62ms	46.5% $1/q$=125ms	45.7% $1/q=\infty$
		ISI	53%	46%	44.2%
0-500 ms	Turtle	Cost-based	56.8% $1/q$=125ms	62.6% $1/q$=1000ms	56.8% $1/q$=500ms
		ISI	54.5%	59.1%	51.6%
	Fish	Cost-based	60.8% $1/q$=62ms	54.4% $1/q=\infty$	48.8% $1/q$=500ms
		ISI	60.8%	46.3%	44.2%
300-500 ms	Turtle	Cost-based	50.5% $1/q$=62ms	51.9% $1/q$=500ms	47.7% $1/q$=250ms
		ISI	53%	56.6%	48.3%
	Fish	Cost-based	52.7% $1/q$=31ms	47.2% $1/q$=1000ms	44.4% $1/q$=500ms
		ISI	47%	47.6%	45%

Table 5.11: Highest median of estimation results for the changes in the motion speed of the moving stimulus, obtained by applying spike cost-based metrics and ISI metrics on the activity of single RGC within the three tested time intervals.

STIMULUS FEATURE	TIME INTERVAL	METRICS	LEFT-DSC	NON-DSC	RIGHT-DSC
0-200 ms	Turtle	Cost-based	40.5% $1/q$=62ms	40.8% $1/q$=62ms	38% $1/q$=62ms
		ISI	41.3%	38.6%	38.6%
	Fish	Cost-based	47.1% $1/q$=125ms	40% $1/q$=31ms	36.8% $1/q$=62ms
		ISI	41.44%	33.5%	32%
0-500 ms	Turtle	Cost-based	42.6% $1/q$=250ms	40.7% $1/q$=125ms	40.3% $1/q$=250ms
		ISI	41.3%	38.8%	38.6%
	Fish	Cost-based	48.6% $1/q$=1000ms	36.8% $1/q$=250ms	34.3% $1/q$=1000ms
		ISI	46.7%	37%	33%
300-500 ms	Turtle	Cost-based	36.2% $1/q$=∞	35.6% $1/q$=250ms	33.7% $1/q$=500ms
		ISI	35%	34.5%	35.7%
	Fish	Cost-based	% $1/q$=125ms	% $1/q$=∞	% $1/q$=1000ms
		ISI	40.5%	33.7%	30.9%

Table 5.12: Highest median of estimation results for the changes in the motion direction of the moving stimulus, obtained by applying spike cost-based metrics and ISI metrics on the activity of single RGC within the three tested time intervals.

STIMULUS FEATURE	TIME INTERVAL	METRICS	LEFT-DSC	NON-DSC	RIGHT-DSC
0-200 ms	Turtle	Cost-based	24.8% $1/q$=31ms	25.6% $1/q$=31ms	22.8% $1/q$=62ms
		ISI	25.3%	25.3%	21.9%
	Fish	Cost-based	21.8% $1/q$=62ms	18.7% $1/q$=62ms	18% $1/q$=62ms
		ISI	23.3%	17.3%	16%
0-500 ms	Turtle	Cost-based	26.4% $1/q$=125ms	27.2% $1/q$=250ms	24.4% $1/q$=500ms
		ISI	25.6%	25.6%	20.5%
	Fish	Cost-based	28.3% $1/q$=125ms	20.2% $1/q$=250ms	18.7% $1/q$=125ms
		ISI	24.7%	17.8%	16.2%
300-500 ms	Turtle	Cost-based	19.4% $1/q$=125ms	18.7% $1/q$=62ms	17.2% $1/q$=∞
		ISI	21%	22.6%	19%
	Fish	Cost-based	% $1/q$=250ms	% $1/q$=1000ms	% $1/q$=500ms
		ISI	22.4%	17.2%	16.3%

Table 5.13: Highest median of estimation results for the combined changes in the motion speed and direction of the moving stimulus, obtained by applying spike cost-based metrics and ISI metrics on the activity of single RGC within the three tested time intervals.

Time interval	Animal	Metrics	Pooled Population	Labelled Line	Functional Group
0-200 ms	Turtle	Cost-based	33.8% $1/q$=250ms n=18	38.2% $1/q$=∞ n=18	43.4% $1/q$=1000ms n=18
		ISI	36.1% n=18	51.5% n=18	50.6% n=15
	Fish	Cost-based	18.1% $1/q$=∞ n=6	18% $1/q$=∞ n=6	
		ISI	21.6% n=6	21.3% n=6	
0-500 ms	Turtle	Cost-based	46.8% $1/q$=125ms n=18	60.3% $1/q$=∞ n=18	64.2% $1/q$=∞ n=18
		ISI	46.8% n=18	54.6% n=18	62.1% n=15
	Fish	Cost-based	25.3% $1/q$=250ms n=6	28.1% $1/q$=∞ n=6	
		ISI	26% n=6	23.4% n=6	
300-500 ms	Turtle	Cost-based	36.8% $1/q$=1000ms n=	34% $1/q$=∞ n=	48.9% $1/q$=∞ n=
		ISI	31.3% n=15	51.4% n=18	46.7% n=15
	Fish	Cost-based	21.4% $1/q$=250ms n=6	23.7% $1/q$=∞ n=6	
		ISI	20.2% n=6	22.9% n=6	

Table 5.14: Highest median of estimation results for the motion velocity of the moving stimulus, obtained by applying spike cost-based metrics and ISI metrics on the activity of populations of RGC within the three tested time intervals.

Stimulus feature	Time interval	Metrics	Pooled Population	Labelled Line	Functional Group
0-200 ms	Turtle	Cost-based	53.% $1/q$=64ms n=15	58.2% $1/q$=∞ n=15	68.9% $1/q$=∞ n=18
		ISI	58.1% n=9	63% n=18	73.9% n=15
	Fish	Cost-based	37.1% $1/q$=∞ n=6	43% $1/q$=∞ n=6	
		ISI	46.8% n=6	42.7% n=6	
0-500 ms	Turtle	Cost-based	65% $1/q$=125ms n=15	79% $1/q$=∞ n=15	86% $1/q$=∞ n=15
		ISI	65.7% n=15	63.2% n=15	81.4% n=15
	Fish	Cost-based	49.4% $1/q$=500ms n=6	54.4% $1/q$=∞ n=6	
		ISI	50.5% n=6	48.6% n=6	
300-500 ms	Turtle	Cost-based	63% $1/q$=125ms n=15	51.7% $1/q$=∞ n=15	76.2% $1/q$=∞ n=15
		ISI	58.4% n=15	62.4% n=15	74% n=15
	Fish	Cost-based	46.3% $1/q$=∞ n=6	39.4% $1/q$=∞ n=6	
		ISI	46% n=6	46% n=6	

Table 5.15: Highest median of estimation results for the motion direction of the moving stimulus, obtained by applying spike cost-based metrics and ISI metrics on the activity of populations of RGC within the three tested time intervals.

STIMULUS FEATURE	TIME INTERVAL	METRICS	POOLED POPULATION	LABELLED LINE	FUNCTIONAL GROUP
0-200 ms	Turtle	Cost-based	0.36 $1/q=\infty$ $n=18$	0.54 $1/q=\infty$ $n=18$	0.39 $1/q=\infty$ $n=18$
		ISI	0.37 $n=18$	0.39 $n=18$	0.3 $n=18$
	Fish	Cost-based	0.88 $1/q=\infty$ $n=6$	0.88 $1/q=\infty$ $n=6$	
		ISI	0.81 $n=6$	0.85 $n=6$	
0-500 ms	Turtle	Cost-based	0.24 $1/q=\infty$ $n=18$	0.28 $1/q=\infty$ $n=18$	0.22 $1/q=\infty$ $n=18$
		ISI	0.26 $n=18$	0.39 $n=18$	0.21 $n=18$
	Fish	Cost-based	0.67 $1/q=\infty$ $n=6$	0.66 $1/q=\infty$ $n=6$	
		ISI	0.7 $n=6$	0.76 $n=6$	
300-500 ms	Turtle	Cost-based	0.37 $1/q=\infty$ $n=18$	0.72 $1/q=\infty$ $n=18$	0.33 $1/q=\infty$ $n=18$
		ISI	0.46 $n=18$	0.43 $n=18$	0.32 $n=18$
	Fish	Cost-based	0.83 $1/q=\infty$ $n=6$	0.93 $1/q=\infty$ $n=6$	
		ISI	0.87 $n=6$	0.82 $n=6$	

Table 5.16: Lowest median of absolute normalised estimation errors for the motion speed of the moving stimulus, obtained by applying spike cost-based metrics and ISI metrics on the activity of populations of RGC within the three tested time intervals.

Stimulus feature	Time interval	Metrics	Pooled Population	Labelled Line	Functional Group
0-200 ms	Turtle	Cost-based	21.5% $1/q$=31ms n=18	19% $1/q$=125ms n=15	26.6% $1/q$=62ms n=18
		ISI	22.3% n=18	41.2% n=18	35.9% n=18
	Fish	Cost-based	4.5% $1/q$=31ms n=6	5.2% $1/q$=125ms n=6	
		ISI	6.2% n=6	6.8% n=6	
0-500 ms	Turtle	Cost-based	28.5% $1/q$=31ms n=18	31.2% $1/q$=500ms n=18	35% $1/q$=62ms n=18
		ISI	28.8% n=18	41.1% n=18	41.6% n=18
	Fish	Cost-based	6.9% $1/q$=62ms n=6	9.1% $1/q$=125 n=6	
		ISI	8.7% n=6	8.4% n=6	
300-500 ms	Turtle	Cost-based	8.1% $1/q$=31ms n=6	11.4% $1/q$=1000ms n=18	12.5% $1/q$=62ms n=12
		ISI	6% n=18	27.9% n=18	13.5% n=18
	Fish	Cost-based	3.9% $1/q$=62ms n=6	5.2% $1/q$=500ms n=6	
		ISI	3.3% n=6	7% n=6	

Table 5.17: Highest median of estimation results for the instantaneous velocity changes of the moving stimulus, obtained by applying spike cost-based metrics and ISI metrics on the activity of populations of RGC within the three tested time intervals.

STIMULUS FEATURE	TIME INTERVAL	METRICS	POOLED POPULATION	LABELLED LINE	FUNCTIONAL GROUP
0-200 ms	Turtle	Cost-based	29.6% $1/q$=16ms n=18	30.4% $1/q$=125ms n=18	34% $1/q$=31ms n=18
		ISI	31.8% n=18	49.3% n=18	45.4% n=18
	Fish	Cost-based	18.4% $1/q$=125ms n=6	18.7% $1/q$=250ms n=6	
		ISI	19.9% n=6	17.5% n=6	
0-500 ms	Turtle	Cost-based	34.8% $1/q$=31ms n=18	36.9% $1/q$=125ms n=18	40.4% $1/q$=62ms n=18
		ISI	36.5% n=18	48.1% n=18	48.2% n=18
	Fish	Cost-based	20.1% $1/q$=125ms n=6	20.8% $1/q$=250ms n=6	
		ISI	21.3% n=6	20.4% n=6	
300-500 ms	Turtle	Cost-based	14.8% $1/q$=31ms n=18	18.7% $1/q$=1000ms n=18	18.4% $1/q$=62ms n=18
		ISI	13.9% n=6	35.4% n=18	20.8% n=6
	Fish	Cost-based	13.1% $1/q$=31ms n=6	13.9% $1/q$=∞ n=6	
		ISI	11.9% n=6	17.1% n=6	

Table 5.18: Highest median of estimation results for the motion velocity of the moving stimulus before the instantaneous velocity changes, obtained by applying spike cost-based metrics and ISI metrics on the activity of populations of RGC within the three tested time intervals.

STIMULUS FEATURE	TIME INTERVAL	METRICS	POOLED POPULATION	LABELLED LINE	FUNCTIONAL GROUP
0-200 ms	Turtle	Cost-based	56.3% $1/q$=16ms n=18	61.6% $1/q$=125ms n=15	66.5% $1/q$=31ms n=18
		ISI	59% n=15	72% n=18	72.4% n=18
	Fish	Cost-based	46.7% $1/q$=16ms n=6	48.6% $1/q$=125ms n=6	
		ISI	51.7% n=6	49.4% n=6	
0-500 ms	Turtle	Cost-based	59.5% $1/q$=31ms n=18	64.6% $1/q$=250ms n=18	68.7% $1/q$=62ms n=18
		ISI	62.8% n=18	71.2% n=18	73.4% n=18
	Fish	Cost-based	49.8% $1/q$=31ms n=6	52.6% $1/q$=125ms n=6	
		ISI	52.7% n=6	51% n=6	
300-500 ms	Turtle	Cost-based	44.2% $1/q$=125ms n=9	50.4% $1/q$=125ms n=18	46.6% $1/q$=16ms n=18
		ISI	42% n=6	62.2% n=18	48% n=6
	Fish	Cost-based	44.6% $1/q$=125ms n=6	46.4% $1/q$=500ms n=6	
		ISI	37.9% n=6	47% n=6	

Table 5.19: Highest median of estimation results for the motion direction of the moving stimulus before the instantaneous velocity changes, obtained by applying spike cost-based metrics and ISI metrics on the activity of populations of RGC within the three tested time intervals.

Stimulus feature	Time interval	Metrics	Pooled Population	Labelled Line	Functional Group
0-200 ms	Turtle	Cost-based	0.66 $1/q$=16ms n=18	0.68 $1/q$=250ms n=18	0.66 $1/q$=62ms n=18
		ISI	0.54 n=18	0.45 n=18	0.44 n=18
	Fish	Cost-based	0.82 $1/q$=16ms n=6	0.77 $1/q$=125ms n=6	
		ISI	0.78 n=6	0.83 n=6	
0-500 ms	Turtle	Cost-based	0.57 $1/q$=31ms n=18	0.62 $1/q$=250ms n=18	0.58 $1/q$=62ms n=18
		ISI	0.52 n=18	0.49 n=18	0.44 n=18
	Fish	Cost-based	0.79 $1/q$=62ms n=6	0.73 $1/q$=250ms n=6	
		ISI	0.78 n=6	0.72 n=6	
300-500 ms	Turtle	Cost-based	0.92 $1/q$=8ms n=18	0.8 $1/q$=8ms n=18	0.86 $1/q$=8ms n=18
		ISI	0.93 n=6	0.64 n=18	0.85 n=6
	Fish	Cost-based	0.94 $1/q$=16ms n=6	0.83 $1/q$=8ms n=6	
		ISI	0.95 n=6	0.79 n=6	

Table 5.20: Lowest median of absolute normalised estimation errors for the motion speed of the moving stimulus before the instantaneous velocity changes, obtained by applying spike cost-based metrics and ISI metrics on the activity of populations of RGC within the three tested time intervals.

STIMULUS FEATURE	TIME INTERVAL	METRICS	POOLED POPULATION	LABELLED LINE	FUNCTIONAL GROUP
0-200 ms	Turtle	Cost-based	39.6% $1/q=31$ms $n=18$	42.5% $1/q=\infty$ $n=18$	48.5% $1/q=125$ms $n=18$
		ISI	40.4% $n=18$	55.5% $n=18$	46.4% $n=18$
	Fish	Cost-based	17.3% $1/q=31$ms $n=6$	17.6% $1/q=250$ms $n=6$	
		ISI	22.1% $n=6$	22.7% $n=6$	
0-500 ms	Turtle	Cost-based	50.6% $1/q=62$ms $n=18$	67.4% $1/q=\infty$ $n=18$	69.1% $1/q=250$ms $n=18$
		ISI	52.5% $n=18$	57% $n=18$	68.5% $n=18$
	Fish	Cost-based	26.1% $1/q=125$ms $n=6$	29.2% $1/q=1000$ms $n=6$	
		ISI	28.1% $n=6$	24.7% $n=6$	
300-500 ms	Turtle	Cost-based	37.3% $1/q=62$ms $n=18$	39.4% $1/q=\infty$ $n=18$	50.3% $1/q=500$ms $n=18$
		ISI	30.9% $n=18$	50.2% $n=18$	46.4% $n=15$
	Fish	Cost-based	21.6% $1/q=62$ms $n=6$	25.3% $1/q=\infty$ $n=6$	
		ISI	19.7% $n=6$	23.8% $n=6$	

Table 5.21: Highest median of estimation results for the motion velocity of the moving stimulus after the instantaneous velocity changes, obtained by applying spike cost-based metrics and ISI metrics on the activity of populations of RGC within the three tested time intervals.

Stimulus Feature	Time Interval	Metrics	Pooled Population	Labelled Line	Functional Group
0-200 ms	Turtle	Cost-based	58.3% $1/q$=62ms n=18	64.6% $1/q$=∞ n=15	72.2% $1/q$=500ms n=15
		ISI	59.9% n=18	63.4% n=18	76% n=18
	Fish	Cost-based	45.6% $1/q$=500ms n=6	48.3% $1/q$=500ms n=6	
		ISI	48.3% n=6	45.9% n=6	
0-500 ms	Turtle	Cost-based	67.8% $1/q$=125ms n=15	83.4% $1/q$=∞ n=18	88.3% $1/q$=1000ms n=15
		ISI	68.4% n=15	62.7% n=18	82.7% n=18
	Fish	Cost-based	52.2% $1/q$=250ms n=6	59.3% $1/q$=∞ n=6	
		ISI	50.9% n=6	50.1% n=6	
300-500 ms	Turtle	Cost-based	63.3% $1/q$=500ms n=18	58.1% $1/q$=∞ n=12	78.6% $1/q$=∞ n=15
		ISI	58.1% n=15	60% n=15	73.6% n=15
	Fish	Cost-based	45.8% $1/q$=250ms n=6	44.2% $1/q$=∞ n=6	
		ISI	46% n=6	49.6% n=6	

Table 5.22: Highest median of estimation results for the motion direction of the moving stimulus after the instantaneous velocity changes, obtained by applying spike cost-based metrics and ISI metrics on the activity of populations of RGC within the three tested time intervals.

Stimulus feature	Time interval	Metrics	Pooled Population	Labelled Line	Functional Group
0-200 ms	Turtle	Cost-based	0.33 $1/q=62$ms $n=18$	0.46 $1/q=\infty$ $n=18$	0.34 $1/q=125$ms $n=18$
		ISI	0.32 $n=18$	0.39 $n=18$	0.26 $n=18$
	Fish	Cost-based	0.72 $1/q=62$ms $n=6$	0.74 $1/q=500$ms $n=6$	
		ISI	0.74 $n=6$	0.78 $n=6$	
0-500 ms	Turtle	Cost-based	22.2 $1/q=62$ms $n=18$	21.8 $1/q=\infty$ $n=18$	17.5 $1/q=250$ms $n=18$
		ISI	0.22 $n=18$	0.41 $n=18$	0.17 $n=18$
	Fish	Cost-based	0.65 $1/q=1000$ms $n=6$	0.6 $1/q=\infty$ $n=6$	
		ISI	0.61 $n=6$	0.72 $n=6$	
300-500 ms	Turtle	Cost-based	0.37 $1/q=125$ms $n=18$	.6 $1/q=\infty$ $n=18$	0.32 $1/q=\infty$ $n=18$
		ISI	0.47 $n=18$	0.49 $n=18$	0.31 $n=18$
	Fish	Cost-based	0.76 $1/q=\infty$ $n=6$	0.81 $1/q=\infty$ $n=6$	
		ISI	0.77 $n=6$	0.74 $n=6$	

Table 5.23: Lowest median of absolute normalised estimation errors for the motion speed of the moving stimulus after the instantaneous velocity changes, obtained by applying spike cost-based metrics and ISI metrics on the activity of populations of RGC within the three tested time intervals.

Stimulus feature	Time interval	Metrics	Pooled Population	Labelled Line	Functional Group
0-200 ms	Turtle	Cost-based	84% $1/q$=16ms n=18	75.6% $1/q$=125ms n=18	81.3% $1/q$=31ms n=18
		ISI	82% n=18	80.1% n=18	83.2% n=18
	Fish	Cost-based	56.8% $1/q$=62ms n=6	55.2% $1/q$=250ms n=6	
		ISI	57.7% n=6	56.3% n=6	
0-500 ms	Turtle	Cost-based	83.6% $1/q$=31ms n=18	77.4% $1/q$=250ms n=18	81.6% $1/q$=62ms n=18
		ISI	81.7% n=18	78.9% n=18	83.8% n=18
	Fish	Cost-based	64.7% $1/q$=125ms n=6	64.8% $1/q$=500ms n=6	
		ISI	63.4% n=6	57.3% n=6	
300-500 ms	Turtle	Cost-based 61.3%	59.8% $1/q$=31ms n=18	60.8% $1/q$=∞ n=18	$1/q$=62ms n=18
		ISI	58.6% n=6	73.5% n=18	65.8% n=6
	Fish	Cost-based	51.5% $1/q$=250ms n=6	56.3% $1/q$=∞ n=6	
		ISI	53% n=6	59% n=6	

Table 5.24: Highest median of estimation results for the changes of motion speed of the moving stimulus, obtained by applying spike cost-based metrics and ISI metrics on the activity of populations of RGC within the three tested time intervals.

Stimulus feature	Time interval	Metrics	Pooled Population	Labelled Line	Functional Group
0-200 ms	Turtle	Cost-based	68.5% $1/q$=31ms n=18	54.5% $1/q$=250ms n=18	64% $1/q$=62ms n=18
		ISI	74.3% n=18	63.1% n=18	75.8% n=18
	Fish	Cost-based	46.9% $1/q$=31ms n=6	47.3% $1/q$=62ms n=6	
		ISI	54.5% n=6	46.6% n=6	
0-500 ms	Turtle	Cost-based	71% $1/q$=31ms n=18	61% $1/q$=500ms n=18	68% $1/q$=62ms n=18
		ISI	75.9% n=18	61% n=18	74.6% n=18
	Fish	Cost-based	52.9% $1/q$=250ms n=6	51.7% $1/q$=250ms n=6	
		ISI	55.5% n=6	48.4% n=6	
300-500 ms	Turtle	Cost-based	46.9% $1/q$=∞ n=15	41.5% $1/q$=∞ n=18	47.3% $1/q$=1000ms n=18
		ISI	43.2% n=9	50% n=18	44.9% n=18
	Fish	Cost-based	42.5% $1/q$=125ms n=6	41.1% $1/q$=∞ n=6	
		ISI	35.8% n=6	47.6% n=6	

Table 5.25: Highest median of estimation results for the changes of motion direction of the moving stimulus, obtained by applying spike cost-based metrics and ISI metrics on the activity of populations of RGC within the three tested time intervals.

STIMULUS FEATURE	TIME INTERVAL	METRICS	POOLED POPULATION	LABELLED LINE	FUNCTIONAL GROUP
0-200 ms	Turtle	Cost-based	58% $1/q$=31ms n=18	42.9% $1/q$=250ms n=18	52.5% $1/q$=62ms n=18
		ISI	62.9% n=18	53.7% n=18	65.2% n=18
	Fish	Cost-based	24.4% $1/q$=250ms n=6	25.1% $1/q$=125ms n=6	
		ISI	31.4% n=6	27.4% n=6	
0-500 ms	Turtle	Cost-based	60.9% $1/q$=31ms n=18	50.1% $1/q$=250ms n=18	57.4% $1/q$=62ms n=18
		ISI	63.4% n=18	50.9% n=18	63.7% n=18
	Fish	Cost-based	33.2% $1/q$=250ms n=6	33.1% $1/q$=500ms n=6	
		ISI	36.7% n=6	29.2% n=6	
300-500 ms	Turtle	Cost-based	28.9% $1/q$=125ms n=18	26.5% $1/q$=∞ n=18	31.7% $1/q$=125ms n=18
		ISI	26.7% n=15	39% n=18	32.9% n=18
	Fish	Cost-based	22.3% $1/q$=125ms n=6	24.6% $1/q$=∞ n=6	
		ISI	24.6% n=6	25.7% n=6	

Table 5.26: Highest median of estimation results for the combined changes of motion speed of the moving stimulus, obtained by applying spike cost-based metrics and ISI metrics on the activity of populations of RGC within the three tested time intervals.

Curriculum Vitae

Personal Data

Name:	León Mauricio
Surname:	Juárez Paz
Date and place of birth:	February 7th, 1977, Mexico D.F., Mexico
Citizenship:	Mexican
Marital status:	Single
Private address:	Schäferstrasse 4, D-26123, Oldenburg
Telephone No.:	+49(0)176-2017-1611
e-mail:	l.m.juarez.paz@uni-oldenburg.de

Higher Education

Dr. rer. nat.	December 2006
Retinal Ensemble Coding Under Dynamic Conditions	November 2012
Carl von Ossietzky University Oldenburg	
Oldenburg, Germany	
Master of Science	March 2004
Biomedical Engineering	August 2006
Aachen University of Applied Sciences	
Jülich, Germany	
Engineering	August 1994
Electronic Engineering	May 2000
Autonomous University of Baja California	
Mexicali, Mexico	

Relevant Academic Background

Computational Neuroscience, Biomedical Engineering and Electronic Engineering

Anatomy, Physiology, Neurophysiology, Electrophysiology, Artificial Organs, Biosensors, Biomechanics, Medical Imaging, Mathematics, Physics, Medical Statistics, Programming, Instrumentation, Control, Signal Processing, Analogue and Digital Electronics.

Research Interest

Brain-Machine Interfaces, Neuroprosthetics, Neuronal Coding, Analysis of Multi-Unit Channel Recordings, Robotics, Machine Learning.

Research Positions

PhD Student	December 2006
Research Unit Dynamics and Stability of Retinal Processing	August 2012
Carl von Ossietzky University Oldenburg	
Oldenburg, Germany	
Research Assistant	October 2005
Medical Engineering and Neuroprosthetics Department	May 2006
Fraunhofer Institute for Biomedical Engineering	
St. Ingbert, Germany	
Research Assistant	January 2005
Laboratory for Chemical Sensors and Biosensors	October 2005
Aachen University of Applied Sciences	
Jülich, Germany	

Teaching Experience

MATLAB Teaching assistant
Involvement in the supervision of Diploma and Master theses
Carl von Ossietzky University Oldenburg, Oldenburg, Germany

Programming and Computer Skills

Basic knowledge:	C, R
Good knowledge	Pascal, LaTeX
Very good knowledge	MATLAB, LabVIEW, Microsoft Office

Languages

Spanish	Native speaker
English	Fluent speaking, reading and writing
German	Fluent speaking and reading
French	Passive language skills

Courses and Certificates

8th BCI2000 Workshop The Rudolf Magnus Institute, University Medical Center Utrecht and BCI2000 Utrecht, The Netherlands	2011
Analysis and Models in Neurophysiology Workshop Bernstein Center for Computational Neuroscience Freiburg, Germany	2008
Theoretical Neuroscience and Complex Systems Summer School Frankfurt Institute for Advanced Studies Frankfurt, Germany	2007
2nd Advanced Data Analysis and Modelling Summer School Universidad CEU San Pablo Madrid, Spain	2007
Neurosensory and Cognitive Science in the North Spring School Hanse Institute for Advanced Study, Carl von Ossietzky University of Oldenburg and Bremen University Delmenhorst, Germany	2007
NEUROBOTICS Summer School NEUROBOTICS Consortium and University of Umea Umea, Sweden	2006
Industrial Automation Qualification Festo and Autonomous University of Baja California Mexicali, Mexico	1998

Working Experience

Engineer   June 2000
Engineering Department   March 2004
Plataforma de Profesionales y Técnicos, Mexico

Process Engineer   September 1999
Printed Circuit Board Engineering Department   April 2000
NEC Nippon Electronic Corporation, Mexico

Line Engineer   December 1998
Printed Circuit Board Production Department   September 1999
Nippon Electronic Corporation, NEC, Mexico

References

Prof. Dr. Jutta Kretzberg (PhD advisor)
Research Group Computational Neuroscience
Carl von Ossietzky University Oldenburg
Carl von Ossietzkystr. 9-11
D-26129 Oldenburg, Germany   Tel.: +49(0)441/798-3314
e-mail: jutta.kretzberg@uni-oldenburg.de   Fax: +49(0)441/798-3250

P.D. Dr. Jan Freund (PhD advisor)
Research Scientist
Research Group Theoretical Physics / Complex Systems
Carl von Ossietzky University Oldenburg
Carl von Ossietzkystr. 9-11
D-26129 Oldenburg, Germany   Tel.: +49(0)441/798-3231
e-mail: jan.freund@uni-oldenburg.de   Fax: +49(0)441/798-3404

Acknowledgements

After more than five years working on this project it is difficult for me to mention all the persons that have helped me through this journey. This time has been very challenging, but I have really enjoyed it. I would like to start thanking Jutta for her great support, but especially, her patience through all this time. As always, her valuable advices helped me improve greatly the structure of this thesis and stress the important findings of my investigation. This task is easier said than made. Also, I would like to thank Jan for helping me broaden my knowledge to interesting theoretical concepts that were unknown for me. In turn, regarding the experimental part of my investigation, my deepest thanks go to Josef and Malte, who patiently taught me the interesting and the not so nice aspects in electrophysiology. I am also very grateful for the nice atmosphere in our small work group.

Of course, my parents and my sister deserve much of the credit for this work. Their support and encouragement kept me going even in uncertain times. These sincere thanks go also to Alex. His friendship is one of the most valuable by-products of these work. Most of all, I am grateful for having the chance of working in this interesting project, which in turn allowed me to live in this nice and friendly city.

288

Erklärung

Hiermit erkläre ich, dass ich die vorliegende Dissertation selbständig verfasst habe und nur die angegebenen Hilfsmittel verwendet habe. Die Dissertation hat weder in Teilen noch in ihrer Gesamtheit einer anderen wissenschaftlichen Hochschule zur Begutachtung in einem Promotionsverfahren vorgelegen.

Oldenburg, den 28. November 2012.

_____

León Mauricio Juárez Paz

Eidesstattliche Erklärung des Doktoranden zur Abgabe einer Dissertation in elektronischer Form

1. Der Doktorand erklärt hiermit an Eides statt, dass die bei der Tauschstelle des Bibliotheks- und Informationssystems (BIS) der Universität Oldenburg abgegebenen fünf gedruckten Exemplare seiner Dissertation sowie die abgegebenen Dateien inhaltlich und formal vollständig mit dem bei der Fakultät eingereichten und von dieser genehmigten Prüfungsexemplar übereinstimmen.

2. Der Doktorand verpflichtet sich, die im Internet zu veröffentlichende elektronische Version seiner Dissertation auf Vollständigkeit und Übereinstimmung mit dem genehmigten Prüfungsexemplar zu prüfen und dem BIS etwaige Fehler mitzuteilen.

3. Der Doktorand erklärt sich damit einverstanden, dass das BIS und die Deutsche Nationalbibliothek die elektronische Version seiner Dissertation auf ihren Dokumentenservern zur freien Nutzung bereitstellen.

4. Der Doktorand ist damit einverstanden, dass auch seine zur Dissertation gehörenden persönlichen Daten (Lebenslauf) maschinell gespeichert und, sofern sie Element des genehmigten Prüfungsexemplares seiner Dissertation sind, vom BIS und der Deutschen Nationalbibliothek auf ihren Dokumentenservern zur freien Nutzung bereitgestellt werden.

Oldenburg, 13. Februar 2013

....
(Doktorand)

Name des Doktoranden: Leon Mauricio Juarez Paz

Titel der Dissertation: Retinal Ensemble Coding under Dynamic Conditions

Fakultät: Fak. V, Institut für Biologie und Umweltwissenschaften (IBU)